GENETIC STUDY OF A BRECCIA IN THE TEMAGAMI GREENSTONE BELT, ONT

MASTER OF SCIENCE (1990)
(Geology)

McMASTER UNIVERSITY
Hamilton, Ontario

TITLE: A Structural-Geochemical Investigation of a Mineralized Breccia and Associated Vein System at the Contact of the Strathy Batholith and the Temagami Greenstone Belt, Strathy TWP., Ontario.

AUTHOR: Mark Enne Baknes
B.Sc. (University of British Columbia)

SUPERVISOR: Dr. J.H. Crocket

NUMBER OF PAGES: xiii, 331

(lacking title page)

ABSTRACT

A 400 by 80 m tabular chalcopyrite-molybdenite mineralized breccia body and associated vein system, are hosted in basic tholeiitic metavolcanics of the Temagami greenstone belt, adjacent to the contact with the Strathy-Chambers batholith.

Mapping of the breccia and enclosing volcanics was conducted on a 400 by 600 m grid at a scale of 1:500. Features of the breccia measured were, fragment size, proportion of matrix, aspect ratio of fragments, attitude of tabular fragments and the thickness of plagioclase rims on fragments. Mapping of the remaining 4 km^2 study area at a scale of 1:2000 established the nature of the volcanic-Strathy-Chambers batholith contact zone and the extent of quartz veining and related structural features.

Structural orientations measured were primarily of joints, veins, breccia fragments, faults and foliations. Joint densities were also recorded to establish any spatial relation between joint density and proximity to the breccia.

Major, trace and rare earth element analysis were conducted on a suite of granitic samples away from the breccia, toward the core of the batholith. A suite of the tholeiitic basalts that host the breccia and a collection of basalt breccia fragments were analysed for major and trace elements.

The dominantly quartz cemented breccia varies in style from zones of pervasive breccia, where fragmentation is extensive, and the breccias are matrix supported, to areas of low matrix incipient breccia, where the breccias contain large (> 30 cm) unrotated blocks. Plagioclase feldspar often forms selvages on fragments as well as in veins within close proximity to the breccia. Sulphide mineralization is concentrated in breccias without plagioclase and in areas of relatively small fragment size. All fragmental material is of the basaltic host and these fragments are exclusively angular, and are often tabular. No evidence of fragment abrasion or matrix rock flour were noted. These features, together with the tabular unrotated fragments and a lack of rebrecciation indicates brecciation was relatively instantaneous, and passive in so much as fluid streaming was not important.

Two and possibly three steeply dipping joint populations were defined. One set essentially parallels the long axis of the breccia, the other cuts accross the breccia at a high angle. Analysis of joint densities suggests that the density of joints increases with proximity to the breccia. This feature and the observation that tabular fragments are orthogonal to the joint sets suggests that the joints were the failure or tensile fractures along which brecciation occurred.

Quartz veins trend toward 071/85NW, parallel to, and perhaps related to a significant shear zone on the east side of Net Lake. Within approximately 150 m of the breccia veins have a much more variable orientation suggesting that the more regional stresses controlling veins were overridden by forces related to breccia formation.

Gresens calculations for the identification of element mobility indicated that volcanic breccia fragments associated with sulphide mineralization and biotite alteration had experienced K and Rb metasomatism similar to that found in porphyry coppper deposits.

Major, trace element, and REE modelling indicate that compositional variation identified in the intrusive suite resulted primarily from plagioclase fractionation, with minor fractionation of biotite hornblende, ilmenite, magnetite, sphene, apatite and allanite. Granitic rocks are more differentiated and display fluid saturation textures toward the contact zone opposite the breccia, suggesting that this zone represents the apical portion of a differentiated and fluid saturated magma chamber.

Brecciation is thought to have been caused by second boiling processes related to differentiation of the Strathy-Chambers batholith that subsequently caused tensile failure and brecciation of the overlying volcanic roof rocks. Based on the similarity of vein-breccia mineral assemblages to

contact metamorphic assemblages the breccia and veins likely formed during peak metamorphism (475-550 ^{0}C) at a depth of less than 8-10 km.

Acknowledgments

I express my great thanks to Dr. J.H. Crocket for his keen interest in the project and for his many insightful ideas and suggestions. Dr. Crocket showed extreme patience as time went on and on. I would also like to thank Andy Fyon of the Ontario Geological Survey for proposing the project and for his critical suggestions in the early stages of field work.

Steve Zymela was a great help to me, as he is to everyone in the department, when it came to computer obstacles. Jack Whorwood provided expert photographic work as did Lens Zwicker in the preparation of thin sections.

Without the encouragement, patience and hard work of Donna James this work would never have been completed.

Finally I would like to acknowledge the financial support, given through Dr. J.H. Crocket, from the Natural Sciences and Engineering Research Council (NSERC) grant OGP 0001780.

Table of Contents

List of Figures

List of Tables

List of Photographic Plates

List of Maps

CHAPTER 1

INTRODUCTION

1.1 Location and Previous Work

The study area is a 4 km^2 block, located 6 km north of the town of Temagami in northeastern Ontario, between 79^0 46' and 79^0 48' west longitude and 47^0 6'and 47^0 8' north latitude (Fig. 1-1). The area is within the Temagami greenstone belt, which is situated in the SE portion of the Superior province of the Canadian Shield.

Extensive early work was carried out in the area by Barlow (1907) and Moorehouse (1946), but the first comprehensive mapping of Chambers, Strathy, Briggs and Strathcona townships was published by Bennett (1978). Fyon and Crocket (1986) produced a preliminary stratigraphic analysis of field results from Strathy township, and Fyon et al. (1988) published a synthesis of geology for Chambers, Strathy and Briggs townships, which included the subject

area of this study. Regional lithogeochemical and mineralogical studies were conducted by Soucie (1979) and Beswick and James (1984). Portions of Strathcona and Riddel townships were the subject of a stratigraphic and geochemical investigation in an M.Sc. thesis by Johnston (1987), and the metamorphism associated with the Chambers-Strathy batholith was studied in a M.Sc. thesis by Brons (1989).

1.2 General Geology

Fyon and Cole (1989) distinguished five lithostratigraphic subdivisions (Sequences: A, B, C ,D, E) in the greenstone belt, which is comprised of tholeiitic and calc-alkalic metavolcanic rocks and associated clastic and chemical metasediments. Below is a brief summary of the stratigraphic interpretation put forth by Fyon and Cole (1989). Sequence A, which occupies a large proportion of the northern half of the belt, has a south facing basal unit of iron-rich, tholeiitic basalt flows, but most of the sequence consists of intermediate and felsic calk-alkalic effusive and fragmental rocks overlain by 100-200 m of oxide-facies iron-formation. The boundary between sequence A and B is complex, but the main feature is a major NE

trending structure known as the Net Lake-Vermilion Lake (NLVL) deformation zone. Sequence B, which encompasses most of the study area, is a south facing sequence having a lower unit of tholeiitic basalt flows and an upper unit of intermediate felsic, calk-alkalic, effusive and fragmental rock. Sequence C is a south facing succession of clastic and metasedimentary rocks. Sequence D consists of iron-rich tholeiitic basalt flows, occupying the core of the east of northeast trending Tetapaga Syncline (Fig 1-1). Sequence E which lies south of the synclinal axis has a lower unit of Fe rich tholeiitic basalt, a central unit of intermediate andesite and rhyolite, effusive and fragmental flows and an upper unit of oxide-facies iron formation.

The belt is bounded by three major granitoid intrusions. The Strathy-Chambers batholith, located largely in northern Chambers and Strathy townships is comprised largely of granite in Strathy township and chlorite-bearing trondhjemite in Chambers township. The Iceland Lake batholith, located on the southern margin of the volcanic belt, is a composite chlorite trondhjemite-granodiorite intrusion. The Spawning Lake stock is a microcline-megacrystic, hornblende biotite granite. It is considered a post tectonic intrusion whereas the other two batholiths are pre- to syntectonic (Bennett, 1978; Fyon et al., 1988).

Four major zones of ductile shear are recognized: Northeast Arm, Net Lake-Vermillion Lake (NLVL), Link Lake (LL) and Tasse Lake (TL) (Bennett, 1978; Fyon and O'Donnell, 1987). The kinematics of the NLVL and TL structures indicate oblique sinistral movement, while the LL and Northeast Arm zones represent zones of flattening parallel to the axial planar foliation of the Tetapaga Syncline (Fyon et al., 1988). Development of the LL and Northeast Arm zones of deformation may have been contemporaneous with the formation of the Tetapaga Syncline, which in turn may have been caused by north-south compression due to granitic diapirism (Fyon et al., 1988). The NLVL zone and possibly the TL zone appear to post date the above structures and at least the outer margin of the Strathy-Chambers intrusive (Fyon et al., 1988). The greenstone belt is metamorphosed to lower greenschist facies, while a hornblende hornfels facies assemblage define a contact metamorphic aureole around the Strathy-Chambers intrusion (Bennett, 1978; Fyon et al., 1988; Brons, 1989).

1.3 Thesis Area Geology

The study area is centred on the contact between the Strathy-Chambers batholith and tholeiitic metabasalts

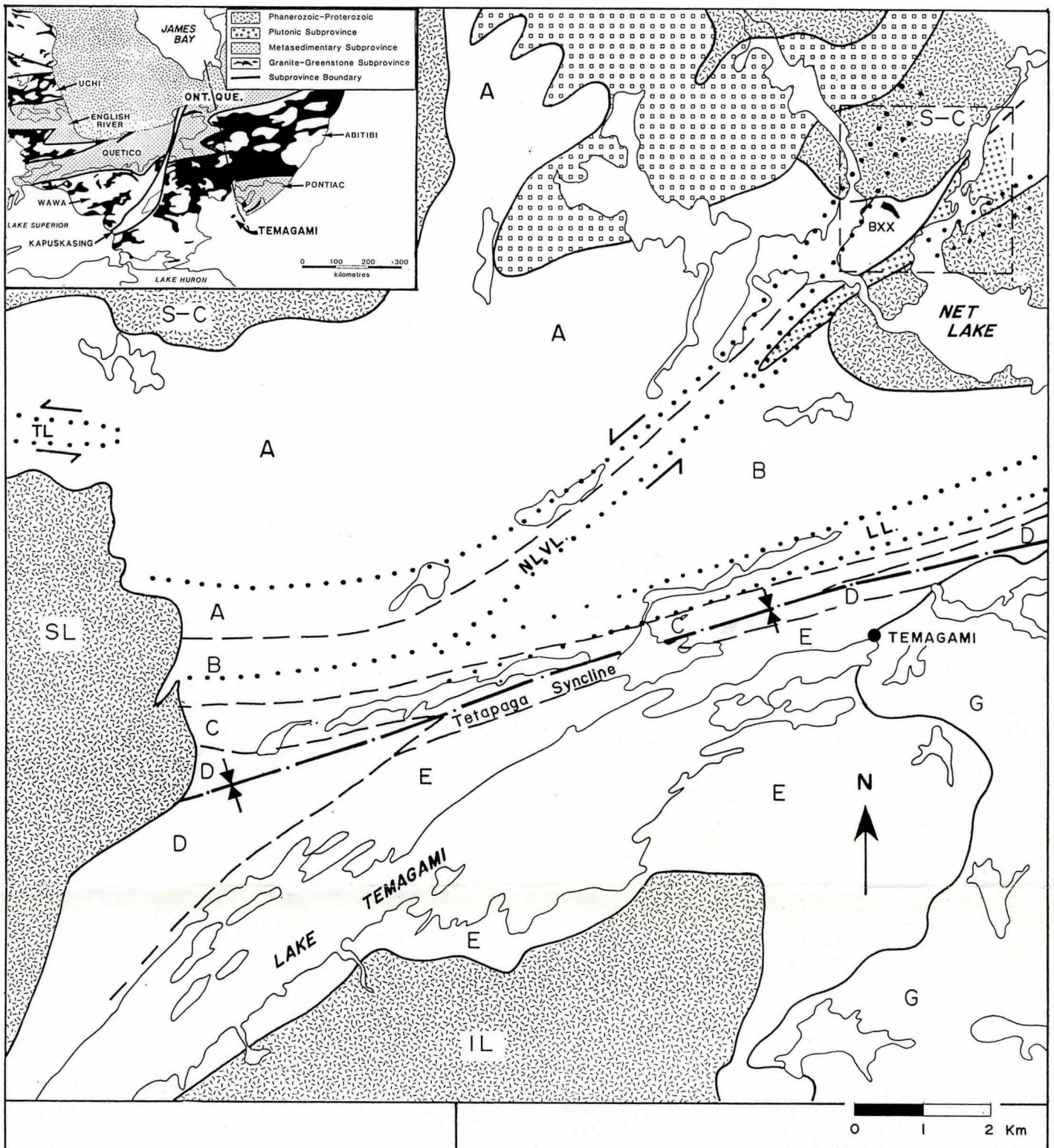

LEGEND

Archean

Metavolcanic Sequence: A B D E

Mafic Intrusion

Clastic Metasedimentary Sequence: C

Granitoids

Proterozoic

Gowganda Formation G

Nippissing Mafic Intrusion

Figure 1-1: Simplified geology of the Temagami greenstone belt after Bennett (1978) and Fyon and Cole (1989). Dashed area in the NE corner shows boundaries of the study area and the location of the breccia (BXX). Deformation zones are within the dotted areas. NLVL-Net Lake-Vermillion Lake deformation zone; LL-Link Lake deformation zone; TL-Tasse Lake deformation zone. A,B,D,E are metavolcanic sequences, C is a metasedimentary sequence. Intrusions: S-C - Strathy-Chambers batholith; SL - Spawning Lake stock; IL - Iceland Lake pluton.

belonging to sequence B of Fyon and Cole (1989, Map 1, Fig. 1-1). For the sake of brevity the prefix meta is implied but deleted in all following discussions. In this zone the volcanics form a trough or salient bounded by two lobes of the Strathy-Chambers batholith. Near the contact there is a sulphide mineralized breccia body comprised of volcanic fragments cemented by a quartz-plagioclase matrix. A consistently NE striking system of sulphide mineralized quartz veins extends from the breccia 1 km south to the village of Temagami North.

1.4 Methodology

1.4.1 Mapping

The allowable detail in geological mapping was dependent on the proportion of outcrop exposure, which varied from nearly 25 % within the immediate vicinity of the breccia to nil in areas south of the breccia. Mapping on the west side of Net Lake including the breccia and points south was at a scale of 1:500, while areas north and on the east side of Net Lake were mapped at 1:2000 scale. A 500 m by 400 m grid with 40 m line spacing was established over the breccia (Map 2). Areas with less exposure north and

south of the grid were located with respect to the grid by tie lines. Outcrops on highway 11 were located with air photos and published maps.

The mapping was carried out with several specific objectives in mind. The first was to map volcanic lithologies that had not been previously differentiated in the map area and to characterize any associated hydrothermal alteration. Secondly, intrusive rocks were mapped mainly to document features such as pegmatites that were thought to be related to the crystallization and emplacement of the intrusion. Thirdly, structural data including joint, fault, shear, foliation and vein attitudes were collected to evaluate whether the formation of the breccia and veins could be correlated with a unique or regionally controlled stress regime. Several textural features of the breccia were also measured to describe the textural variability within the breccia and establish relationships between these features and others, such as mineralization.

1.4.2 Geochemistry

Analysis of intrusive rocks for major and selected trace elements was done by X-ray fluorescence (XRF) and instrumental neutron activation analysis (INAA) (Appendix

A). This investigation was carried out to classify the intrusive rocks and define any compositional variability that might be spatially related to the contact adjacent to the breccia. Major and trace element analysis of volcanic rocks were required to aid in distinguishing lithologies identified during mapping and to identify any alteration that might be related to hydrothermal or intrusive activity. Analysis of quartz for trace constituents was conducted to determine any differences in the composition of vein and breccia quartz, and mineralized versus unmineralized quartz. Sulphide separates were also analyzed for some trace elements and sulphur isotopes to investigate the source of hydrothermal fluids and the temperature of mineral deposition.

1.5 Thesis

The field and laboratory investigations were directed toward testing the hypothesis that the breccia and vein hydrothermal systems were developed as a consequence of differentiation and subsequent separation of a hydrothermal fluid from an apical zone of the Strathy-Chambers batholith. This fluid is thought to have exerted pressure on volcanic roof rocks causing their failure and brecciation, and to

have released the mineralizing fluids into the breccia matrix and a system of quartz veins that were oriented in response to the regional north-south compressional stress regime.

CHAPTER 2

GENERAL GEOLOGY AND PETROGRAPHY

2.1 General Geology of The Thesis Area

The thesis area encompasses an approximately 4 km^2 area in the NE corner of Strathy township, where a 1 km wide salient of volcanic rocks lies between two lobes of the Strathy-Chambers batholith (Fig. 1-1). The volcanics are mainly iron-rich tholeiitic basalts belonging to sequence B of Fyon and Cole (1989). They are hornfelsic, fine-grained, massive to pillowed, with pillows that consistently indicate a SE facing orientation. These basalts are intruded by a layered gabbro-anorthosite body that is approximately conformable to the NE trending volcanics (Map 1) (Fyon and Cole, 1989). The Strathy-Chambers batholith, which varies compositionally from mainly trondhjemite in Chambers township to dominantly granite in the study area, (Fyon and Cole, 1989) intrudes the volcanics and the gabbro-

anorthosite body in a variety of styles. One type of intrusive contact comprises an extensive intrusion breccia (Harker 1909, Wright and Bowes, 1963) where large blocks of volcanics founder in a matrix of varying proportions of medium grained granite. These volcanic blocks show evidence of being intruded prior to granite intrusion by the gabbro-anorthosite gabbro, making clear the temporal intrusive relationships (Plate 2-1a). The existence of intrusion breccia and the relationship of the elevation contours with the intrusive volcanic contact suggest that here the contact dips very shallowly towards the SE (Map 1).

A distinctive feature of the granite-greenstone contact in the study area is a 340 m long by 90 m wide tabular breccia body that lies adjacent to the approximately south dipping intrusive contact (Map 1). Fragments are exclusively volcanic, angular and often blocky. In some zones they are distinctly tabular, forming well aligned, steeply dipping units (Plate 2-1b;2-2a,b,c). The matrix is dominantly milky white quartz, but in many areas fragments are rimmed with selvages, up to 4 mm, of subhedral plagioclase (Plate 2-1b;2-2a,c). Rock flour, or a significant proportion of fine fragments are absent in the matrix.

Plate 2-1a (page 12): Intrusion breccia with tabular blocks of basalt that appear to be intruded by gabbroic intrusive. A partially consumed fragment of anorthosite/gabbro is visible beneath the scale.

Plate 2-1b (page 12): Basaltic breccia fragments with plagioclase selvages.

Plate 2-2a (page 13): Pervasive quartz-feldspar breccia with aligned tabular fragments.

Plate 2-2b (page 13): Alignment of tabular fragments in a quartz only breccia.

Plate 2-2c (page 13): Well developed plagioclase selvages in a pervasive breccia.


A

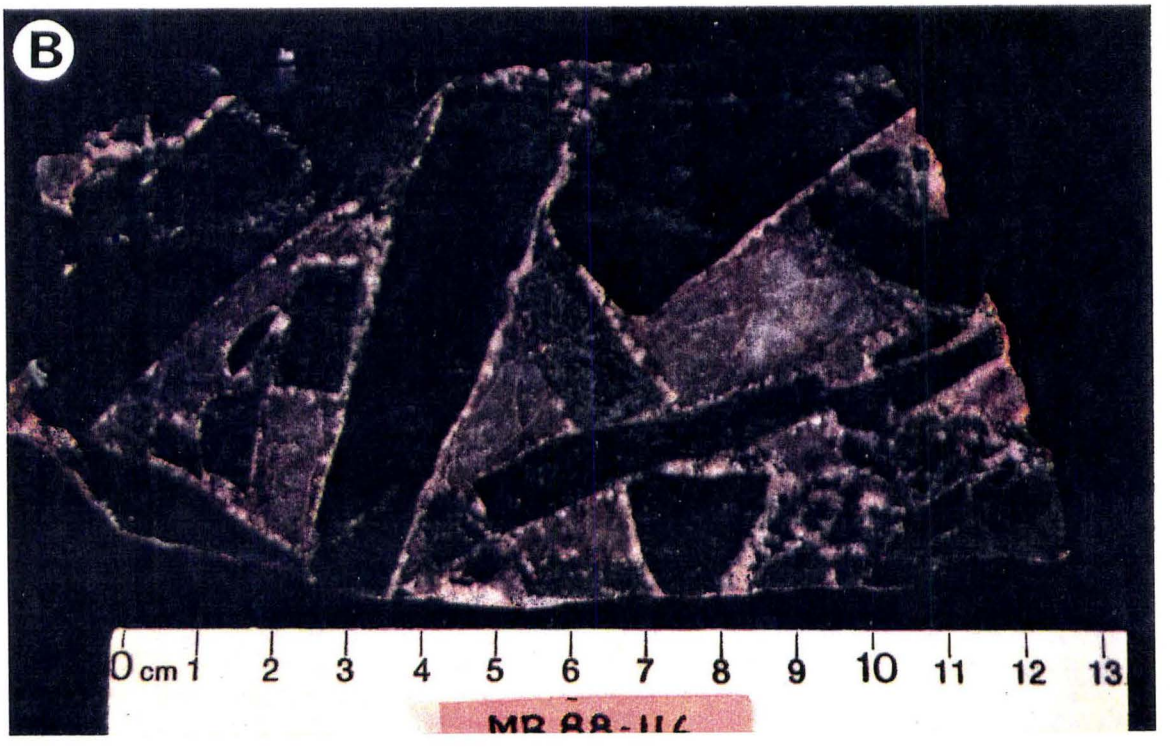
B
0 cm 1 2 3 4 5 6 7 8 9 10 11 12 13


B


A


C

Fragment size varies considerably in the NE portion where large blocks, on the order of a meter or more, of unbrecciated basalt are bordered by margins of quartz and or fine-grained breccia. These breccias are termed incipient (Walker and Cregheur, 1982), implying that fragments have not experienced significant movement or rotation and that fragmentation is only weakly developed, producing a mosaic structure where the fragments appear to fit together (Plate 2-3a,b;2-4a). To the SE of the incipient breccia the breccia is termed pervasive meaning fragmentation is much more extensive, fragments are often matrix supported, and of relatively small size. These pervasive breccias are also characteristic in that on the scale of at least 3-4 m across an outcrop the brecciation is continuous (Plate 2-4b;2-5a,b). The matrix proportions in the pervasive breccias are also generally greater (>20 %) than the areas of incipient breccia. There are two satellite breccias, at the NW end on either side of the main mass of breccia (Map 2). One is a 15-20 m wide incipient breccia, on the north side of the main breccia, where the volcanic fragments are highly altered to biotite and chlorite. The other is a 30-40 m long, by 1-2 m wide, lens shaped breccia body on the south side of the main breccia, which is similar in character to the main body. Obvious alteration of breccia fragments is

Plate 2-3a (page 15): Incipient breccia where blocks of basalt are fractured, but not brecciated and are bordered by finer-grained breccia.

Plate 2-3b (page 15): Incipient breccia where fragmentation is apparent, but there is essentially no matrix.

Plate 2-4a (page 16): Incipient breccia, large unrotated blocks with marginal zones of finer-grained breccia.

Plate 2-4b (page 16): Pervasive quartz-only breccia. Largely matrix supported, equant blocky fragments.

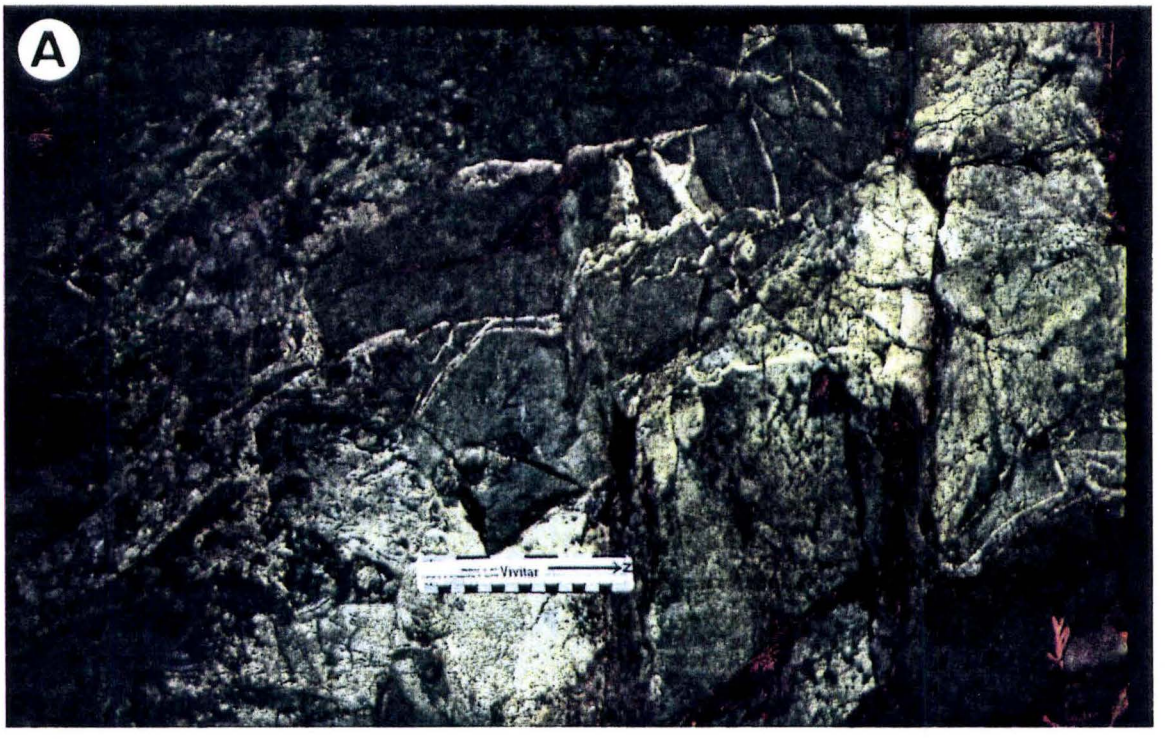
A
Vivitar

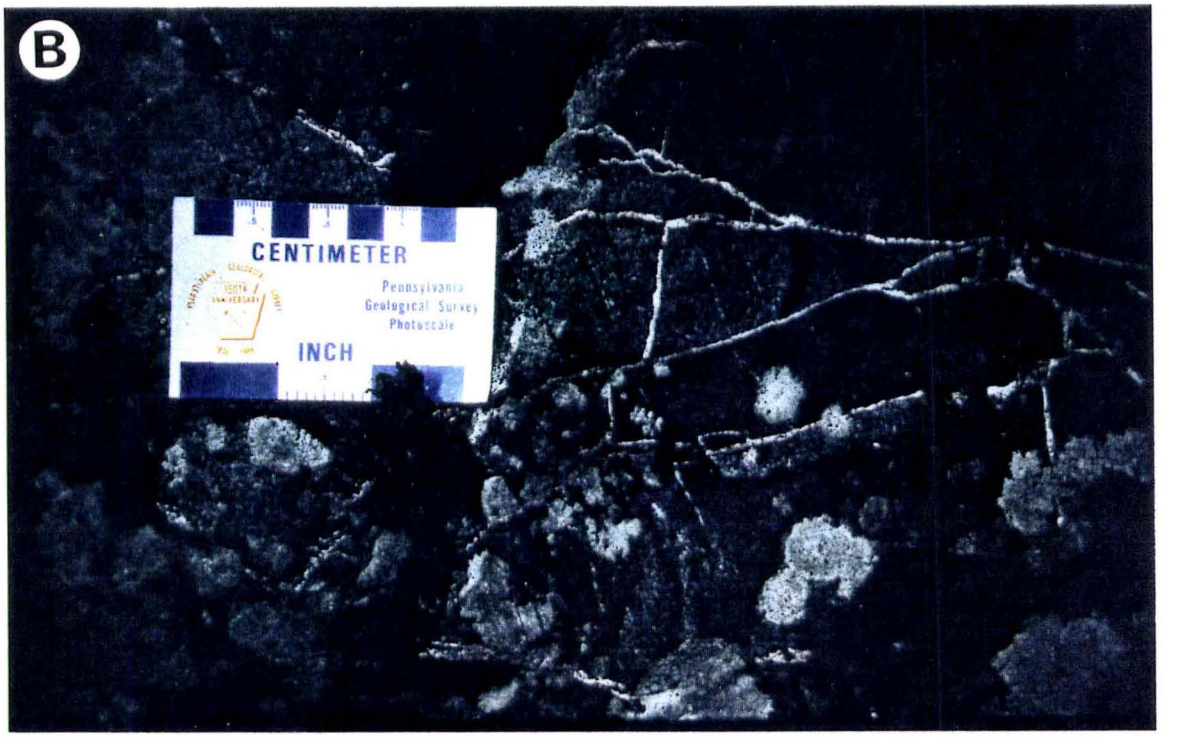
B
CENTIMETER
Pennsylvania
Geological Survey
Photoscale
INCH

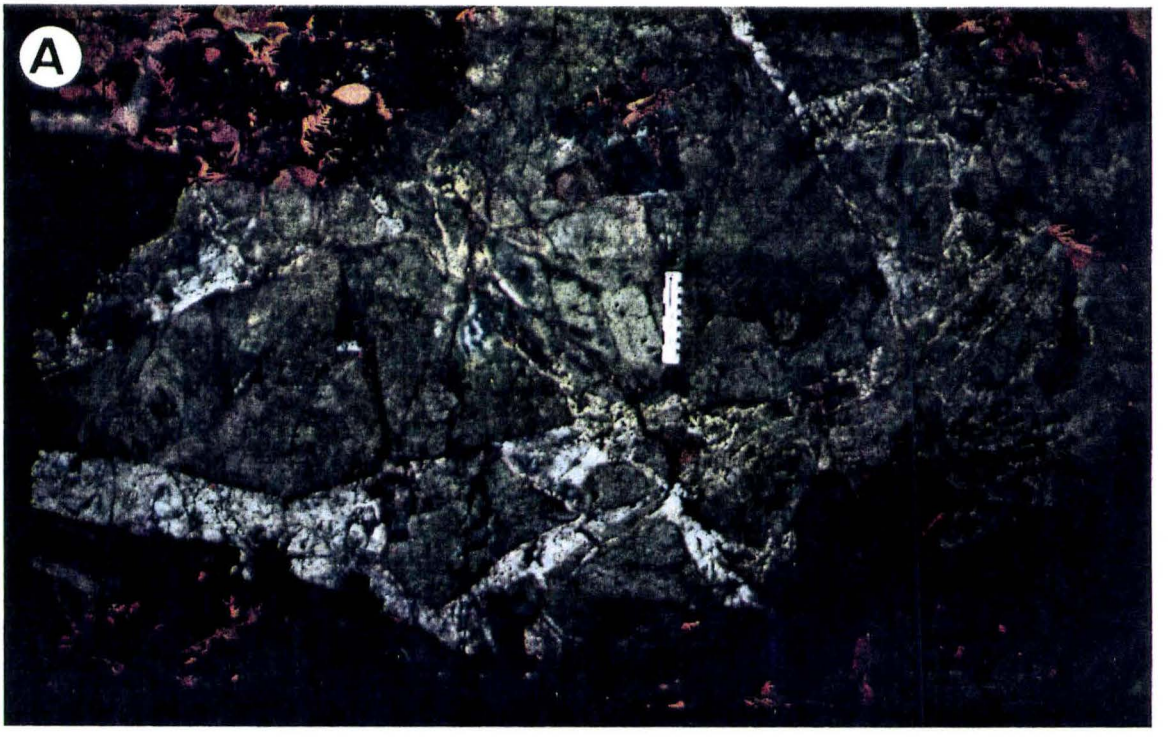
A


B

generally absent, but alteration does concentrate in mineralized zones where higher concentrations of disseminated and selvage biotite and chlorite are present. Mineralization is present mostly at the SE end of the main breccia and is comprised primarily of chalcopyrite and molybdenite, which form selvages on volcanic fragments.

Quartz veins are distributed throughout the study area and are hosted in both volcanics and the Strathy-Chambers batholith. From the breccia extending south to North Temagami there is a persistent set of veins that trend near 071^0 and dip steeply to the NW. These veins are often mineralized with selvages of chalcopyrite and molybdenite in the same way that breccias are mineralized. At a distance of about 100 m on either side of the breccia, veins still trend near 071^0, but there is considerably more variability in attitude. In this area of variable vein orientations a moderate number of the veins have feldspar selvages much like that observed within the breccia. On the east side of Net Lake there are many largely unmineralized veins that coalesce in a zone of shearing referred to as the 069^0 shear zone (Map 1). These veins trend subparallel to the shear zone and often exhibit a sugary texture leading to the conclusion that their formation is related to shearing.

Dykes in the study area include feldspar and quartz feldspar porphyry, basaltic, granite and aplite. The basaltic dykes clearly postdate the felsic magmatism and hydrothermal activity whereas the granitic and aplitic dykes coincide with it and are spatially restricted to the contact zone. Quartz and quartz feldspar porphyry dykes occur throughout the Temagami belt. According to Bennett (1978) there are two distinct types: 1) those associated with major felsic intrusions that are likely comagmatic with the intrusions, and 2) porphyries, not associated with major intrusions, which are probably subvolcanic equivalents to local felsic volcanic units (Bennett, 1978; Fyon and O'Donnell, 1987, Johnston, 1987). In the area surrounding the breccia the feldspar porphyry dykes appear to be associated with the breccia emplacement and show evidence of intrusion possibly during and immediately after breccia solidification. Geochemical evidence is highly suggestive that the porphyry dykes and the Strathy intrusive are comagmatic, suggesting that the intrusive emplacement was approximately coincident with the formation of the breccia.

The most prominent structural elements in the vicinity of the study area are the NLVL zone of deformation and the 069^0 shear zone (Fig. 1-1; Map 1). The NLVL zone is considered to have experienced a dominant, oblique,

subvertical component of motion, with a lesser, sinistral, horizontal component (Fyon et al. 1988). The kinematics of the 069^0 shear zone are uncertain, but the few indications suggest movement was sinistral and subhorizontal. The consistent vein orientations are also considered to be an important structural component probably genetically related to the major sinistral component of shear (see section 3.5.1). Concentrated near the breccia, but extending as far south as Temagami North, are two prominent sets of orthogonal joints, which are thought to be related to the breccia emplacement.

2.2 Description of Lithologies

2.2.1 Strathy Granite

Thin sections of the Strathy-Chambers granite, from a traverse extending from the contact opposite the breccia northward for 1.8 km along highway 11, were studied. The findings are similar to those of Fyon and Wheatley (1988). Grain size is generally medium- to coarse-grained (Plate 2-5c), but there are local variations in the vicinity of pegmatites and aplitic rocks. Plagioclase occurs as subhedral to euhedral laths often displaying albite twins,

Plate 2-5a (page 20): Pervasive breccia with 2-4 mm feldspar selvages.

Plate 2-5b (page 20): Close up of pervasive quartz-only breccia shown in figure 2-4b.

Plate 2-5c (page 20): Granite typical of that which outcrops along highway 11. 'Kf' refers to the tartan twinned K-feldspar which occurs as an interstitial phase.

Plate 2-5a (page 20): Pervasive breccia with 2-4 mm feldspar selvages.

Plate 2-5b (page 20): Close up of pervasive quartz-only breccia shown in figure 2-4b.

Plate 2-5c (page 20): Granite typical of that which outcrops along highway 11. 'Kf' refers to the tartan twinned K-feldspar which occurs as an interstitial phase.

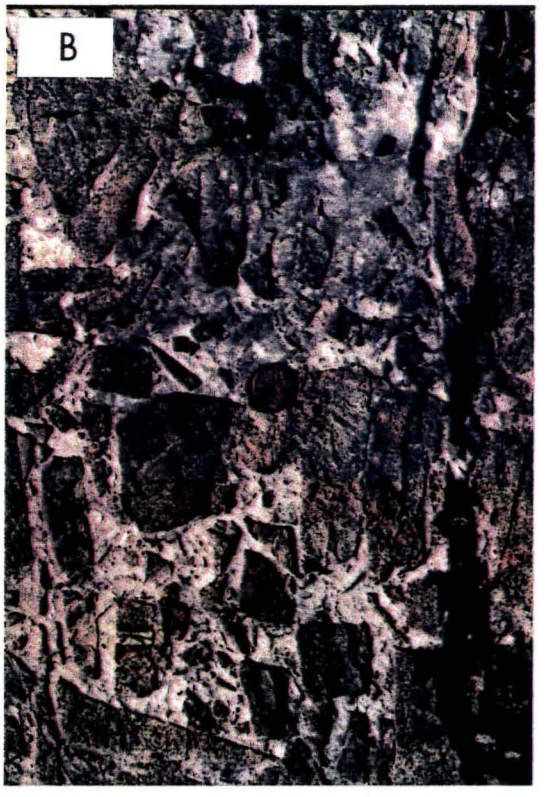

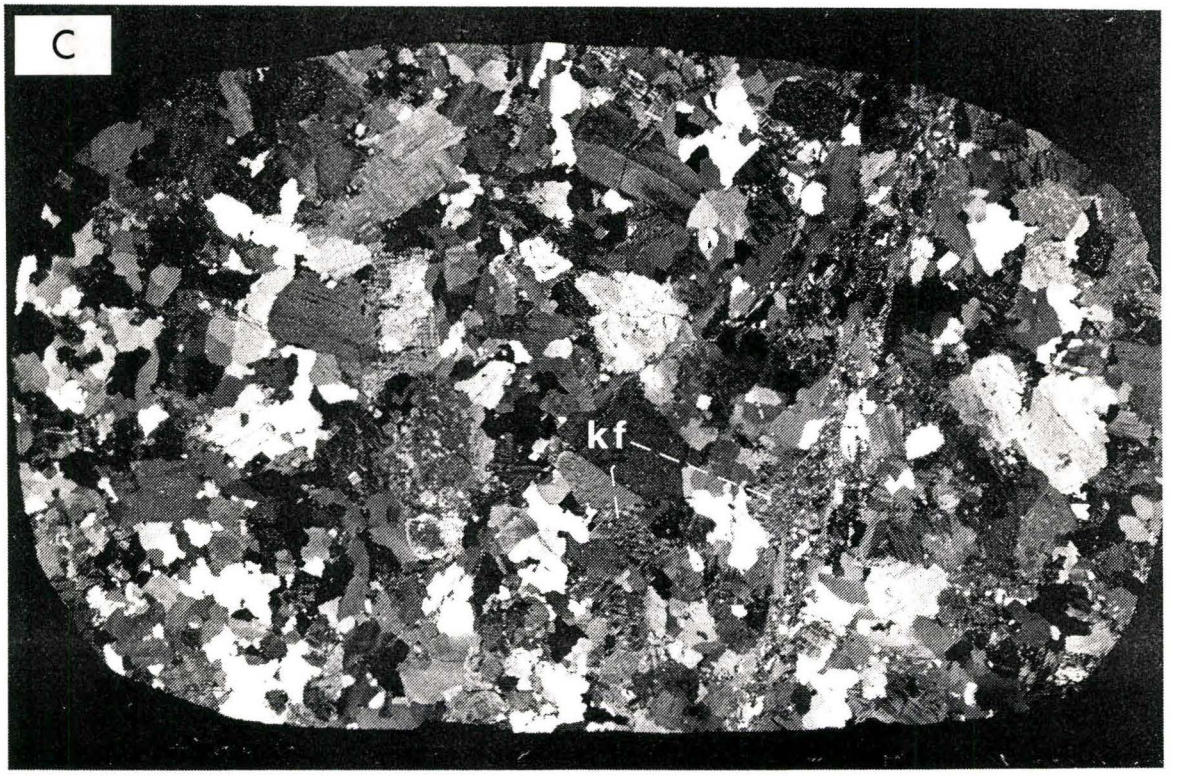

1 cm

which indicate compositions averaging An_{34}, and as perthitic exsolutions and irregular inclusions in K-feldspar. Perthitic alkali feldspar occurs most often interstitial to plagioclase and quartz, and appears to partially replace both of these minerals. Quartz invariably occurs as equant anhedral grains interstitial to and enclosing plagioclase. Chlorite is present in two habits: as euhedral books adjacent to plagioclase grains with rims of fine-grained epidote, and as finer-grained laths and radiating aggregates replacing plagioclase. Chlorite may also occur as rare pseudomorphs after amphibole as evidenced by long acicular aggregates of chlorite. The well-formed books of chlorite often have internal diffuse lenses of biotite suggesting that chlorite is a pseudomorph after biotite. Epidote is associated with chlorite and also commonly an alteration product of plagioclase. Sericite replaces plagioclase and chlorite. Other accessory minerals include zircon as inclusions in chlorite (biotite), hematite, carbonate, apatite and clinozoisite. Point counts were not made, but visual estimates of modes suggest that the amount of chlorite decreases and that alkali feldspar increases in samples nearest the contact.

2.2.1.2 Pegmatites, Aplites and Related Lithologies

Pegmatites, pegmatoids and aplites are exposed in a restricted zone of outcrops along highway 11 close to the intrusive-volcanic contact (Map 1). The term pegmatoid is used here in reference to pegmatite-like features that do not display the normal pegmatite textures, but still appear to have developed as late stage differentiates formed in the presence of a separate aqueous phase (Jahns and Burnham, 1969). Pegmatites are largely comprised of pegmatitic intergrowths of quartz and pink perthitic alkali feldspar and minor plagioclase. Chlorite sometimes forms massive aggregates filling interstices between quartz and alkali feldspar. Muscovite is a minor phase, occurring at the margins of chlorite masses and as pseudomorphs of feldspar laths. Epidote usually forms isolated aggregates associated with muscovite. In some pegmatites small blebs of pyrite and chalcopyrite are visible as late stage open space filling. Although not identified within the pegmatites molybdenite rarely occurs as isolated grains in granite or in quartz stringers in close proximity to the pegmatite zones.

Aplites often form undulating dyke-like bodies that sometimes have central pegmatitic lenses (Plate 2-6a). In thin section they are comprised of quartz and perthitic

feldspar sometimes as graphic intergrowths. Plagioclase is usually present as ragged exsolutions in perthite, but it also forms discrete euhedral inclusions in the perthite, which are partially replaced by sericite. Quartz occurs as anhedral grains, displaying sutured margins with adjacent quartz and feldspar.

In addition to the pegmatites and aplites, pegmatoids having a peculiar bulbous shape and a banded structure were identified. These features are termed bubble structures (Plate 2-6b;2-7a,b). In the photographs the dark layers are comprised of granitic material having a higher proportion of chlorite than the light layers. In some similar examples there are small pegmatitic segregations in the basal part of the spherical structure. The striking spherical form at the base of these structures and the occasional association with pegmatites indicates that they are not xenolith. It is proposed that they formed by exsolution of fluid from crystallizing magma. The remarkable banding and symmetrical distribution of features is suggestive of derivation by some process related to fluid diffusion.

Pegmatites are generally considered to develop as late residual differentiates crystallizing from volatile-enriched melts resulting from granitic differentiation on a plutonic scale (Cerny, 1982). In the classification scheme of

Plate 2-6a (page 24): Aplite with lensoidal pegmatitic segregation.

Plate 2-6b (page 24): Bubble structure with dark bands of mafic rich granitic material. On the left side of the photo, which is interpreted as the top of the bubble structure, the form flattens out into a planar layer that extends laterally (dotted lines). A probably spherical bubble-like form is developed in the 'bottom' on the right side of the photo (B).

Plate 2-7a (page 25): A bubble structure with a pegmatitic segregation (P) in the 'basal' portion. The planar layer shown by the dotted line is shared with another poorly developed bubble structure in the extreme left of the photo.

Plate 2-7b (page 25): Bubble structure similar to previous examples but here there is no basal bubble or pegmatite. The top portion, which grades laterally into the apical layer (dotted line) is weakly pegmatitic.

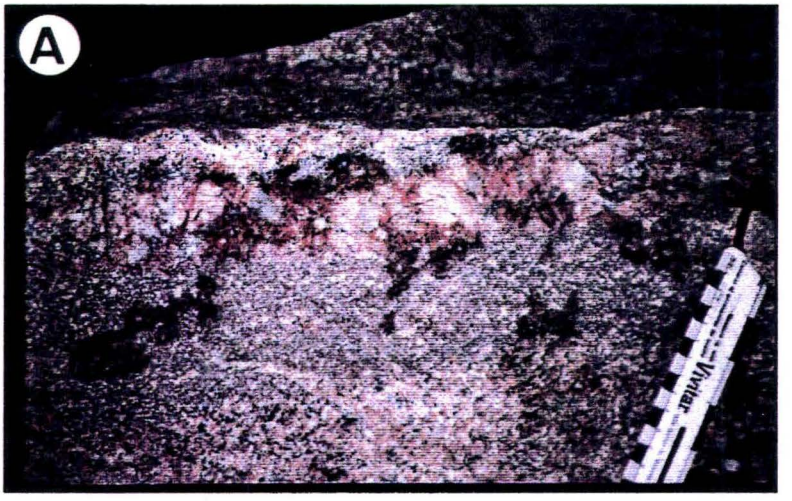
A


B


A
P


B

Ginsburg et al. (1979) the pegmatites described here correspond to the miarolitic pegmatite class. Such pegmatites are situated largely within cupolas of shallow-seated, epizonal to subvolcanic granites and in their adjacent host rocks. Aplites are often closely associated with pegmatitic zones and are thought to develop as a pressure quench brought on by a loss of fluids (Cerny et al., 1985). Zonation that is apparent along the highway traverse is of this nature, where pegmatites are suggested to lie in the most apical zones of the magma body with aplites occurring immediately beneath the pegmatitic aureole (Map 1;Cerny et al., 1985).

2.2.2 Feldspar Porphyry Dykes

With the exception of one example all the dykes encountered were feldspar phyric and did not have a quartz phenocryst component. Plagioclase phenocrysts are typically 0.2 - 1.5 mm, euhedral-subhedral, unzoned, simple twinned crystals. Invariably they are extensively altered by fine-grained epidote and chlorite. Estimates of the plagioclase composition were difficult to obtain because of the alteration, but most results indicate a composition near An_{50}. The matrix is often very fine-grained and in some

samples glassy, but where microcrystalline it consists of subhedral-anhedral plagioclase and interstitial quartz. The occasional myrmekitic-like texture suggests the presence of matrix K-feldspar (Deer et al., 1983). Chlorite and epidote are minor phases in the matrix while in one dyke that cuts the granite, sericite is significant and increases as a matrix component near the intrusive contact. Compositional determinations from matrix feldspar consistently average to An_{32}, which is considerably less calcic than the phenocrysts and similar to compositions in the granitic samples, which averaged An_{34}.

In the southern part of the study area to the west of Temagami North and east of Highway 11, there are a few exposures of granitic rocks. In hand specimen these rocks ranged from aphanitic to medium-grained porphyritic. The exposures did not indicate that these were dyke-like bodies nor did they resemble the more common porphyry dykes encountered. The unique porphyritic texture and the nearby presence of probable crenulated quartz and feldspar layers, a texture considered to indicate the presence of fluids (Moore and Lockwood, 1973; Stewart, 1983; Kirkham and Sinclair, 1985), as well as abundant quartz veins suggest that these rocks may represent pressure quenched granites (Plate 2-8a)(see chap.6). In thin section the rocks range

from porphyritic to aphyric, with both subhedral and euhedral plagioclase (An_5), rounded quartz phenocrysts and minor chlorite pseudomorphs. The groundmass is a very fine-grained intergrowth of quartz and feldspar that, in some zones is myrmekitic.

2.2.3 Gabbroic Intrusive

In the study area gabbroic rocks occur primarily in the intrusive breccia zone and on the east side of Net Lake, although there are possibly some limited exposures in the vicinity of the water tower (Map 1). Fyon and O'Donnell (1987) refer to these rocks as part of the Net Lake layered complex. To the SW of Net Lake, the complex is mainly a pyroxenite overlain by heterogeneous, gabbro-anorthositic gabbro, the uppermost part of which is quartz-rich and feldspathic (Fyon and O'Donnell, 1987). Northeast of the Temagami North settlement, along the NE shore of Net Lake, the pyroxenite phase of the intrusion is missing, and coarse-grained gabbro and anorthositic gabbro predominate (Fyon and O'Donnell, 1987). Within the study area the mineralogy is totally secondary with original pyroxenes replaced by xenoblastic amphibole. Original ophitic textures remain, but xenoblastic plagioclase and minor

quartz embay and replace the margins of amphibole. Quartz, biotite, epidote and chlorite are closely associated and occur as aggregates surrounding partially replaced magnetite-ilmenite grains. Net and skeletal textured pyrite and chalcopyrite are unevenly distributed and display textures suggestive of remobilization.

2.2.4 Mafic Volcanics

In general the volcanics can be described as massive to pillowed flows of tholeiitic basalts. They are fine- to medium-grained, weather a medium greenish grey and are dark greenish grey on the fresh surface. The volcanics within the study area are noticeably hornfelsic and darker in color than the volcanics more distant from the intrusive contact. The study area is encompassed in the inner contact metamorphic aureole of the Strathy-Chambers batholith and is characterized by the hornblende-hornfels facies mineral assemblage: ferro-hornblende + actinolite + epidote + plagioclase + quartz + ilmenite + apatite + magnetite $\pm$ chlorite $\pm$ sericite $\pm$ biotite $\pm$ microcline (Brons, 1989). Brons (1989) also delineates a biotite zone or halo within the volcanics parallel to the intrusive contact.

Within the area of the breccia detailed mapping allowed for the distinction of several different basaltic lithologies within the greater package of tholeiitic basalts. In the following sections they are distinguished petrographically, but chemical distinctions and classification are discussed in chapter 5.

High- Magnesium Tholeiites, Group 2i On the weathered surface these medium-to fine-grained rocks are typically medium greenish grey and have a characteristic salt and pepper distribution of dark and light minerals. Fresh surfaces are granular textured with uneven to sub-conchoidal fracture and are coloured dark grey to greenish grey. Outcrops are usually massive showing no primary flow textures. In thin section these basalts are comprised mainly of a framework of pale green subidioblastic to idioblastic hornblende and xenoblastic plagioclase (Plate 2-8b). The matrix is a complex intergrowth of untwinned feldspar, lesser quartz, granular epidote, sericite, and chlorite. Rarely relic plagioclase laths are evident but these are largely replaced by granular epidote (Plate 2-9a,b). Apatite occurs as a trace phase within the quartz and feldspar. Opaques usually comprise less than one modal percent and occur as anhedral disseminated grains often adjacent to, or as inclusions in hornblende. Epidote is

Plate 2-8a (page 31): Quenched granite; phenocrysts of quartz and plagioclase in a fine-grained matrix.

Plate 2-8b (page 31): 2i or high-Mg tholeiite. Subidioblastic hornblende (yellows and orange) in a fine grained matrix of quartz feldspar and epidote.

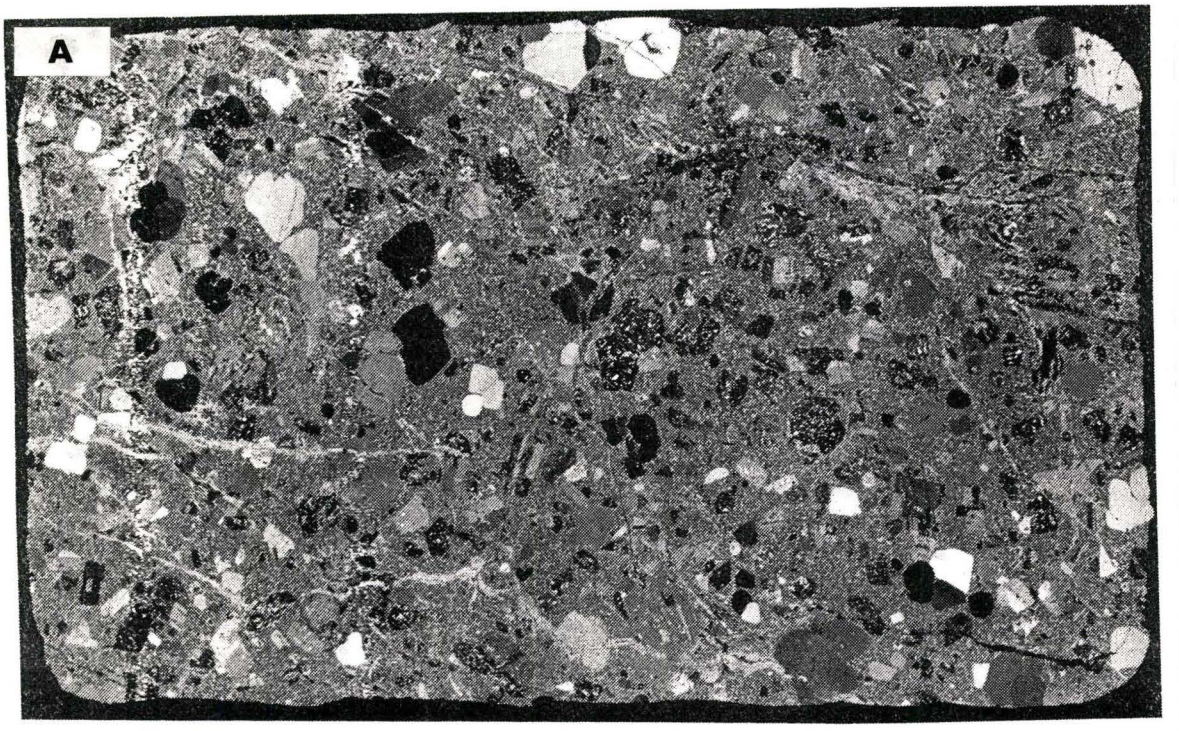

1 cm

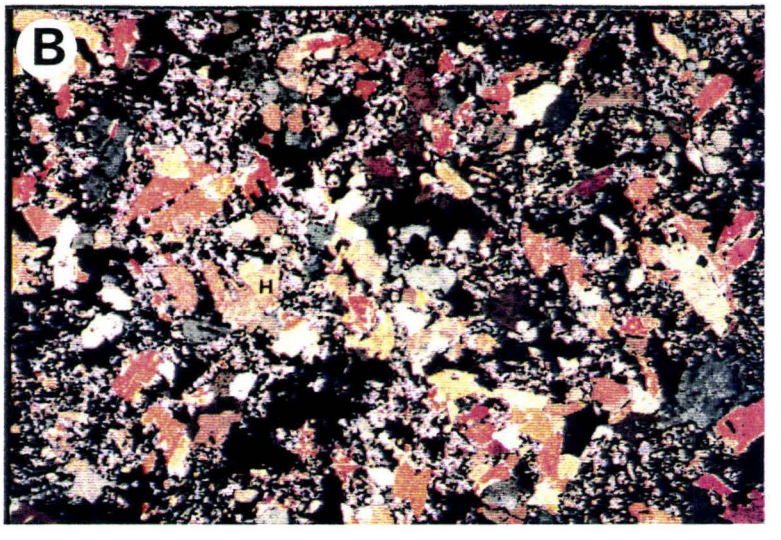

1 mm

usually present as fine aggregate replacements of feldspar, but it also occurs rarely as discrete grains and in thin veinlets associated with quartz and carbonate. Other replacement textures observed are sericite replacing feldspar, quartz and chlorite replacing hornblende and very rarely, biotite replacing hornblende.

High-Iron Tholeiites, Groups 2j and k On the weathered surface these rocks are fine-grained, dark grey to dark green. The fractured surface, which is often conchoidal, is dark greenish grey to black with occasional fine flecks of biotite. Group 2j rocks are usually massive and display no primary textures, but outcrops are often highly fractured. Group 2k rocks, otherwise the same as 2j, are differentiated on the basis of extensive primary textures, such as pillow selvages and amygdules (Plate 2-9c,d). In thin section both 2j and k are comprised of a framework of fine-grained, dark green, subidioblastic hornblende. The matrix is mainly xenoblastic feldspar, but sometimes relic plagioclase is present with sparsely disseminated aggregates of granular epidote. The fine-grain texture of these rocks is often interrupted by zones of coarse-grain size and different mineralogy that probably correspond to pillow selvages and amygdules. In these areas hornblende becomes coarse, quartz appears as equant grains in sometimes polygonal masses and

Plate 2-9a (page 33): 2j or high-Fe tholeiite with fine-grained hornfelsic texture.

Plate 2-9b (page 33): 2k or high-Fe tholeiite with fine-grained texture with possible chlorite filled amygdules (dark grey).

Plate 2-9c (page 33): 2i or high-Mg tholeiite with relic plagioclase laths, which are largely replaced by epidote.

Plate 2-9d (page 33): More typical salt and pepper 2i or high-magnesium tholeiite.

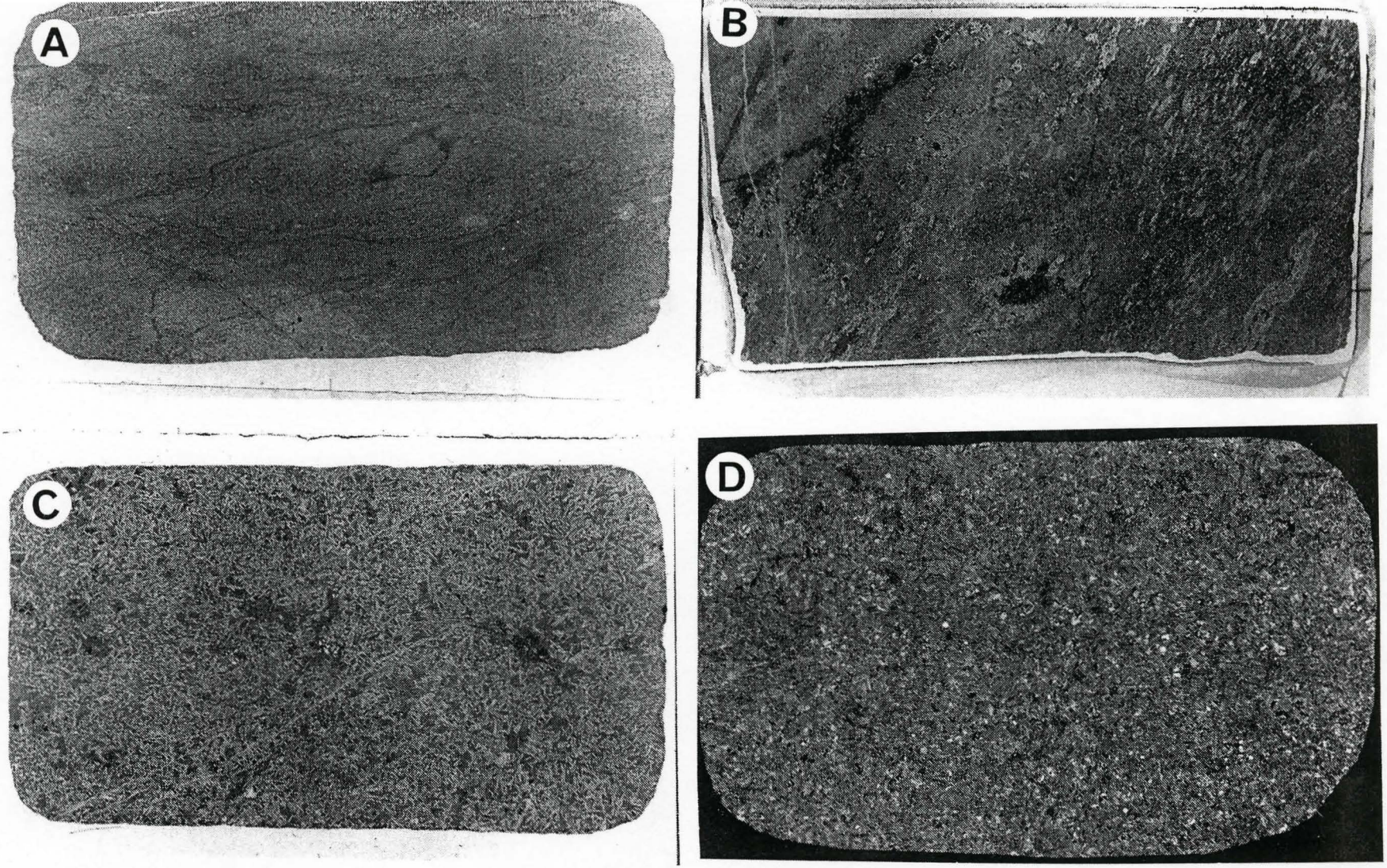
A
B
C
D
1 cm

chlorite and epidote form patches of intergrown aggregates. In some of the chlorite-filled amygdules, lenses of biotite are visible within chlorite grains suggesting that chlorite may be a pseudomorph after biotite. The more common habit of biotite is diffuse patches in hornblende grains, sometimes in association with clusters of opaques, indicating a replacement origin (Plate 2-10a). Opaque phases are heterogeneously distributed and comprise 1-2 %. They are often associated with biotite.

Medium-Grained Tholeiites, Group 2o The weathered surface is medium to light greenish grey with a distinctive salt and pepper texture like the 2i group except that the grain size is coarser and the proportion of light coloured minerals greater. The fresh surface is medium grey, with uneven to subconchoidal fracture, and granular texture. In some exposures it is clear that shearing has taken place and the rock takes on a layered texture of alternating light and dark mineral bands with infrequent lenses of quartz. In thin section the framework hornblende is pale green and has a distinctive ragged appearance (Plate 2-10b). The matrix is comprised of an xenoblastic intergrowth of feldspar and granular and polygonal quartz. Sericite is abundant in the matrix replacing up to 25 % of feldspar and similarly quartz embays and replaces hornblende. Carbonate, quartz, chlorite

Plate 2-10a (page 35): 2j containing disseminated biotite (blue) as interstitial grains and replacements of hornblende.

Plate 2-10b (page 35): 2o or altered high-Mg tholeiite. Secondary textures include veinlets of chlorite (chl) and epidote, quartz (q) replacement of hornblende (H) and secondary carbonate (ca).

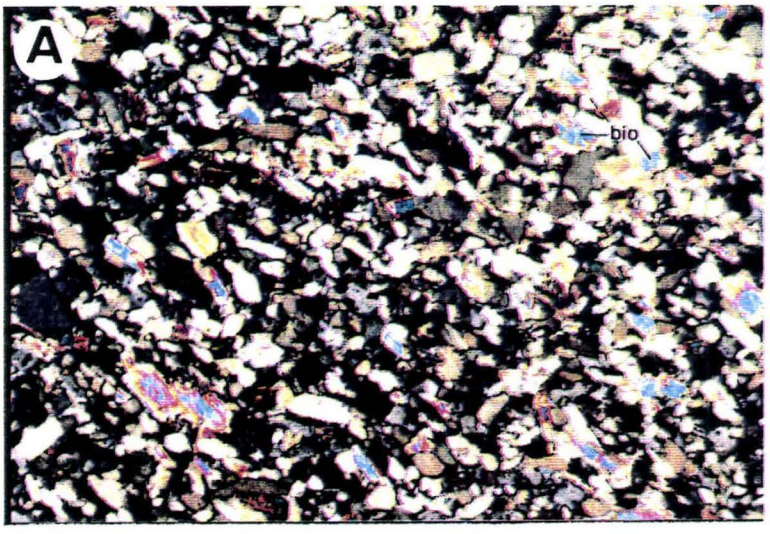
A
bio
1mm

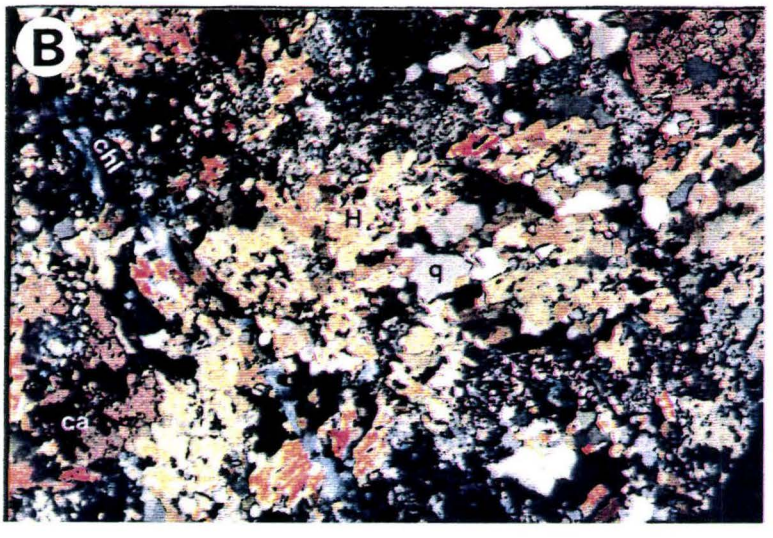
B
chl
H
q
ca
1mm

and epidote all occur in subparallel veinlets. Opaques, which include hematite are associated with the veinlets.

2.2.4.1 Interpretation of Volcanic Lithologies

The most distinctive petrographic contrast between the high-Fe tholeiites and the high-Mg tholeiites is the colour of hornblende, the distribution of biotite and the texture and mineralogy of the matrix. The hornblendes in the high-Fe tholeiites have darker green pleochroism and higher interference colours, which may be a reflection of higher Ti contents. The greater proportion of biotite in the high-Fe tholeiites may also be an indication of higher Fe and Ti content. The high-Mg tholeiites also differ from the high-Fe tholeiites in the greater content of secondary matrix minerals, such as epidote and sericite. They also rarely contain relic plagioclase laths indicating these rocks underwent less recrystallization during metamorphism.

In outcrop, 2i and 2j/k units usually have gradational contacts, but in some instances they are in direct contact having interfingering complex boundaries. The irregular outcrop pattern does little to confirm or imply a stratigraphic relationship between these rocks and it is therefor unclear whether or not the divisions represent

primary lithological units or relatively less altered and more altered equivalents (Map 2).

The 2o unit clearly represents a more intensely altered zone since it displays abundant petrographic evidence of secondary mineralogy and deformation. The similar chemical composition and appearance of 2o rocks to 2i rocks suggests that 2o is a more intensely altered and deformed equivalent to 2i.

CHAPTER 3

STRUCTURAL GEOLOGY

3.1 Introduction

Collection and analysis of structural data was carried out to develop models for the formation of the breccia body and related structures. Any model for these local structural features should take into account the more regional structural synthesis put forth by Fyon et al. (1988). Structural data were collected primarily from areas immediately adjacent to the breccia body with some additional data taken from specific areas up to 1.5 km from the breccia. Data consisted primarily of vein, joint, foliation, and fault orientation data, and additional measurements on breccia fragments, dykes, pegmatites and related structures. To better interpret variations in the structural data and their dependence on location and host lithology, the area was divided into structural domains,

first defined by lithology. Additional domains represent the area SW of the breccia, which is divided into two areas in order that contrasts in structure might be identified relative to distance from the breccia and along the strike of veins. Domains adjacent to the breccia are small to allow for identification of subtle changes over short distances that may reflect breccia forming processes. Domains are also defined for the area on the east side of Net Lake since this area is influenced by intense shearing. The boundaries and names of domains for each structure category, such as veins and joints, may not coincide, according to circumstances. Table 3-1 lists the various domains according to structural category and summarizes the main characteristics of each, while Figure 3-1 shows the areal distribution of the various domains. After separation into domains, stereographic projections of the data were used to demonstrate the geometry of features and the relationships between structural elements. Contours at intervals of $E + 2\sigma$ were determined using the method proposed by Robin and Jowett (1986). E is the expected number of points to be found on the surface of the stereonet within an area A, and is equal to NA where N is the total number of data points (Kamb 1959). From the structural geometry and kinematic indicators, estimates of possible

TABLE 3-1

Summary of Structural Domains

Quartz Vein Domains

Domain	Location and Extent	Features and purpose
3	north side of bxx	contrast veins north and south of breccia
14	south side of bxx	" " " " "
6,7	south side bxx	test persistence of veins and variation distant from the bxx
8	east side Net L.	test if veins similar and genetically related to veins on west side, relation to 069 shear zone

Joint Domains

5	north side of bxx	test if joint density decrease with dis. from the bxx, if contact zone influenced joints
N,E	on north side bxx	test density variation and if strike varied with trend of bxx
W,S	on south side bxx	" " " " "
19,20	on south side bxx	test if joints sets persisted beyound the immediate breccia area

Miscellaneous domains are defined in the same way as the quartz domains; bxx = breccia

Figure 3-1: Boundaries of structural domains for the three main structural categories: veins, joints and miscellaneous features, which include foliations, faults, shears and attitudes of pegmatoids.

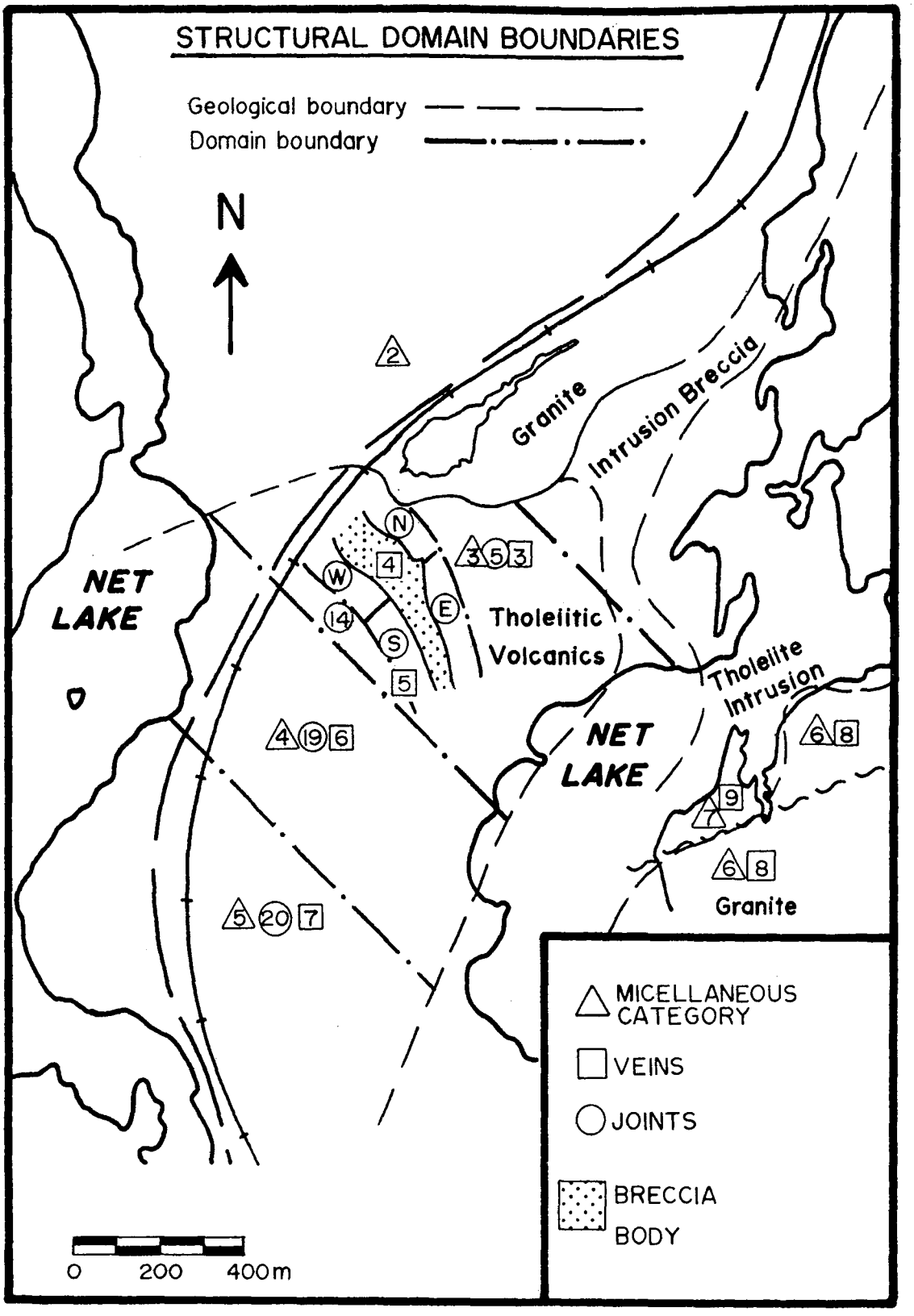
STRUCTURAL DOMAIN BOUNDARIES
Geological boundary
Domain boundary
N
NET LAKE
Granite
Intrusion Breccia
Tholeiitic Volcanics
Tholeiite Intrusion
NET LAKE
Granite
MICELLANEOUS CATEGORY
VEINS
JOINTS
BRECCIA BODY
0 200 400m

stress orientations were made and then compared with the findings of Fyon et al. (1988).

3.2 Regional Structure

Based on field mapping carried out in Chambers, Strathy and Briggs townships Fyon et al. (1988) recognize three distinct foliations in the Temagami greenstone belt. The earliest foliation termed S_0/S_1 trends eastward in the Chambers and Strathy townships and generally follows, and is deformed with bedding. The S_2 foliation trends 030^0 in Strathy Township and is considered to be a shear foliation related to deformation within the Net Lake-Vermilion (NLVL) and Tasse Lake zones of deformation. Steep plunging mineral elongations and the offset of dykes and some veins indicate a minor sinistral horizontal, and a major vertical component, where the NW block is up relative to the SE. The youngest foliation S_3 is N-S trending and thought to be axial planar to open folds.

Based on these structural features Fyon et al. (1988) proposed that S_0/S_1 was the first foliation developed in response to a N-S directed compression that was also responsible for the formation of the Tetapaga syncline to the south in Strathcona township. Neglecting other major

faults to the south, the S_2 fabric developed in response to a process of simple shear concentrated on the NLVL and Tasse Lake deformation zones. Kinematic indicators suggest that movement was dominantly oblique subvertical with a minor sinistral component. With this sense of movement the compressive stress would also be directed in an approximate N-S direction. S_3 is believed to be the latest fabric developed in response to an E-W compression that in turn formed the open fold structures. A significant overprinting of structural elements is displayed by the NLVL deformation zone where the S_0/S_1 plane is drawn into parallelism with the S_2 fabric. Another significant paragenetic feature is the apparent cutting of the Strathy-Chambers batholith by the probable northward extension of the NLVL shear zone, indicating that the fault postdates that portion of the batholith.

3.3 Local Structural Features and Structural Domains

3.3.1 Quartz veins

Quartz veins are common throughout the study area occurring in the immediate vicinity of the breccia, extending southward and to the east on the opposite shore of

Net Lake (Map 1,2). Veins are hosted in both volcanics and granitic rocks of the Strathy-Chambers batholith, although veins hosted in granite occur almost exclusively on the east side of Net Lake. Those veins on the east side of Net Lake are largely unmineralized in contrast to those on the west side, which are often mineralized with chalcopyrite and molybdenite. The structure of veins is usually simple with straight margins, slickensides absent and vein filling comprised of massive white quartz. In some veins slivers of wall rock, sometimes sheared, are distributed within the vein. In one vein, thin bands of wall rock were conspicuously distributed in symmetrical ribbons parallel to the walls, suggesting more than one episode of vein opening (Plate 3-1a). On the east side of Net Lake vein quartz appears to be more fine-grained and in hand specimen looked sugary or chalcedony-like. Considering that these veins are in a zone of intense shearing, it is likely that the texture resulted from syn- or post-vein shearing.

For the structural analysis vein orientation data were divided into nine different domains (Fig. 3-1; Table 3-1). Only domains 3, through 9, contained significant numbers of veins and only these will be considered in the following discussions. Domains 3 and 5 were defined to test for any contrast in vein characteristics on either side (NE and SW)

of the breccia while domain 4 includes veins within the breccia body. Domains 6 and 7 encompass the large area south of the breccia extending south to the road into Temagami North. Domains 8 and 7 include veins on the east side of Net Lake. Those in domain 8 within the granitic rocks and those in 7 are within the mafic rocks.

3.3.2 Joints

Joints represent a very prominent feature in the volcanics that host the breccia body. They comprise steep, often well-defined joint sets, that do not offset other features nor have slickensides on their surfaces. In outcrop, joints often occur in two strong sets intersecting at high angles to form blocky and hackled surfaces. The number or density of joints on individual outcrops is highly variable and joint densities were, therefore, measured at each outcrop station. The variation in joint density was deemed important because hydrothermal brecciation is often accompanied by sheeted joints or fractures tangential to the breccia margins (Sillitoe and Sawkins, 1971). These sheeted fractures are thought to represent tensile fractures along which the breccia propagates and expands. One reason for measuring joint densities was to test the hypothesis that

increased joint densities and tangential joints might be expected if there was a genetic link between joints and breccia. Densities were measured by counting the number of joint planes having a consistent attitude across a distance of 1 meter perpendicular to the joint surface. At each outcrop station, individual sets of joints were identified and their attitude and density measured. In total, 544 joint attitudes and 544 corresponding joint density measurements were taken at 295 different locations within the breccia and surrounding volcanics. Domains near the breccia are narrow and run parallel to it, while those greater than 80 m from the breccia margin have the same boundaries as domains 6 and 7 designated for the quartz veins (Fig. 3-1). Joint orientations were not recorded on the east side of Net Lake within the intrusive, or in the intrusive breccia zone to the north, since these areas did not display prominent joint sets.

3.3.3 Foliations, Shear planes and Faults

Attitudes for foliations, shears and faults were taken throughout the study area including the east side of Net Lake. The distinction between faults and shear zones was sometimes difficult due to poor exposure or because the

assignment of somewhat ambiguous planar elements into the category of fault or shear. Lineations, usually consisting of slickensides and more rarely mineral elongation in some of the foliated granites, were also recorded. Data were collected from all areas, but these structural features are uncommon in the intrusive breccia zone, so this domain was omitted. Domain boundaries are otherwise like those defined for the quartz veins (Fig. 3-1). In the interpretation, foliations, shears, faults, pegmatites and related structures are all put into the miscellaneous category because of their similar orientations.

3.3.4 Pegmatites and Related Structures

In many examples pegmatites were lens shaped enabling measurement of an approximate attitude (Plate 3-1b). The bubble structures (refer chap.2, section 2.2.1.2) showed consistency in the attitude of the apical and interior layering between different occurrences, confirming that the orientation of these structures were relevant structural elements. In some instances aplites also had a planar morphology and their attitudes were also included in the interpretation with pegmatites and bubble structures. Pegmatites, bubble structures and aplites were only

recognized in the intrusive outcrops on highway 11 directly north of the breccia; that is, domain 2 of the miscellaneous category.

3.3.5 Dykes

The four major types of dykes encountered in the study area were: quartz feldspar porphyry, feldspar porphyry, granite and basalt. Only the feldspar porphyry and granitic dykes are considered. All of these are within domain 3 of the miscellaneous category.

3.4 Descriptive Geometry

3.4.1 Quartz Veins

The composite stereo plot of all 267 vein orientations reveals that there is a strong concentration of veins trending toward 071/85NW (Fig. 3-2a); however, on plots of individual domains it is clear that differences exist between domains. Domain 6 shows a simple distribution of primarily mineralized veins concentrated at 071/85nw (Fig. 3-2b). Domain 7 is similar, with mineralized veins clustered at 071/85NW, but it differs in that there is a

distribution of points that appear to define a small circle (Fig. 3-3a). Domain 8 also has a concentration of veins near 071/85NW, but in contrast to domains 6 and 7, these veins are not significantly mineralized (Fig. 3-3b). Many of the veins in domain 8 differ significantly in attitude from the dominant trend of 071^0. When the three domains 6, 7 and 8 are plotted together these off-trend veins show a small circle array and three separate great circle distributions that lie in the planes: 157/26W, 157/56W and 157/66E (Fig. 3-4a). The small circle distribution is defined primarily by data from domain 7, while the great circle arrays are mostly comprised of data from domain 8. If the great circle arrays of poles to quartz veins are a true reflection of the geometry it indicates that there are at least three imaginary planes with equal strike, but different dips. Such a geometry would arise from the refolding of a subhorizontal anticline roughly perpendicular to the fold axis (Fig. 3-5a). In terms of the analogy the limbs of the fold are represented by quartz veins. A concept that will be discussed later suggests that all of the veins once had a common axis of intersection which was subsequently deformed. The small circle distribution of poles defines a different, but possibly related geometry to those veins lying on great circles. Figure 3-5b shows that

Figure 3-2a: Composite stereonet of quartz veins from all domains. Symbols: filled triangles feldspar-bearing veins; open squares non-mineralized veins; filled squares mineralized veins.

Figure 3-2b: Stereonet of quartz veins from domain 6, south of the breccia. Symbols same as for figure 3-2a.

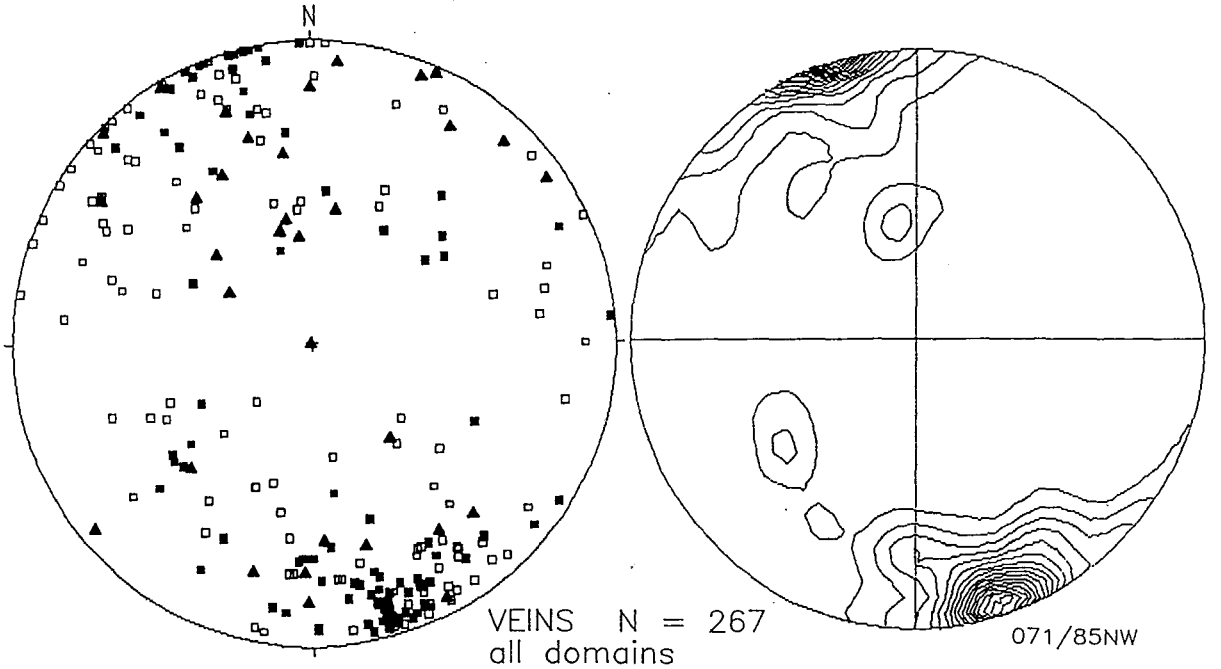

VEINS N = 267
all domains

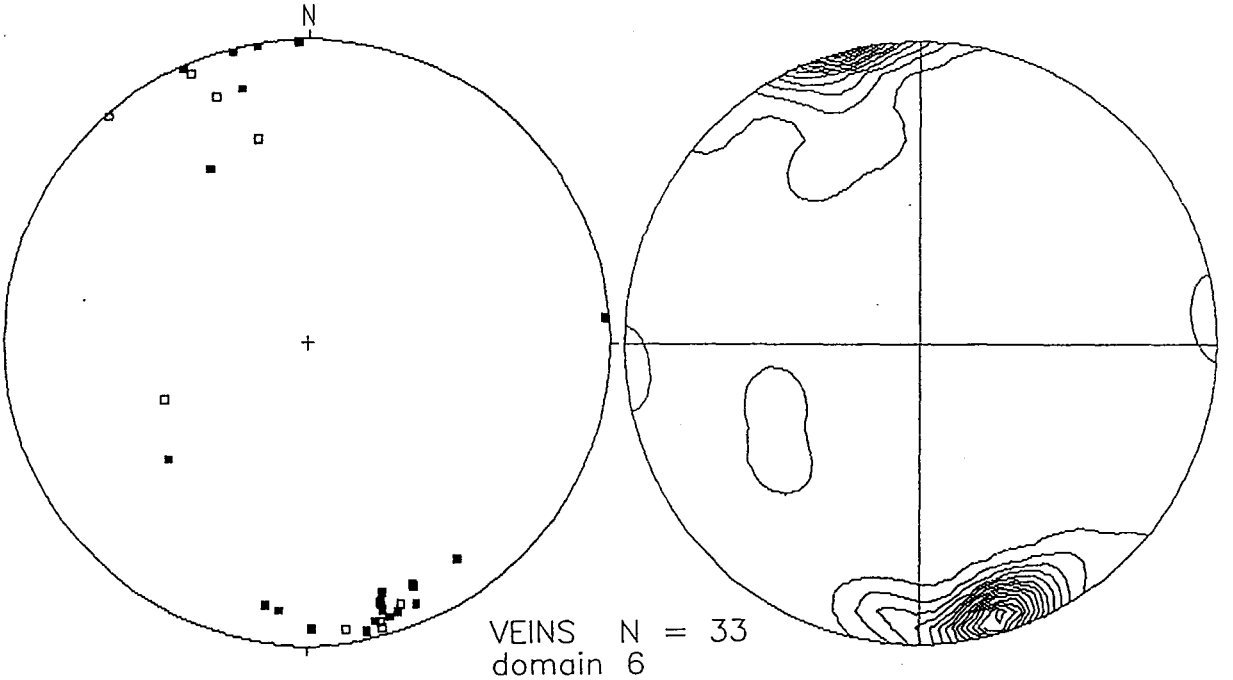

VEINS N = 33
domain 6

Figure 3-3a: Stereonet of quartz veins from domain 7, south of the breccia in the area of North Temagami. Symbols same as for figure 3-2a.

Figure 3-3b: Stereonet of quartz veins from domain 8, on the east side of Net Lake. Veins are hosted in granitic rocks and are within the vicinity of the 069 shear zone. Symbols same as for Figure 3-2a.

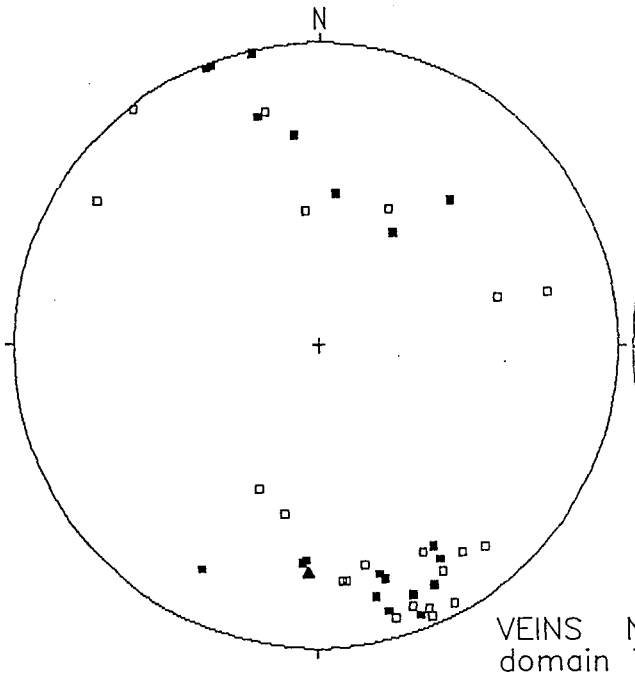

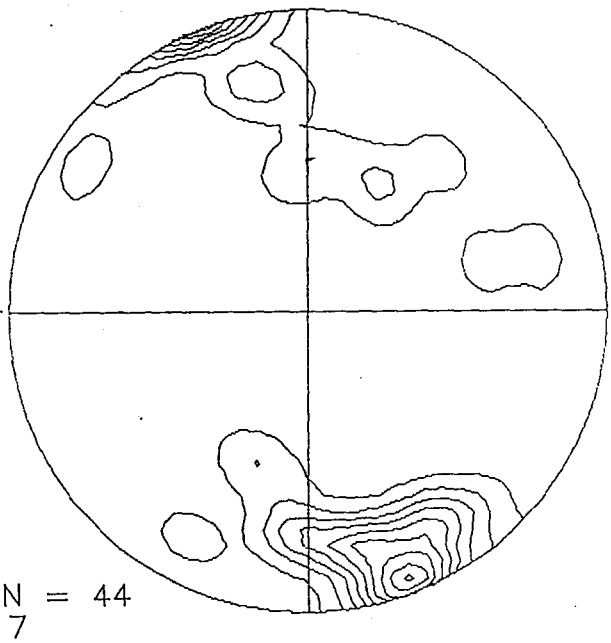

VEINS N = 44
domain 7

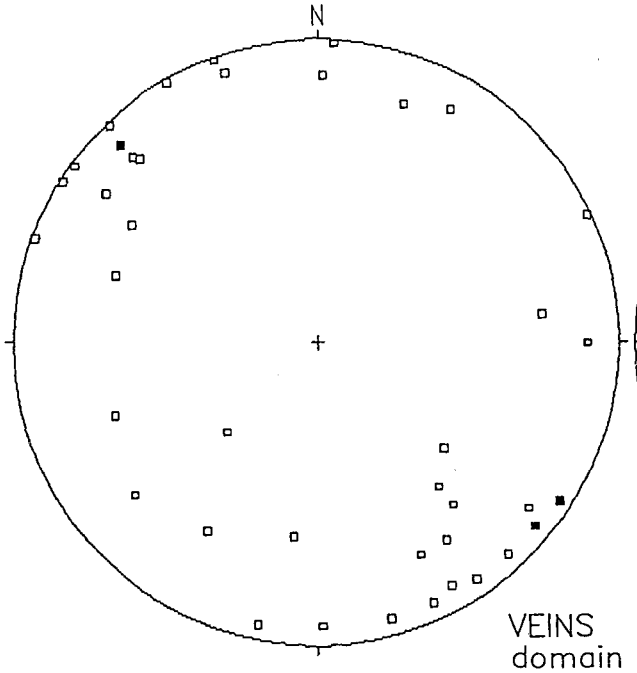

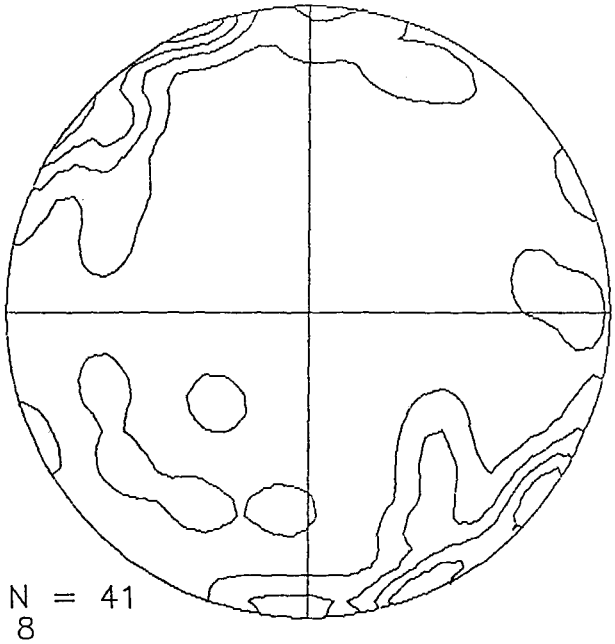

VEINS N = 41
domain 8

Figure 3-4a: Composite stereonet of quartz veins from domains 6, 7 and 8, all of which are well south of the breccia. Poles to veins appear to define three great circle distributions and one small circle array. symbols same as for figure 3-2a.

Figure 3-4b: Stereonet of veins from domain 3, north of the breccia. Symbols same as for figure 3-2a.

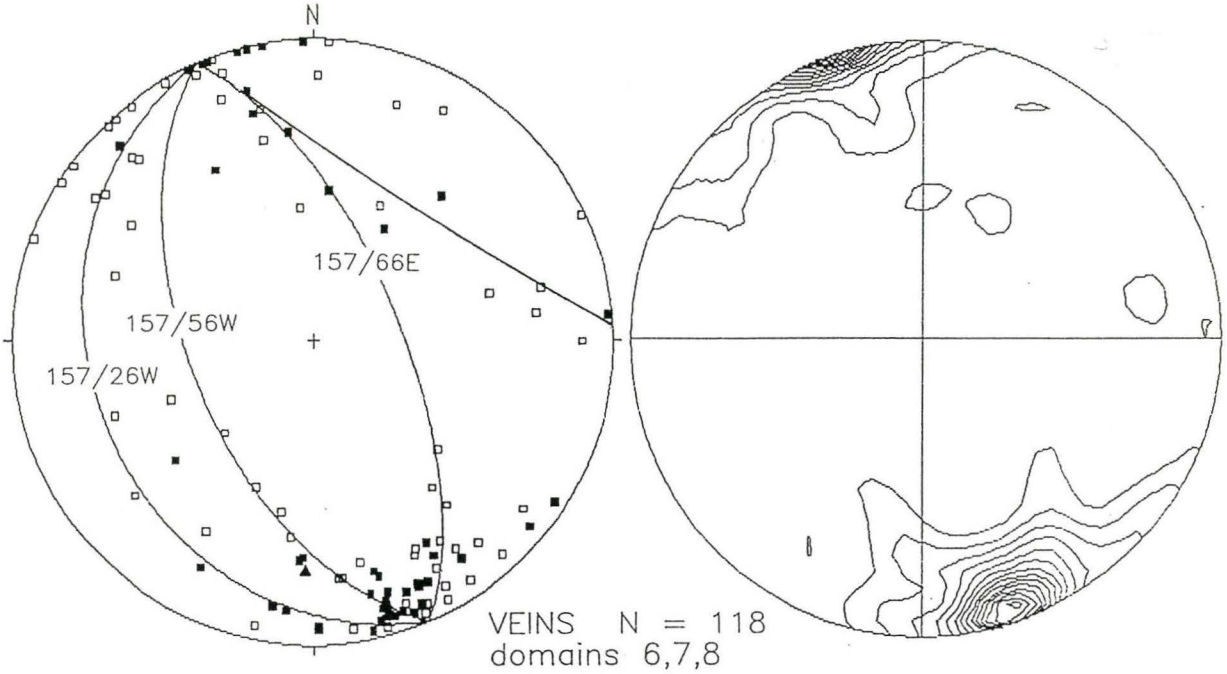

VEINS N = 118
domains 6,7,8

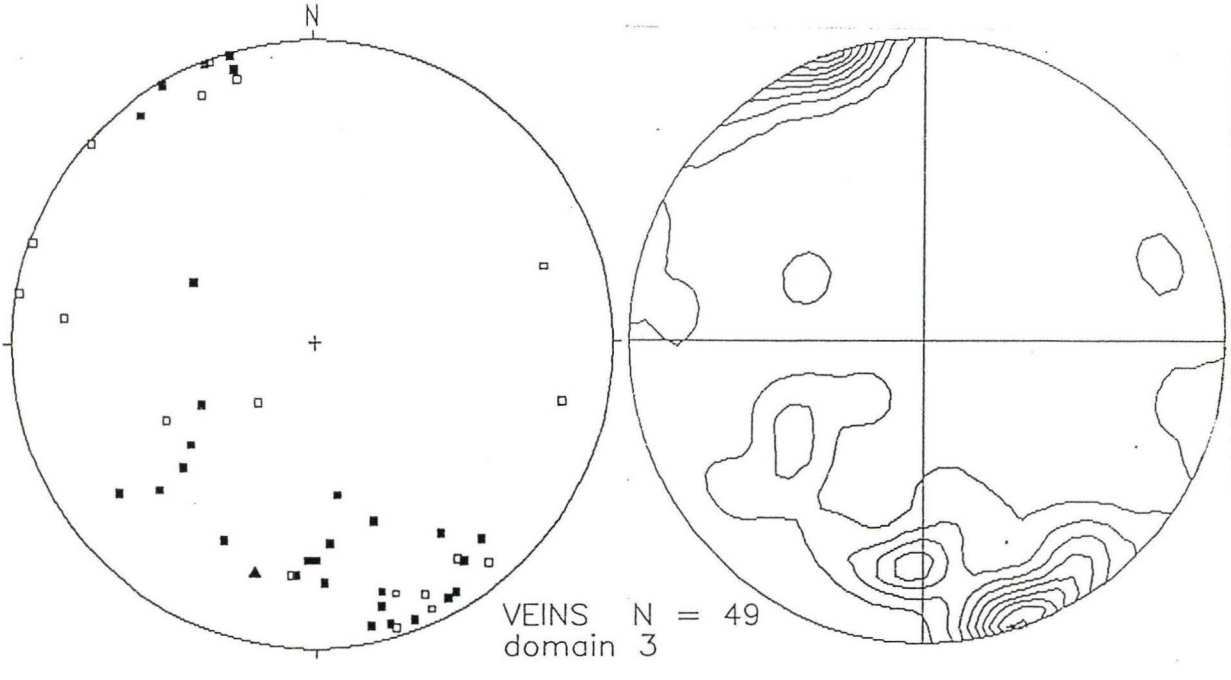

VEINS N = 49
domain 3

Figure 3-5a: Schematic representation of the vein geometries defined by the great circle distributions of poles to quartz veins. This geometry is defined by the composite of quartz veins and it does not imply that a single vein posses this geometry.

Figure 3-5b: Schematic representation of the vein geometries defined by the small circle distribution of poles to quartz veins. As above this sketch does not represent the geometry of a single vein.

a

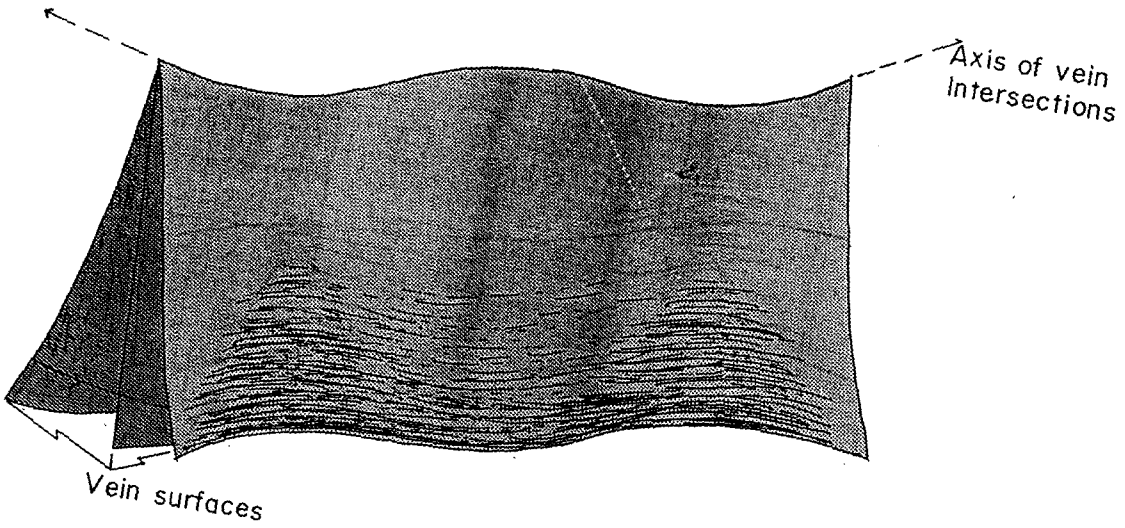
Axis of vein
Intersections
Vein surfaces

b

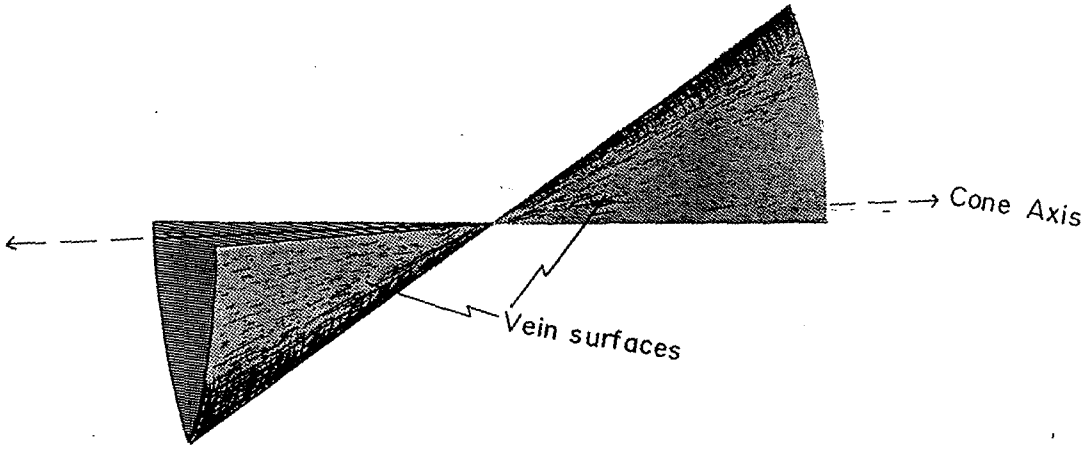
Cone Axis
Vein surfaces

the sum of vein orientations that lie on the small circle, mostly from domain 7, define a section of a cone with a vertex angle of 70^0 and a cone axis plunging 11^0 toward 215^0. This seemingly complex geometry is not so different from the other veins and in fact many of the veins defining the conic surface have orientations similar to the other vein populations.

Domains 3, 4 and 5 are the domains located near the breccia body (Fig. 3-1). Domain 4, which encompasses the breccia, contains very few quartz and feldspar-bearing veins and is, therefore, not shown. Domain 3, which is to the north of the breccia has a cluster of veins near 071^0 but there is a significant number of veins that dip steeply to moderately northward (Fig. 3-4b). Domain 3 also contains a moderate number of mineralized veins and a few feldspar-bearing quartz veins. Domain 5 to the south of the breccia has a strong cluster of mineralized veins at 071^0, but a preponderance of unmineralized and feldspar-bearing veins that generally dip southward (Fig. 3-6a). Considering domains 3, 4 and 5 together, the greatest contrast with the other domains is the larger degree of vein attitude variation and the existence of feldspar-bearing quartz veins (Fig. 3-6b). An important similarity with the other domains is the existence of mineralized veins concentrated about

Figure 3-6a: Stereonet of veins from domain 5 from the area not extending beyond 170 m south of the breccia. Symbols same as for figure 3-2a.

Figure 3-6b: Composite stereonet of veins from domains 3,4,5. Domain 4 is within the breccia, domain 3 north and 5 south of the breccia. Symbols same as for figure 3-2a.

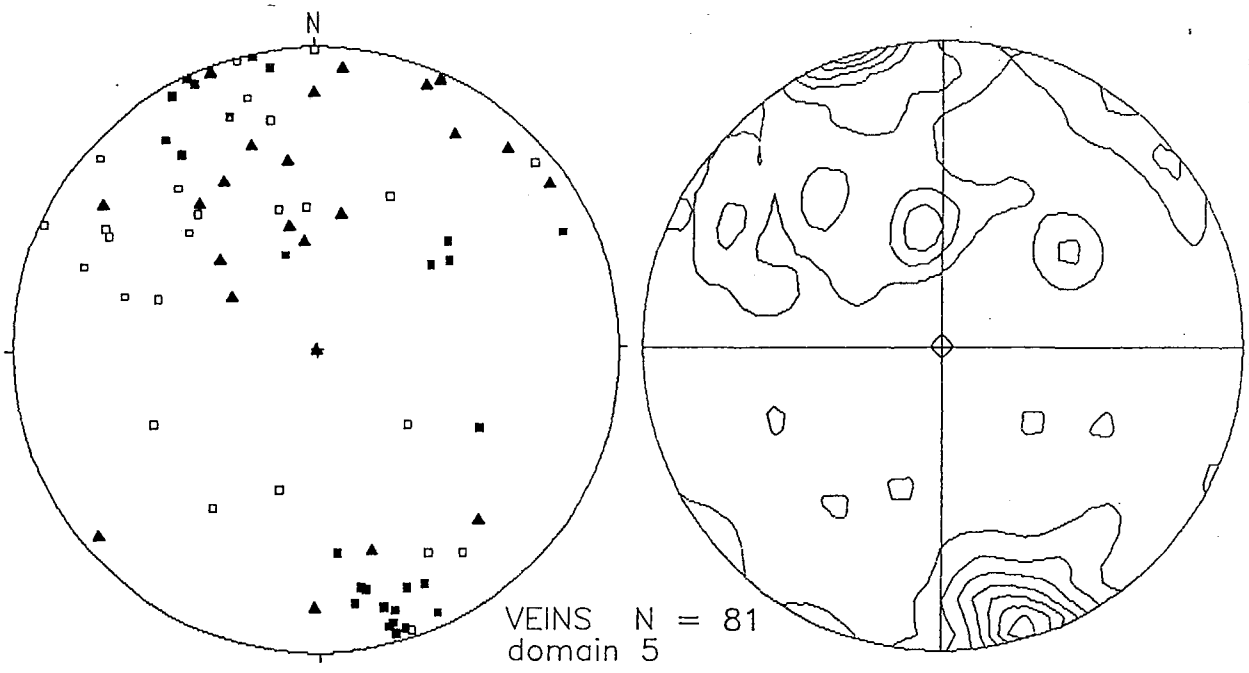

VEINS N = 81
domain 5

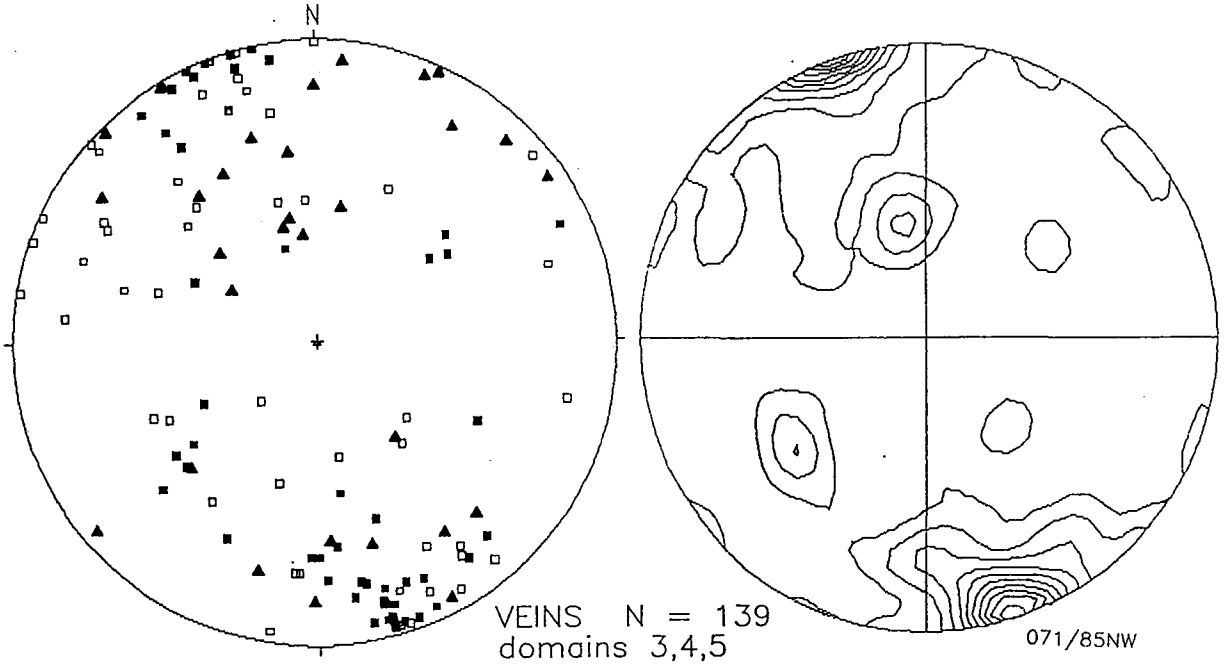

VEINS N = 139
domains 3,4,5

071/85NW

071/85NW. The apparent outward dip of veins, with respect to the breccia, is not necessarily well defined, but it may have significance in the context of breccia formation. If the apparent geometry of outward dipping veins is real it may represent a brittle response to the fluid overpressures developed during breccia formation. Outward dipping fractures and veins might represent the response to a sudden pressure decrease or relaxation immediately following brecciation.

Vein thicknesses were also investigated to test for any spatial or attitude relationships. In general vein thicknesses ranged from a 1 or 2 cm to greater than 20 cm, however typically they were on the order of 7 to 13 cm wide. Contours of vein thickness in the area of the breccia and southward indicate that the thickest veins occur within the breccia and toward the breccia centre (Fig. 3-7b)(refer appendix D for discussion of contouring). Unfortunately because of poor exposure there is poor lateral distribution of stations so that vein thicknesses for the breccia zone and areas to the south is difficult to interpret. Tentatively it appears that the thickest veins lie on a trend extending from the central part of the breccia to the outcrops exposed on highway 11, west of Temagami North.

Figure 3-7a: Map showing the locations of veins relative to the breccia body. Grid coordinates are shown on the map boundaries.

Figure 3-7b: Contour map of vein thickness taken at the locations shown in figure 3-7a.

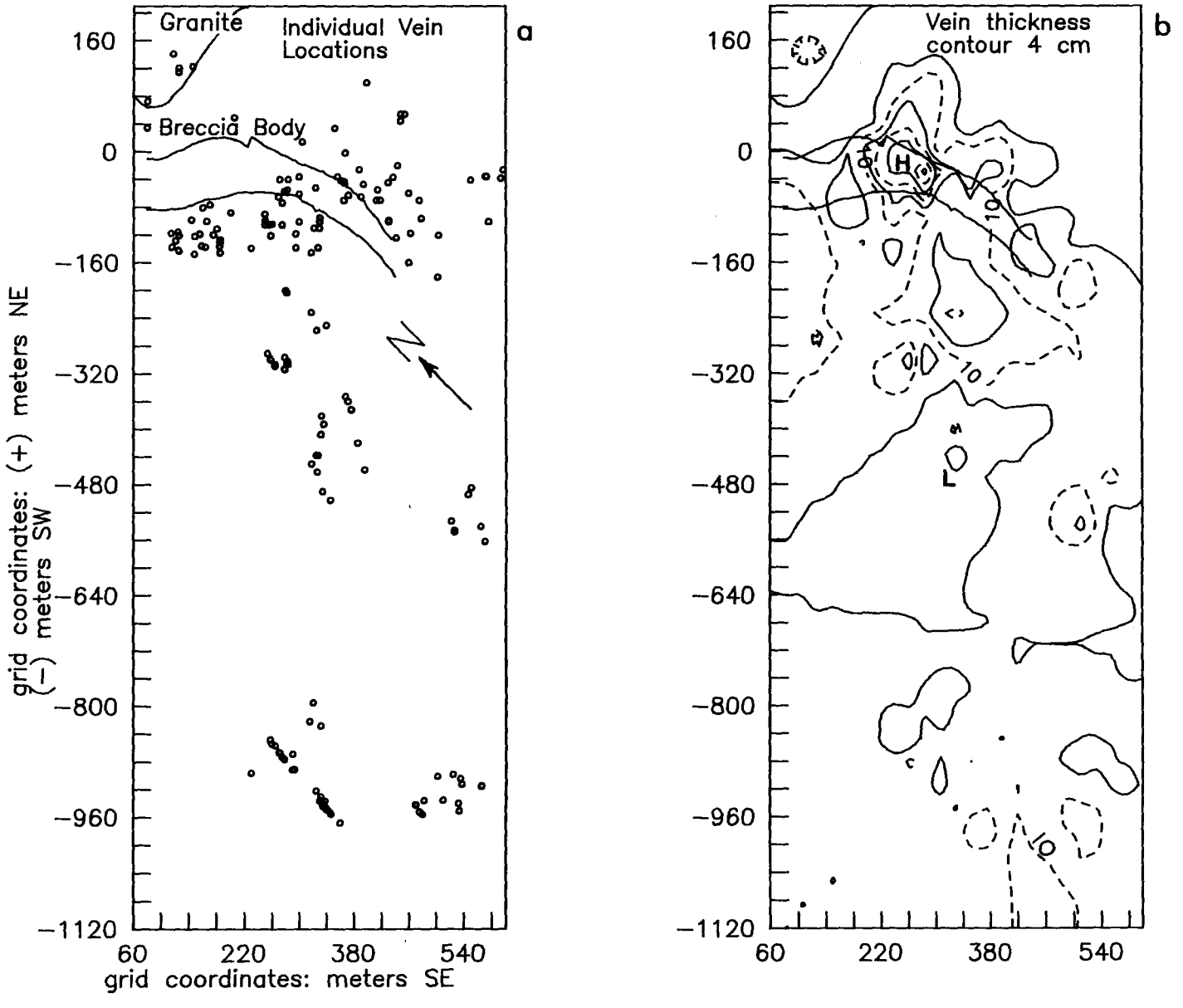
Granite
Individual Vein Locations
a
Breccia Body
N
160
0
−160
−320
−480
−640
−800
−960
−1120
60
220
380
540
grid coordinates: (+) meters NE
(−) meters SW
grid coordinates: meters SE
Vein thickness contour 4 cm
b
H
L
10
5
0

3.4.2 Joints

In analysis of the joint orientation data two and possibly three distinct populations of joints were identified. Each one of these populations is referred to as a joint set in the following discussion. On a stereo plot of all domains the most tightly constrained population, joint set 1, is centred at 038/82 NW. In the SW quadrant a more diffuse cluster is evident centred at 116/83 NE (Fig. 3-8a). The acute angle of intersection between these two clusters, which defines the characteristic blocky fracture on many outcrops and possibly the rectangular shape of breccia fragments, is 78 degrees. Considering the attitudes of joints, domain by domain, reveals that the 116^0 trend may actually be better characterized as two separate populations; set 2, 119/90 and set 3, 142/89 NE, as defined by the attitude averages of joints in the breccia domain and the north and east domains (Fig. 3-9a,b;3-10a). There are few consistent differences in the orientations of joints amongst the domains, but there are differences in how well the trends are defined. Stereo plots covering the study area shows that the degree of variability around the joint set averages differs from one domain to the next (Fig. 3-8 - 3-12). In general domains nearest to the breccia show the

Figure 3-8a: Stereonet of joints from all domains.

Figure 3-8b: Stereonet of joints from domain 5, north of the breccia body.

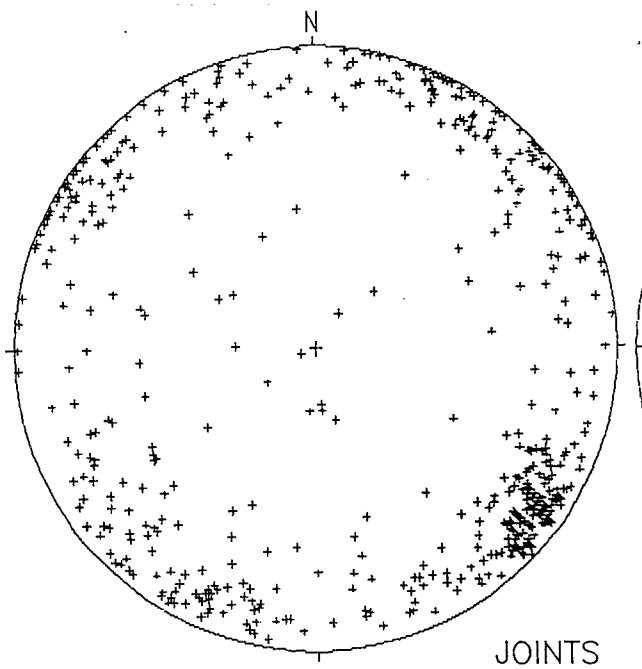

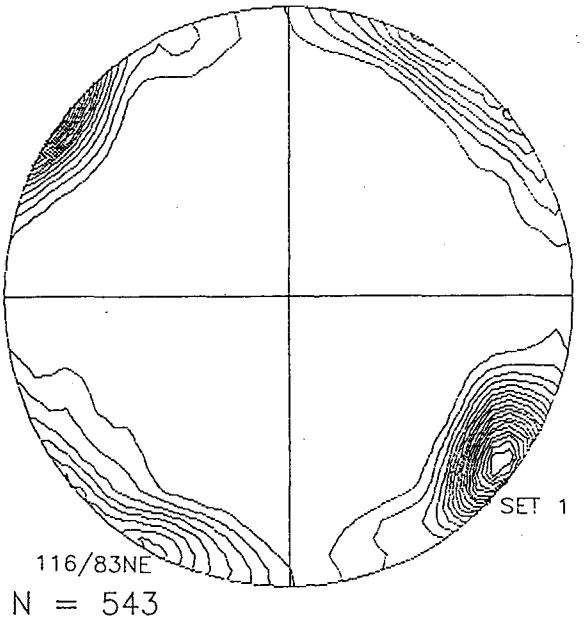

JOINTS N = 543
all domains

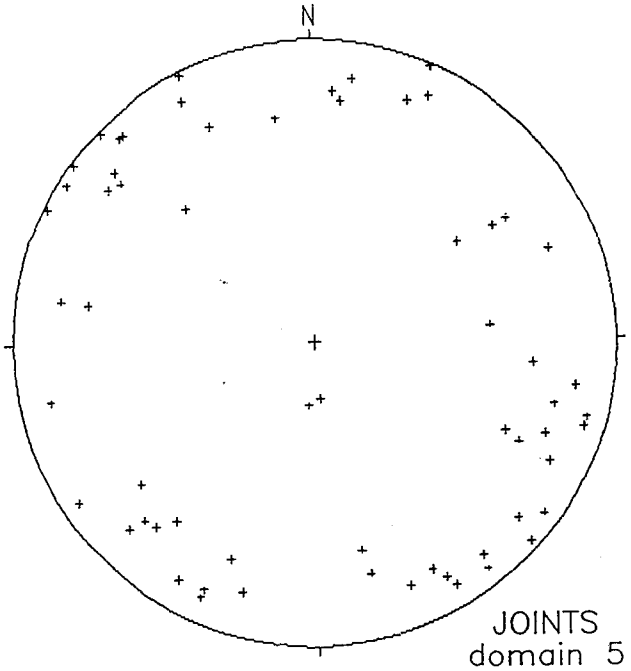

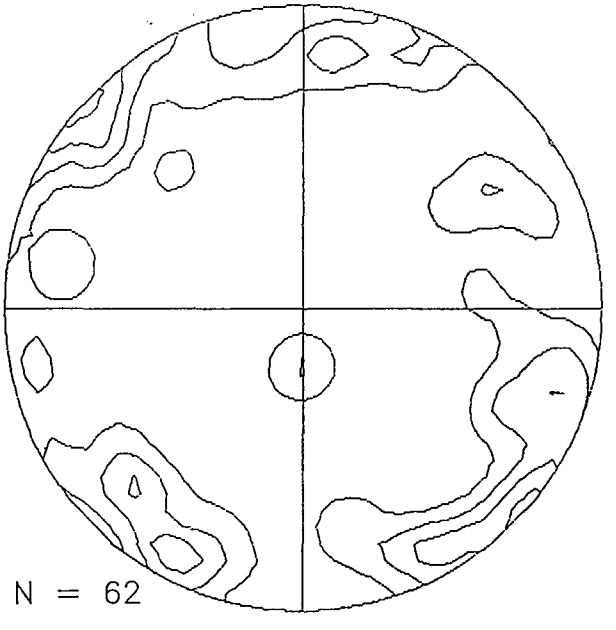

JOINTS N = 62
domain 5

Figure 3-9a: Stereonet of joints from the north domain, situated on the north east margin and north end of the breccia.

Figure 3-9b: Stereonet of joints from the breccia domain.

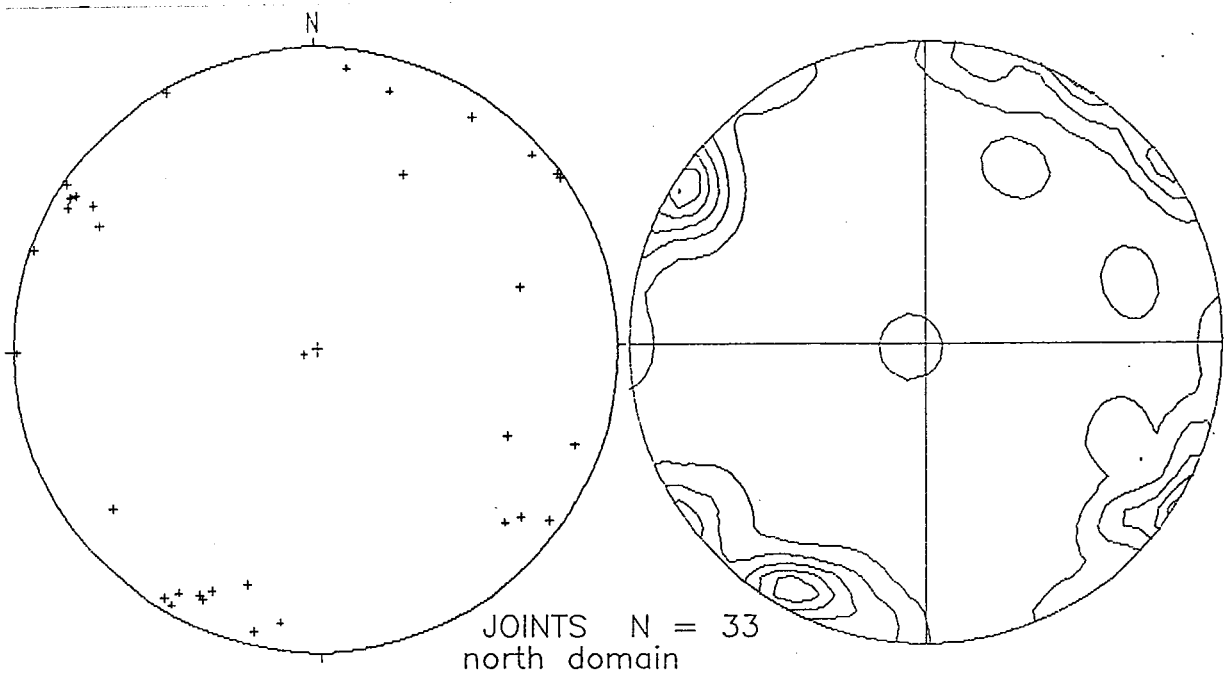

JOINTS N = 33
north domain

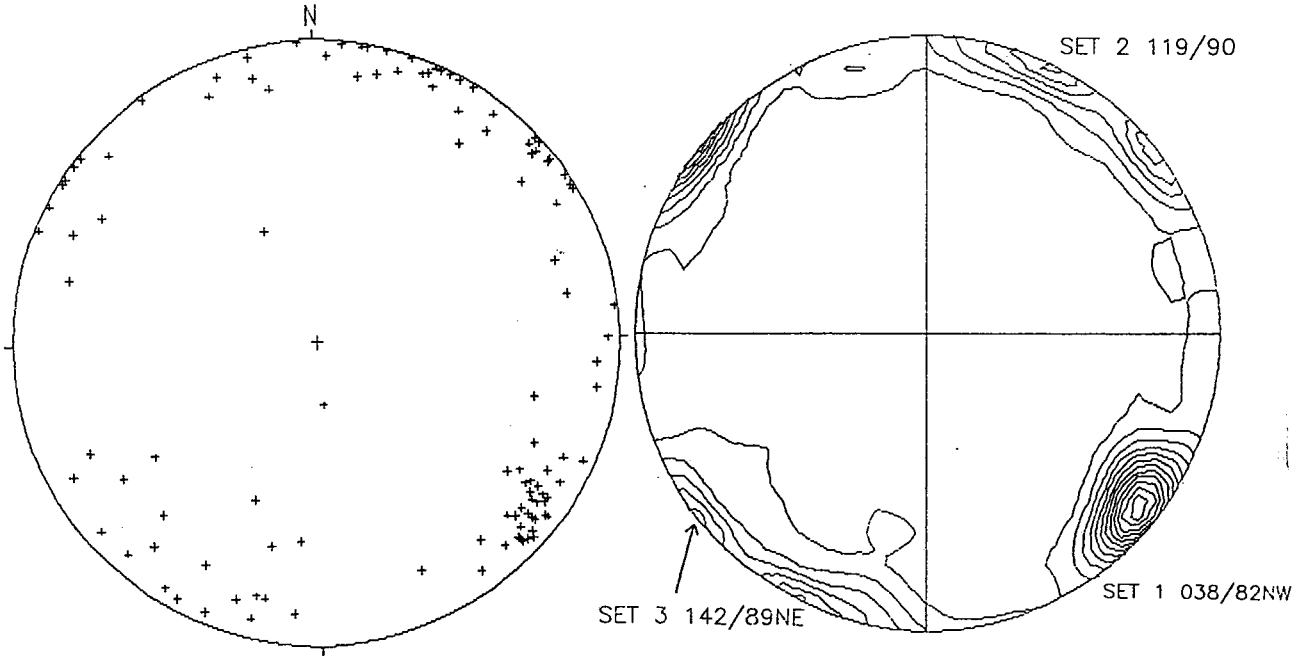

JOINTS N = 117
breccia domain

Figure 3-10a: Stereonet of joints from the east domain situated on the northeast margin at the south end of the breccia.

Figure 3-10b: Stereonet of joints from the west domain situated on the southwest margin of the breccia at the north end of the breccia.

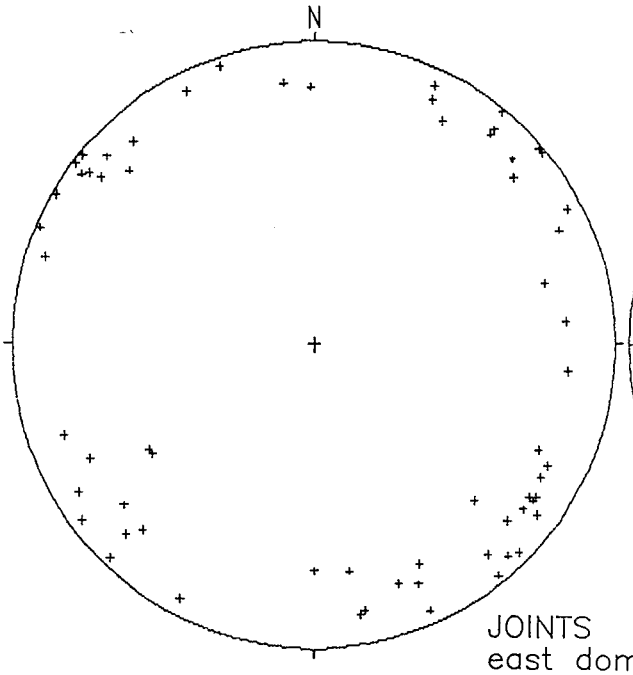

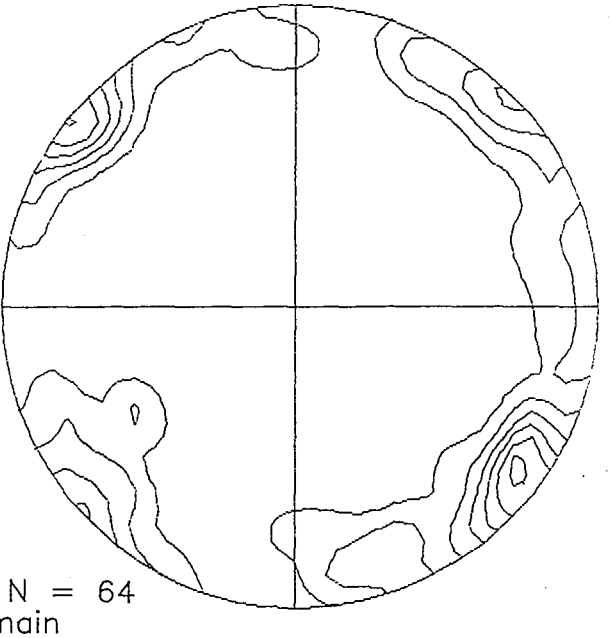

JOINTS N = 64
east domain

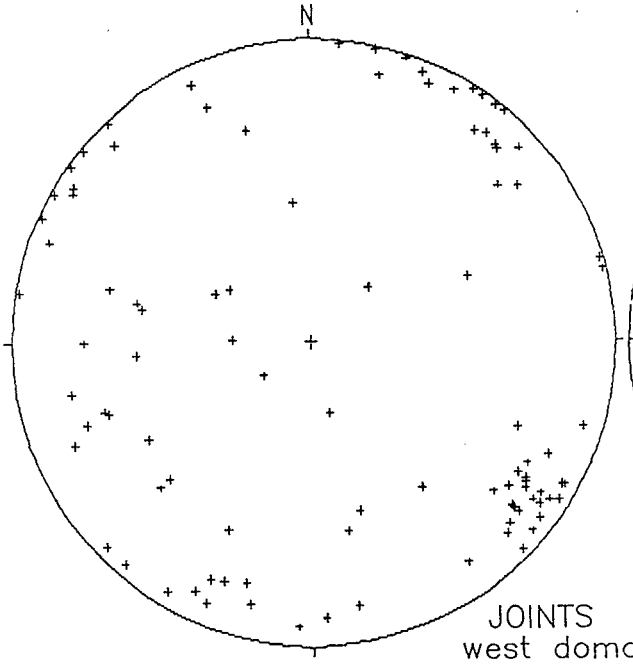

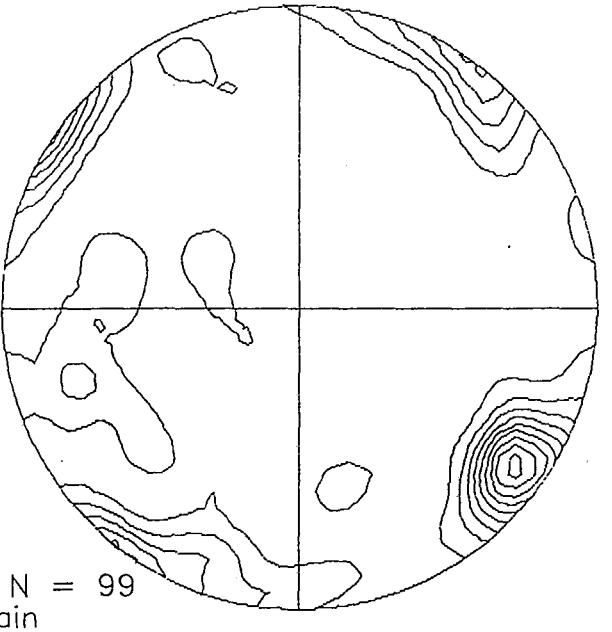

JOINTS N = 99
west domain

Figure 3-11a: Stereonet of joints from the south domain situated on the southwest margin of the breccia at the south end of the breccia.

Figure 3-11b: Stereonet of joints from domain 14, south of the breccia.

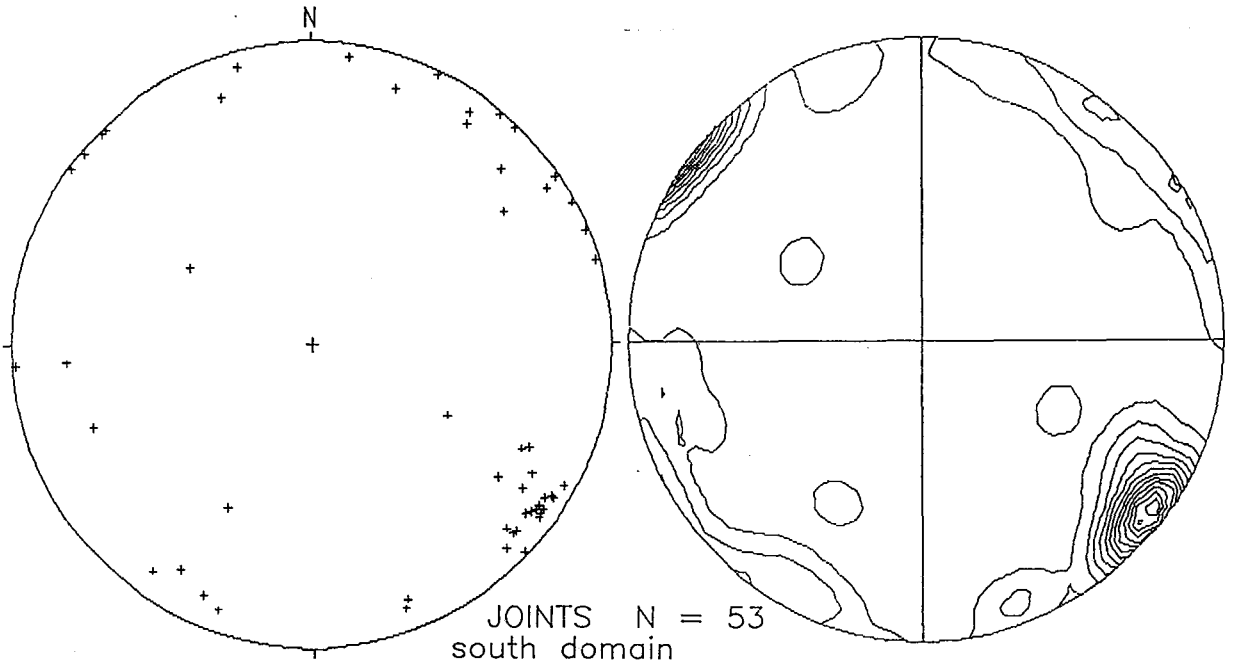

JOINTS N = 53
south domain

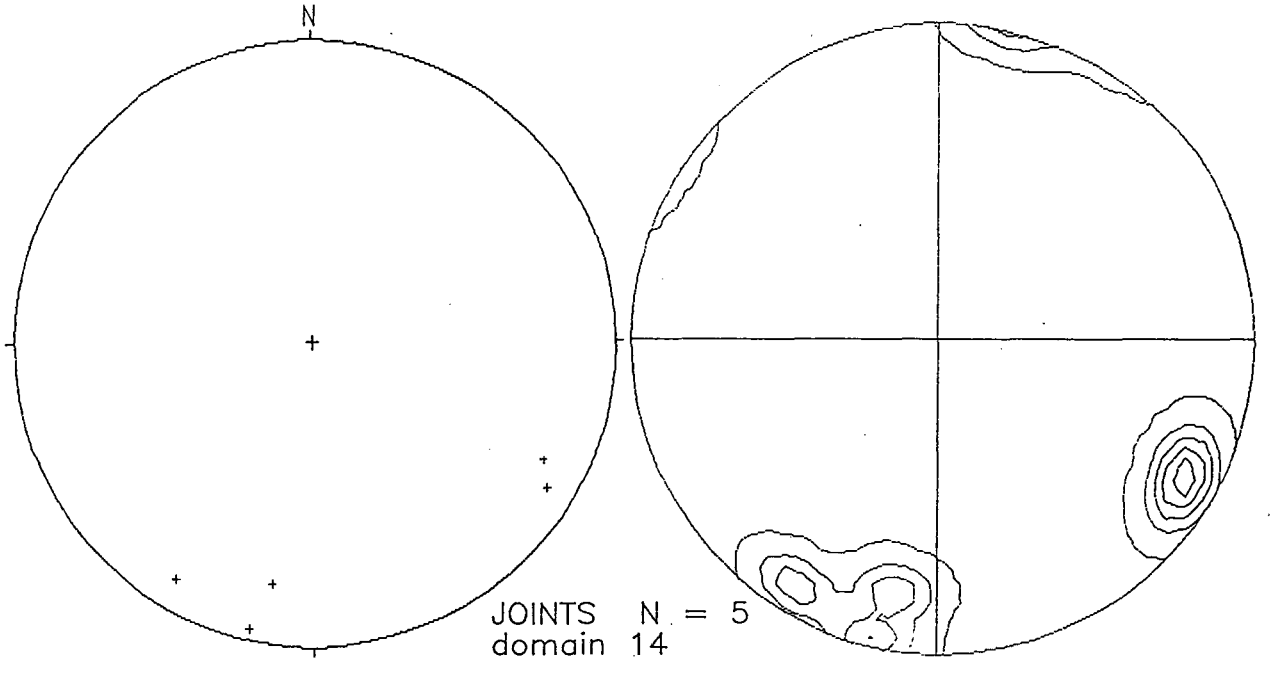

JOINTS N = 5
domain 14

Figure 3-12a: Stereonet of joints from domain 19, south of the breccia.

Figure 3-12b: Stereonet of joints from domain 20, in the area of Temagami North.

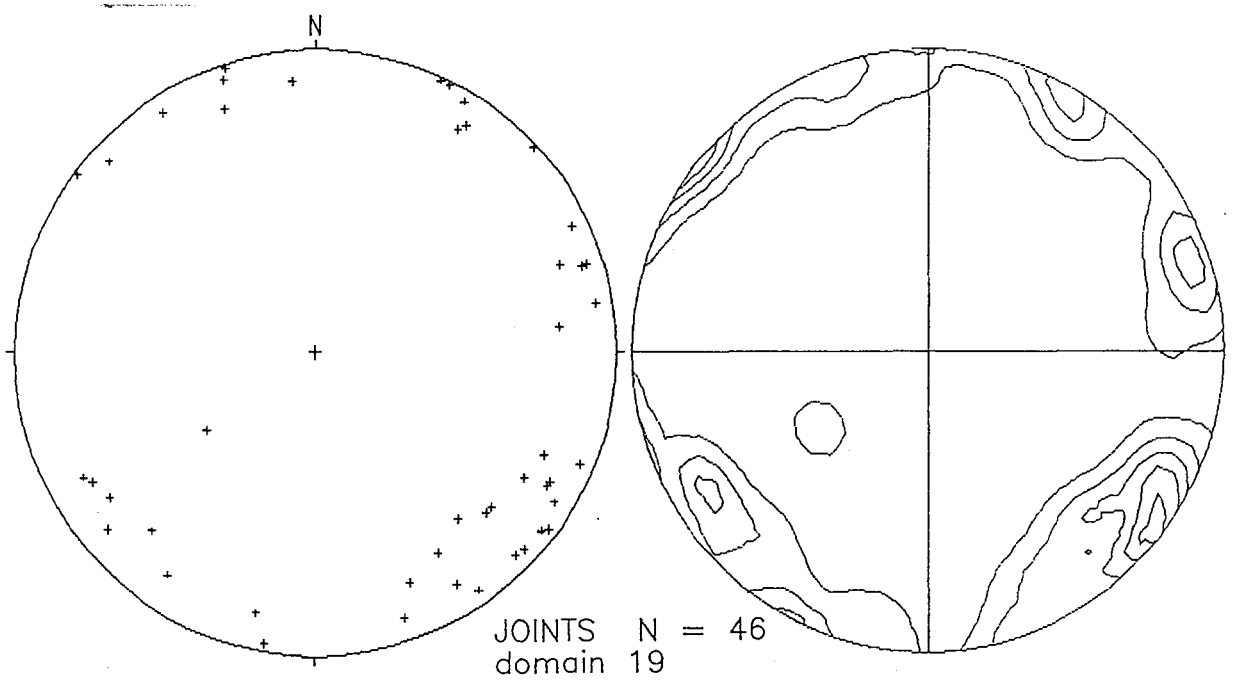

JOINTS N = 46
domain 19

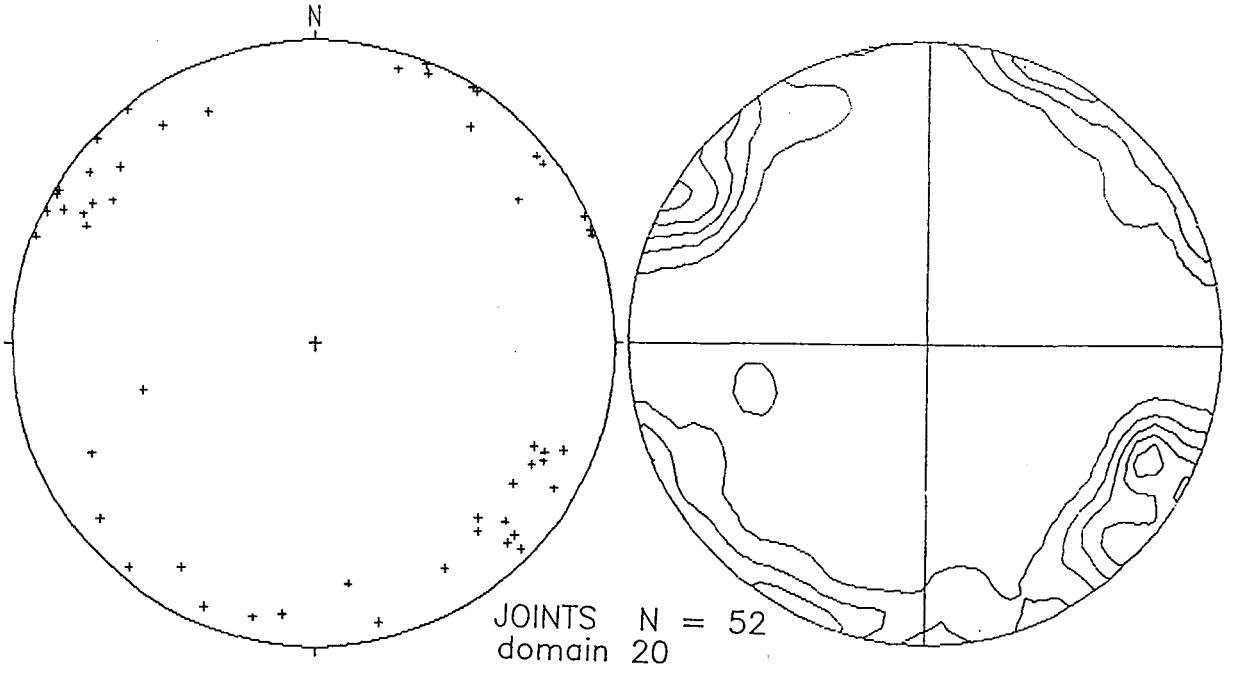

JOINTS N = 52
domain 20

least amount of variation while those more distant, such as domains 5, 19 and 20, show significantly more variation.

Joint density results are illustrated on plots of joint density versus domain or distance from the breccia margin (Fig. 3-13,14). The plot of joint set 1 data indicate little variation in joint with respect to distance from the breccia (Fig. 3-13a). The plots of joint set 2 and 3 data are similar and show a fairly constant average density except for domains bordering the north side of the breccia (Fig. 3-14a,b). In order to reduce the influence of spuriously high density values an additional trend line is shown where a modified density average is calculated by deleting the highest and lowest values of a domain. The joint densities are contoured in Figures 3-15 and 3-16. All three joint sets are generally more dense in the central regions of the breccia although in detail they do not correlate well with one another. The locations of density highs differ between sets, but in general they lie near or on the breccia margins. Again poor coverage makes interpretation of the joint contours for the area to the south of the breccia more difficult. Set 1 joints form a ridge of high density that extends through the centre of the breccia to an area 450 m SW of the grid base line which is host to veins and two small exposures of quartz cemented

Figure 3-13a: Map showing the boundaries of the joint domains in the close vicinity of the breccia body. The narrow domains paralleling the breccia margin were defined so as to decern the variation of joint density as a function of distance from the breccia margin.

Figure 3-13b: Plot of joint density versus domain for joints in the range of joint set 1. In reference to figure 3-13a this plot is essentially a cross section of joint density perpendicular to the long axis of the breccia body. The open circles are the density of joints at a particular outcrop station. The closed circles are the average density calculated for the particular domain. The filled triangles are the average of a domain calculated after removing the highest and lowest values from the data.

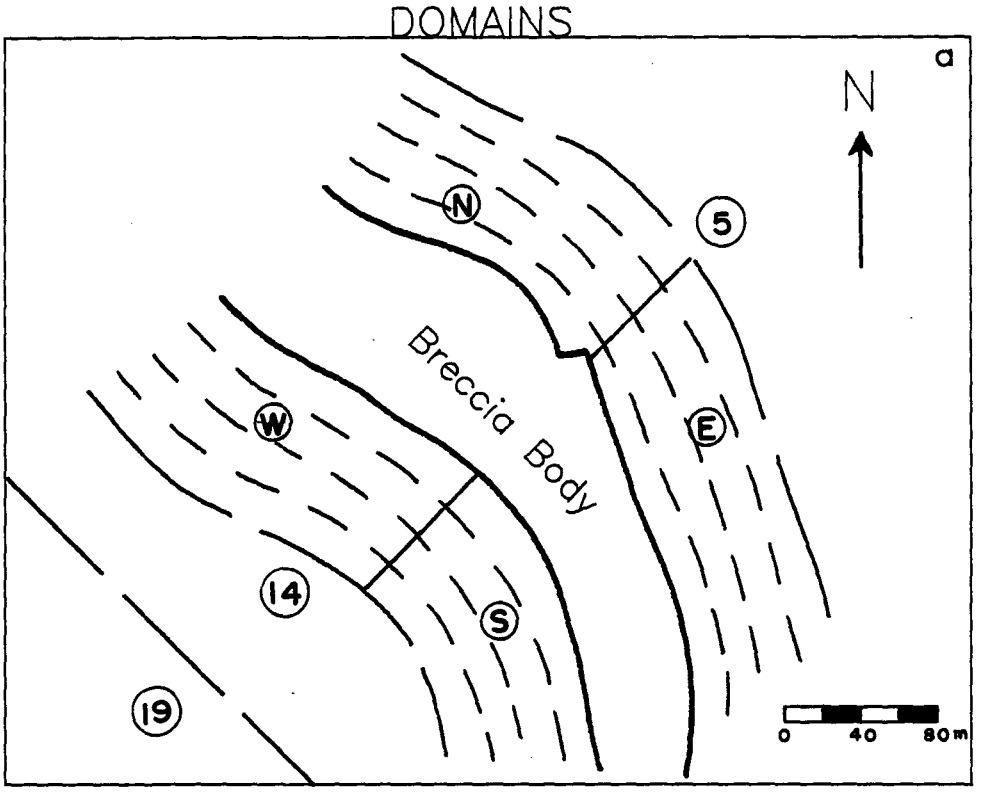
DOMAINS
a
N
N
5
W
E
S
14
19
Breccia Body
0
40
80m

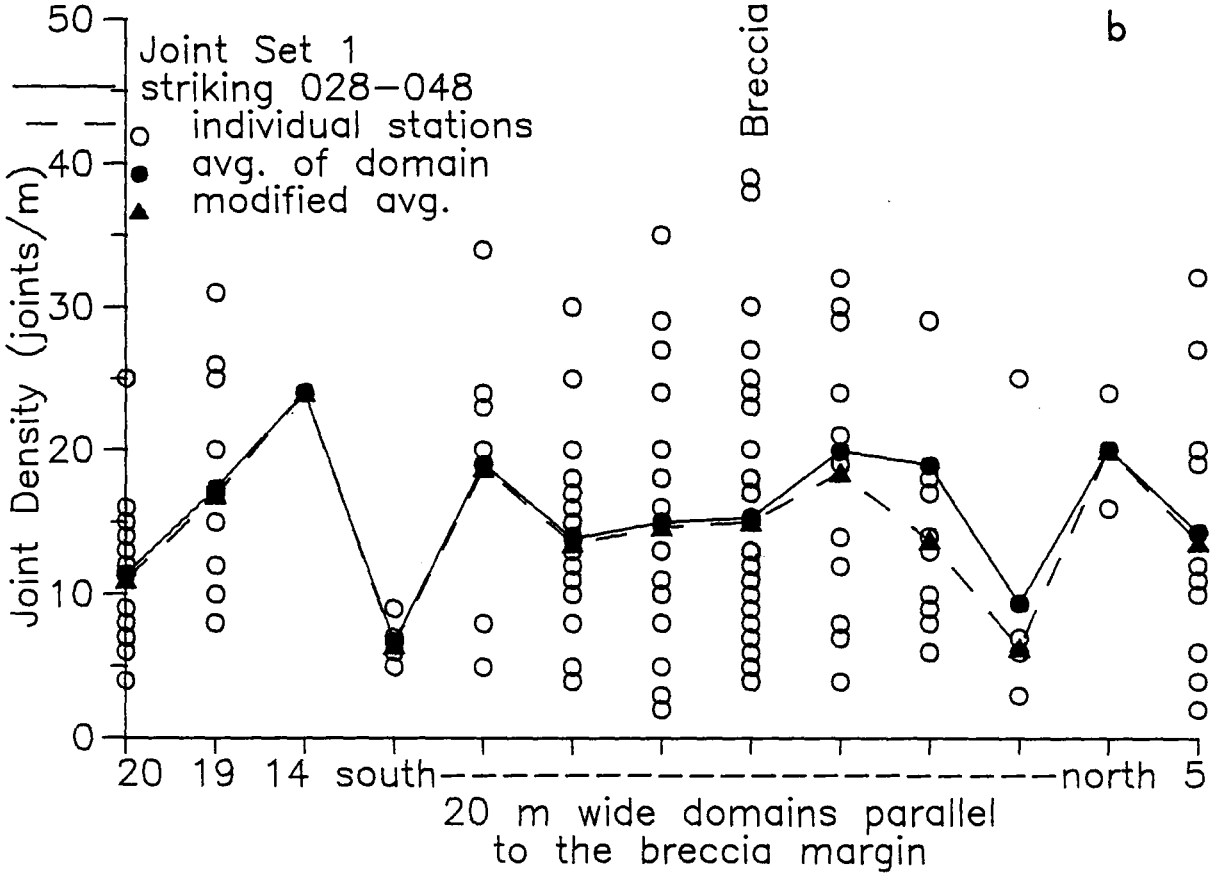
b
Joint Set 1
striking 028–048
individual stations
avg. of domain
modified avg.
Breccia
Joint Density (joints/m)
50
40
30
20
10
0
20 19 14 south
north 5
20 m wide domains parallel
to the breccia margin

Figure 3-14a: Plot of joint density versus domain for joints in the range of joint set 2.

Figure 3-14b: Plot of joint density versus domain for joints in the range of joint set 3.

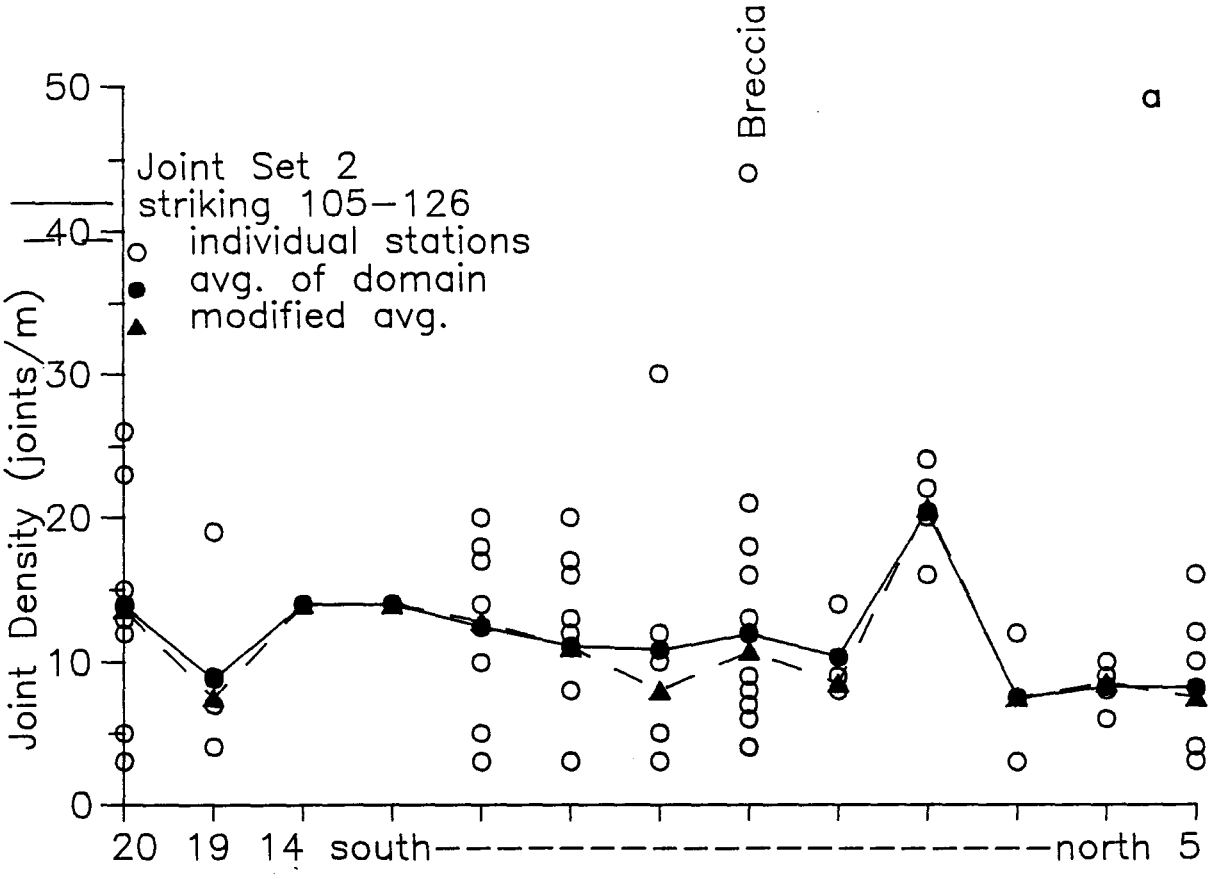
a
Joint Set 2
striking 105–126
individual stations
avg. of domain
modified avg.
Breccia
Joint Density (joints/m)
50
40
30
20
10
0
20 19 14 south
north 5

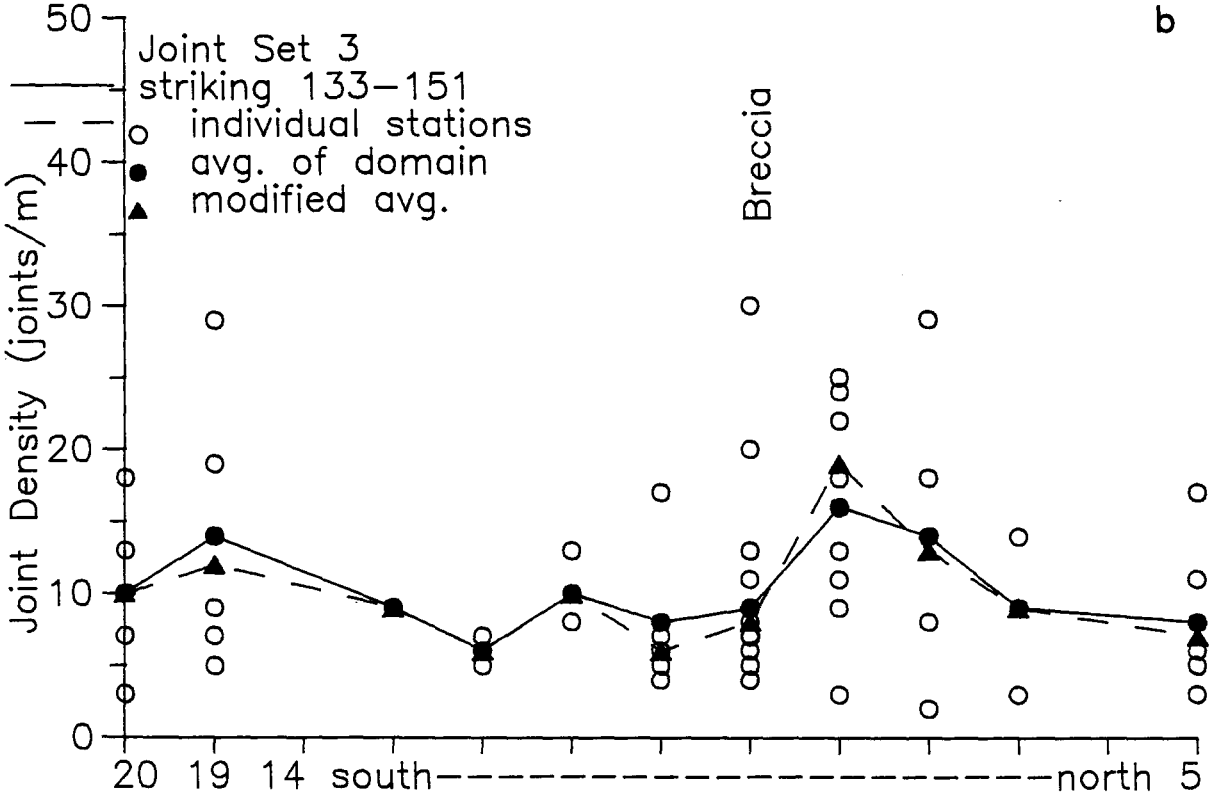
b
Joint Set 3
striking 133–151
individual stations
avg. of domain
modified avg.
Breccia
Joint Density (joints/m)
50
40
30
20
10
0
20 19 14 south
north 5

Figure 3-15a: Map showing the distribution of stations where joint attitudes and densities were measured. The filled squares are locations of significant mineralization uncovered by trenches, shafts and pits.

Figure 3-15b: Contour map of joint densities in the range of joint set 1. "H" marks high and "L" relatively low density areas.

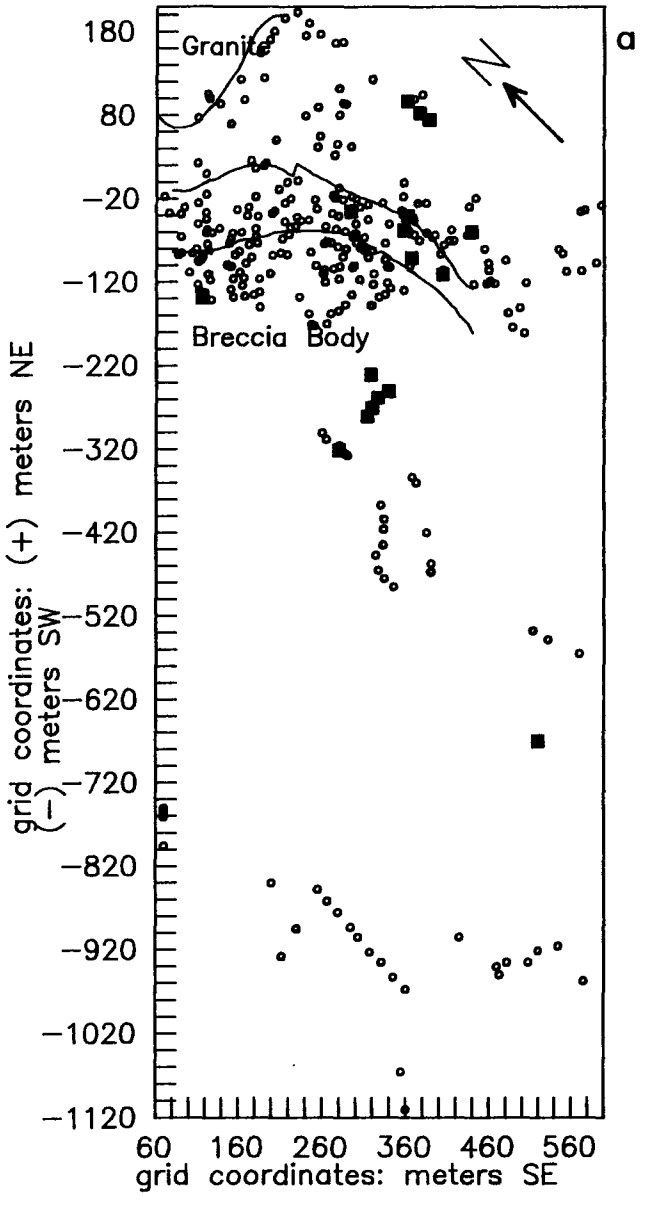
a
Granite
Breccia Body
N
180
80
−20
−120
−220
−320
−420
−520
−620
−720
−820
−920
−1020
−1120
grid coordinates: (+) meters NE
(−) meters SW
60
160
260
360
460
560
grid coordinates: meters SE

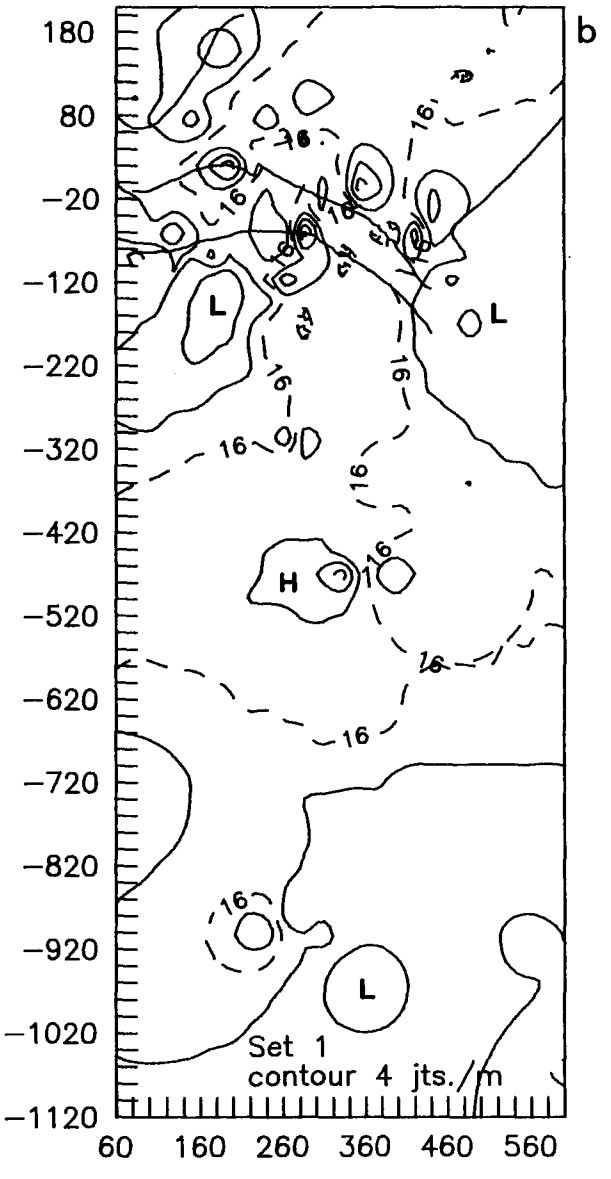
b
180
80
−20
−120
−220
−320
−420
−520
−620
−720
−820
−920
−1020
−1120
L
H
16
Set 1
contour 4 jts./m
60
160
260
360
460
560

Figure 3-16a: Contour map of joint densities in the range of joint set 2.

Figure 3-16b: Contour map of joint densities in the range of joint set 3.

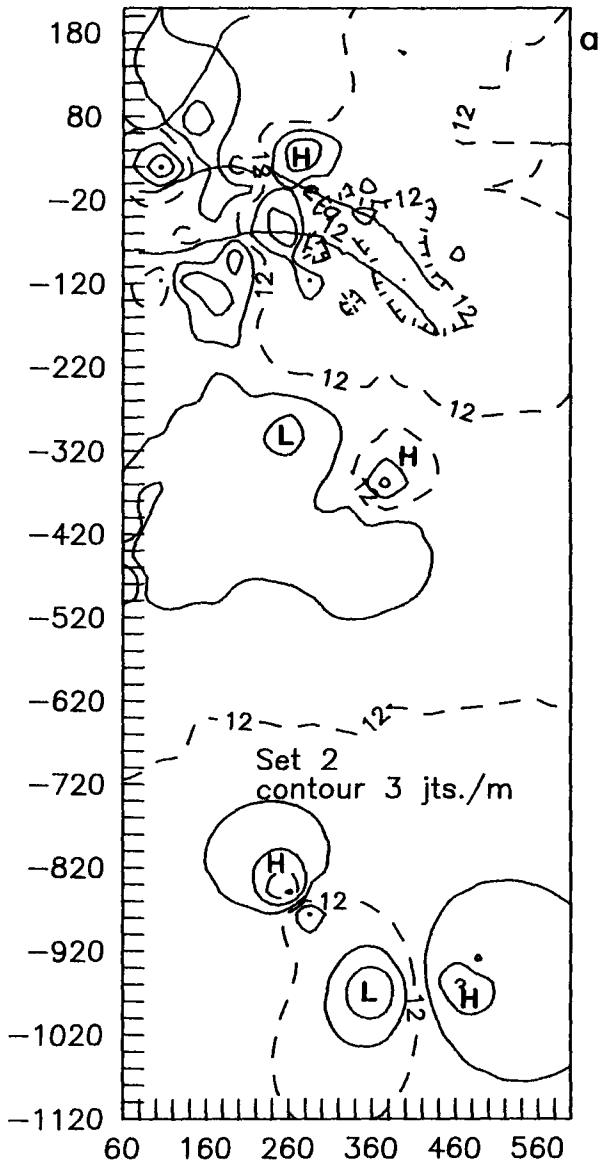
a
180
80
-20
-120
-220
-320
-420
-520
-620
-720
-820
-920
-1020
-1120
60
160
260
360
460
560
H
L
12
Set 2
contour 3 jts./m

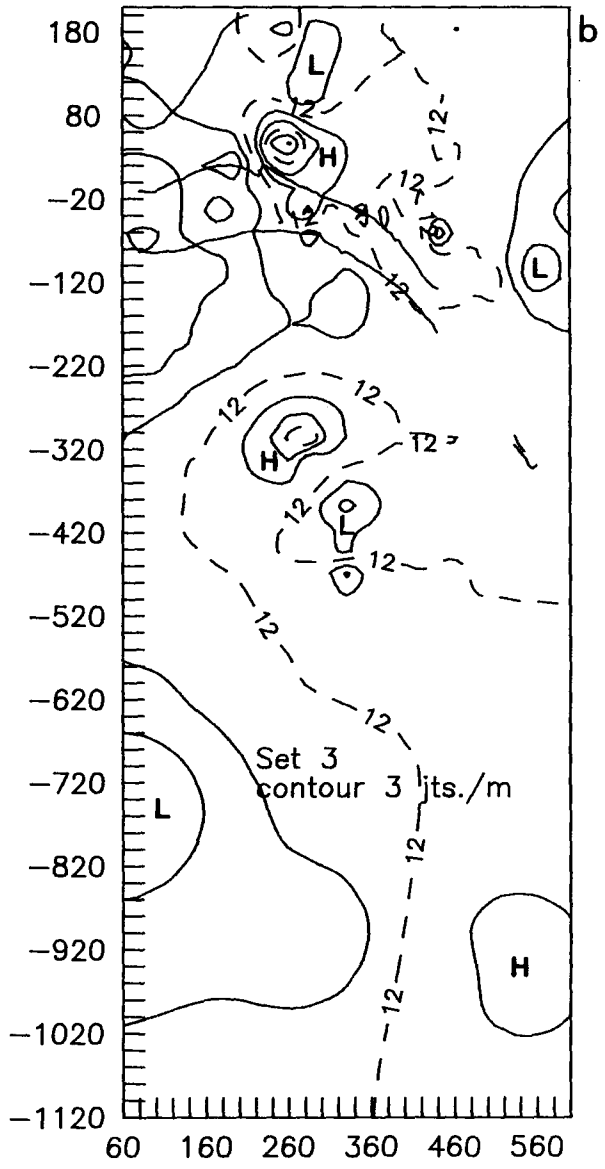
b
180
80
-20
-120
-220
-320
-420
-520
-620
-720
-820
-920
-1020
-1120
60
160
260
360
460
560
H
L
12
Set 3
contour 3 jts./m

breccia. Density highs for set 2 and 3 joints do not form such a ridge, however, there is an isolated high in the extreme SW corresponding to an area of volcanics pervaded by veins and intruded by what is interpreted as quenched granite.

3.4.3 Miscellaneous Features

The majority of data taken from domain 2, which covers the intrusive north of the breccia, were of pegmatite, bubble structures (refer chap.2) and aplite orientations. Both domain 6 and 7 are situated on the east side of Net Lake, domain 7 being comprised of mafic and domain 6 of granitic rocks. Within these two domains most of the data gathered were foliation attitudes. Individual plots of each of these three domains reveal strong similarities between them and therefore, a single plot of all three domains is shown to illustrate the trends (Fig. 3-17a). There are possibly three attitudinal populations that can be defined from the data within domains 2, 6 and 7. The strongest, consisting primarily of foliations, shears, pegmatites and related structures, centres on 058/66 NW. Another less well defined group of foliations and shears trends toward 028/62 E and the third, made up of foliations, clusters near 005/87

E. The 028^0 foliation may well correspond to the S_2 foliation developed in the NLVL zone of deformation, while the 005^0 direction could represent the expression of S_3. The cause of the 058 trend is not obvious, but it may represent effects of the 069^0 shear.

Domain 3 covers the area immediately surrounding the breccia while domains 4 and 5 lie to the south of the breccia. As was the case above, individual plots of the domains lead to the conclusion that the three are better treated as one group. On the resulting stereo plot the strongest concentration of data trends 168/86 W and is defined by faults, shears, and both granitic and feldspar porphyry dykes (Fig. 3-17b). A weaker concentration of fault and foliation data centres on 030/86 E, while a poorly defined cluster of granitic and porphyry dykes trend near 080^0 and dip steeply south. The 168^0 trend does not correspond to any previously defined planar features and so its origin or affinity is unknown. In a general sense the 168^0 direction lies perpendicular to the granite greenstone contact, and consequently this feature may represent a tensional weakness or fault plane related to intrusive emplacement. The 030^0 trend parallels the S_2 surface defined by Fyon et al. (1988), although this may be insignificant since the trend is so weakly defined.

Figure 3-17a: Stereonet plot of miscellaneous features from domains 2, 6 and 7, in dominantly granitic rocks. Symbols: open circles-shear zones; filled circles-pegmatoids; crosses-foliations; squares with tic marks-feldspar porphyry dykes; circles with tic marks-granitic dykes.

Figure 3-17b: Stereonet plot of miscellaneous features from domains 3, 4 and 5, located on the west side of Net Lake, exclusively in volcanic rocks. Symbols same as for figure 3-17a.

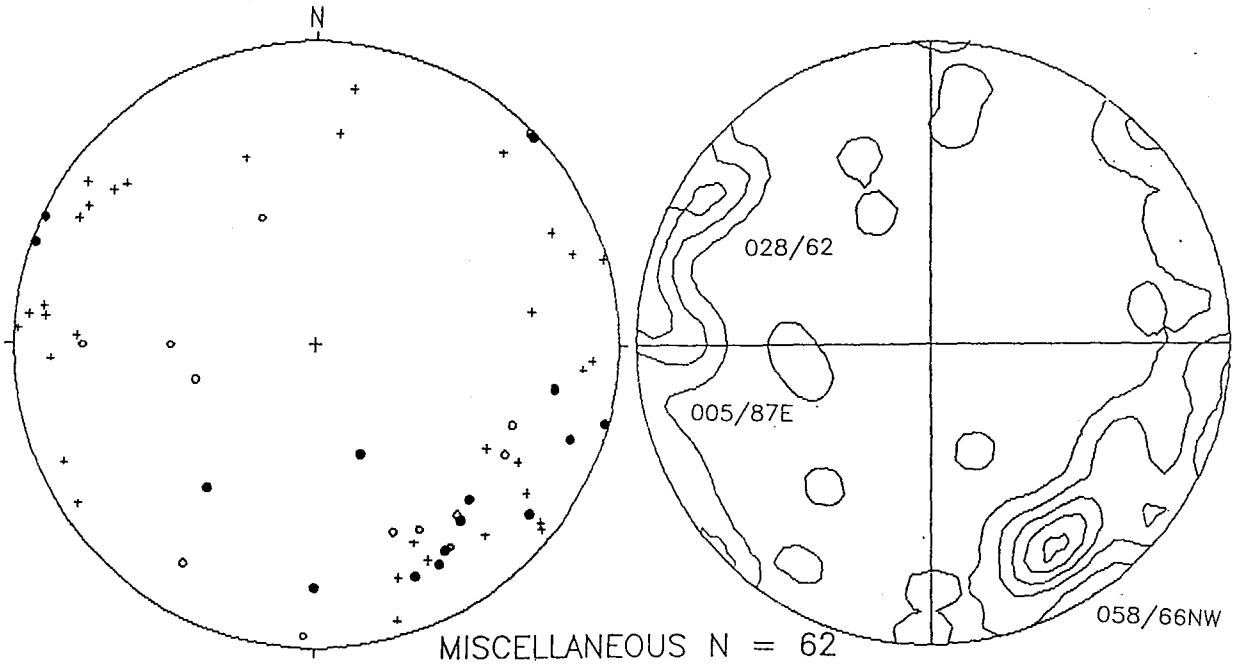

MISCELLANEOUS N = 62
FEATURES
domains 2,6,7

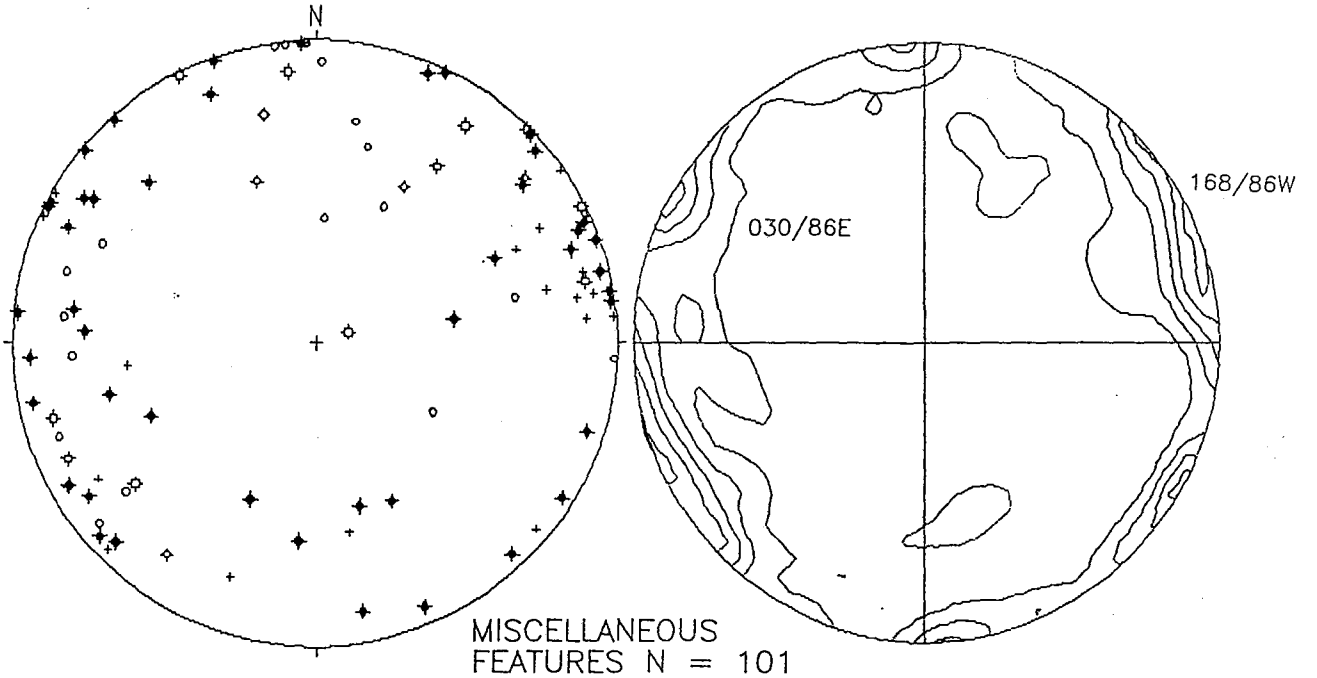

MISCELLANEOUS
FEATURES N = 101
domains 3,4,5

3.5 Dynamic and Kinematic Analysis

3.5.1 Quartz Veins

Quartz veins were usually featureless structures having homogeneous vein fillings, well defined straight walls and a lack of included wall-rock material. In a relatively few veins slickensides were observed and most of these indicated subhorizontal movement. When wall-rock fragments were present they were typically elongate, parallel to the walls and had both angular and streamlined cross sections. The veins on the east side of Net Lake had several different characteristics, the most notable being that they were hosted in granitic rocks and were largely unmineralized. These veins often had quartz filling with a sugary to chalcedony-like texture, which differed from the usual coarse-grained vitreous quartz found on the west side of Net Lake. Often the veins contained highly foliated wall-rock fragments and had trends parallel to, or at a low angle to, the penetrative foliation. Often veins coalesced to form stockworks, zones of brecciation and horse-tailing terminations. In the vicinity of the 069^0 shear zone the frequency of quartz veins and brecciation intensifies and

within the core of the shear zone silicification is pervasive (Plate 3-1c,d;3-2a). The intensity of silicification in the shear zone is similar to that found in the probable extension and intersection of the NLVL deformation zone with the Strathy-Chambers batholith (Fyon et al. 1988). Based on the field textures and coincidence in distribution and orientation of the veins and the shear zone it is thought that the veins in this area developed during and in response to the shear zone activity. The development of this shear zone along the volcanic intrusive contact suggests that shearing was localized along the contact in response to the emplacement of the batholith. Development of shear stresses within and parallel to the volcanic trough or salient is implied by the gross morphology of the contact, where the salient is defined by the two impinging lobes of the batholith. It is probably not coincidental that the trend of the salient (065^0), the quartz veins (071^0) and the trend of the 069^0 shear zone are all subparallel (Map 1;Fig. 1-1). In what may be a somewhat analogous situation, diapirism during the emplacement of the Strathy-Chambers and Iceland Lake intrusions has been implicated in the formation of the Northeast Arm and Link Lake zones of deformation (Fyon et al. 1988). By virtue of their internal structure and distance from the 069^0 shear,

Plate 3-1a (page 74): Ribbon quartz vein located near the SW end of the breccia body. Ribbons consist of chloritic slivers, likely of the adjacent wall rocks and may indicate repeated vein opening and closing (crack and seal).

Plate 3-1b (page 74): Large pegmatite in the Strathy-Chambers batholith along highway 11. Pegmatite is mainly comprised of euhedral perthitic K-feldspar and massive milky white quartz. (15 cm scale in bottom left corner of photo)

Plate 3-1c (page 74): Series of subparallel anastomosing veins hosted in granitic rock in the vicinity of the 069 shear zone. The sheared contact with the mafic intrusion is approximately 4 m to the left, in the field of the photograph.

Plate 3-1d (page 74): Anastomosing quartz veins and pervasive silicification of granitic host rocks in the vicinity of the 069 shear zone.


A
MB 88-257
0 cm 1 2 3 4 5 6 7 8 9 10 11 12 13 14 15

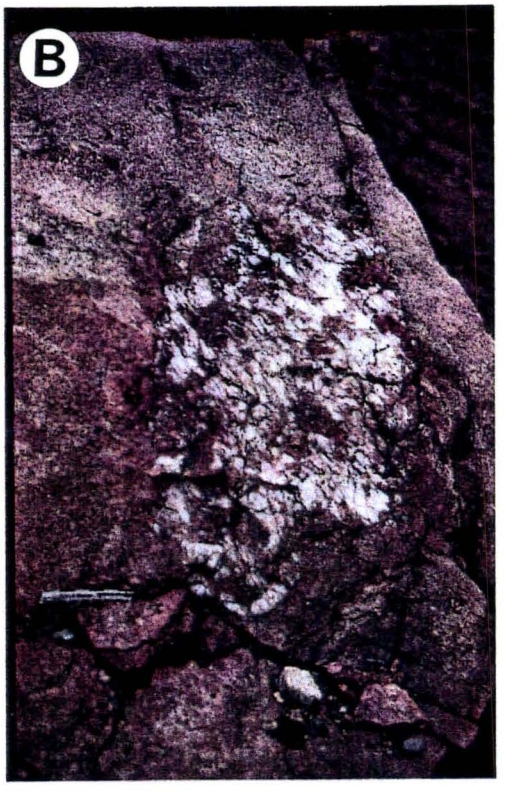
B


C


D

veins on the west side of Net Lake do not lend themselves to this hypothesis of a shear origin quite so readily. There are some features though, such as the alignment and parallelism of veins on either side of Net Lake, that suggest these two areas may be one continuous zone. There is also small scale evidence that favours a shear-related origin for veins on the west side of Net Lake. The example in figure 3-18a shows a pair of mineralized veins, trending 085/58 N, with some narrow quartz filled splays that extend a few cm beyond the vein margins. The orientation, and mineralized nature of the veins suggests that they are an example of the dominant vein set trending 071/85 NW. In this geometric configuration it is possible that the main body of the vein represents the shear direction while the splays represent tension or gash veins. It is clear that compression directed in the plane of these supposed tension veins would result in a sinistral, subhorizontal sense of movement. Another example is shown in figure 3-18b where a thick mineralized vein, trending 073/87 N, shows some possible kinematic indicators. Adjacent to the vein one set of high density joints parallels the vein while another set intersects the vein at a moderate angle. In addition chloritic slivers inside the vein parallel these joints which intersect the vein. Subhorizontal slikensides

Figure 3-18a: Sketch of quartz vein located near the southwest end of the breccia body which shows possible kinematic features. The 040 vein splays are interpreted to be gash veins representing a tensional plane and the main body of the vein a shear or fault plane. Such a configuration indicates an approximate north-south compression with a subhorizontal, sinistral sense of shear.

Figure 3-18b: Sketch of quartz vein located approximately 300 m southwest of the breccia body which shows possible kinematic features. The 030 joints in this example as in the above sketch are interpreted to be tensional features. The geometry is interpreted to imply approximate north-south compression and a subhorizontal sinistral sense of shear.

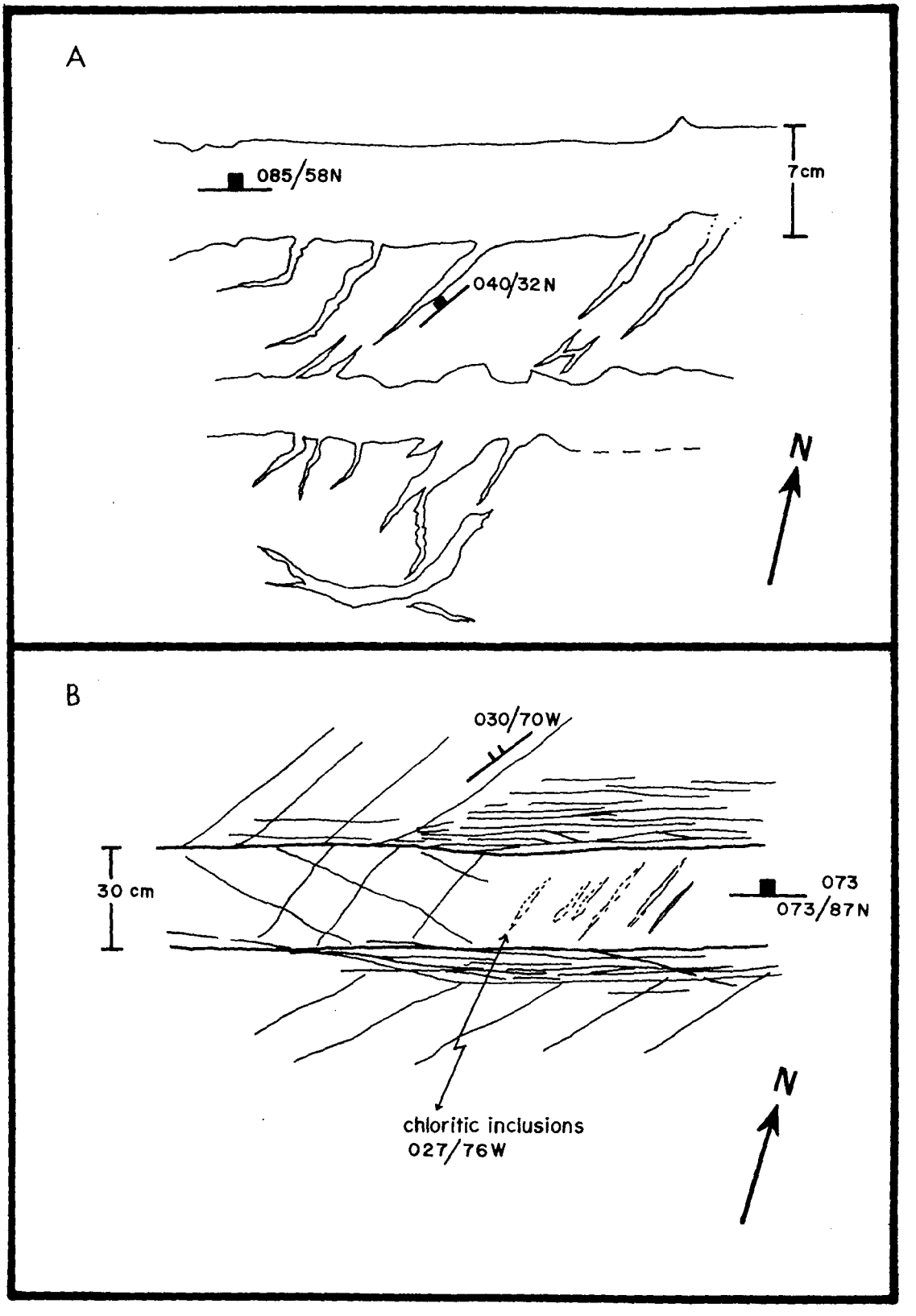
A
085/58N
7cm
040/32N
N
B
030/70W
30 cm
073
073/87N
chloritic inclusions
027/76W
N

indicate the latest direction of movement, but not the sense of movement. If the intersecting joints are tensional features, analogous to the vein splays in the previous example, the vein would have experienced sinistral, subhorizontal movement.

For the following discussions it is assumed, based on the few slickensides, that the veins lie within a plane of shear and that movement was sinistral and horizontal. It is then possible to estimate the principal strain directions using the model of Anderson (1951) (Fig. 3-19a). It follows that if rotational strain was not significant the strain axes approximate the principal stress directions. In Anderson's model the conjugate fault planes are at 30 degrees, and the conjugate shear planes 45 degrees, to the compressive stress direction. The intersection of the conjugate planes define the intermediate stress direction while the extensional vector is at 90 degrees to both σ_1 and σ_2. The compressive vector also lies in a X-Z plane, defined as containing the slickensides (net slip direction) and oriented at 90 degrees to the shear plane, which here is defined by the veins. The intermediate stress vector is a pole to this X-Z plane and the extension direction lies within the X-Z plane at 90 degrees to σ_1. Using these relationships estimates of the stress distribution are, σ_1

$4^0/208^0$, σ_2 $83^0/342^0$ and σ_3 $5^0/117^0$ (Fig. 3-19b). A similar derivation of stress vectors can be defined for the individual examples shown in figure 3-18a,b. In these examples lineations are not apparent, but tensional features are, allowing for the definition of σ_2 at the intersection of the veins and supposed tensional planes. The results of this method derive σ_1 vectors of $10^0/26^0$ and $15^0/24^0$, results remarkably similar to those derived in the example based on horizontal lineations (Fig. 3-20a,b).

Fyon et al. (1988) suggests an approximate N-S compression and a largely vertical, minor sinistral component along the NLVL zone of deformation. The results herein suggest that conditions forming the quartz veins, which may be analogous to those that created the 069^0 shear zone, require a roughly N-S compression. In contrast the orientation of the estimated intermediate stress is such that movements would be largely strike-slip as opposed to thrust-slip for the NLVL zone. It may be presumptuous to assume that the dynamics responsible for the two deformation zones are related, but general similarities in style, timing and general setting are compatible with a similar origin. The limited number of kinematic indicators obtained from quartz veins unfortunately limits the confidence to be put on the results of the dynamic analysis. In addition, data

Figure 3-19a: Sketch shows the ideal geometry of tensional and shear planes in a compressional regime. The sense of movement is indicated by arrows as are the orientation of slickensides (SS). From Anderson, (1951).

Figure 3-19b: Kinematic construction based on quartz vein representing a plane of shear and the slickensides the net slip direction. Symbols: filled triangles slickenside lineations; filled square, pole to veins; open square, pole to joints; cross, stress vector. Sigma 1 maximum, sigma 2, intermediate and sigma 3 minimum compressive stress directions.

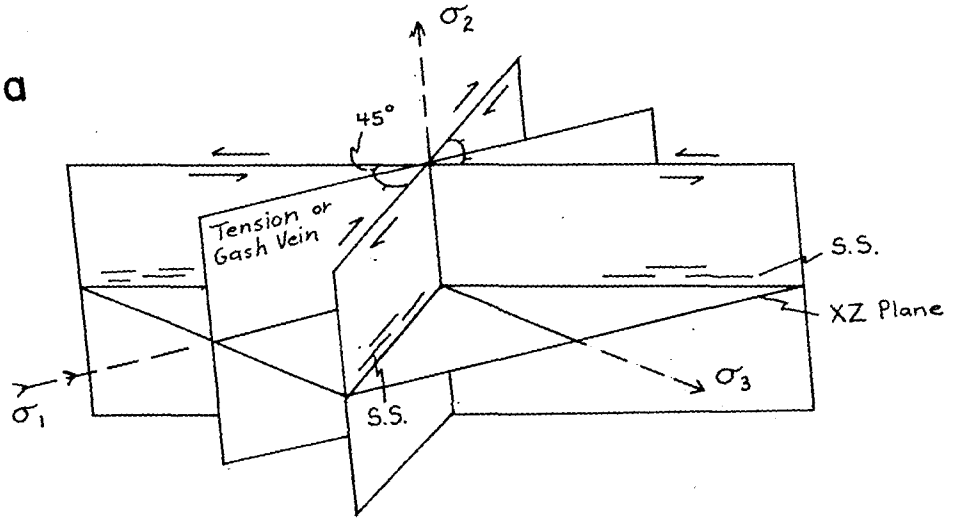
a
σ2
45°
Tension or
Gash Vein
S.S.
XZ Plane
σ3
σ1
S.S.

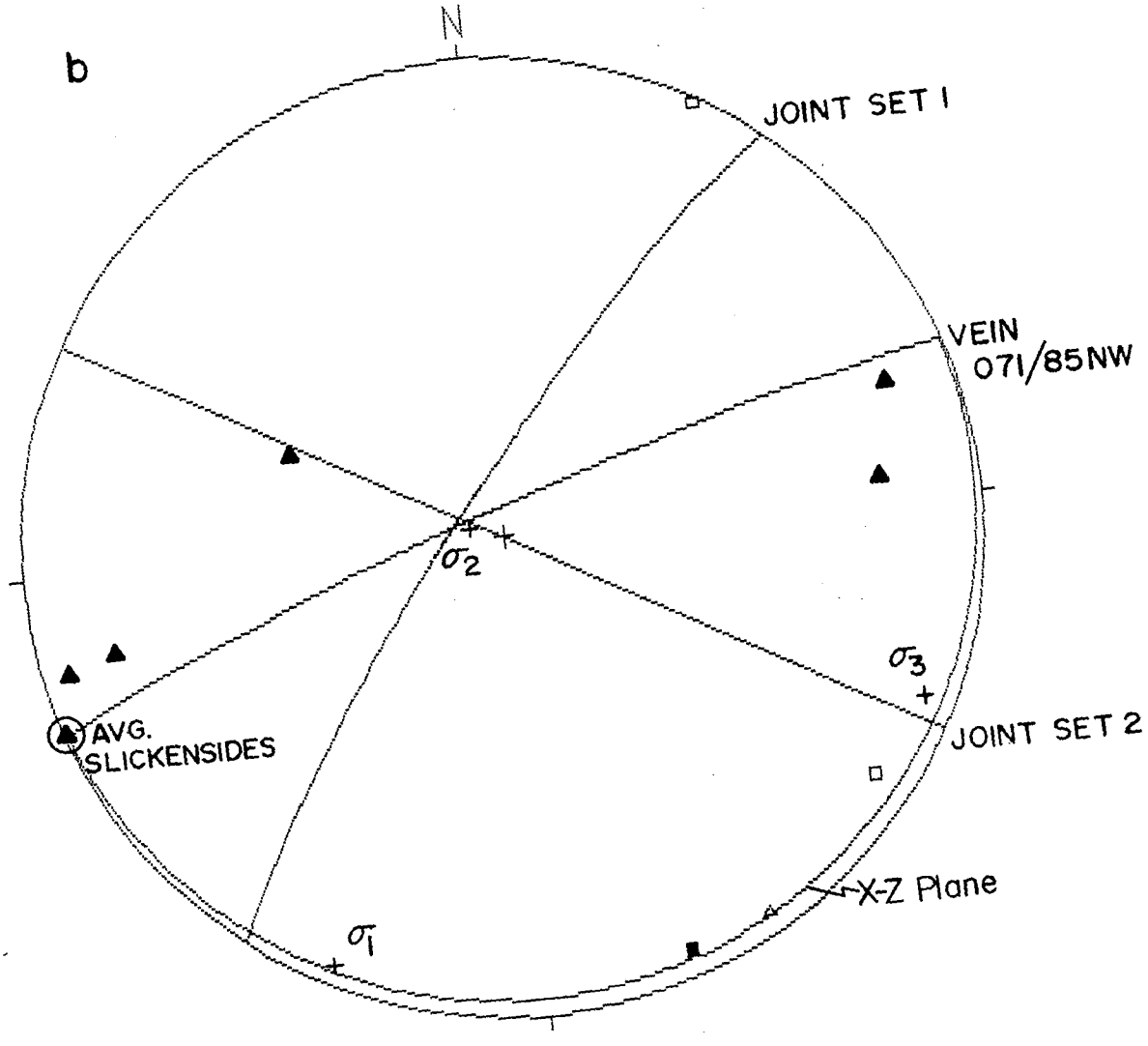
b
N
JOINT SET 1
VEIN
071/85NW
σ2
σ3
JOINT SET 2
AVG.
SLICKENSIDES
X-Z Plane
σ1

Figure 3-20a: Kinematic construction based on vein in figure 3-18a representing a plane of shear and the vein splays representing tension gash veins containing the compressive stress direction.

Figure 3-20b: Kinematic construction based on vein in figure 3-18b representing a plane of shear and the intersecting joints a tensional plane containing the compressive stress vector.

(a)

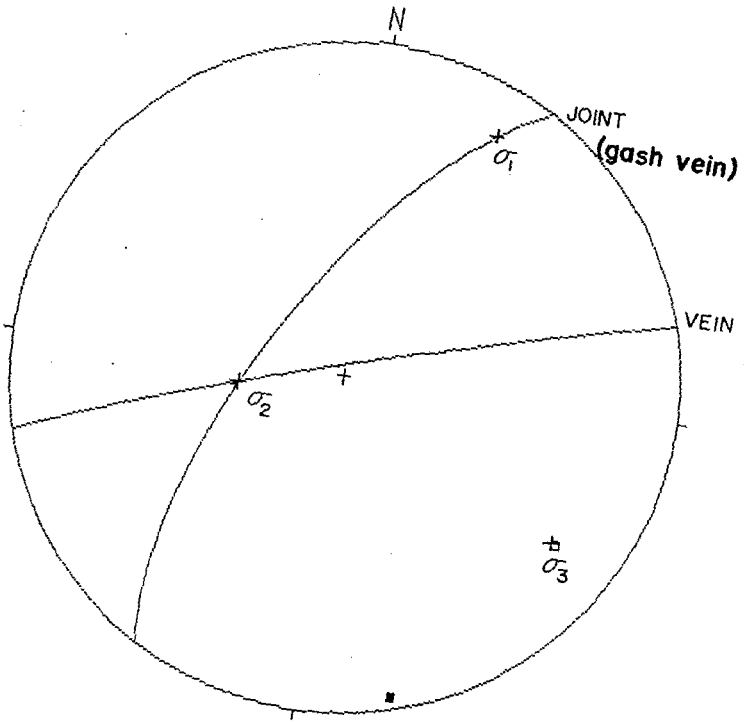
N
JOINT
(gash vein)
σ_1
VEIN
σ_2
σ_3

(b)

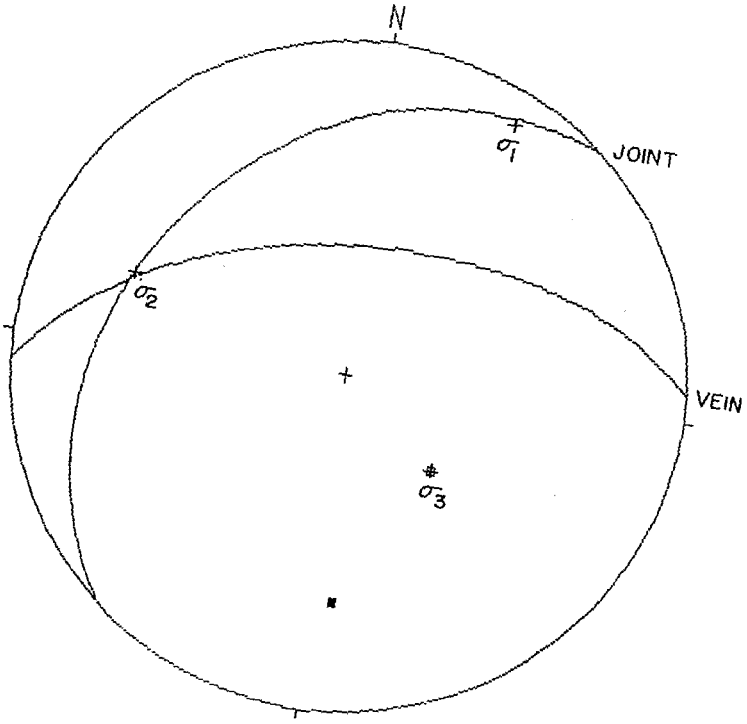
N
σ_1
JOINT
σ_2
VEIN
σ_3

were gathered from a small area as opposed to the findings of Fyon et al. (1988), which are based on a composite of features from a large area. The difference in results in results is problematic, but it must be considered that the stress field may have been heterogeneous during the development of structures allowing for contrasts in stress distribution within a relatively small area. If the few kinematic indicators used for this analysis are incorrect it is still possible, given the subparallelism of the veins to the NLVL, to consider that the veins could be related to the movements on that fault. Alternatively the kinematic interpretation of the 069^0 shear zone may be incorrect and it may have experienced largely vertical movements more like the NLVL zone in which case the veins could still be viewed as shear veins related to the 069^0 structure. Under this latter interpretation it is possible that the NLVL and 069^0 structures developed under similar stress conditions and at nearly the same time.

Stereonet plots for domains 6, 7 and 8 indicate a distinctive vein geometry in which curviplanar veins intersect in a curvilinear axis (Fig. 3-4a;3-5a). The simplest analogy to this geometry is a fold that has been compressed perpendicular to the fold axis and refolded into open folds. In terms of the fold analogy, the fold limbs

are represented by quartz veins and the fold axes are defined by the intersection of these veins. Fyon et al. (1988) describe the existence of an S_3 foliation, which they believe is an axial planar foliation to small scale open folds documented within the greenstone belt. It seems plausible that the apparent folding of the E-W trending quartz veins may be a response to the folding event that produced the minor folds and S_3 foliation. If this is the case the folding of the veins has produced open folds with a steep axial plane striking 160^0 and interlimb angles of about 90 degrees. Further evidence in favour of this folding concept is that both S_3 foliation and the apparent folding of veins are best developed in the same area, the east side of Net Lake. Unless vein emplacement was along anisotropy caused by folding the simplest interpretation is that the E-W trending veins formed prior to the S_3 foliation.

In earlier discussion, it was suggested that the thickness of veins and possibly the density of joints were coincident along a zone that trends across the breccia toward the SW (Fig. 3-7,15,16). As will be discussed in chapter 4, the strongest mineralization, in both veins and breccia, follows this same 045^0 trend or zone. Bearing in mind the limitations of exposure and lateral coverage of

these features, it is suggested that there is a linear band characterized by stronger mineralization, vein thickness and jointing. If the trend is real it may represent a zone of stronger brittle deformation that cuts across the 071^0 vein trend. If, as has been suggested, the veins represent a shear plane then the orientation of this brittle deformation zone may correspond to a conjugate fault zone. The ideal angle between fault and shear is 15^0 (Anderson, 1951) whereas in this case the angle is roughly 25^0. Although the evidence is modest, the possibility of a fault could explain the apparent trend of mineralization since increased strain would enhance vein opening and fluid permeability.

The above discussions are primarily concerned with veins belonging to the domains lying to the south and east of the breccia zone. This same population of veins exists in the vicinity of the breccia in domains 3 and 5; however, other classes of veins are also present in these domains. The most notably different feature of these domains is a greater variation in vein attitude and a preponderance of feldspar bearing veins (Fig. 3-4b;3-6a,b). Based on mineralogical similarities it is believed that the 071^0 veins, other veins in the area of the breccia and the breccia filling itself were all formed at the same time. The stress that probably created these seemingly random

veins may be related to that which produced the 071^0 veins, but it appears that other forces or anisotropies in the rock disrupted the regularity in vein attitudes. The only systematic character of these veins is weak 071^0 strike and a tendency to dip northward on the NE side of the breccia and south on the SW side. These factors suggest that the stress field in the region of the breccia was modified to that existing outside the immediate area of brecciation. At distances of a hundred or more meters beyond the breccia the regional stress regime probably dominated and controlled the strain features such as veins and possibly joints. Within this peripheral zone forces created by retrograde boiling would have caused vertical and perhaps nearly hydrostatic stress, which may have greatly exceeded regional stress for a relatively short period of time. The apparent symmetry displayed by the veins on either side of the breccia is compatible with stress localization within the breccia zone and may represent relaxation of stress immediately after brecciation.

3.5.2 Joints

The interpretation of forces responsible for the formation of joints is dependent on the timing of joint

formation and their relationship to breccia development. There are essentially three possible temporal relationships that might apply. The first would have the joints formed much later than the breccia in response to unrelated regional stresses. Another possibility is that joints formed by regional stresses prior to formation of the breccia and that the breccia cuts these features, being influenced by the inherent weakness caused by their presence. Lastly the joints may have been surfaces of failure for brecciation and developed just prior to and during breccia formation in response to fluid overpressures immediately beneath the breccia. Contrary to these possibilities the two or three joint sets could have formed independently at distinctly different times, although data discussed in chapter 4 indicates that some of the joints developed synchronously with the breccia. It is clear that joints cut the breccia, but there is also evidence that quartz veinlets are controlled by joint surfaces, in particular the 038^0 set (Plate 3-2b). It also seems apparent that the density of joints and the variability of their attitudes is dependent on the proximity to the breccia. An important additional feature is that the alignment of rectangular fragments within the breccia is very close to the directions of the joint sets (see chap.

Plate 3-2a (page 86): Silicification and brecciation of the granitic rocks in the vicinity of the 069 shear zone.

Plate 3-2b (page 86): Jointed volcanics within 30 m of the breccia body contact. In this example a small quartz stringer trending 070 is deflected along the 034 joint plane indicating that the joint predates the quartz stringer.


A

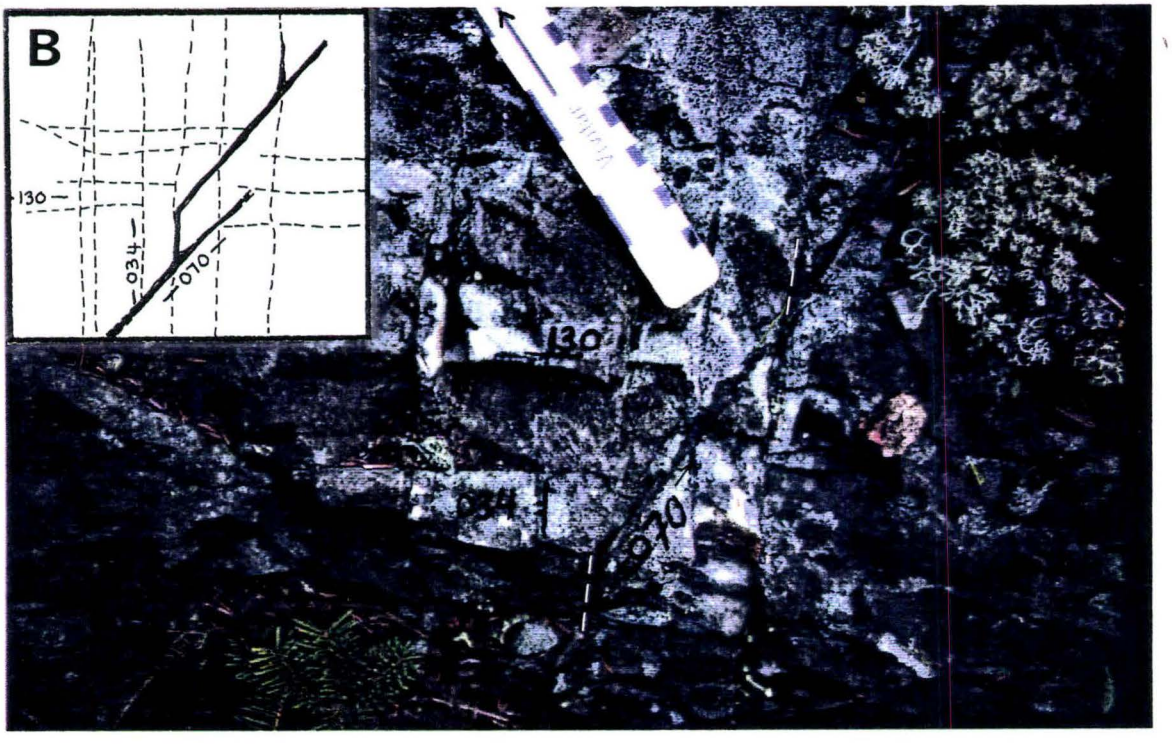
B
130
034
070
130
070

4). The results are not conclusive, but it appears that the joints are closely related to breccia formation.

If the model of Burnham (1979, 1985) is adopted then it is proposed that joints result from subvertical compressive stress emanating from the underlying intrusive. In response to stress focused on a central point fractures may delineate radial and concentric patterns above an intrusive stock or plug. In these circumstances the intermediate and minimum stress vectors are equal and horizontal, a condition that allows for these tensile fractures to develop radial or concentric patterns (Anderson, 1936). In Temagami it is clear that the intrusion was not symmetric nor plug-like in form so it is not surprising that radial and concentric fractures are absent. Even so, the joints may have developed under analogous conditions of vertically directed non-radial stress resulting in the orthogonal patterns now evident.

An alternative model would have the joints related to the same stress regime responsible for the development of quartz veins. Plotting joint set 1 and joint set 2 with the stress orientations derived earlier reveals that joint set 1 contains σ_1, and that σ_1 is essentially a pole to joint set 2 (Fig. 3-19b). This geometry is convenient in explaining joint set 1 as a tensional feature; however, it does not fit

as an explanation for the derivation of joint set 2 or set 3, unless they formed in response to vertically directed stress, which likely dominated near the breccia. If the latter hypothesis is adopted joint set 1 is seen to form in response to more regional stresses akin to those responsible for the 071^0 veins. In the vicinity of the breccia, increasing pressures prior to brecciation would mean σ_1 would be orientated in the vertical direction. In addition σ_3 would lie in the horizontal so as to define a pole and extension direction to joint set 2 and roughly set 3. If, as is suggested, σ_3 is a pole to joint set 2 prior to and during brecciation it might be expected that brecciation would propagate parallel to joint set 2 and 3 leading to the development of a tabular breccia body as observed. This explanation is compatible with several key observations such as the subparallelism of breccia fragments with joint set 2 and 3, and the better attitudinal definition of set 2 and 3 joints adjacent to the breccia (Fig. 3-8 - 3-16). The variable distribution of joints in domain 5 may reflect the complex interplay of forces operating at the intrusive volcanic contact. The fact that joints in this area appear to be effected by proximity to the contact suggests that the formation of these joints took place during intrusive and hydrothermal activity.

The occurrence of high joint density areas near and adjacent to the breccia, in addition to other evidence, favours the concept that joints were planes of failure exploited by brecciation (Fig. 3-15,16). In addition to this association there is evidence linking joints to vein and mineralization distribution. Plots of joint density show that the areas of high density correspond to areas of known mineralization indicated by shafts, trenches and mineral showings (Fig. 3-15,16). The correspondence of large vein thickness with joint density highs is also suggestive that joints influence vein formation, but as is the case for joints and mineralization, poor coverage makes an extension of these trends beyond grid location 550 SW uncertain (Fig. 3-7). The existence of a high density area of set 2 and 3 joints in the area of grid location 920 m SW may be significant as it is an area where quenched intrusive rocks are exposed (Map 1). As noted in chapter 2 these rocks may have formed by exsolution of fluids and quenching of magma that resulted from failure of the roof rocks. The prominent joints, like the breccia itself, may result from pressures exerted by the shallow underlying intrusive as magmatic-hydrothermal fluids escaped. An indication that the jointing in this area may be related to processes analogous to those responsible for the main breccia is

illustrated near this area on highway 11 where a small exposure of vein breccia, shows on a small scale, features much like those in the main breccia (Plate 3-3; Map 1).

3.5.3 Possible Conjugate Faults Bordering the Breccia

In the areas immediately north and south of the breccia a set of fault or high strain zones were tentatively identified (Map 2). The sense and amount of displacement was indicated by minor offsets of cross cutting stringers and aplite dykelets. The stereonet of fault and foliation data from domain 3 reveals a recognizable trend, but on a composite of domains 3, 4 and 5 there is slightly better resolution of the near vertical data at 168^0 and a weak concentration at 030^0 (Fig. 3-17b). Because of the apparent sense of movement and geometry one interpretation of these high strain zones is that they represent a conjugate pair of faults with one fault, the 168^0 fault, more strongly developed than the other. Theoretically the angle between fault planes should be near 60^0 (Anderson, 1951); however, the planes considered here are separated by 46^0. Knowing the sense of movement and the point of intersection between planes allows approximate definition of the stress directions. The resulting stress vectors, σ_1 $16^0/8^0$, σ_2

Plate 3-3 (page 91) Small exposure of breccia on highway 11 near Temagami North. Breccia displays textures similar to the main breccia body 800 m to the north.

$74^0/190^0$ and σ_3 $1^0/99^0$ are very similar to those obtained by considering the quartz veins as a plane of shear (Fig. 3-19b;3-21). In regards to timing it is likely that the 168^0 structure formed during or prior to the breccia formation, as the structure does not appear to cut the breccia, and feldspar porphyry and granite dykes, known to cut the breccia, follow the 168^0 trend. The prominent protuberance on the north margin of the breccia (grid location 230 SE, 10 NE) where the 168^0 structure would appear to offset the breccia may in fact be a point where the breccia expanded further into the country rock due to the inherent weakness of the highly fractured host. The chronologic indications and the agreement between stress estimations by different means suggest that the 168^0 and 030^0 structures were likely related to the stresses that prevailed prior to, and possibly during, breccia formation.

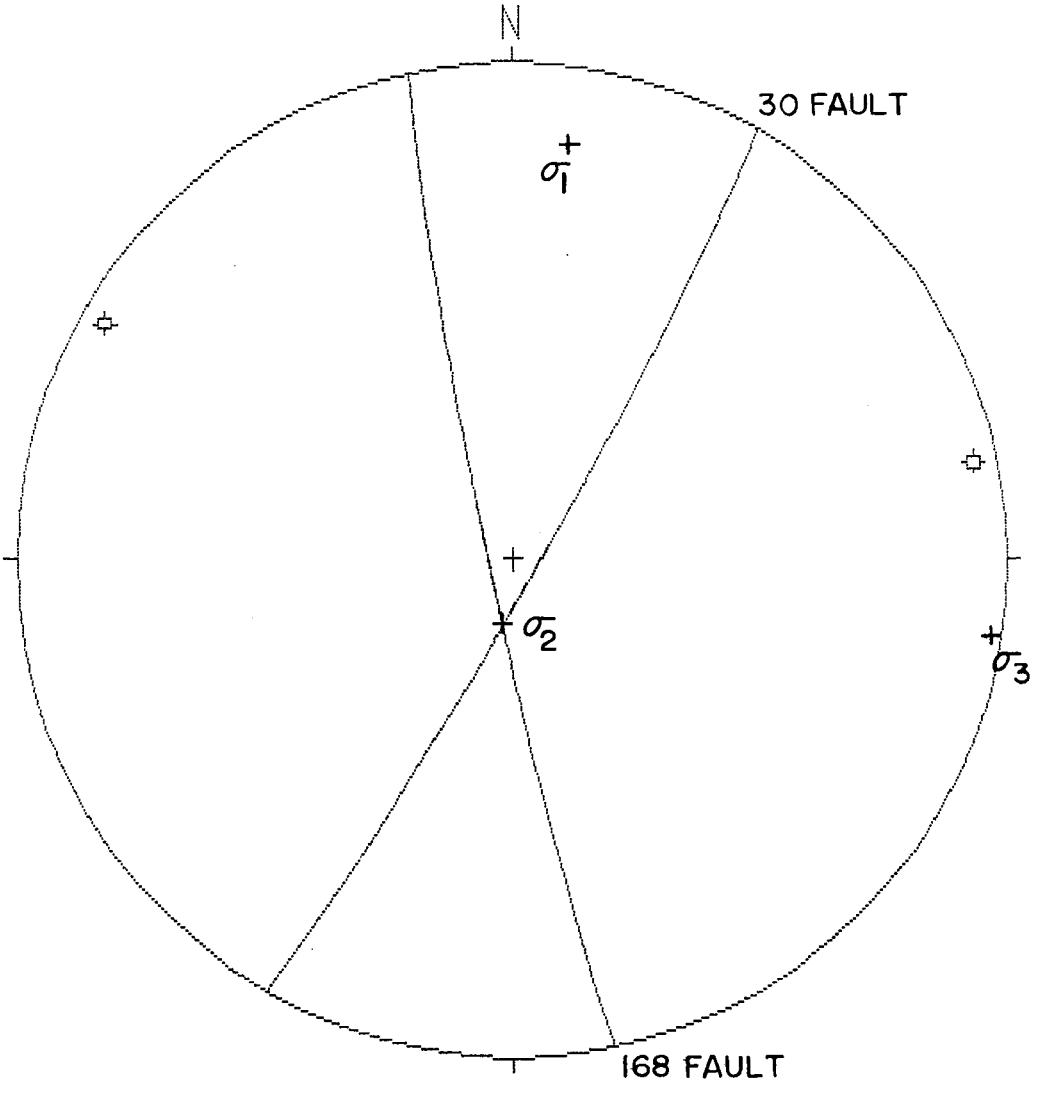

Figure 3-21: Kinematic construction assuming that the faults or planes of weakness in the immediate area of the breccia represent conjugate fault planes. In this configuration the intermediate stress direction is defined by the intersection of the faults and the maximum compressive direction bisects the acute angle of fault intersections.

CHAPTER 4

THE BRECCIA BODY

4.1 General Features of the Breccia

4.1.1 Breccia Form and Extent

The breccia is an elongate body that trends roughly NW-SE having a long dimension of at least 340 meters and a width of 90 meters at the widest point (Map 2). The breccia outcrops on a 40 m high resistant knoll that may represent a roche moutonnée. At the NW end brecciation diminishes in intensity before being obscured by cover, while at the SE end the breccia thins to a width of 40 m before being covered by overburden. The shape and relationship of the breccia with elevation contours suggests that the zone is tabular, striking 140^0 and dipping shallowly to the SW. There is, however, no reason to presume that the breccia conforms to a consistent geometric shape or attitude with

depth. In the middle section of the breccia where exposure is best and brecciation most intense the contact with unbrecciated rock is often sharply defined. In other areas where brecciation is not well developed the margin between breccia and non-brecciated rock is gradational (Map 2). Generally the margin of the breccia is regular with one exception on the central south margin where a 50 m, by 1-3 m, narrow finger of breccia extends from and trends subparallel to the main body (Map 2). Near this locality and about 40 m south from the main body there is a 30-40 m long, by 1-2 m wide, lens-shaped satellite breccia hosted in unbrecciated volcanics. Another satellite breccia occurs on the NE side of the main body near the NW end (Map 2). In this breccia rock fragments are intensely altered to biotite and chlorite, unlike the main mass of breccia.

4.1.2 Relation of Breccia Zones to Geologic Features

Proximity to the Strathy-Chambers batholith The breccia is hosted in mafic volcanics some 75 to 240 m SW of the contact of volcanics and the Strathy-Chambers batholith (Map 1,2). Several features suggest that the granite intrusive lies at a shallow depth. At the extreme SE end of the grid (grid location 480 SE, 950 SW) there are exposures of silicified

volcanics and small exposures of granitic rocks (Map 1). Silicification of volcanics also occurs in the area of grid location 640 SE, 100 SW. Another indication of the proximity of the intrusive is found near the satellite breccia at the north end of the grid where breccia matrix is comprised of medium- to fine-grained felsic material in place of the usual quartz matrix. These features, plus the occurrence of granitic and porphyry dykes, indicate that the granitic rocks lie only a short vertical distance, perhaps 50 to 150 meters, below the present breccia exposure (see sec. 4.3.2).

Granitic dykes that outcrop to the north of the breccia are never seen in contact with the breccia; however, the porphyry dykes, believed to be comagmatic with the intrusive, (refer chap.6) do outcrop within and adjacent to the breccia. One such dyke is in contact with the long finger-like breccia that extends from the main body on the SW breccia margin. In this exposure the dyke cuts the breccia as evidenced in outcrop and in thin section where angular inclusions of quartz are incorporated in the dyke (Plate 4-1a,b;4-2a). Two other exposures of porphyry occur within the main mass of the breccia. One of these clearly postdates the breccia while the other has a very irregular form, so that temporal relations with the breccia are

Plate 4-1a (page 97): Contact between breccia and feldspar porphyry dyke. Upper area of the photo consists of a large breccia block rimmed with feldspar. In the lower half the dyke cuts the breccia and conforms to the shape of the breccia block.

Plate 4-1b (page 97): Same contact as above located 15m along strike. In a similar manner as above, the dyke can be seen to conform to a breccia block. The contact here is curvyplanar and there is no evidence of the dyke being fractured or brecciated.


A
Vivitar
Z
Q


B
Vivitar
Z

difficult to decipher. Spatial association of porphyritic rocks with intrusion-related hydrothermal breccias is not uncommon and several studies argue that these magmas were intruded in association with brecciation (Sillitoe and Sawkins, 1971; Burnham, 1979; Warnaars et al., 1985).

Relative ages of breccia and veins Physical evidence for vein formation greatly preceding or postdating the breccia is lacking. No fragments of vein material were found within the breccia and no examples of veins truncated by the breccia were found. The few veins within the breccia did not clearly display features indicating formation after breccia solidification. In most instances the vein quartz appears to be continuous with the breccia matrix. Another type of vein that occurs within the breccia transects large blocks or zones of incipient breccia (refer chap.2, sec. 2.1) and can be difficult to distinguish as a vein or part of the breccia matrix. In addition to the physical evidence relating to breccia-vein age relationships there is mineralogical evidence from veins and enclosing breccia that suggests veins and breccia matrix were derived from the same hydrothermal fluid. Veins adjacent to zones of feldspar-bearing, quartz-only or mineralized breccia almost invariably have the same matrix components. On a larger scale it is evident that the broad elongate zone of greatest

sulphide vein mineralization coincides with, or intersects, the zone of greatest breccia-hosted sulphide mineralization (Map 2). In a similar way the greatest concentration of feldspar-bearing veins outside the breccia are not only close to the breccia but seem to be most prevalent where the adjacent breccia has the thickest feldspar selvages (Map 2). All these features, both textural and mineralogical, suggest that the vein and breccia matrices were derived from the same fluid, and at nearly the same time.

Relationship between breccia and joints The relationship of the joint sets to the breccia, discussed in chapter 3, revealed that the joint density seemed highest adjacent to and toward the centre of the breccia body (Fig 3-15,16). The joints were found to penetrate the breccia indicating that some zones were affected by jointing after solidification. The timing of joints, like the timing of quartz veins, is uncertain in that there is conflicting evidence which indicates jointing may have occurred prior to, during and after brecciation. Evidence indicating either pre-breccia or syn-breccia joint formation is the occurrence of quartz filled joint planes (Plate 3-2b). Less direct evidence of the timing of joint formation is the remarkable parallelism of tabular breccia fragments and set 2 and 3 joints (Fig. 4-1), which implies that the joints

Figure 4-1: Map of the breccia body and average strike of tabular breccia fragments. Trend of dominant joint sets are shown in the upper right hand corner. The stereonet inset shows the poles to breccia fragment alignment.

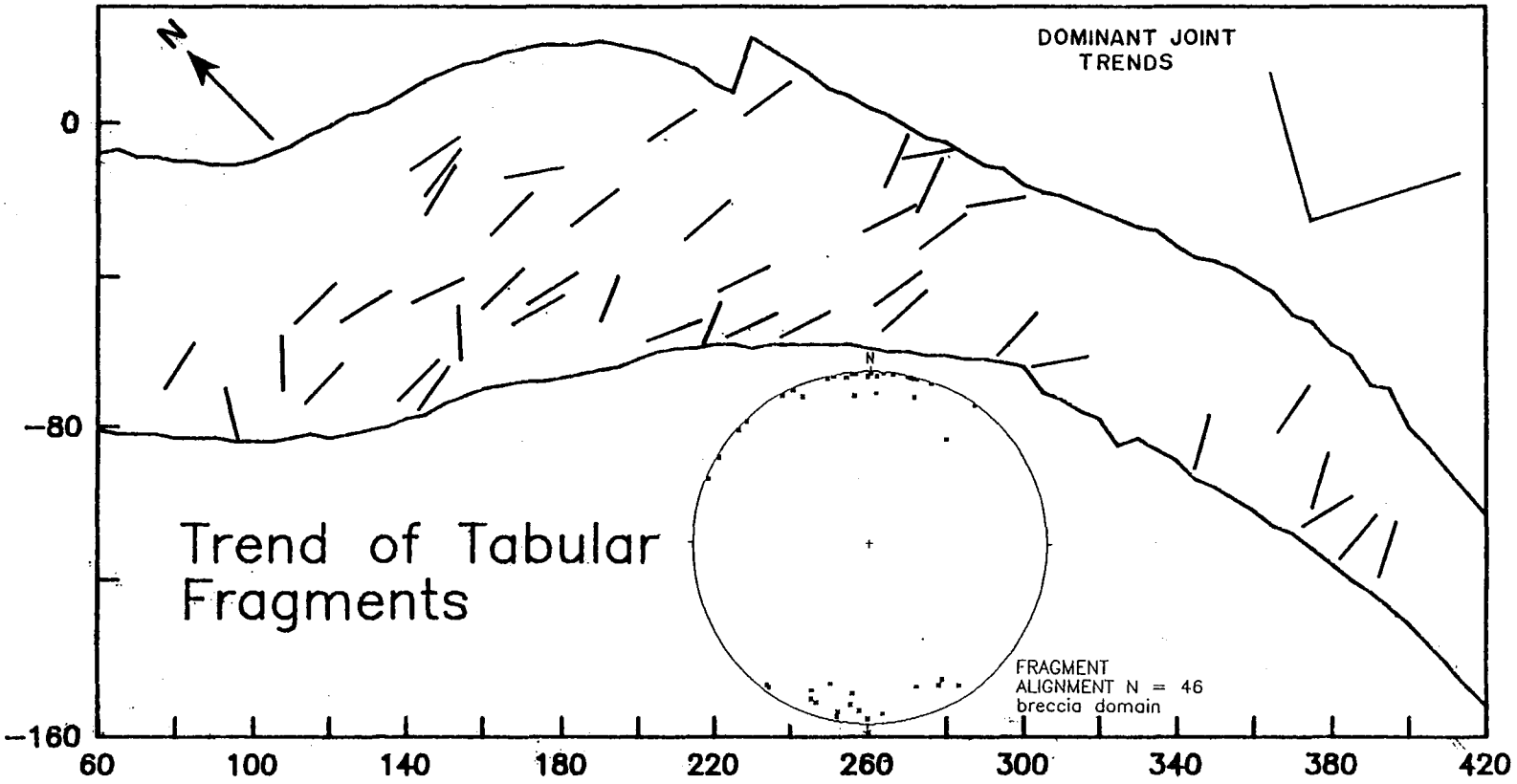
N
DOMINANT JOINT
TRENDS
0
-80
-160
60
100
140
180
220
260
300
340
380
420
Trend of Tabular
Fragments
N
FRAGMENT
ALIGNMENT N = 46
breccia domain

were actually the surface of failure along which the breccia expanded.

4.1.3 Internal Breccia Textures

The breccias framework is comprised of the basalt subtypes 2i, 2j and 2k. It was difficult to identify the proportions of each basalt type at individual stations and no correlation between basalt host lithology and fragment lithology could be defined. Fragment size varies from larger than a meter in areas of incipient brecciation to consistent 3 to 10 cm size fragments in zones of pervasive brecciation (refer chap.2, sec. 2.1). Rock flour or finely granulated material, often present in breccias (Sillitoe, 1985), is not present (Plate 4-2b). Fragments are exclusively angular and in some areas the fragments are tabular showing marked parallel alignment.

The breccia matrix is dominantly massive white translucent quartz with a few examples of euhedral cockscomb quartz filling. Plagioclase feldspar when present occurs as subhedral to euhedral selvages on fragments and some vein walls, ranging from < 1 mm to 4 mm in thickness (Plate 4-2c,d). Chlorite and biotite are seldom visible except in the satellite breccia on the north side of the main breccia, and in the mineralized zones. Potassium feldspar is a rare

Plate 4-2a (page 102): Thin section of feldspar porphyry in contact with the breccia from the same site as shown in figure 4-1. On the left of the photo fragments of quartz (breccia matrix) are included, fractured and infilled with porphyritic igneous matrix.

Plate 4-2b (page 102): Fine grained-breccia with polygonal quartz matrix, which is free of rock flour.

Plate 4-2c (page 102): Euhedral plagioclase as selvages and crystals suspended in the quartz breccia matrix (b).

Plate 4-2d (page 102): Selvage of a breccia fragment with both plagioclase (pl) and thin blades of chlorite (chl) projecting into the quartz matrix (q).

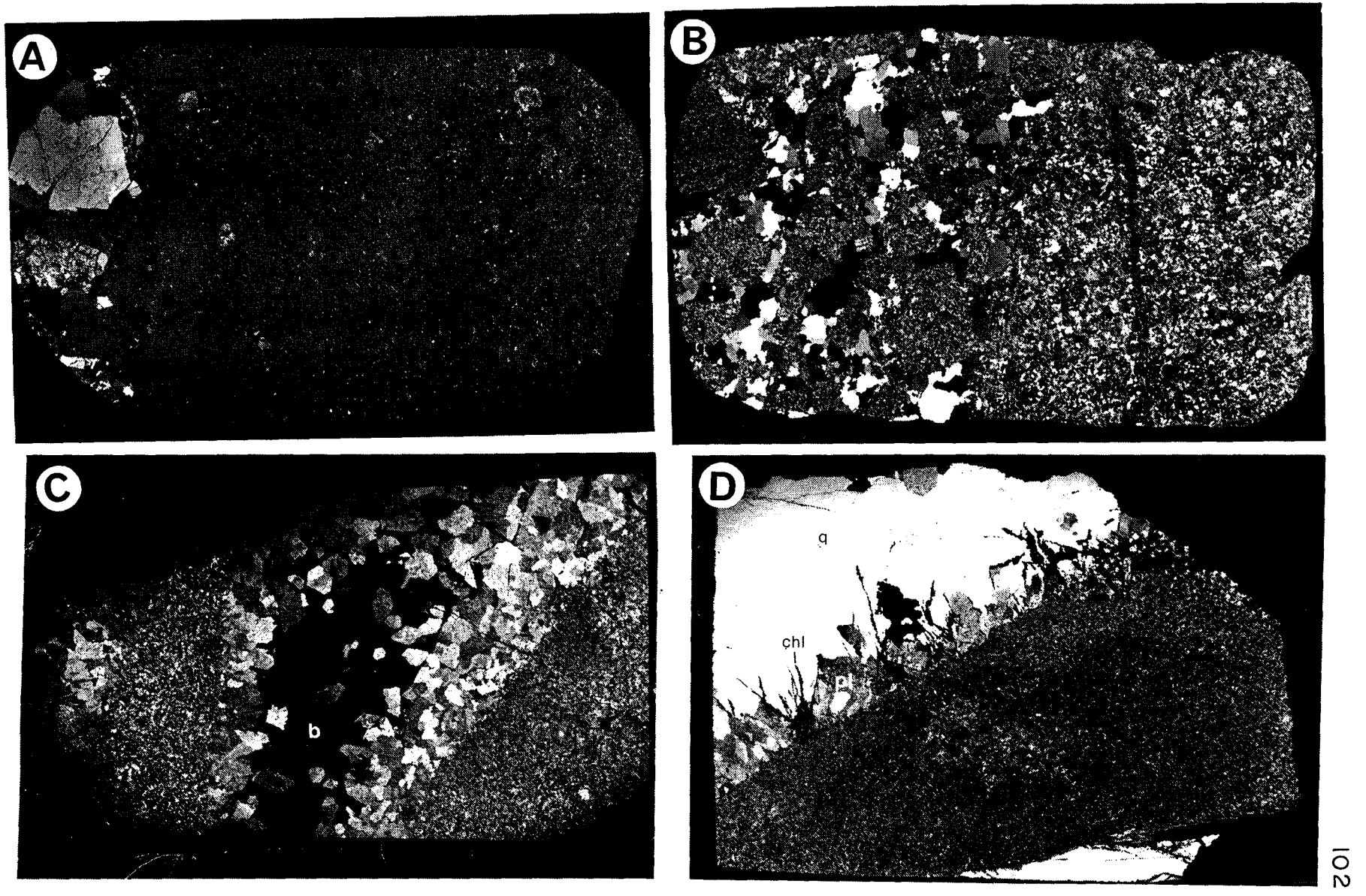

1 cm

constituent occurring as cross cutting 1-3 mm veinlets that clearly postdate the brecciation and sometimes replace plagioclase selvages (Plate 4-3a). Two separate occurrences of fluorite, in association with the potassium feldspar, were identified suggesting that fluorite is also a late phase. There is sulphide mineralization, consisting mainly of coexisting molybdenite and chalcopyrite, but it is only significant (1-5 % combined sulphides) between grid lines 300 and 400 SE.

Within the satellite breccia on the north side of the main breccia body there are two distinctive exposures thought to illustrate the genetic relationship between igneous and hydrothermal regimes. In one example (Plate 4-3b) the breccia matrix grades from a quartz matrix to a felsic matrix of medium-grained felsic material. The contact between the two types of matrix is bounded by subhedral feldspar crystals projecting into the massive quartz matrix. Disseminated crystal aggregates of feldspar occur within the quartz dominated matrix suggesting that the quartz and feldspar coprecipitated in equilibrium. In the other example, quartz and pinkish aplite to granitic material coexist in a dyke-like body that displays textures similar to the previous example (Plate 4-4a). This latter example may be a vein dyke as described by Spurr (1923); as

Plate 4-3a (page 104): Thin pink stringer (dyklet) of K-feldspar cutting brecciated volcanics. In some instances the K-feldspar replaces plagioclase selvages in feldspar-bearing breccias.

Plate 4-3b (page 104): Example of a breccia thought to have formed under processes transitional between hydrothermal and igneous. The yellow area is felsic-aplitic material the dark grey is quartz (Q). Lower left of photo shows volcanic fragments with both aplitic and quartz matrix. In the centre of the photo a quartz stringer cross cuts the aplitic material.

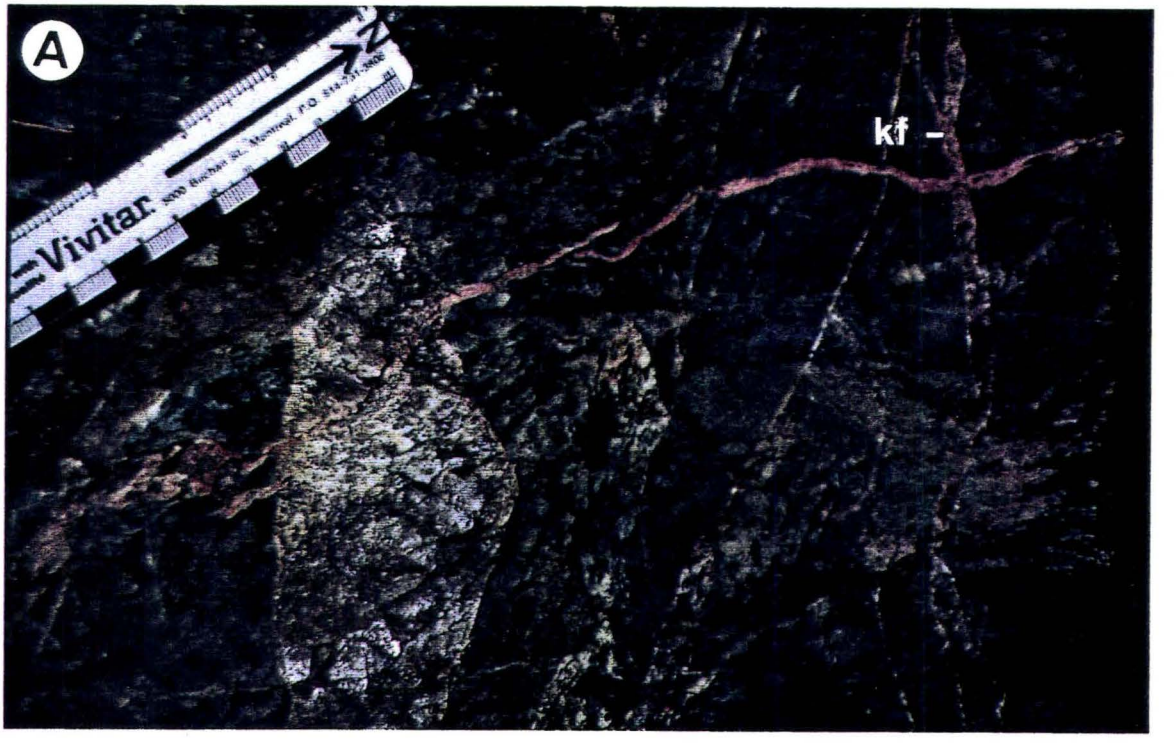
A
kf
Vivitar


B
Q
Vivitar

crosscutting intrusive bodies that display features transitional between igneous dykes and hydrothermal veins. Vein dykes are found in the Climax molybdenite deposits where they typically occur near the intrusive contacts (White, 1981). Shannon et al. (1982) indicated that many vein dykes have unidirectional quartz along their walls and aplitic centres, which suggest a close relationship between comb quartz layers (Moore and Lockwood, 1973), aplite dykes, vein dykes and hydrothermal quartz veins. Based on these, and other, features it is proposed that there was a continuum or coexistence between the igneous and hydrothermal systems represented by the granite and the breccia-vein end members.

4.2 Textural Analysis

4.2.1 Purpose and Definition of Textural Parameters

Field mapping of the breccia indicated that the style of brecciation and several textural features varied systematically throughout the breccia. A useful division could be made between incipient breccia and pervasive breccia (refer chap.2, sec.2.1). Another mappable feature was the thickness of feldspar selvages which varied

gradationally throughout the breccia. Other changes were too subtle and gradual to be usefully mapped in qualitative terms. To better define systematic variations within the breccia a more quantitative survey was conducted and various textural measurements made. The quality of outcrops, in terms of size and visibility of features, did not allow stations to be equally spaced and as a result stations locations are somewhat unevenly distributed (Fig. 4-2). Measurements were taken at 162 stations, providing an average area of about 130 m^2/station.

Because in some cases fragment size varied from meters to centimetres on a single outcrop, a semi-quantitative approach was used to describe the size distribution. At each station a visual estimate of the 25th and 75th percentile fragment size was made as well as an average size estimate. Percentiles were estimated mainly to deal with the problem of characterizing incipient breccias where fragment size ranges were extremely large. With such large size ranges average size is virtually meaningless and therefore, an estimation of the 'average' small fraction and 'average' of the large is more relevant. In the case of incipient breccias the 25 percentile is essentially a measure of the small size fraction which forms the matrix to large undisturbed blocks. The size range was defined to be

Figure 4-2: Map of the breccia body showing the distribution of stations where textural measurements were made on the breccia.

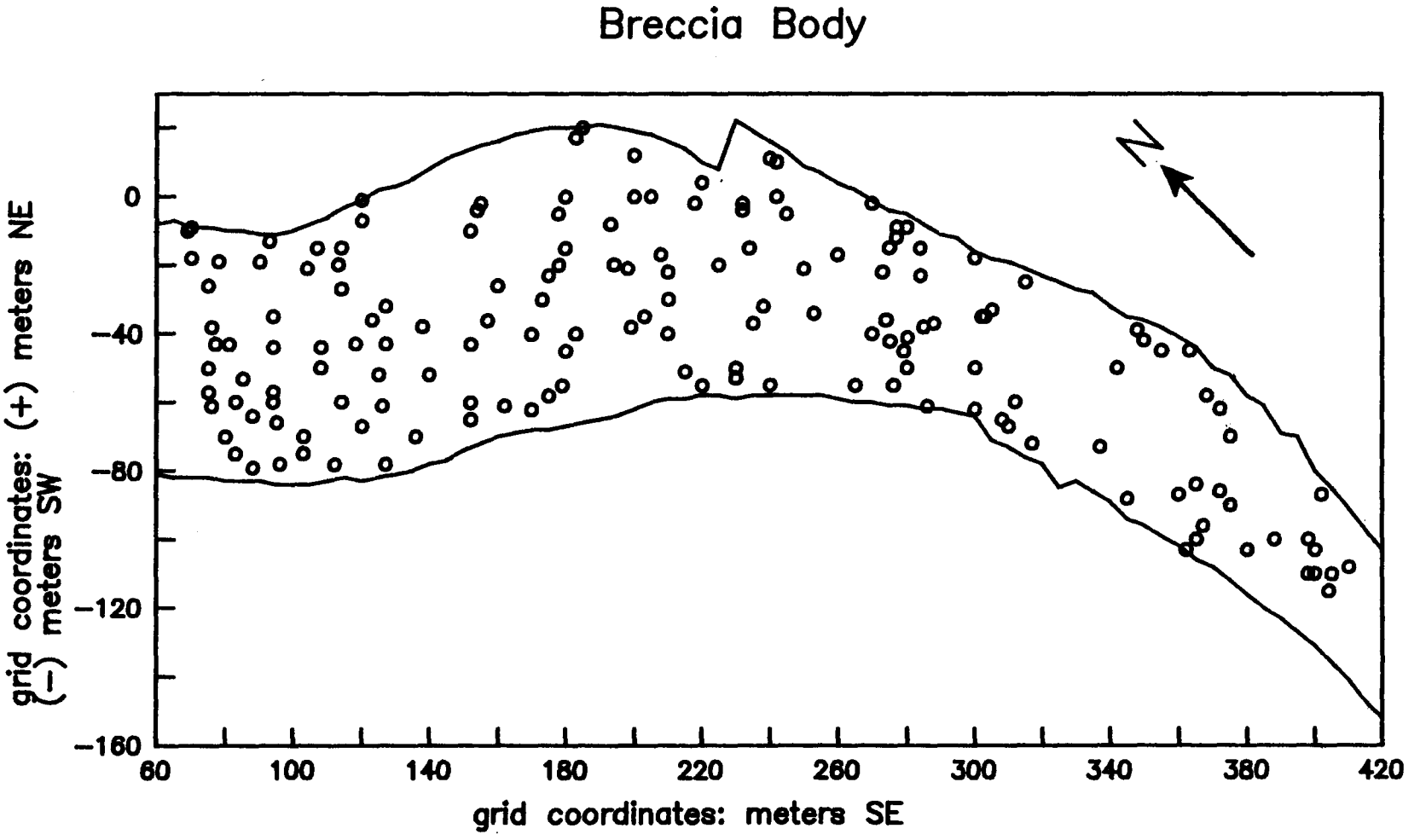
Breccia Body
N
0
-40
-80
-120
-160
60
100
140
180
220
260
300
340
380
420
grid coordinates: (+) meters NE
(-) meters SW
grid coordinates: meters SE

the difference between the 75th and 25th percentile. In some cases the average of the percentiles were used as an estimate of the average fragment size.

The aspect ratio of fragments (longest dimension/shortest dimension) was also estimated to quantify the degree to which tabular shape was characteristic of fragments. For this parameter approximately 10 fragments were measured for the longest and shortest dimension, and an average calculated from which the aspect ratio was determined.

The percentage of matrix was estimated with use of diagrams for visual estimation of the percentage composition of rocks (Shvetsov, 1955). The difficulty in estimating matrix proportions proved to be greatest in areas of incipient brecciation where the small size of individual exposures relative to fragment size limited accurate estimations.

Feldspar selvage thickness was the most easily measured parameter since the selvage usually enveloped the entire fragment. In some localities, however, only part of the fragment perimeters had selvages. In these cases the percentage of a fragment rim consisting of feldspar selvages was also estimated and taken into account in determination of an average feldspar selvage thickness.

The total surface area of breccia fragments was also calculated for each breccia station, mainly to test the hypothesis that surface area might provide some control on the percentage of feldspar and sulphides. An estimation of the total surface area of breccia fragments can be made by assuming that fragments are cubes and that the two dimensional measurement is an effective estimate of the three dimensional fragment. The effect of differing fragment shapes, for example cubes versus tabular shapes, was tested and found to be insignificant relative to other uncertainties in the calculations. A simple derivation of a number proportional to the total fragment surface area is shown below.

Surface Area = (total no. fragments)(average surface area of each fragment)

no. frags. = vol. of total frags./vol. of each frag.

An estimate to the volume of total fragments is taken as 100 % - matrix volume %. If it is assumed that each fragment approximates a cube then the volume of each fragment equals the cube of the average size. The surface area of each fragment is simply the surface area of one side of the cube times 6. Cancellation of

terms yields the expression:

$$\text{Surface area} = [(100 - \%\ \text{matrix})/(\text{avg. frag. size})^2][6]$$

Since the result is only a relative number we can eliminate the constant. From this relationship it is clear that the surface area is most dependent on the squared term, fragment size.

4.2.2 Results of the Textural Analysis

Spatial Variation Results of the textural data have been contoured to show the spatial variation and correspondence of breccia textures to features within and adjacent to the breccia. The size data all illustrate the same general trend of large fragment size and size range to the NW end and along the NE margin of the main breccia body (Fig. 4-3,4). In most areas of large fragment size and large fragment range the brecciation is dominantly incipient. The aspect ratio data indicates an area of tabular fragments in the central and SW portion of the breccia (Fig. 4-5a). The matrix percentage is highest in the central and SW with subsidiary highs at the NW and SE extremes (Fig. 4-5b). The feldspar selvage thickness is greatest in the central and SW portion, but the high extends to the NW along the SW margin

Figure 4-3a: Contour of the average breccia fragment size.

Figure 4-3b: Contour of the breccia fragment size range, defined as the difference between the 25th and 75th percentile fragment size.

Figure 4-4a (page 112): Contour of the 25th percentile breccia fragment size.

Figure 4-4b (page 112): Contour of the 75th percentile breccia fragment size.

Figure 4-5a (page 113): Contour of the average breccia fragment aspect ratio.

Figure 4-5b (page 113): Contour of the percent breccia matrix (ie quartz + plagioclase).

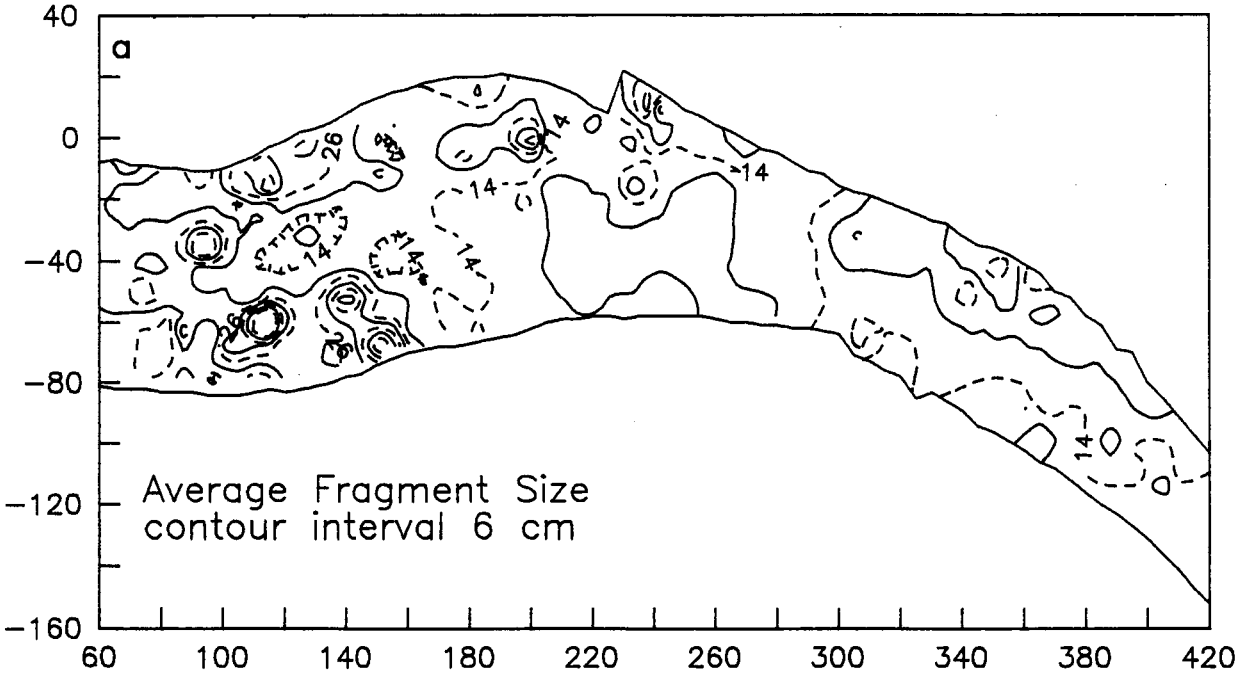
a
Average Fragment Size
contour interval 6 cm
40
0
-40
-80
-120
-160
60
100
140
180
220
260
300
340
380
420

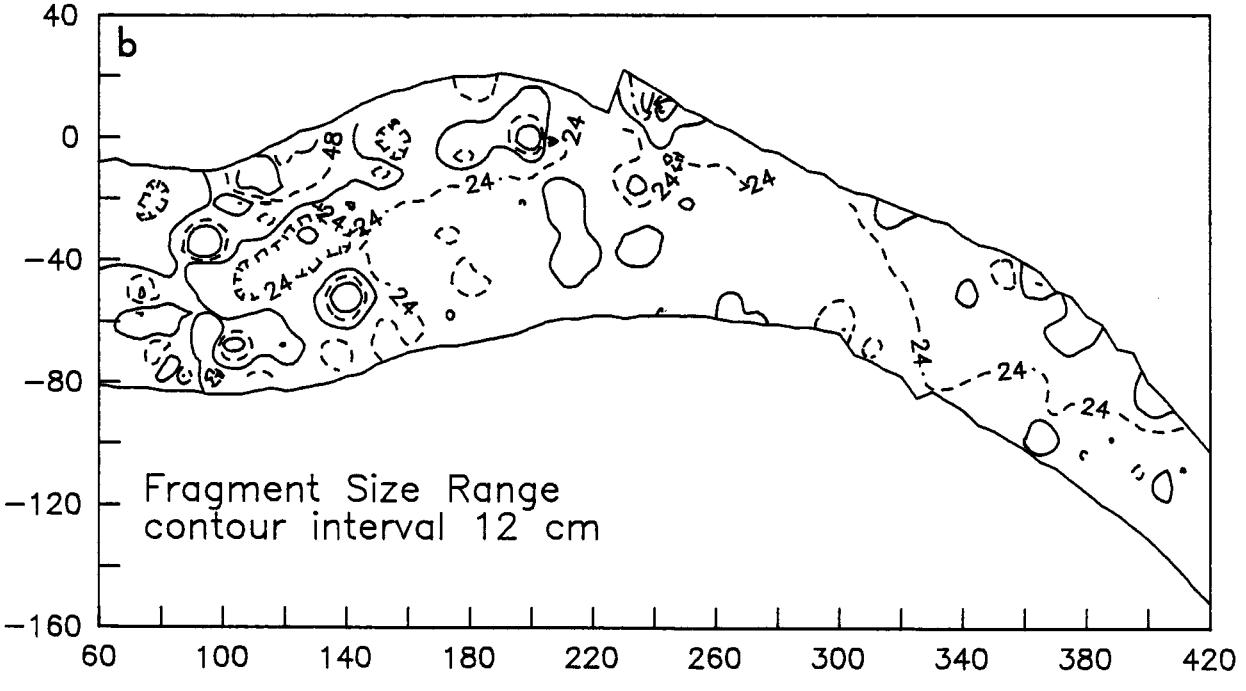
b
Fragment Size Range
contour interval 12 cm
40
0
-40
-80
-120
-160
60
100
140
180
220
260
300
340
380
420

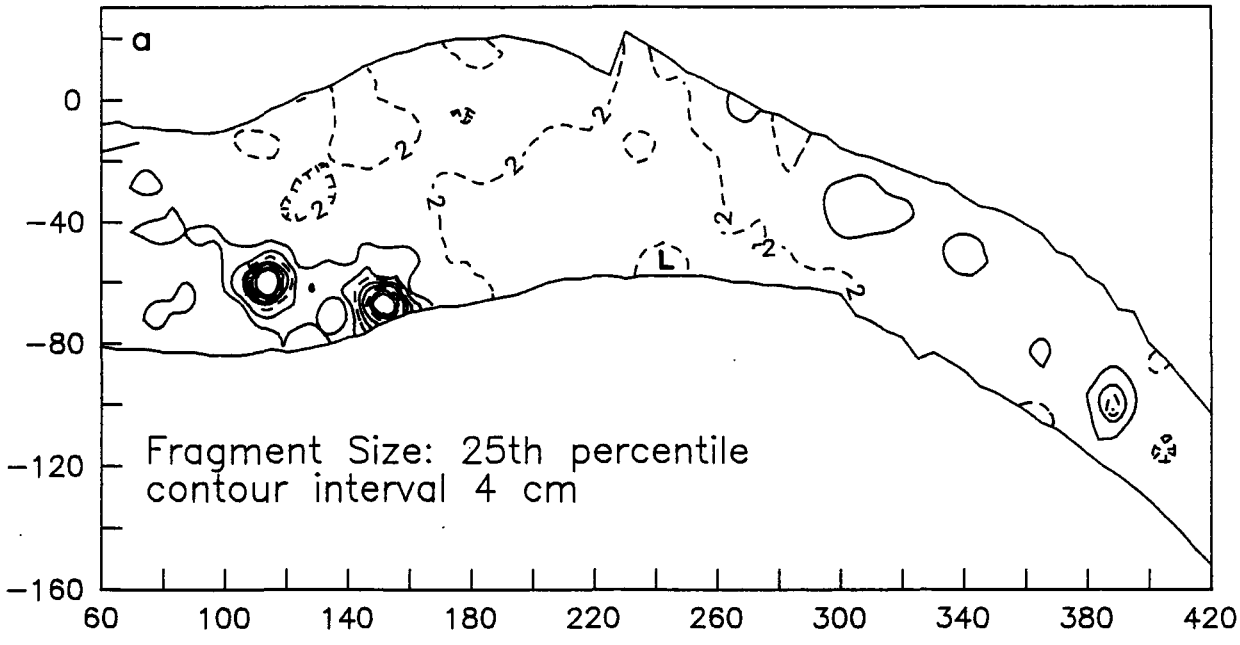
a
0
-40
-80
-120
-160
60
100
140
180
220
260
300
340
380
420
Fragment Size: 25th percentile
contour interval 4 cm

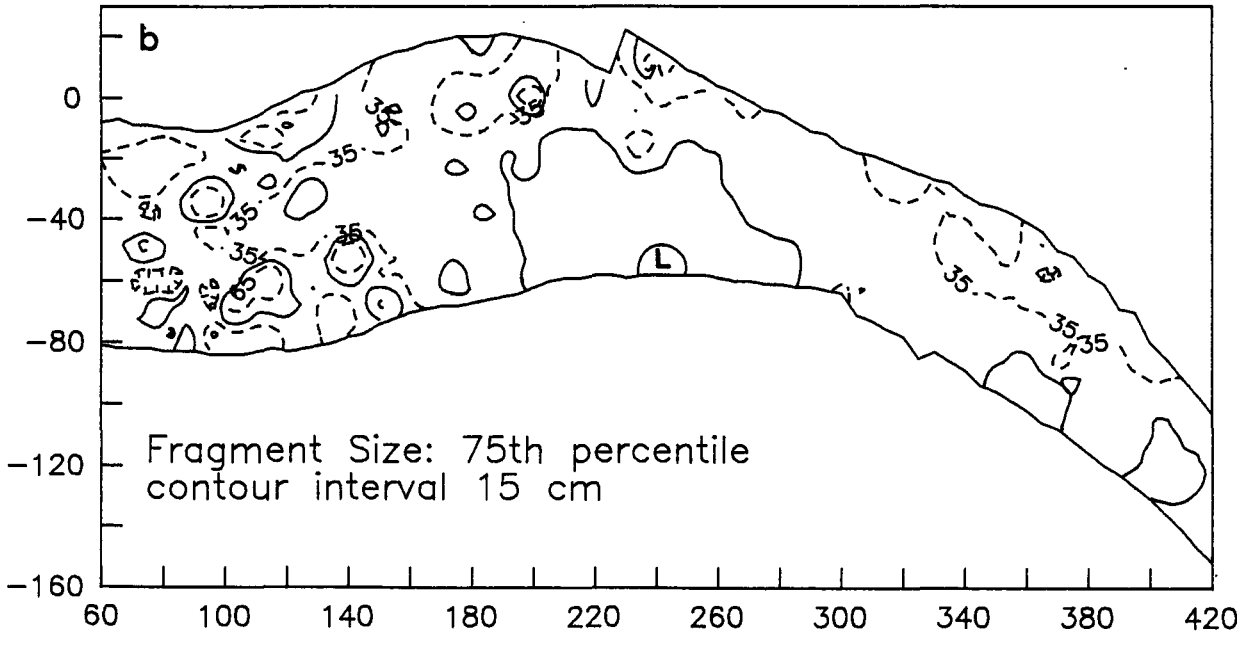
b
0
-40
-80
-120
-160
60
100
140
180
220
260
300
340
380
420
Fragment Size: 75th percentile
contour interval 15 cm

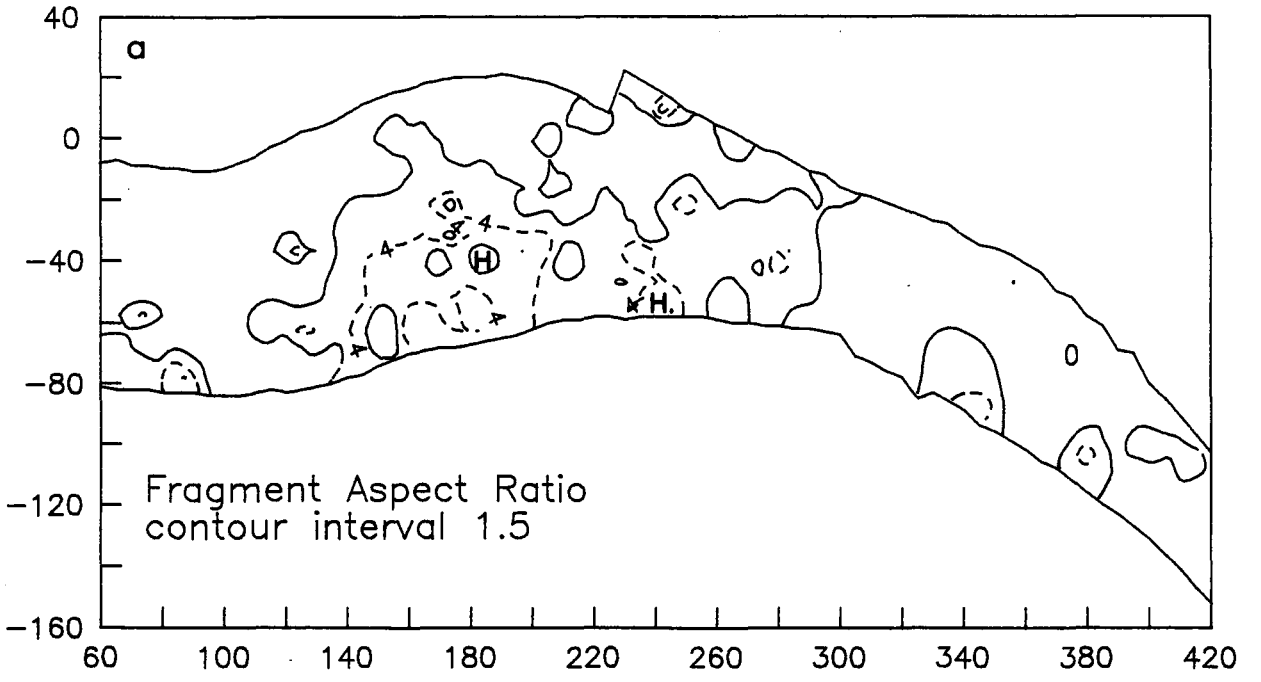
a
40
0
−40
−80
−120
−160
60
100
140
180
220
260
300
340
380
420
Fragment Aspect Ratio
contour interval 1.5

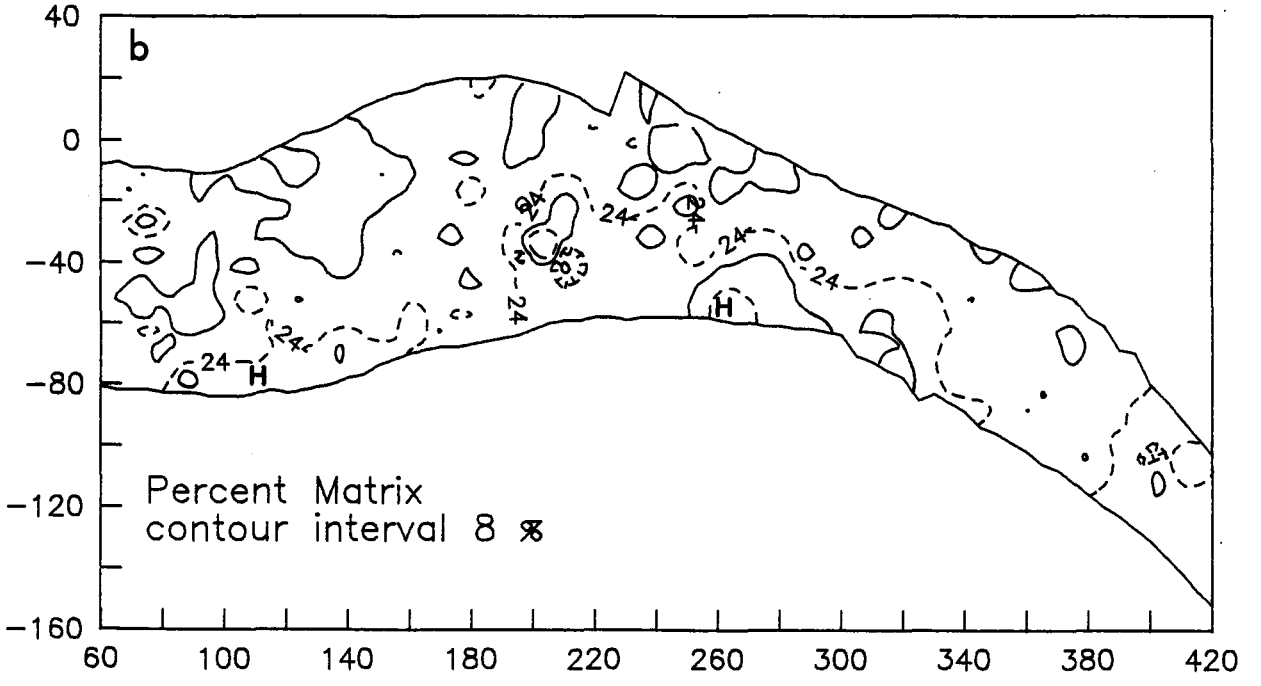
b
40
0
−40
−80
−120
−160
60
100
140
180
220
260
300
340
380
420
Percent Matrix
contour interval 8 %

(Fig 4-6a). The calculated surface area simply shows the inverse of the size data and not surprisingly there is little or no correspondence with the percent matrix (Fig. 4-6b).

A somewhat interpretive designation, termed in situ breccia, is applied to areas having high aspect ratio (≥ 3), good fragment alignment and large fragment size (≥ 20 cm). In situ breccias include incipient breccias, and in addition breccias where fragment are well-aligned and tabular. Tabular well-aligned fragments imply that brecciation was passive and that relative movement of fragments minimal. These implications are also true for incipient breccias and therefore the area designated as in situ implies passive brecciation with very little relative movement of fragments. The intervening areas are termed pervasive breccias and these zones represent extensive fragmentation with some degree of fragment rotation and mixing. The resultant map indicates that the pervasive zone of breccia is largely in the SE end of the breccia with the exception of an isolated area in the NE (Fig. 4-7).

Correlations between breccia textures Relationships between breccia textures are illustrated on X-Y plots, which include symbols differentiating four classes of breccia: mineralized quartz only, mineralized quartz and feldspar-bearing,

Figure 4-6a (page 115): Contour of feldspar selvage thickness.

Figure 4-6b (page 115): Contour of total relative fragment surface area.

Figure 4-7 (page 116): Map of the breccia showing the extent of pervasive (hatchured) and in situ breccia (blank). In situ breccia is defined as those areas with large fragment size and aspect ratio. The filled squares are areas of vein type or breccia and vein associated mineralization. The filled squares with tic marks are areas of mineralized breccia not associated with veins.

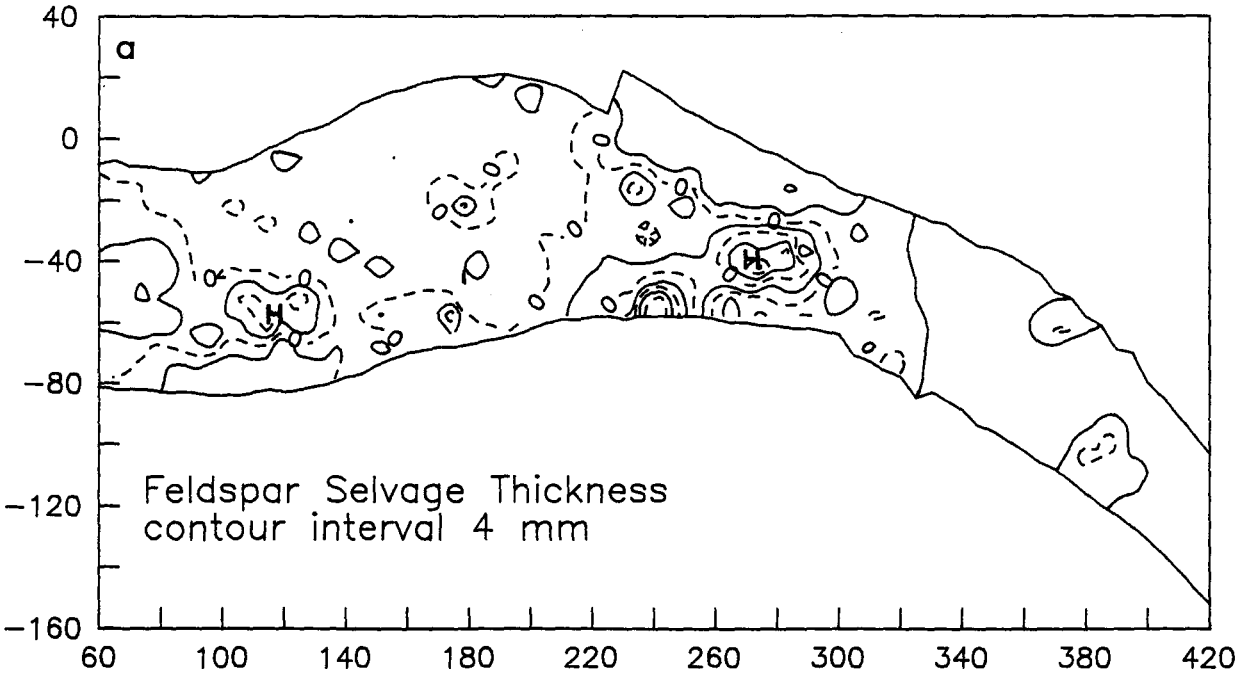
a
40
0
−40
−80
−120
−160
H
H
Feldspar Selvage Thickness
contour interval 4 mm
60
100
140
180
220
260
300
340
380
420

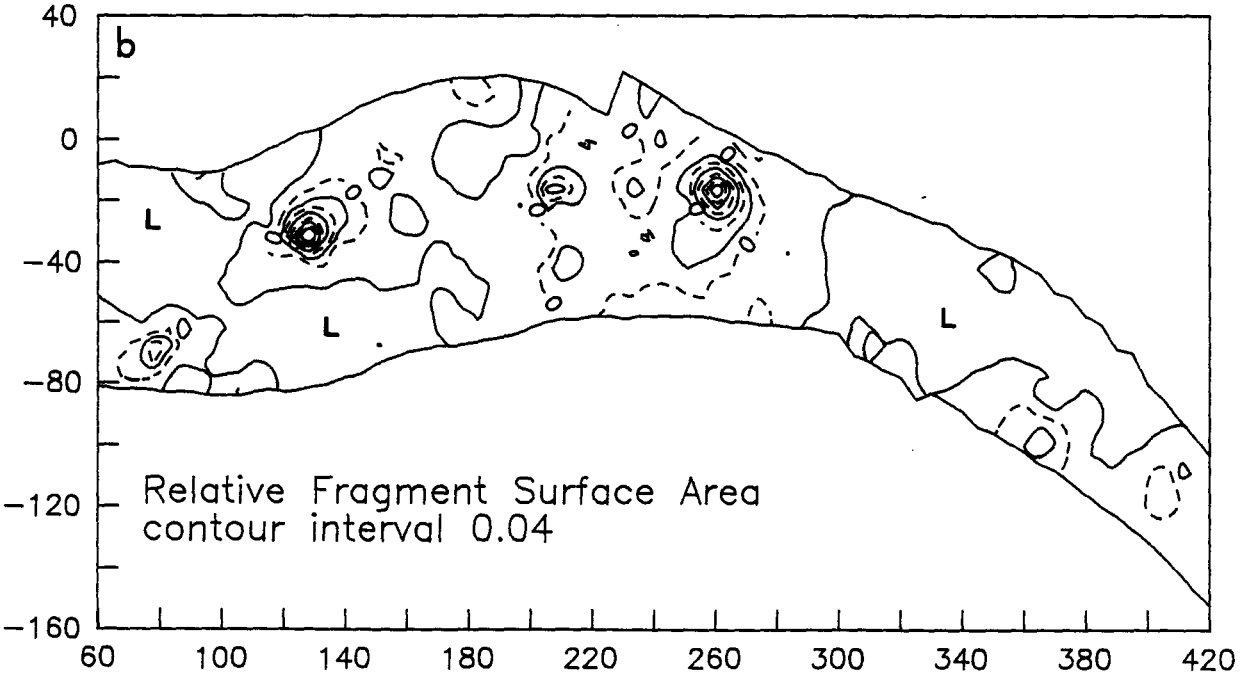
b
40
0
−40
−80
−120
−160
L
L
L
Relative Fragment Surface Area
contour interval 0.04
60
100
140
180
220
260
300
340
380
420

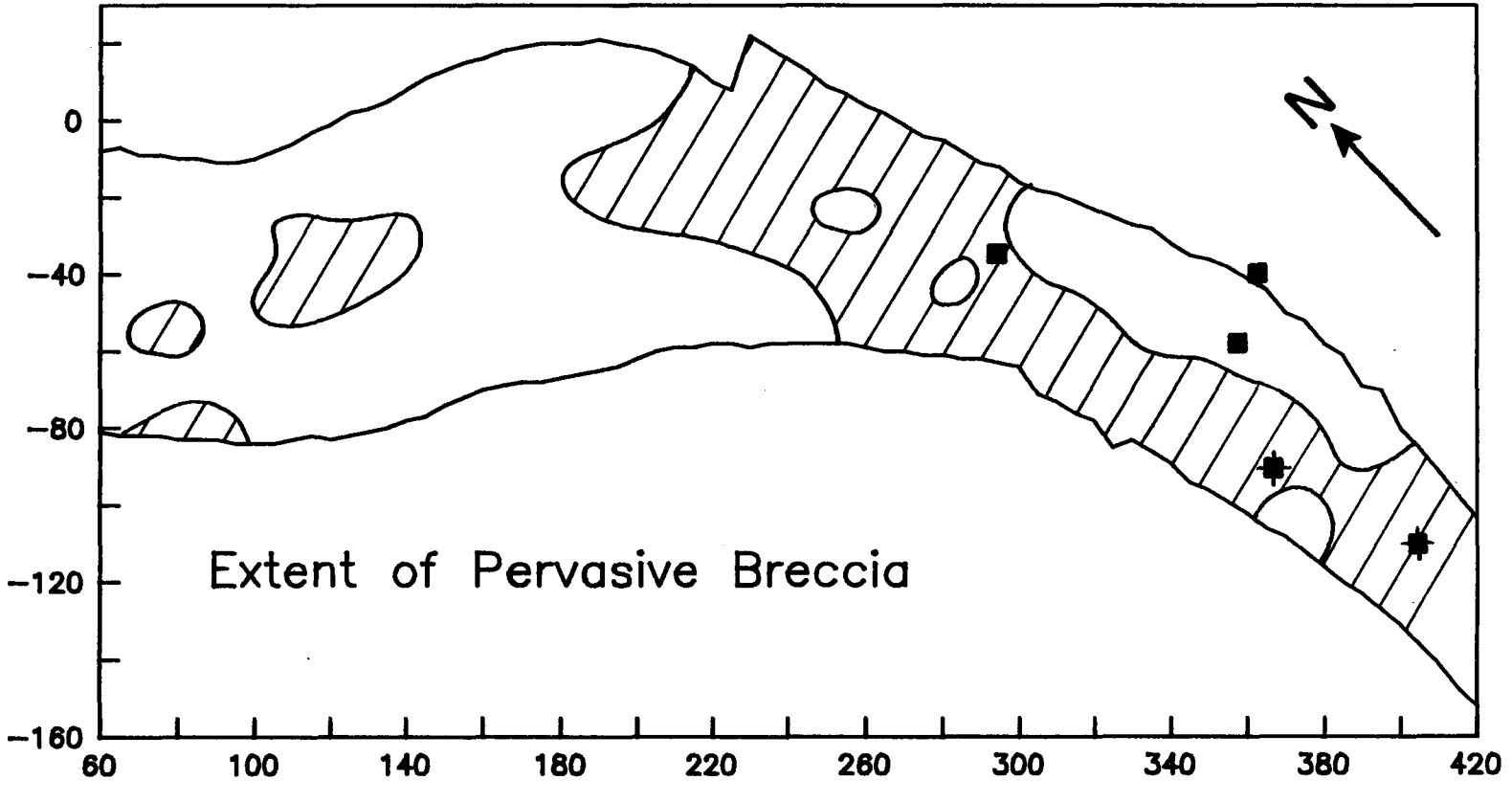
0
-40
-80
-120
-160
60
100
140
180
220
260
300
340
380
420
N
Extent of Pervasive Breccia

unmineralized quartz only, unmineralized quartz and feldspar-bearing. The purpose in this analysis is to test the hypothesis that mineralization of feldspar and sulphides may be correlated with textural aspects of the breccia, which in turn are linked to physical and chemical processes.

The inverse correlation of surface area with fragment size is apparent in figure 4-8a,b. The strong correlation of surface area with fragment size makes it clear that the changes in matrix proportions are of little consequence to fragment surface area. A weak positive correlation may exist between the thickness of feldspar selvage and the proportion of matrix, although it is not necessarily true that a high percentage of matrix coincides with a high feldspar content (Fig. 4-9a). More convincing is the apparent coincidence of greatest feldspar selvage thickness with zones of in situ brecciation (Fig. 4-6a;4-7). The relation between aspect ratio and matrix suggests that the highest aspect ratios are coincident with intermediate matrix proportions (Fig. 4-9b). The aspect ratio versus fragment size exhibits the same pattern (Fig 4-10). This is not surprising since mapping indicated that the most tabular fragments only occurred in breccias of intermediate fragment size (Fig. 4-3;4-5a). The matrix versus fragment size data suggests an inverse relationship between these parameters,

Figure 4-8a (page 118): Relative breccia fragment surface area versus average breccia fragment size. The relative surface area calculation includes the average fragment size term.

Figure 4-8b (page 118): Relative fragment surface area versus the 75th percentile fragment size.

Figure 4-9a (page 119): Feldspar selvage thickness versus the percent breccia matrix.

Figure 4-9b (page 119): Aspect ratio of fragments versus percent matrix.

Figure 4-10a (page 120): Aspect ratio of breccia fragments versus average fragment size.

Figure 4-10b (page 120): Aspect ratio versus the 75th percentile fragment size.

Figure 4-11 (page 122): Percentage of breccia matrix versus the average fragment size.

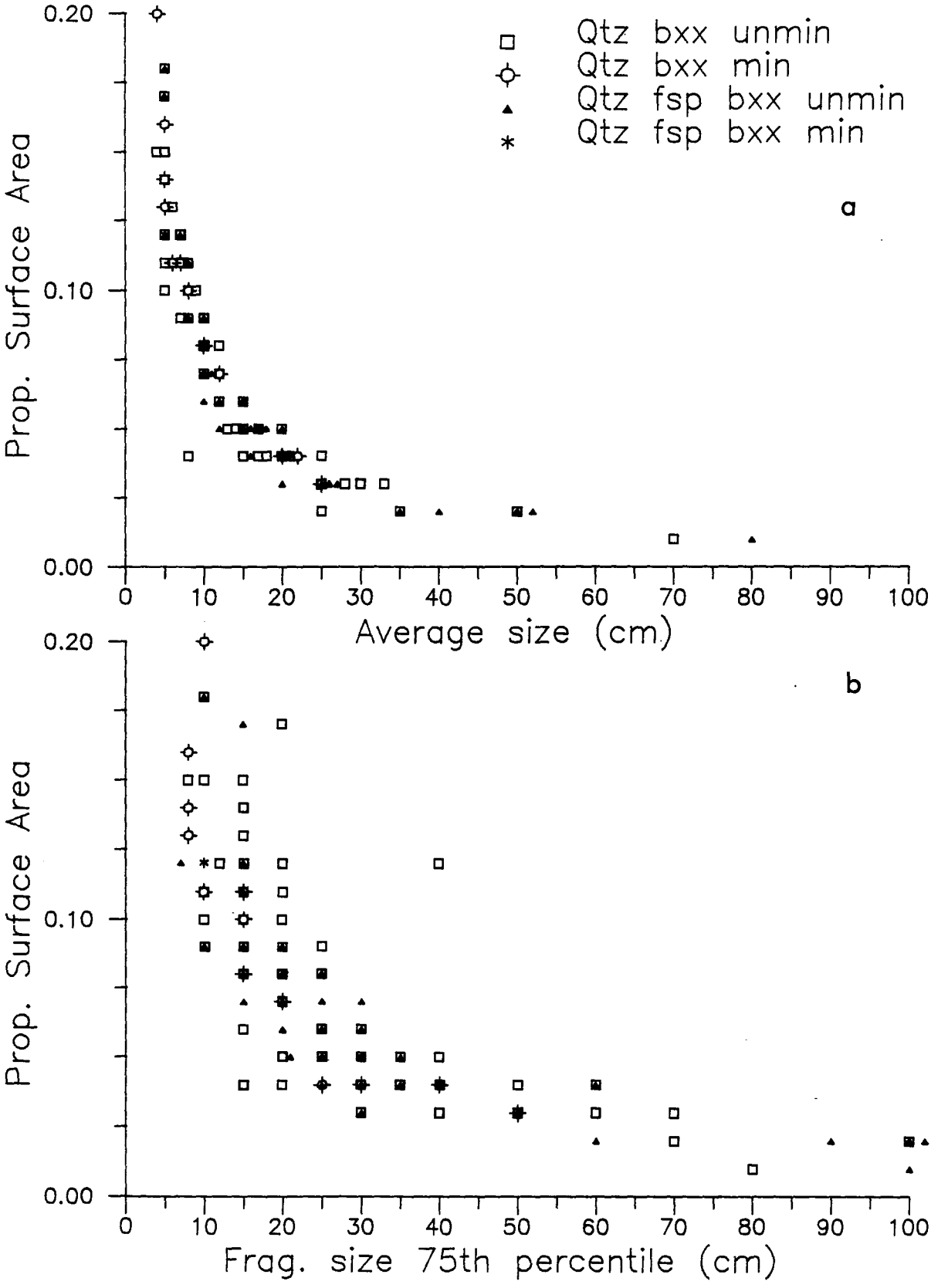
Qtz bxx unmin
Qtz bxx min
Qtz fsp bxx unmin
Qtz fsp bxx min
a
Prop. Surface Area
0.20
0.10
0.00
0
10
20
30
40
50
60
70
80
90
100
Average size (cm)
b
Prop. Surface Area
0.20
0.10
0.00
0
10
20
30
40
50
60
70
80
90
100
Frag. size 75th percentile (cm)

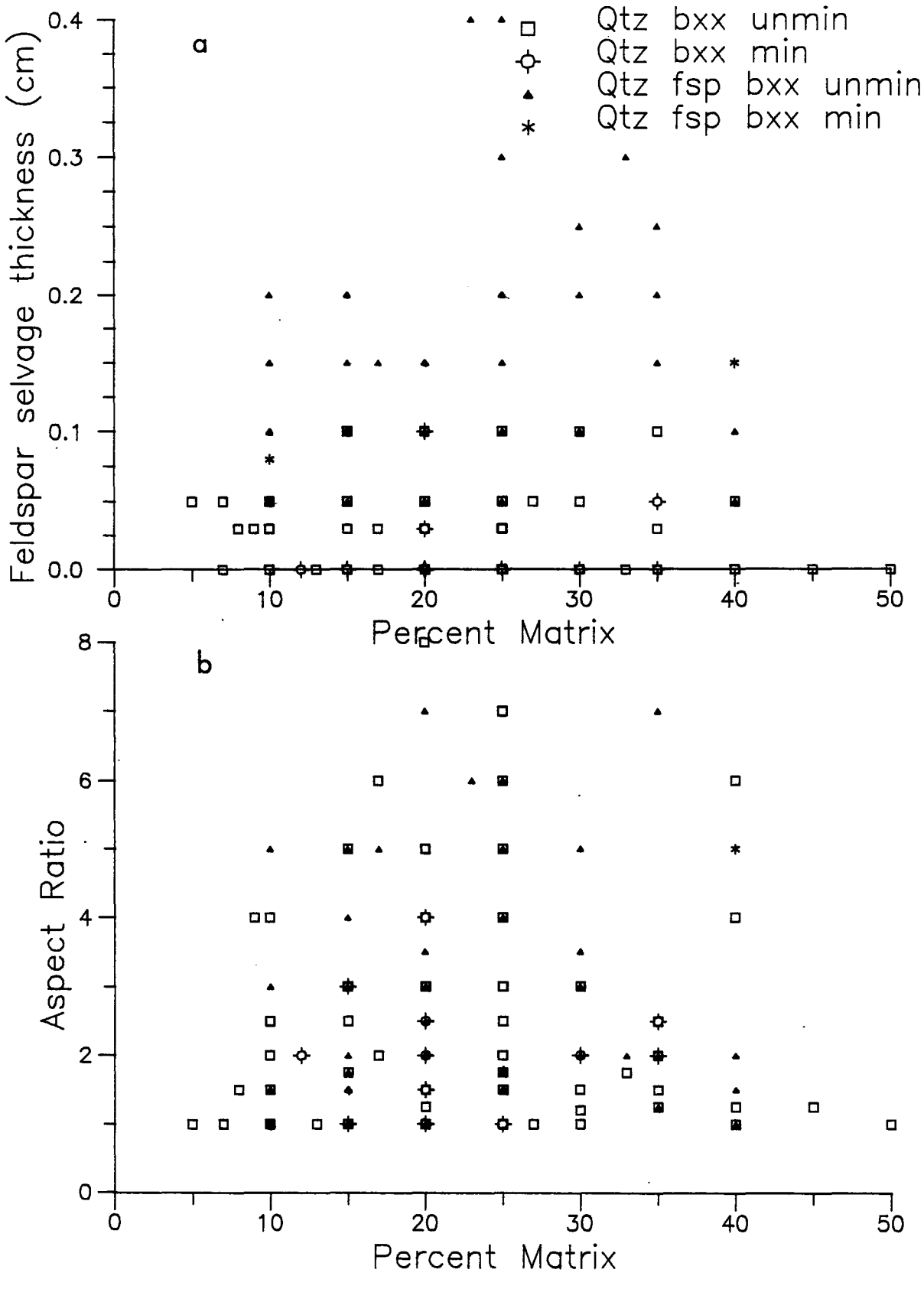
a
Qtz bxx unmin
Qtz bxx min
Qtz fsp bxx unmin
Qtz fsp bxx min
Feldspar selvage thickness (cm)
0.4
0.3
0.2
0.1
0.0
0
10
20
30
40
50
Percent Matrix
b
Aspect Ratio
8
6
4
2
0
0
10
20
30
40
50
Percent Matrix

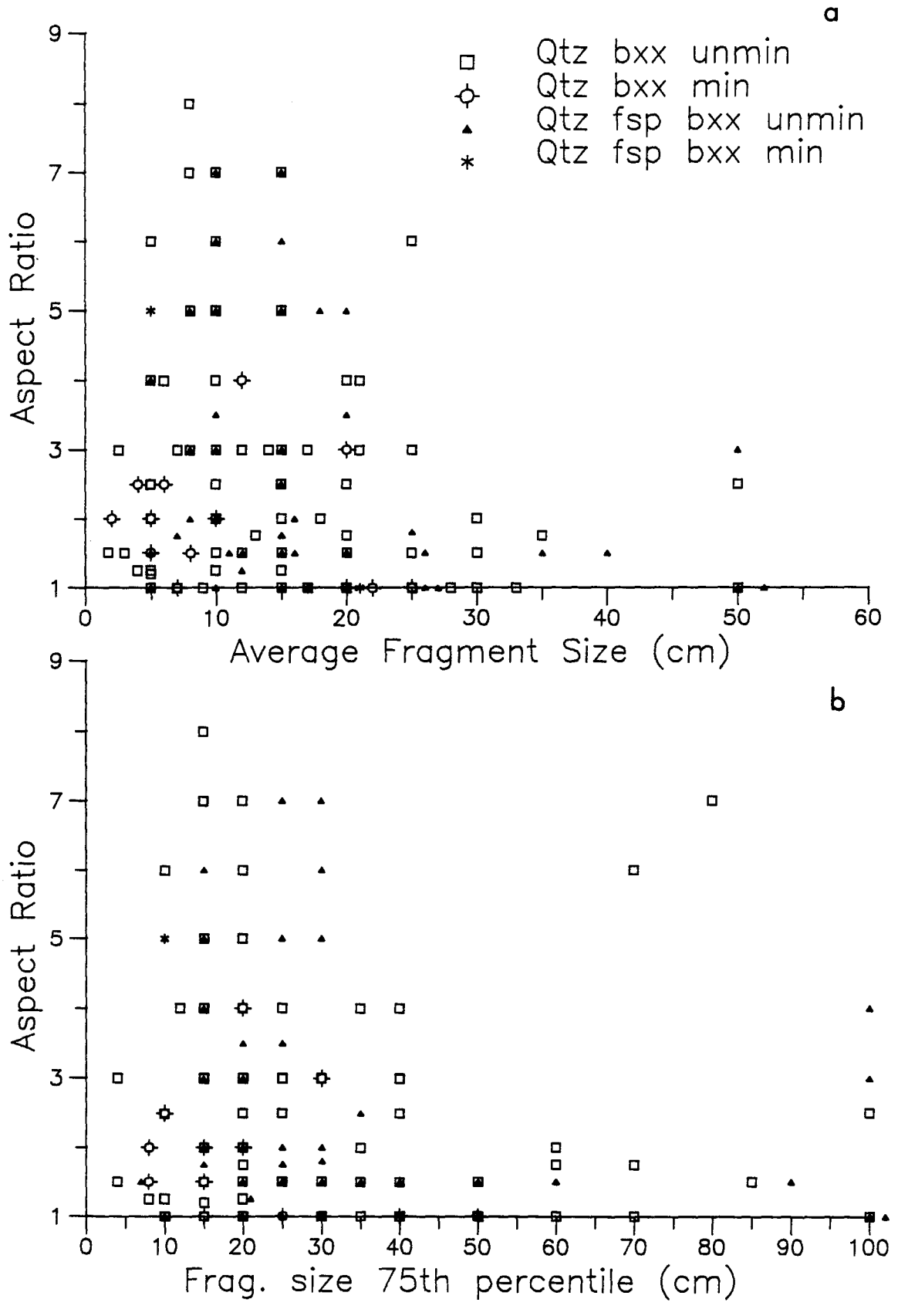
a
Qtz bxx unmin
Qtz bxx min
Qtz fsp bxx unmin
Qtz fsp bxx min
Aspect Ratio
Average Fragment Size (cm)
b
Aspect Ratio
Frag. size 75th percentile (cm)

again consistent with reference to intuitive observations made in the field (Fig. 4-11)

In addition to measuring the aspect ratio, the orientation of tabular fragments was also measured whenever an outcrop displayed a consistent alignment of fragments. The results of this analysis show a strong preferred orientation of tabular fragments at 105^0, dipping steeply to the north, and a smaller group striking 060^0. This orientation is conspicuously close to that of joint set 2 at 116/83 NE, and may be an indication of the genetic link between joints and breccia (Fig. 4-1).

Relationship of mineralization to breccia textures The mineralized occurrences within the breccia are divided into two types: those in close association with breccia-hosted veins and those entirely associated with brecciation. In the former category mineralization is actually hosted in both breccia and in the adjoining vein or veins, but in the latter type there is no spatial association with veins. The relationships between texture and mineralization are most clearly defined for the mineralization associated with mineralized breccia and more difficult to categorize for mineralized breccias associated with veins. The clearest relationship is that strong mineralization occurs in zones where little or no feldspar is apparent (Map 2;Fig.4-6a;4-

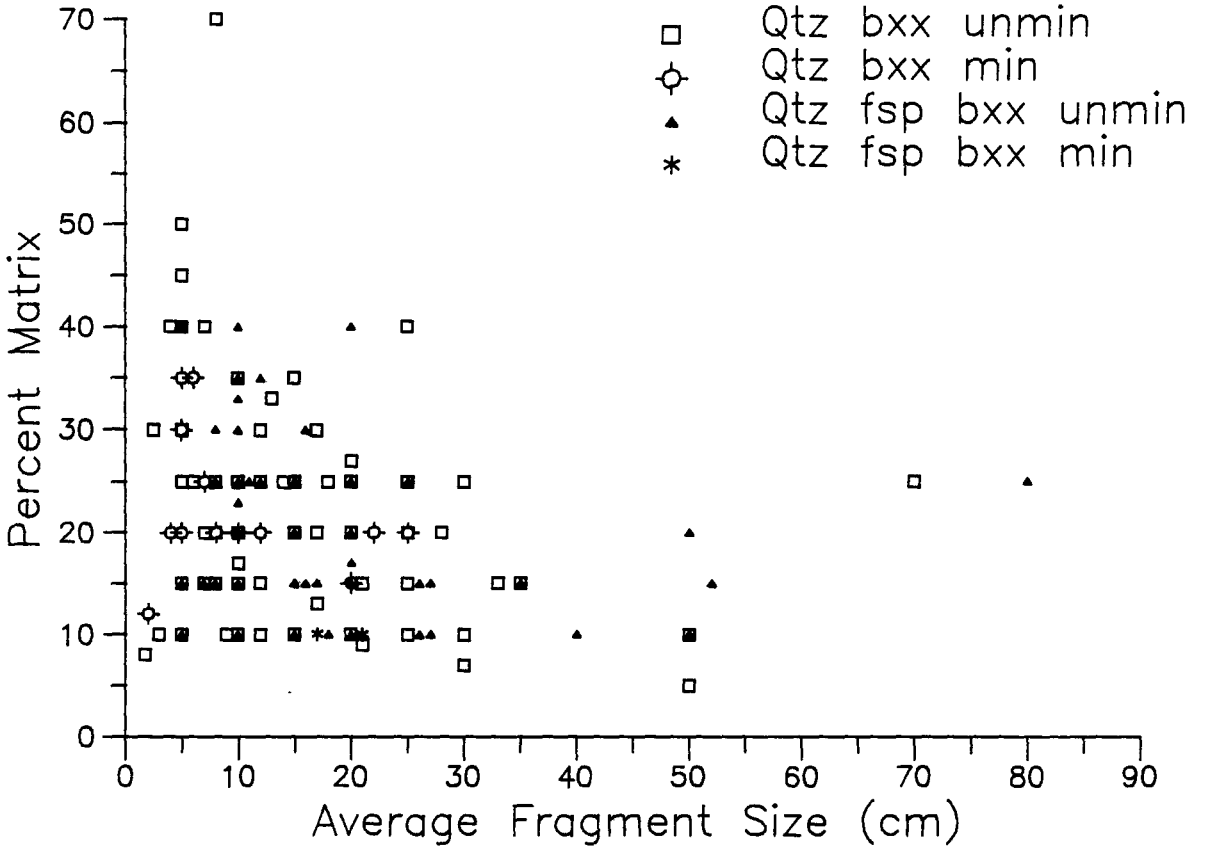
Qtz bxx unmin
Qtz bxx min
Qtz fsp bxx unmin
Qtz fsp bxx min
Percent Matrix
0
10
20
30
40
50
60
70
Average Fragment Size (cm)
0
10
20
30
40
50
60
70
80
90

7). Mineralization is also associated with well-sorted breccias with small fragment size (Fig.4-8 - 4-11). It follows from earlier discussion that because areas of small fragment size have low aspect ratios, the mineralized breccias are often characterized by fragments with low aspect ratios. It also follows that because the fragment size is small the mineralized breccias have large surface areas (Fig.4-8a,b). With the exception of the two vein-related mineralized breccias on the NE flank, mineralized zones appear to coincide with those areas termed pervasive breccias (Fig.4-7).

4.3 Models of Breccia Formation

The formation of intrusion-related hydrothermal breccias usually invokes essentially two classes of models. The first class attribute brecciation to a process where by exsolved hydrous fluid derived from saturation of a magma causes pressure leading to eventual failure and brecciation of roof rocks. The other class argues that a fluid filled void is created between the intrusive and overlying roof rocks and that brecciation proceeds by a process of gravitational slumping. In the subsequent analysis of these two basic models, evidence will be provided that generally

favours the former explanation for the Temagami breccia.

4.3.1 Void Related Models

In the model proposed by Norton and Cathles (1973) a void is produced by expansion of exsolved magmatic water trapped beneath a crystalline rind or carapace situated at the top of a pluton. Once failure occurs the pressure drops, causing the intrusive to crystallize. Pinching of the lower portion of the void by viscous magma would occur and the walls collapse to fill the void, thereby forming a breccia. In a comparable model the hydrous fluid atop the intrusive might be corrosive enough to cause extensive dissolution and subsequent volume reduction of the overlying rocks thereby creating a void (Locke, 1926; McKinstry, 1955; Sillitoe and Sawkins, 1971; Mills, 1972). Magma withdrawal as a means to create a void has also been suggested and in this case brecciation proceeds in a similar manner to the process mentioned above (Perry, 1961; Blecha, 1974; Atkinson et al., 1982).

4.3.2 Models Related to Resurgent (Second) Boiling

Burnham (1979) describes a model applicable to shallow emplacement and solidification of felsic magmas at depths in the order of 2-8 km. Depending on the water content, magmas will rise to a depths of about 3 km before reaching the saturated solidus at which point the magma body begins to solidify from the outside producing a solid, largely impervious rind or carapace. Subsequent cooling and differentiation leads to exsolution of a hydrous fluid that concentrates in the cupola or apical regions of the intrusive. The reaction so described is referred to as second or resurgent boiling, and is expressed by the relation:

H_2O-saturated melt --> crystals + H_2O hydrous phase

This transformation results in a net increase in volume, which can be expressed in terms of energy as $P\Delta V$ energy (Burnham, 1979). If the initial water content of the magma is high enough the energy supplied by this reaction is sufficient to cause brittle failure of roof rocks to depths of less than 8-10 km (Burnham, 1979, 1981, 1983; Burnham and Ohomoto, 1980). This initial failure may result in the development of a myriad of steep, systematically oriented fractures and possibly brecciation. This initial failure

results in decompression, causing further exsolution of hydrous magmatic fluids and the expansion of previously exsolved hydrous phases. This sudden exsolution of hydrous phases causes the residual melt to move below the saturated solidus resulting in pressure quenching of the magma. The amount of energy released during decompression can be greater than that produced by resurgent boiling. This energy is expended by the expansion of fluids and gases causing brecciation, propagation of both new and pre-existing fractures and gas streaming, whereby fragmental material is transported upward in a fluidized suspension. Fractures formed during initial failure may be extended and widened to such an degree as to allow magma to intrude forming intramineral dykes (Wilson, 1978).

The formation of sheeted fractures tangential to the breccia margin may be produced by either initial failure or by the process of decompression (Sillitoe, Sawkins, 1971; Knutson, 1979). If there is an instantaneous drop in fluid pressure sheeted fractures may arise by decompressive shock (Knutson, 1979; Allman-Ward et al., 1982), and spalling and collapse might follow. The latter process is similar to the void-related models except that the driving force causing failure is fluid overpressure while in the other models gravitational forces are thought to be largely responsible

for failure and collapse.

4.4 Genesis of the Temagami Breccia

4.4.1 Comparison of Features To Other Examples

There has been several attempts at classifying intrusion-related hydrothermal breccias based on genetic criteria. Agreement has been elusive, possibly because the various models are not fundamentally different and one or all of these processes may have been important in the creation of different breccia types. Sillitoe (1985), in his overview of ore-related breccias, divided the magmatic-hydrothermal breccias into those associated with porphyry systems and those not. Under this scheme he noted several qualitative distinctions between these types, the most definitive of which are summarized in table 4-1. With respect to deposit type the Temagami breccia does not closely fit the porphyry model since it lacks the typical pervasive and zoned alteration and fracture controlled mineralization. In terms of geometry and shape the Temagami breccia is closest to the non-porphyry system since it is effectively a single regular shaped pipe or body, and is in the appropriate size range. The contact relationships at

Temagami vary from sharp to gradational and thus are ambiguous with respect to classification. As to whether or not there are sheeted contacts, the analysis of jointing indicates that in a strict sense the margins are not sheeted because their density is not intensified in a regular way within 1-5 m of the actual margin (Sillitoe, 1985). The fragments in the Temagami breccia are exclusively angular and often tabular. Rock flour is totally absent. These textural features favour the non-porphyry system classification. Alteration in the Temagami breccia is best termed K-silicate (refer chap.5), which favours the porphyry classification. Breccia formation appears to coincide with the mineralization event, a feature perhaps compatible with a porphyry system. In terms of ore potential previous failed attempts at mining this deposit suggest the deposit is non-economic, another feature consistent with a non-porphyry classification. Even though the Temagami breccia does not fit all of the criteria, it seems most reasonable to classify the system as a member of the non-porphyry group.

A feature of the Temagami breccia common to other magmatic-hydrothermal breccia systems is the existence of porphyritic dykes, plugs and irregular bodies within the breccia. In many of these occurrences the timing of dyke

Table 4-1

Classification of breccia into non-porphyry or porphyry type (Modified from table 10 of Sillitoe, 1985)

Feature	Non-Porphyry System	Porphyry System
ore dep type	isolated pipes	porphyry
geometry	single or multiple pipes	single or multiple pipes, irregular bodies
diameter	50-300m locally >1000 m	up to 200 m
fragments	angular-subrounded	angular-rounded, tabular uncommon, clast supported normal
rock flower	local <30%	common ,50% often heterolithic, more vertical movement, streaming
other	sheeted contacts, shingle breccia, exfoliated frags	same but exfoliated frags uncommon
Alteration	sericite common	K-silicate common
Timing	premineralization	pre-intermin-eralization
contacts	sharp contacts	gradational con-tacts

intrusion appear to vary within a single deposit and may occur before, during and after brecciation (Sillitoe and Sawkins, 1971; Wilson, 1978; Warnaars, 1985). In Burnham's model such dykes might be derived from the upper or interior portions of the associated intrusive body. In the case of Temagami these porphyritic rocks have a less evolved geochemical signature and therefore it is likely the dyke magmas were derived from deeper portions of the granitic magma chamber (refer chap.6). Emplacement of these dykes (intramineral dykes; Wilson, 1978) is facilitated by high fluid pressures that allow significant opening of pre-existing fractures to allow emplacement of viscous magma (Burnham, 1979). In Temagami the dyke paralleling the breccia tongue on the SW margin of the main breccia body may be of this origin since it appears to have taken advantage of an existing weakness, the breccia itself.

An interesting similarity exists between the textures in the Temagami breccia and in the breccia at the Chadbourne mine at Noranda, Quebec. The occurrence of incipient breccia grading into pervasive breccia is much like that observed at Temagami, as is the preferential occurrence of mineralization in the pervasive breccia, a feature indicating a correlation with fragment size and shape (Walker, 1982). At Chadbourne, as at Temagami, tabular

fragments are of a consistent orientation and this attitude corresponds to a system of parallel fractures that cut the breccia (Fig. 4-1).

A great deal of similarity between the Temagami breccia and other examples of magmatic-hydrothermal breccias is apparent. In addition there are other features present in Temagami that explicitly link breccia formation to the Strathy-Chambers batholith. In general terms the close proximity of the breccia to the intrusive is important. The porphyritic dykes are likely derived from the intrusive and these have a strong spatial and possibly genetic relation with the breccia. Although mineralization in the form of chalcopyrite and molybdenite is sparse in the intrusive it is important that both the breccia and intrusive are mineralized. Late stage mineralization of fluorite and K-feldspar found in the breccia may also be significant as both these minerals are commonly associated with late stage fluids of magmatic origin. Intense alteration to biotite noted to the north end of the breccia near the contact may also be significant. For example, in the Rio Blanco, Chile (Warnaars, 1985), biotite and K-feldspar is a common alteration assemblage close to the intrusive contact. The previously discussed occurrence of the vein dyke and the aplitic breccia matrix is important evidence supporting the

intrusive-breccia affinity. Lastly, implicit in all the intrusive related breccia models is the concept that the exsolved magmatic fluid, which generates the breccia is derived as an extension of magmatic differentiation. As discussed in chapter 6, the increasingly differentiated character of the Strathy-Chambers batholith with proximity to the breccia supports this concept.

4.4.2 Processes and Chronology of Breccia Formation

Before developing any model of breccia formation it is necessary to review constraints established by features of the Temagami breccia. One of the most important observations is that the breccia fragments are exclusively angular and often display characteristics that indicate minimal net displacement or rotation. Because of the lack of rock flour and the angularity of fragments it is considered unlikely that there was significant vertical transport of fragments by processes such as gas streaming. Another important relationship noted was that larger blocks of basalt were seen in the process of brecciation where fragments appeared suspended or frozen before the fragmentation had proceeded extensively (Plate 2-3,4). In a similar manner well-aligned tabular fragments, completely

supported by matrix, gave the impression that the matrix formed almost immediately after fragmentation, before the fragments settled or became disrupted by turbulent flow (Plate 2-2a,b). Another factor is the high proportion of matrix in some areas, in particular the breccia tongue and satellite breccia to the SW of the main body (Plate 4-4b). High matrix proportion indicates that fluid pressures were great enough to maintain significant open space to produce these matrix-dominated breccias, and to allow for the intrusion of porphyritic intramineral dykes. Lastly, it is necessary to explain the fact that both joint sets appear to precede and postdate solidification of the breccia.

The mechanisms that created the Temagami breccia are believed to follow closely the model proposed by Burnham (1979). The depth of breccia formation cannot be well constrained, but based on Burnham's conclusions it was probably less than 8-10 km, a figure in agreement with Brons, (1989) who estimated a depth of 7.5 ± 3.5 km (2 ± 1 kb) for the emplacement of the Strathy-Chambers batholith. The geological circumstances, however, indicate that the breccia does not lie above the structurally highest portion of the Strathy-Chambers intrusive, but rather on a shallow dipping margin (Fig. 4-12). This does not provide a problem for the Burnham model but, as stated by Burnham (1985), it

is not consistent with the model of Norton and Cathles (1973) where the energy for brecciation is entirely gravitational. In the case of breccias lying on the margins of an intrusive Burnham suggests that it may be localized by zones of weakness. Without accurate knowledge of the underlying morphology of the intrusive-volcanic contact it is difficult to surmise the possible location of a fluid trap. The contact relationship with elevation contours seems to indicate the intrusive, in the area of the intrusion breccia, dips very shallowly south eastward. Nearest the breccia the contact reveals what may be a three dimensional bulge or cupola (Map 1). This apparent geometry is compatible with the breccia model and also may explain the localization of intrusion breccia, where a flat or shallow contact would cause the roof rocks to founder (Fig 4-12). Furthermore the geometry and distribution of volcanics and intrusive may have differed, at the time of brecciation, from the present configuration. The intrusive contact adjacent to the breccia may initially have been the apex of the intrusive, but subsequent tectonics or continued intrusion may have altered the morphology to the present configuration.

Regardless of the location and form of the fluid trap, it is proposed that resurgent boiling accompanied

Plate 4-4a (page 135): Possible vein dyke or igneous-hydrothermal breccia. Similar to example in plate 4-3b but here the body is dyke-like in form. Quartz, felsite (F) material and fine-grained granitic rock (lower right hand corner) appear to be have crystallized in equilibrium.

Plate 4-4b (page 135): Satellite breccia on the SW side of the main breccia body, that has a very high proportion of quartz matrix.


A
F
Vivitar
N

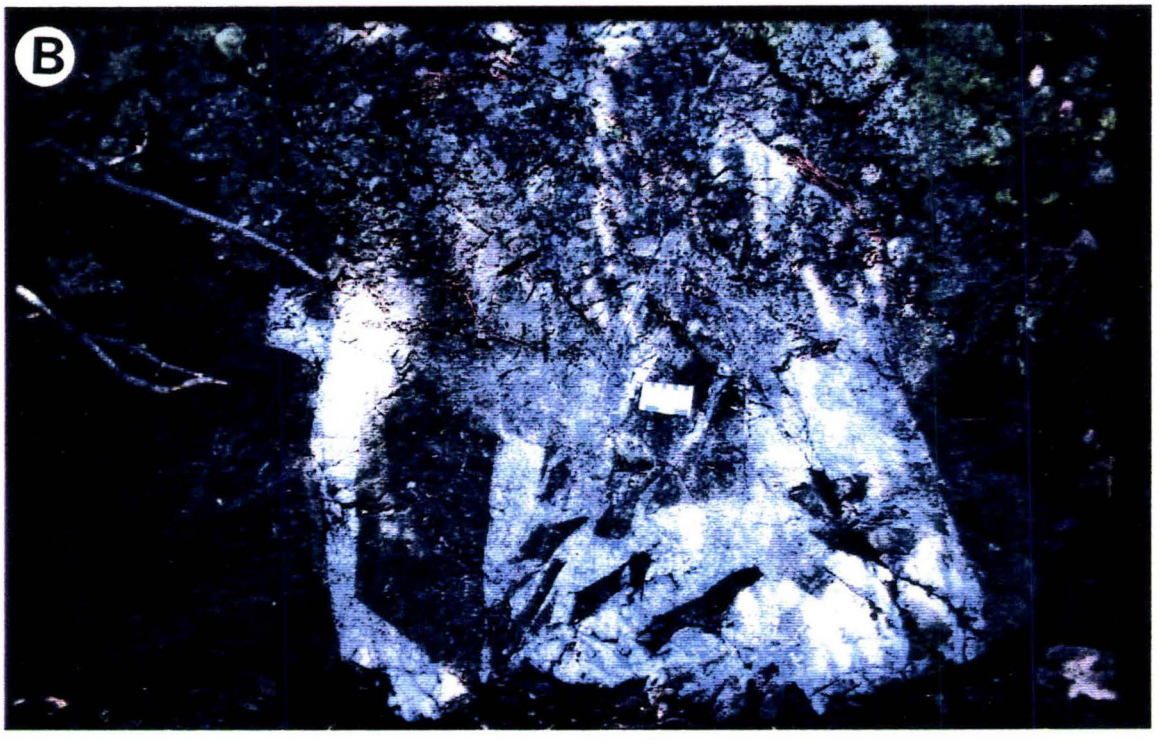
B

Figure 4-12: Schematic NE-SW cross section, looking NW, through the breccia. Features noted in the text, such as the satellite breccias, veins dykes, porphyry and granitic dykes, are shown. Vertical scale is approximately 2X horizontal. Subvertical lines represent joints. Not shown are the great number of quartz veins that occur primarily on the southwest side of the breccia.

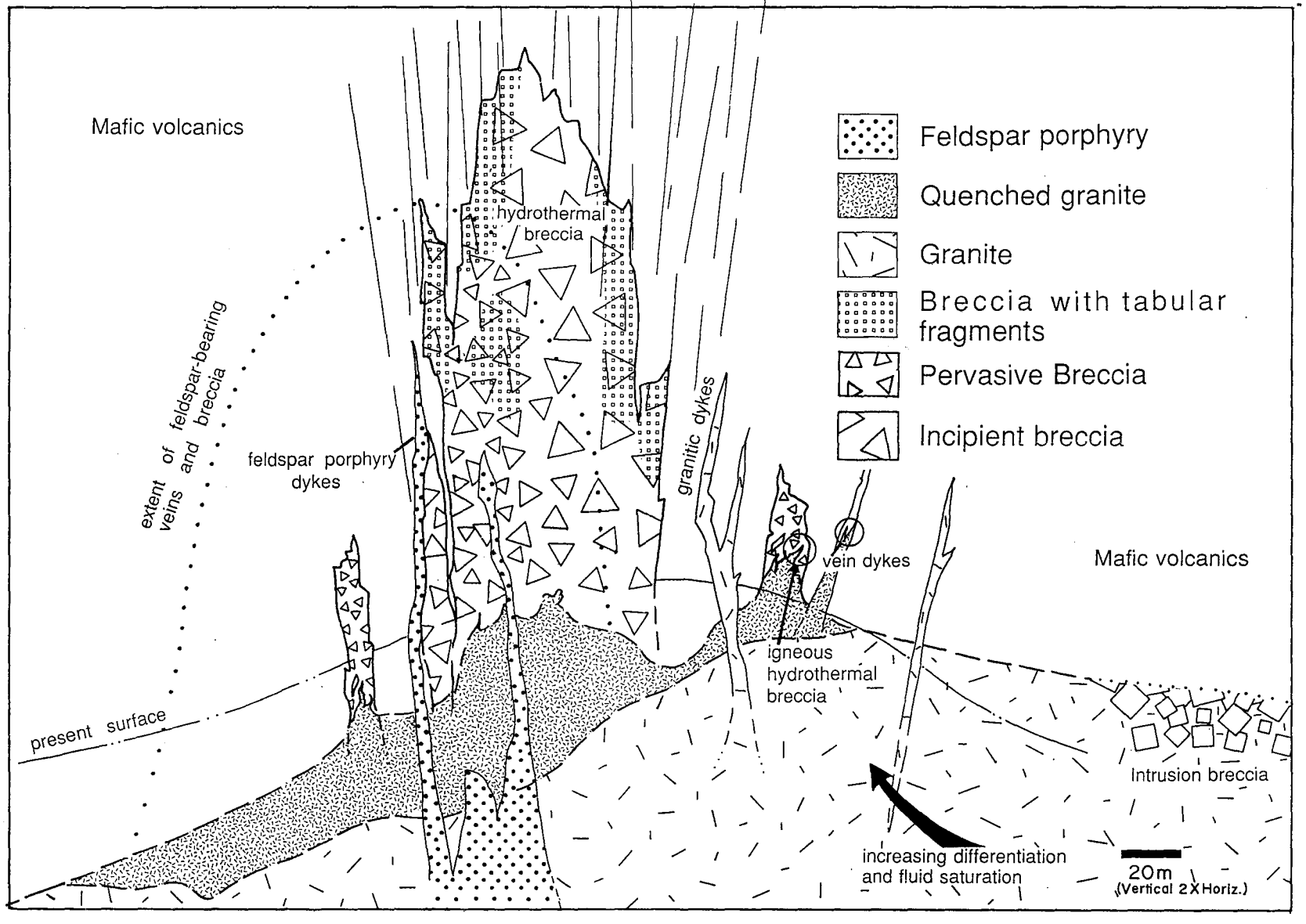
Mafic volcanics
Feldspar porphyry
Quenched granite
Granite
Breccia with tabular fragments
Pervasive Breccia
Incipient breccia
hydrothermal breccia
extent of feldspar-bearing veins and breccia
feldspar porphyry dykes
granitic dykes
vein dykes
Mafic volcanics
igneous hydrothermal breccia
present surface
Intrusion breccia
increasing differentiation and fluid saturation
20m
(Vertical 2X Horiz.)

differentiation, causing the formation of fractures and possibly brecciation. Decompression following initial failure might have caused further brecciation and fracturing ;however, it does not appear to have led to streaming, and fragment mixing and attrition (Sillitoe, 1985).

The absence of any evidence of multiple stages of brecciation and the largely passive style of brecciation suggests that the process was geologically instantaneous and occurred in a single stage. Immediately following breccia solidification it seems that a second period of resurgent boiling or energy creation via decompression occurred. Evidence for continued stress is indicated by the intramineral dyke, which postdates the breccia, and post-breccia jointing. The origin of the joint set 1 structures, discussed in chapter 3, were considered a consequence of essentially regional forces ;however, it is also possible to relate these joints closely with breccia processes. When internal overpressures result in failure, stress is relieved by expansion in the direction of σ_3. As joints, and in this case possibly the breccia itself, were filled strain compensation in this direction became reduced (Allman-Ward et al., 1982). To accommodate this situation the position of σ_2 and σ_3 might change or invert, so as to allow extension in another direction. It seems plausible that

maximum extension might be best accommodated at 90 degrees to the first plane, joint set 1, which intersects at 87 degrees with set 2. It is possible that the renewed forces were sufficient to allow intrusion of the dykes and formation of fractures, but were not sufficient to cause repeated brecciation such as that found in porphyry related systems. Rejuvenation of the system by influx of magmas probably did not occur at Temagami as suggested by the apparent absence of composite plutons in the region. Rebrecciation would also be inhibited if additional fluids were able to escape along other conduits such as the NLVL zone of deformation as suggested by Fyon et al. (1987, 1988, 1989). Such may be the case where fluids originating from the breccia zone appear to have escaped into the 071^0 trending quartz vein system. The extensive quartz veining within the 069^0 shear zone may in fact represent another related hydrothermal centre analogous to the breccia, except that in this case fluid release was into a system of veins influenced by shear stresses rather than the tensile and brittle forces that characterize the breccia and the immediate surrounding area.

4.5 Mineralization of the Breccia and Veins

4.5.1 Relationships and Controls of Breccia Textures on Mineralization

Before discussion of the factors that influenced the distribution of feldspar and sulphides the basic reason for the presence of these minerals in the hydrothermal system is considered. Arguments have so far stressed, that the hydrothermal fluids were largely of magmatic origin. In experiments with fluorine-rich granites extreme alkali enrichment in the fluid phase exsolved from such granitic melts has been observed (Glyuk and Anfiligov, 1974; Kovelenko et al., 1974; Ludington, unpub. data, 1979). These workers observed that the fluid composition approached that of hydrous alkali silicate melts. Extremely high solubilities of molybdenite (>10 wt percent) have been found in such melts (Isuk, 1976). Although traces of fluorite were found in breccias, the fluorine content of the intrusive is not known; even so, these findings may be relevant to the Temagami mineralization. Clearly, the preponderance of feldspar-rimmed breccia fragments attests to significant amounts of Al and alkalis in the hydrothermal fluids. According to the above experimental results, an alkali fluid would have the potential to carry large amounts of molybdenum and perhaps copper in solution. With respect

to the molybdenite source it has been established by many workers that stockwork molybdenite deposits, of which this system may be a variant, derive their constituents from adjacent evolved granite intrusives (Gunow et al., 1981; Mutschler et al., 1981; White et al., 1981).

In general both feldspar and sulphide mineralization occur as selvages in both veins and within the breccia (Plate 4-5a,b). The subhedral to euhedral faces projecting into the quartz matrix along with the selvage habit suggest that both feldspar and sulphides were precipitated early in the vein and breccia paragenesis. In the case of feldspar the fragments and vein walls show little or no evidence of alteration so it would seem that the volcanic material simply acted as a substrate for nucleation. Sulphide mineralization, however, is associated with minor alteration and wallrock-fluid interaction may have been critical for mineralization. The actual precipitation of the minerals was probably controlled by cooling, pressure decrease or changing chemistry of the hydrothermal fluids (Barnes, 1979).

Feldspar mineralization Hydrothermal fluids may have been either homogeneous or heterogeneous. It is plausible that fluids were heterogeneous on the scale of the breccia body, leading to the spatial distribution of matrix

mineralization. Alternatively if fluids were homogeneous then physical conditions must have varied in order to explain the sulphide mineral distribution.

A heterogeneous fluid might originate from density stratification of fluid above the magma (Burnham and Ohmoto, 1980) or perhaps from fluid immiscibility. To some degree such stratification or separation of fluids might be maintained upon release into the vein and breccia system. The preservation of compositional contrasts between fluids would have been promoted by proximity of the fluid source to the breccia and rapid formation and solidification of the breccia. Another possibility is that immiscible fluids could have developed by the pressure release and or temperature drop associated with failure and that these fluids might lead to the present distribution of feldspar.

If the fluids that formed the breccia and vein mineralization were homogeneous then physical and or chemical factors must have varied throughout the breccia and influenced mineralization. This possibility is supported by the weak positive correlation between feldspar and the proportion of matrix and the correspondence of feldspar-bearing breccias with zones of in situ brecciation (Fig. 4-9a). The increased matrix proportions in these areas suggest that the void created in brecciation was greater and

that the fluid/rock ratio was higher than in other areas of brecciation. One possibility is that the fluid/rock ratio allowed for a greater flux of mineralizing fluid over the crystallization boundary resulting in greater feldspar accumulation. Alternatively, the different texture of the breccia in the feldspar zone may indicate that brecciation occurred at a slightly different time in these areas. If fluids permeated this zone first they may have lost feldspar constituents before accessing the rest of the breccia. Another possibility is that the different style of breccia may indicate differing temperature-pressure regimes that favoured feldspar precipitation.

Sulphide mineralization Analogous arguments can be suggested for the sulphides, but an the important difference is that conditions favouring feldspar did not also favour sulphide mineralization. An important contrast in mineral associations is that sulphide mineralization and alteration do seem to be coincedent. Another important relationship is that mineralization is associated with finer fragment sizes, and therefore more pervasive breccias. The smaller fragments, which provide a greater total fragment surface, and the alteration of these fragments suggests that mineralization was dependent on wallrock-fluid interaction. The antipathetic relation of sulphides and feldspar might

then arise because mineralizing fluids would not be able to react with the feldspar-enveloped surface of a vein or fragment. Obviously, other influences were also critical since not all non-feldspar bearing breccias were mineralized and there are isolated examples of mineralized feldspar-bearing breccias. An important feature of these mineralized feldspar-bearing examples is that on the small scale the feldspar and sulphides did not come into contact, thereby maintaining the antipathetic relationship. These isolated occurrences of sulphides and feldspar may indicate that the fluids contained the components to precipitate both sulphides and feldspar but that conditions for precipitation were specific to each. Perhaps as the feldspar precipitated and alkali components became depleted in the solution, molybdenum and copper solubility changed from being undersaturated to oversaturated. This sort of solubility control may explain the spotty mineralization in feldspar-rich zones and the greatest mineralization where feldspar is deficient. This process negates the need to call on fluid wall-rock interaction as the sole factor in sulphide precipitation. It is also possible that both processes were critical for conditions of sulphide precipitation.

4.5.2 Petrography and Paragenesis of the Breccia and Vein Mineralization

4.5.2.1 Opaque Mineralization

The main opaque minerals within the veins and breccia are chalcopyrite, molybdenite, magnetite and pyrite while minor constituents include pyrrhotite, marcasite, hematite, sphalerite, bornite, chalcocite, cubanite, and covellite. In general the chalcopyrite and molybdenite occur together as selvages in veins and partial rims in the breccia matrix and rarely form more than 5 volume percent. Significant mineralization is concentrated in small pockets within the breccia and in veins that lie within a weakly defined linear trend (Map 1,2).

Examination of polished ore mounts allowed for the identification of two distinctive parageneses. The first includes mineralized breccias and veins that lack magnetite, the second includes veins that contain magnetite.

Non magnetite-bearing veins and breccias In this assemblage molybdenite occurs in characteristic deformed plates nucleating directly on the volcanics or commonly on epidote. Chalcopyrite when associated with molybdenite envelops the euhedral crystals and is interstitial between the delicate

cleavages of molybdenite (Plate 4-5c). Pyrite occurs as subhedral to euhedral inclusions in chalcopyrite and sometimes as overgrowths on molybdenite and epidote (Plate 4-5d;4-6a,b). In some instances it has been extensively replaced by marcasite, chalcopyrite and rarely by late stage hematite (Plate 4-5d;4-6b). Pyrrhotite, sphalerite, and rarely cubanite form inclusions in chalcopyrite. Pyrrhotite is closely associated with pyrite. Hematite is a minor constituent that replaces most sulphide phases and is most often associated with cross cutting micro-veinlets of quartz. Covellite is also found in trace amounts primarily as alteration rims on chalcopyrite. The inferred paragenesis for the non magnetite-bearing veins and breccias based on these textures indicates an early stage of primary precipitation of molybdenite, pyrite, pyrrhotite, chalcopyrite followed by exsolution of sphalerite, and cubanite and finally by secondary alteration minerals, hematite, marcasite and covellite (Fig. 4-13a).

Magnetite-bearing veins All of the magnetite-bearing mineralization is found with a series of veins in the vicinity of grid location 250 SE, 320 SW, which is 100 m SW of the breccia within the general zone of mineralized veins (Map 2). Molybdenite displays characteristic bladed habit, but often is largely replaced by MoO_3 or molybdenum ochre

Plate 4-5a (page 146): Molybdenite (mo) laths projecting into vein quartz (q). Chalcopyrite (c) and molybdenite occur as selvages. The dark grey-black material in the lower half of the photo is volcanic wall rock.

Plate 4-5b (page 146): Chalcopyrite (c) between two breccia fragments showing net-like texture occurring as an interstitial phase within the volcanic fragment.

Plate 4-5c (page 146): Molybdenite (mo) lamellae in chalcopyrite (c). Chalcopyrite fills the delicate interstices between molybdenite lamellae. Sphalerite (s) occurs as inclusions in chalcopyrite.

Plate 4-5d (page 146): Pyrite (py) growing as subhedral crystals on sub-euhedral crystals of epidote (ep). Chalcopyrite appears to form after pyrite and epidote. Marcasite (M) and quartz replace pyrite.

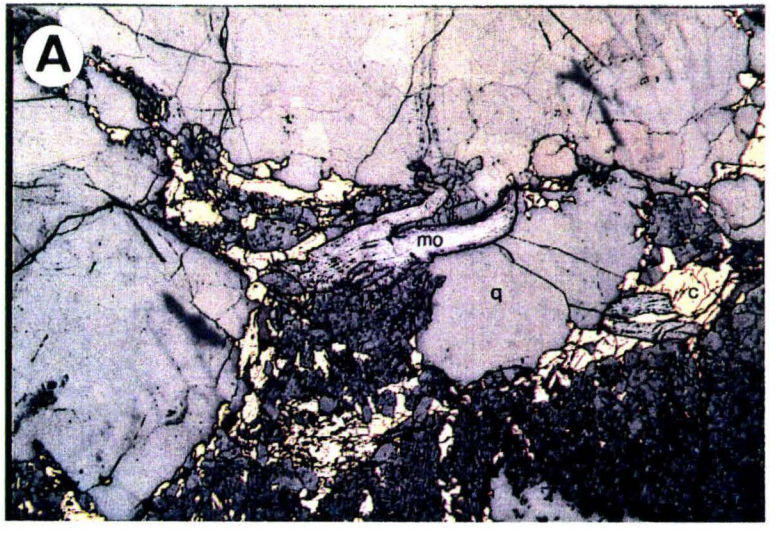
A
mo
q
c
1mm

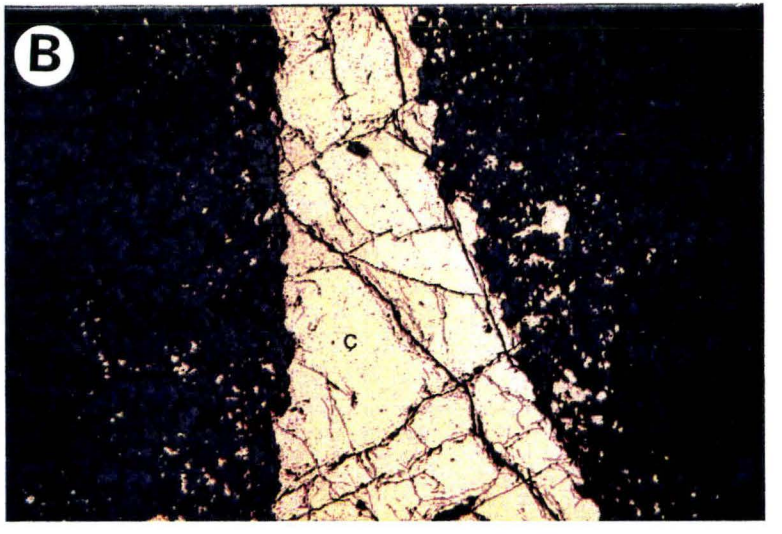
B
c
1 mm

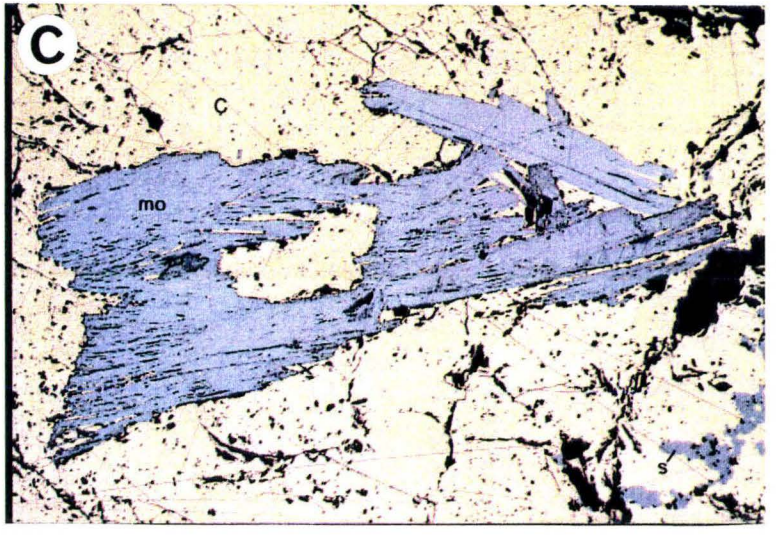
C
c
mo
s
1mm

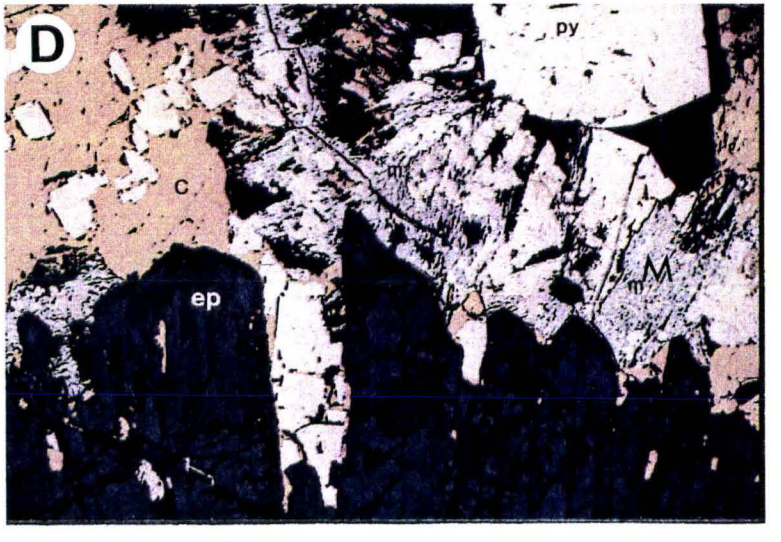
D
py
c
ep
m
M
1mm

(Plate 4-6c; Ramdohr, 1969). Magnetite, with oriented exsolution lamellae of hematite, engulfs and fills delicate interstices between blades of molybdenite in a form similar to chalcopyrite in the magnetite-free assemblages (Plate 4-6c,d). Pyrite occurs as subhedral to euhedral grains within magnetite, sometimes showing evidence of replacement by magnetite. Minute irregular inclusions of bornite occur in magnetite. Within the bornite there are basketweave exsolution lamellae of chalcopyrite. Chalcocite forms some small inclusions within magnetite and these are invariably rimmed with covellite, which also forms abundant small disseminated inclusions within and on the margins of magnetite. Pyrrhotite is rare, forming rounded inclusions in grains of chalcopyrite within magnetite. Hematite occurs mainly as a replacement of magnetite, but it also occurs in micro-veinlets of gangue where it replaces pyrite. Based on these textures the paragenesis indicates a sequence of primary mineralization beginning with molybdenite, followed by pyrite and bornite and then exsolution of chalcopyrite and pyrrhotite. Secondary replacement under oxidizing conditions are suggested by late minerals, magnetite, molybdenum ochre, covellite and hematite (Fig. 4-13b).

4.5.2.2 Vein and Breccia Silicate Paragenesis

Plate 4-6a (page 148): Subhedral pyrite (py) growing on lamellae of molybdenite (mo). The molybdenite is partly replaced by molybdenum ochre (mox). Chalcopyrite appears to be the latest phase.

Plate 4-6b (page 148): Subhedral pyrite growing on molybdenite. The pyrite has been extensively replaced by marcasite (m), quartz and hematite (ht).

Plate 4-6c (page 148): Molybdenum ochre (mox) engulfed in an intergrowth of magnetite (mag) and hematite (ht). Dark grey mineral is vein quartz.

Plate 4-6d (page 148): Molybdenite (mo) and molybdenum ochre (mox) engulfed in magnetite (mag). Covellite (cov) is disseminated within magnetite. Dark grey is vein quartz (q).

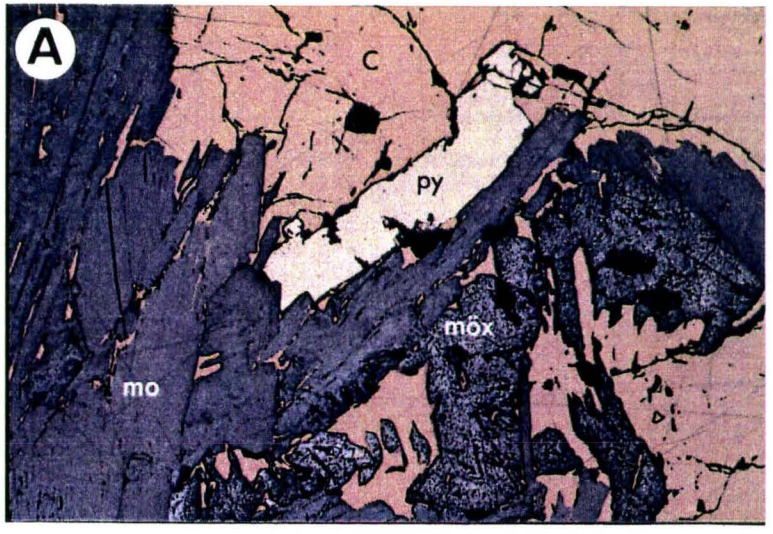
A
c
py
mox
mo
1 mm

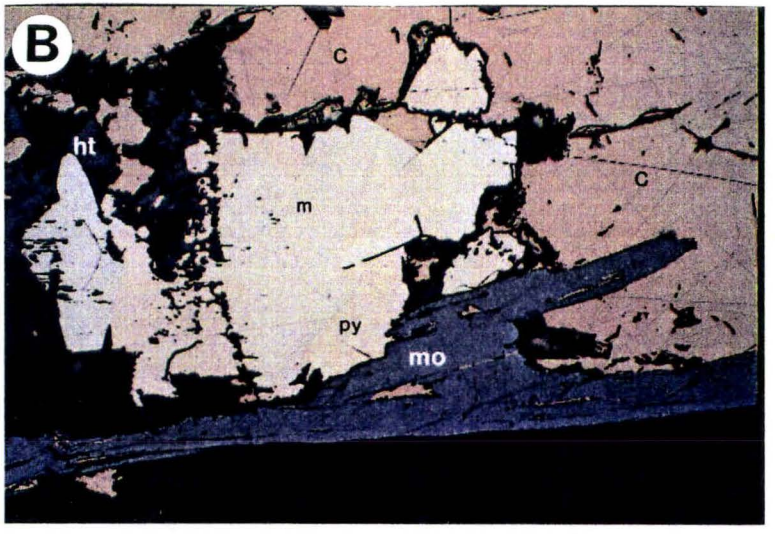
B
c
ht
m
c
py
mo
1 mm

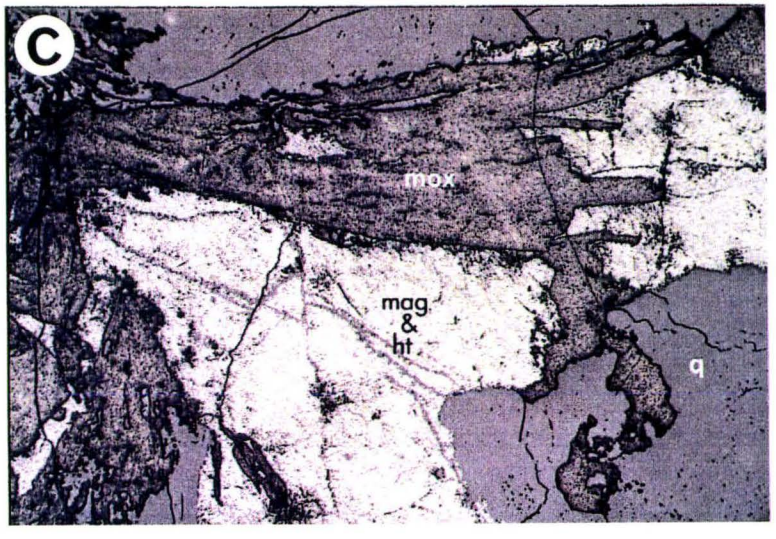
C
mox
mag
&
ht
q
1 mm

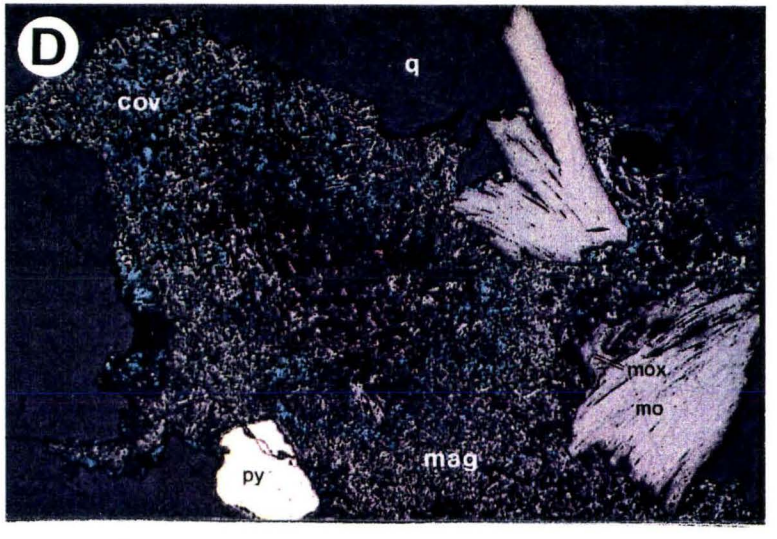
D
q
cov
mox
mo
py
mag
1 mm

Figure 4-13a: Paragenesis diagram for the non-magnetite-bearing, vein and breccia, opaque mineral assemblage.

Figure 4-13b: Paragenesis diagram for the magnetite-bearing, quartz vein, opaque mineral assemblage.

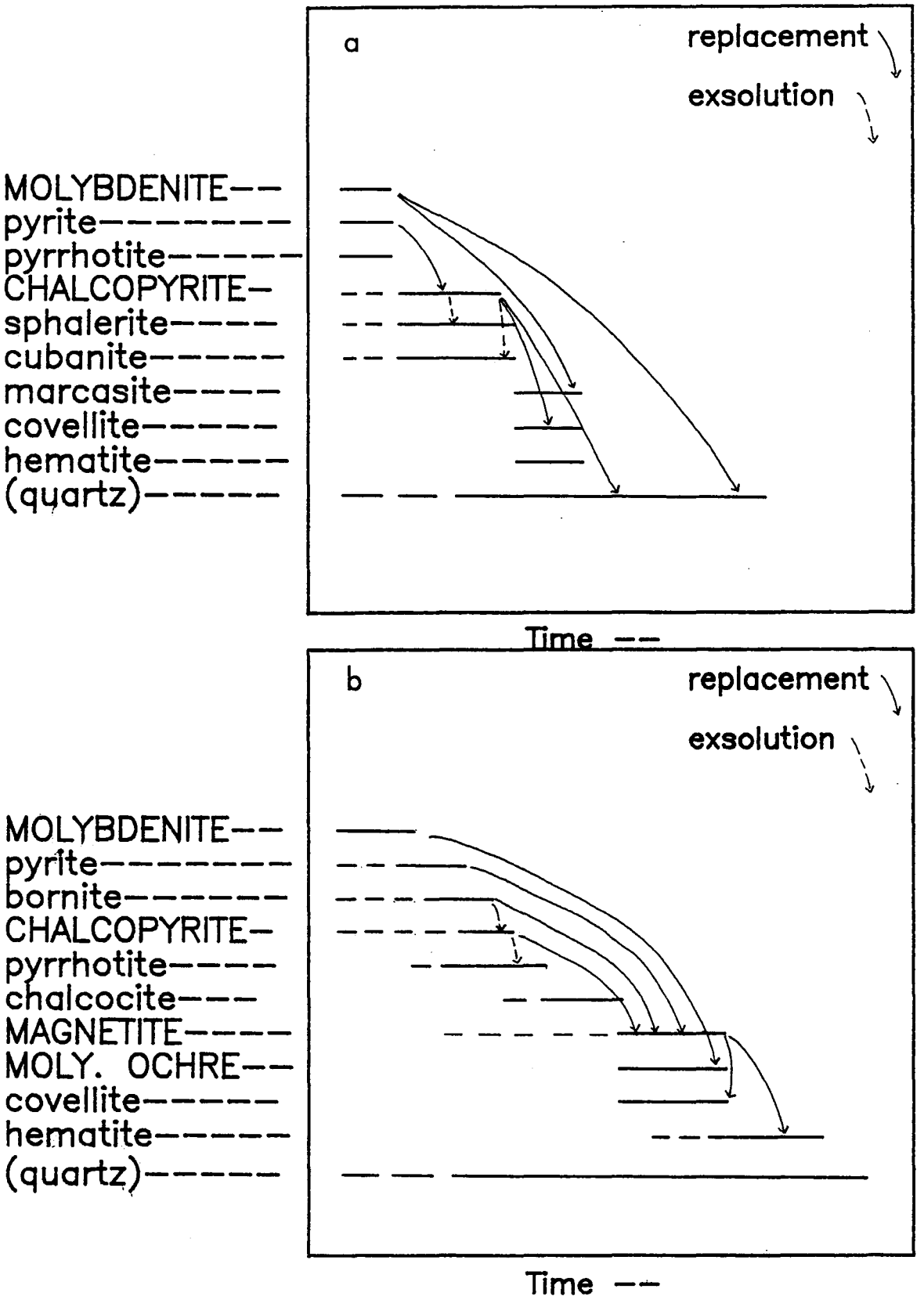
a
replacement
exsolution
MOLYBDENITE--
pyrite--------
pyrrhotite-----
CHALCOPYRITE-
sphalerite----
cubanite-----
marcasite----
covellite-----
hematite-----
(quartz)-----
Time --
b
replacement
exsolution
MOLYBDENITE--
pyrite--------
bornite-------
CHALCOPYRITE-
pyrrhotite----
chalcocite---
MAGNETITE----
MOLY. OCHRE--
covellite-----
hematite-----
(quartz)-----
Time --

Only thin sections of breccia quartz assemblages were examined, but the similarity in mineralization of the breccia and the non-magnetite bearing veins is justification for extending observations made on the breccia to the vein paragenesis.

Feldspar-bearing veins and breccia With few exceptions these areas are almost exclusively unmineralized. Plagioclase (An_{25}) forms subhedral to euhedral selvages on vein margins and breccia fragments. Chlorite occurs as long platy selvages, sometimes with internal lenses of biotite and appears to coprecipitate with plagioclase (Plate 4-2b). Chlorite, with the same anomalous blue pleochroism, also occurs within the volcanic fragments. Replacement of the plagioclase, primarily by sericite and epidote, is extensive within the veins. Replacement textures within the volcanic fragments are similar to, but more extensive, than those noted in the unbrecciated volcanics. Rarely, in both feldspar-bearing and feldspar-deficient examples, where fragments are small, hornblende is almost completely replaced by plagioclase quartz and epidote (Plate 4-7a). In instances where coarse (2i) and fine-grained (2j/k) volcanic fragments exist in the same breccia, the coarse fragments show the most evidence of recrystallization and replacement.

The contact between selvage feldspar and the fine-grained fragments is abrupt, but in the coarse fragments it seems as though the mineralogy within the fragments has recrystallized and is continuous with the hydrothermal assemblage.

Feldspar deficient veins and breccias In unmineralized breccias the mineralogy is usually simple and consists of quartz in direct contact with volcanic fragments, and rarely minor chlorite as selvages and within the fragments. In other examples coarse recrystallized hornblende is extensively replaced by quartz, plagioclase and epidote. In mineralized breccias epidote is common as coarse subhedral mineral aggregates and radiating clusters of euhedral crystals projecting into chalcopyrite and molybdenite (Plate 4-5d). The relative crystallization ages of epidote, hornblende and the sulphides is illustrated by the infilling of voids between silicate crystals and fractures by chalcopyrite (Plate 4-7b,c,d). Prior to crystallization of sulphides, hornblende, growing from recrystallized volcanic fragments, sometimes forms as a hydrothermal mineral projecting into vein quartz and forming a substrate for epidote (Plate 4-8a,b). Chlorite occurs both as selvages and aggregates in fragments, sometimes with inclusions of biotite books. Biotite also occurs as patchy replacements

Plate 4-7a (page 152): Quartz breccia with breccia fragment (dashed area) that has been almost entirely replaced by quartz.

Plate 4-7b (page 152): Chalcopyrite (c) forming after epidote (ep) as evidenced by interstitial habit.

Plate 4-7c (page 152): Chalcopyrite (c) occurring on the margin of, and as fracture fillings in epidote (ep).

Plate 4-7d (page 152): Chalcopyrite (c) forming after hornblende (h) as evidenced by interstitial habit.

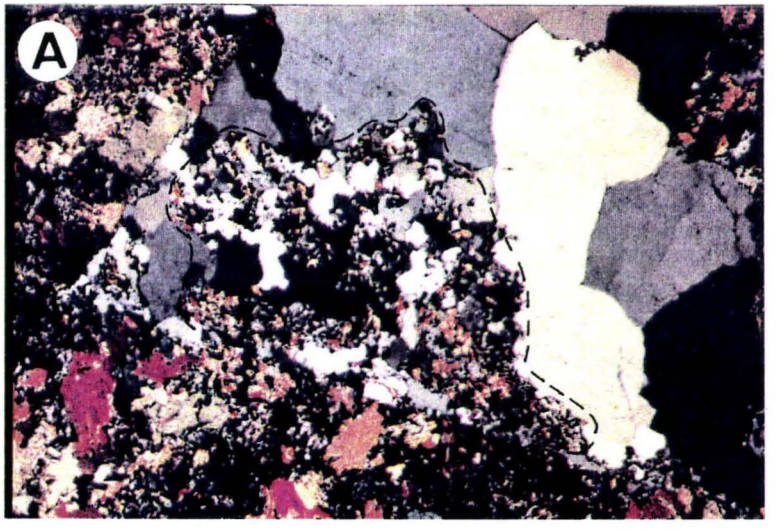
A
1mm

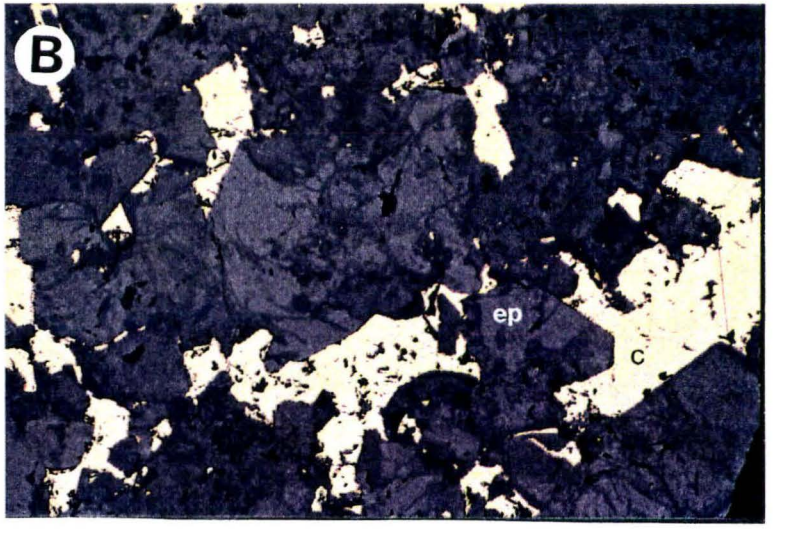
B
ep
c
1mm

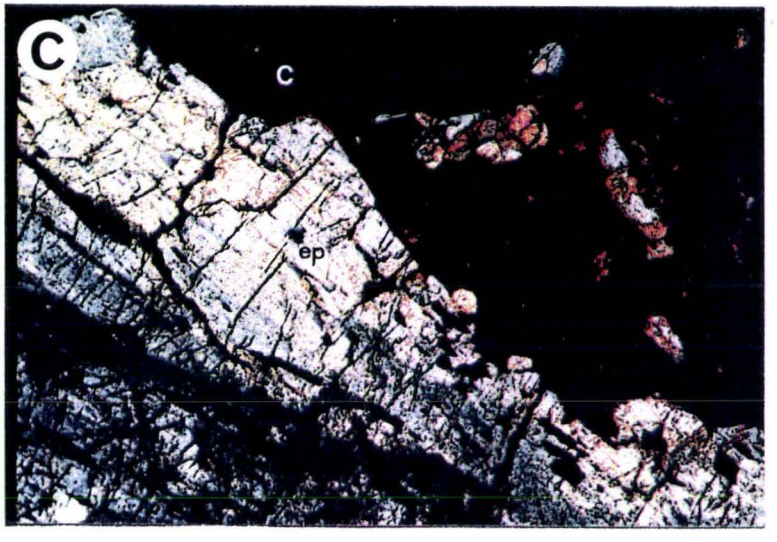
C
c
ep
1mm

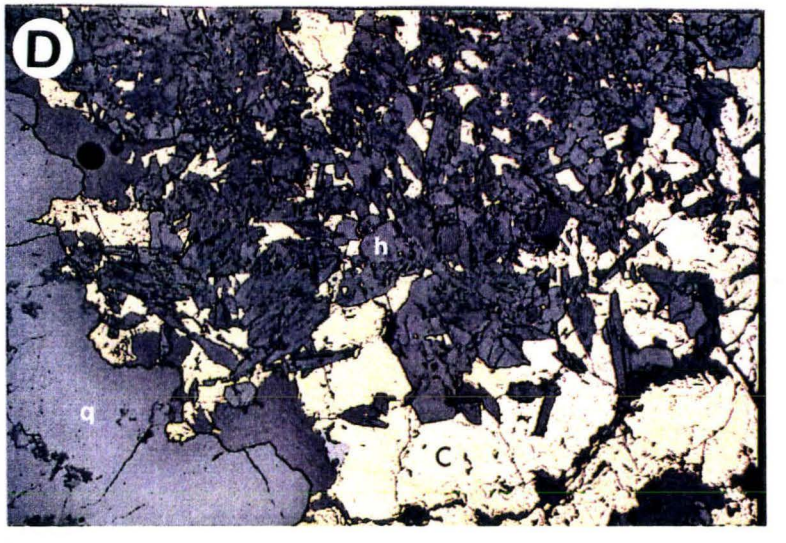
D
h
q
c
1mm

of hornblende within volcanic fragments (Plate 4-8c) and as a late phase where it appears to replace epidote and sulphide minerals. The appearance of biotite and epidote especially in mineralized samples is the most obvious contrast with the feldspar-bearing assemblages aside from the absence of feldspar itself. In the satellite breccia, on the north side of the main breccia zone, biotite and chlorite completely replace volcanic fragments along fractures and on fragment selvages. Based on the morphology of grains it appears that initially the mica was dominantly biotite and that it was later replaced by chlorite (Plate 4-8d). One isolated example of a mineralized breccia contains what is thought to be siderite. Based on textural relationships the siderite precedes the crystallization of both chlorite and epidote. In the same example fluorite occurs in association with late stage K-feldspar veinlets.

4.5.2.3 Interpretation of the Opaque and Silicate Paragenesis

Based on the metamorphic assemblages and mineral chemistry Brons (1989) estimates the following physicochemical conditions within the inner metamorphic contact aureole: 475-550^{0}C, mole fraction of $CO_2 \leqslant 0.10$, oxygen fugacity 10^{-18}

Plate 4-8a (page 154): Breccia matrix with epidote (ep) growth on substrate of hornblende (H).

Plate 4-8b (page 154): Needles of hornblende (H), growing from a breccia fragment, projecting into the quartz matrix (q).

Plate 4-8c (page 154): Breccia fragment in a mineralized breccia that contains abundant biotite as a replacement phase.

Plate 4-8d (page 154): Massive aggregates of biotite and chlorite replacing volcanic fragments in the 'biotite breccia'. Chlorite (dark blue) replaces biotite.

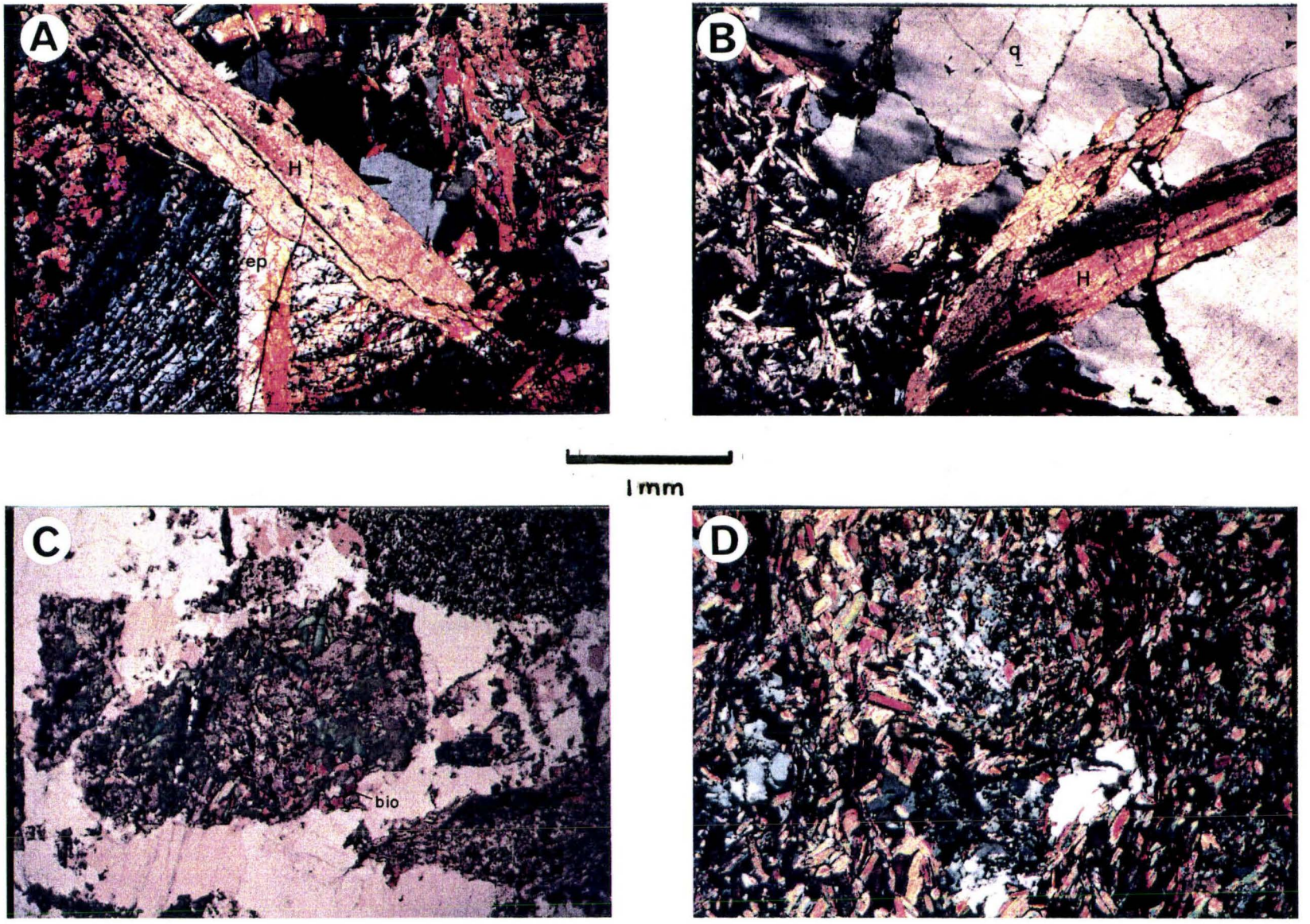
A
H
ep
B
q
H
1 mm
C
bio
D

to 10^{-22} bars. With the exception of actinolite and ilmenite all of the minerals belonging to the hornblende hornfels facies mineral assemblage, which are indicative of the metamorphic conditions, have been identified in the vein and breccia filling. This evidence is highly suggestive, and in agreement with the conclusions of Brons (1989), that the veins and breccia were formed during peak metamorphism.

Petrographic evidence indicates that coarse-grained epidote and plagioclase are in equilibrium, and that sericite and K-feldspar are later replacement phases. The stability fields of these minerals can be plotted in terms of the ratios, log a_{Ca}^{2+}/a_{H}^{+} and log a_{K}^{+}/a_{H}^{+}. The observed assemblages are compatible with increasing activity of K^{+} and a possible decrease in the activity of Ca^{2+} (Fig. 4-14a). K enrichment is likely reflected in the secondary biotite, sericite and K-feldspar which taken together may be indicative of a zone of K-silicate alteration like that noted in porphyry mineral deposits (Lowell and Guilbert, 1970).

According to White et al. (1981), the occurrence of quartz molybdenite mineralization in porphyry mineral deposits, is suggestive of temperatures in the range of 500-600^{0}C. In addition the potassium-silicate mineral assemblage associated with porphyry mineral deposits is considered to

develop under temperatures of 400-600^{0}C. The common opaque mineralogy associated with the K-silicate alteration assemblage, bornite-magnetite, bornite-chalcopyrite, or chalcopyrite without pyrite (Einaudi, 1982), is very similar to the observed Temagami assemblage. The sequence of opaque minerals noted herein, pyrite --> bornite + chalcopyrite --> magnetite --> hematite, may be indicative of decreasing fS_2 and increasing fO_2 (Fig. 4-14b). Figure 4-14b also shows the field of K-silicate alteration denoted by the assemblage biotite, K-feldspar and anhydrite, which, with the exception of anhydrite was observed in association with the mineralization.

Based on these criteria and evidence that will be considered in later chapters, it is assumed that mineralization in the veins and breccia were synchronous with peak metamorphism. The occurrence of an oxidized assemblage in one area of the vein system and the heterogeneous distribution of sulphide and feldspar mineralization is suggestive that hydrothermal fluids varied compositionally, in both space and time. The appearance of secondary K-rich phases is also suggestive of late K-silicate alteration in the mineralized zone.

Figure 4-14a: Stability relations among minerals as a function of activity ratios in a co-existing aqueous phase at 500 bars, 350°C and a_{CO2} = 20. Heavy arrow shows the possible evolution path of the hydrothermal solution as implied by the silicate vein and breccia paragenesis. Modified after Beane, 1982.

Figure 4-14b: Log fS_2 - log fO_2 diagrams. Stippled field represents the estimates of the fugacity environment of K-silicate alteration. Heavy arrow shows the possible evolution path of the hydrothermal solution as implied by the opaque mineral paragenesis. Abbreviations: bio-biotite; Ksp-K-feldspar; Ah-anhydrite; Qz-quartz; Py-pyrite; Cp-chalcopyrite; Cc-calcite; Po-pyrrhotite; Mt-magnetite; Hm-hematite. Modified after Einaudi,(1982).

a

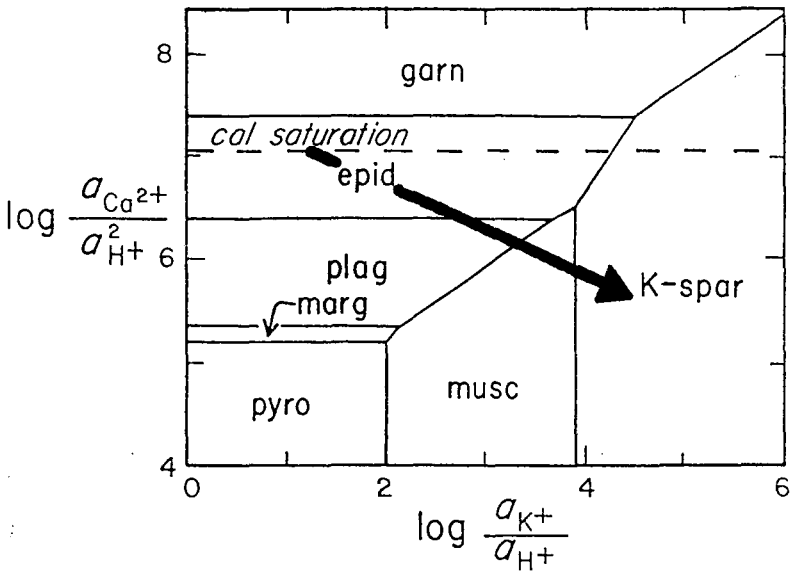

Key to Minerals:

cal = calcite
epid = epidote
garn = garnet (grossular/andradite)
plag = plagioclase (albite/anorthite)
pyro = pyrophyllite
K-spar = K-feldspar
marg = margarite
musc = muscovite

b

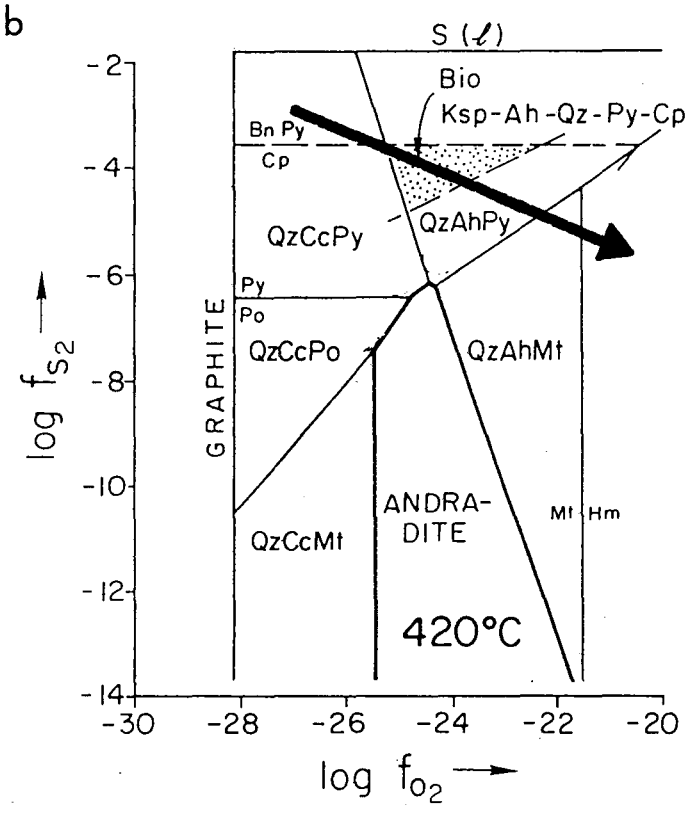

CHAPTER 5

GEOCHEMISTRY OF THE VOLCANIC ROCKS

5.1 Introduction

Forty samples of volcanic and related rocks were analyzed for major and selected trace elements by XRF and INAA techniques (appendix A). The main objectives were to characterize alteration related to the intrusion and/or brecciation, and to chemically differentiate mafic rock units 2i, 2j, 2k and 2o and investigate their origin. Alteration of the volcanics in the area of the breccia was subtle and expressed only by the appearance of biotite in outcrop. The bleaching of volcanics in the silicified zone at the southwest end of the grid (grid location 640 SW, 100 SW) and the potassic alteration evident in the extreme south of the study area (grid location 480 SE, 900 SW) represented the most intense alteration of volcanics outside the breccia (Plate 5-1a,b; Map 1). Three samples of basaltic dykes

Plate 5-1a: Outcrop of tholeiitic basalt within 5 meters of the contact with the Strathy-Chambers batholith. The bleaching is the result of quartz plagioclase alteration, which enhances the primary hyaloclastite texture.

Plate 5-1b: Quartz and K-feldspar altered tholeiitic volcanic from the area of intrusive outcrops near North Temagami. Original minerals have been largely replaced by quartz, plagioclase K-feldspar and carbonate. Myr-myrmekitic texture; H-hornblende; ca-carbonate.

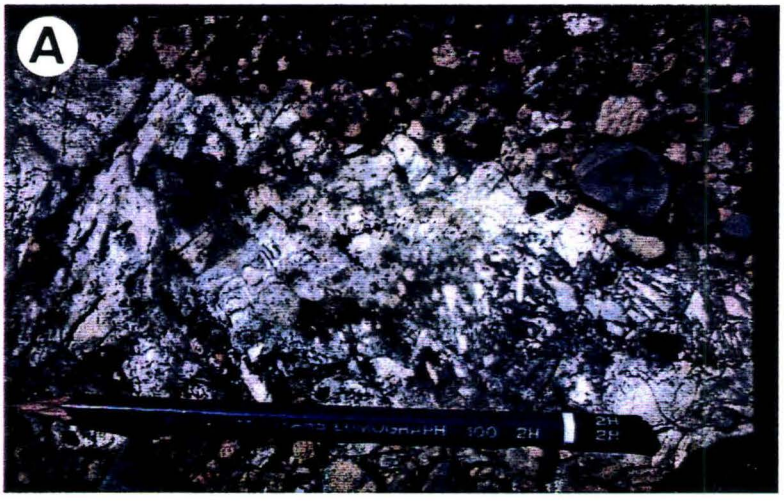

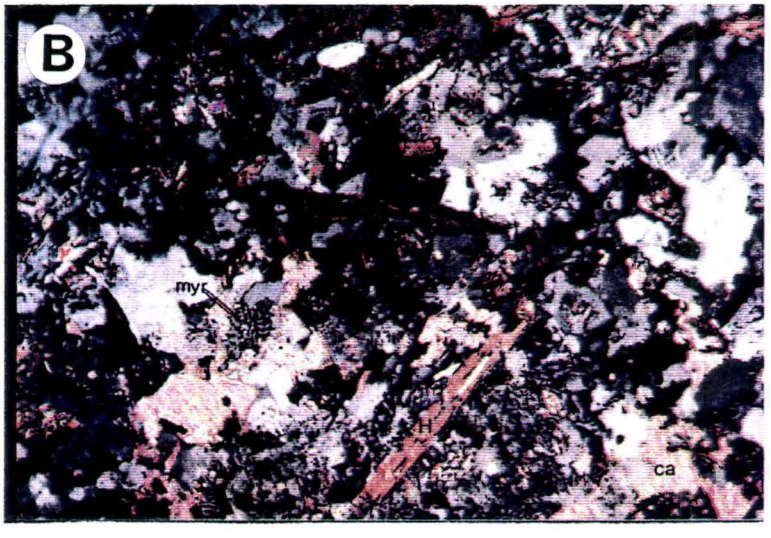

1 mm

(112, 190, 330) and two samples of gabbroic rock (174, 306), thought to be either altered volcanic or mafic intrusive rock, were analyzed. The basaltic dykes were of interest since they cross cut both quartz veins and breccia. If the composition of these dykes characterized them as probable feeders to the volcanics then a relative time constraint on the breccia and vein emplacement would be obtained. The mafic or metasomatic rocks were analyzed to aid in classifying them as volcanics, mafic intrusives or their altered equivalents.

5.2 Classification and Chemical Distinction of Mafic Rock Types

The Jensen cation plot (Jensen, 1976) is most appropriate for the classification of the mafic rocks in this study because it does not use alkali elements, which are particularly susceptible to alteration. On the Jensen plot in figure 5-1 the majority of samples lie in a cluster that spans the iron and magnesium tholeiite fields. No komatiitic compositions were found in the analyzed suite. This is expected, since these rocks are within sequence B of Fyon et al. (1989), the lower unit of which is described as iron-rich tholeiite. Four samples (174,300,112,284) lie

Figure 5-1: Jensen cation plot of volcanic rocks from the study area. Left ternary plot is of individual samples some of which are numbered and discussed in the text. Points plotted on the right are averages of the various lithologies. Field 1, high-Fe tholeiites; Field 2, high-Mg tholeiites (Jensen, 1976).

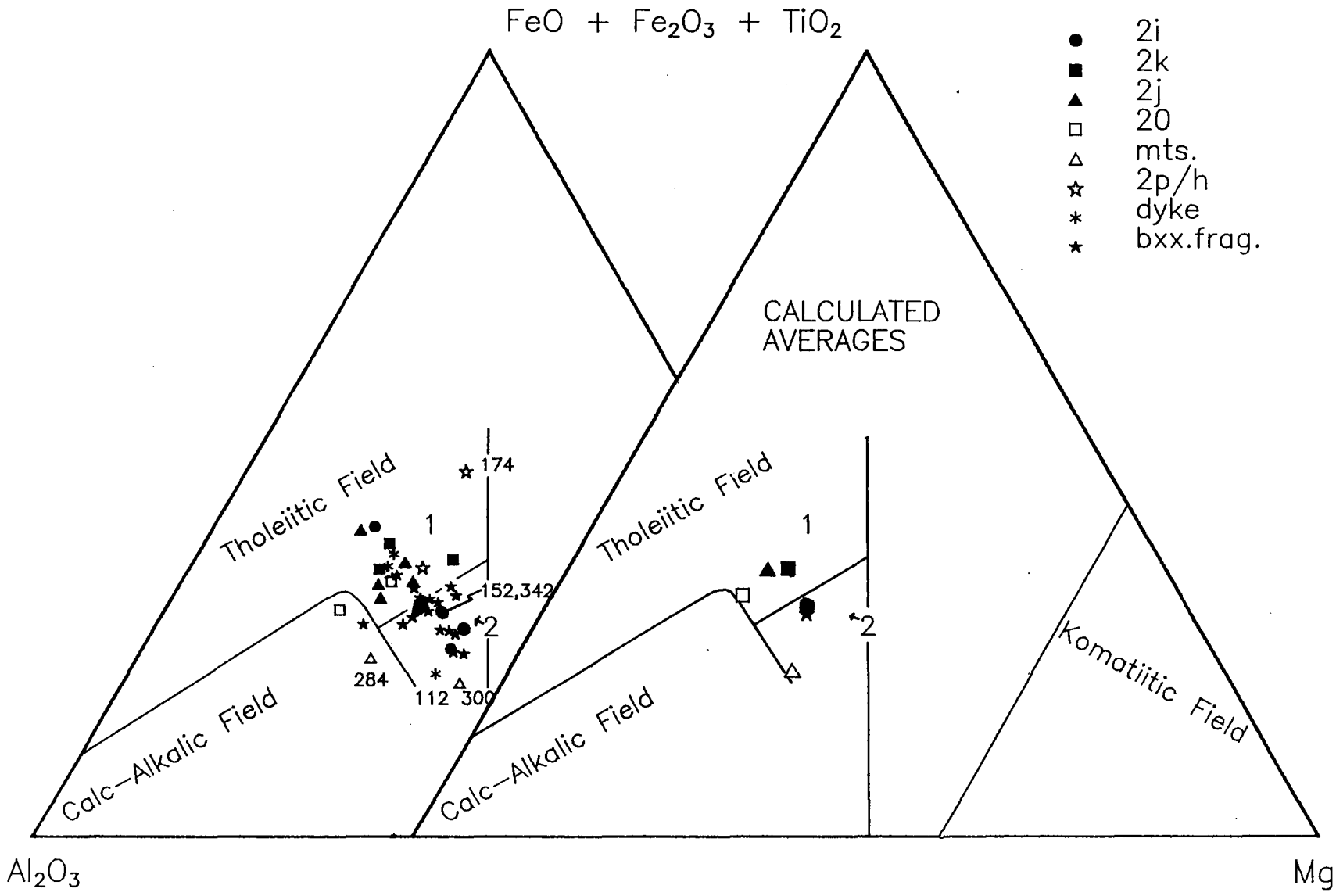
FeO + Fe2O3 + TiO2
2i
2k
2j
20
mts.
2p/h
dyke
bxx.frag.
CALCULATED AVERAGES
Tholeiitic Field
Tholeiitic Field
Komatiitic Field
Calc–Alkalic Field
Calc–Alkalic Field
174
152,342
284
112
300
1
2
1
2
Al2O3
MgO

outside the main cluster suggesting that they may not be comagmatic with the volcanics or that secondary alteration has significantly changed their compositions.

Chemical distinction between the lithological types, 2i, 2j and 2k is apparent on the Jensen plot where groups 2j and 2k lie in the high-Fe tholeiite field and 2i, with the exception of one sample, in the high-Mg tholeiite field (see averages, Fig. 5-1). The average composition of breccia fragments is slightly skewed toward the high-Mg tholeiite field, which is not surprising since unit 2i is the predominant volcanic rock type (Map 2).

There are two different mafic dyke types represented by samples 190, 330 and 112. Samples 190 and 330 lie adjacent to one another and classify as high-Fe tholeiites. The dykes are lower in Si and Ca in comparison to the volcanics and have significantly higher concentrations of Ti, P, Sr, and Zr (Table 5-1). The 112 dyke straddles the basalt/tholeiite field and differs significantly from the volcanics and the other dykes with respect to several elements. Relative to the volcanics, sample 112 is significantly lower in Fe, Ca, and much higher in Si, Mg, Na, P, Ba, Sr and Zr. Considering the significant chemical contrast between all three dyke samples and the volcanics it is assumed that the dykes are not cogenetic character with

TABLE 5-1

Major and Trace Element Results
(Oxides in percent, trace elements in ppm)

Element	2i (high Mg-tholeiite) n = 6 Average	Variance	SD	2k (high Fe-thleiite) n = 4 Average	Variance	SD
SiO_2	51.39	0.72	0.85	51.42	1.78	1.34
Al_2O_3	13.61	0.13	0.37	13.23	0.21	0.46
Fe_2O_3	14.10	3.35	1.83	16.17	3.09	1.76
MgO	7.36	2.49	1.58	6.19	1.32	1.15
CaO	9.27	0.47	0.69	9.05	1.30	1.14
Na_2O	1.90	0.10	0.31	2.06	0.20	0.45
K_2O	1.22	0.02	0.15	0.88	0.11	0.33
TiO_2	0.72	0.04	0.19	0.73	0.00	0.05
MnO	0.17	0.00	0.02	0.20	0.00	0.02
P_2O_5	0.09	0.00	0.02	0.08	0.00	0.01
Ba	290.17	5.3E+4	229.16	198.25	7.9E+3	89.11
V	322.04	1.1E+3	32.75	334.00	609.50	24.69
As	1.72	1.30	1.14	1.40	0.33	0.57
Co	47.61	66.83	8.18	63.30	219.43	14.81
Cu	33.16	365.83	19.13	147.25	3.7E+4	192.64
Cr	287.98	2.0E+4	143.13	318.23	7.9E+3	88.90
Ni	104.88	637.66	25.25	94.75	515.69	22.71
Zn	118.92	2.1E+3	45.92	195.75	4.3E+3	65.73
Rb	55.21	79.62	8.92	20.25	141.15	11.88
Sr	127.56	686.76	26.21	98.00	485.26	22.03
Y	19.00	9.86	3.14	18.23	8.48	2.91
Zr	49.13	146.42	12.10	45.53	9.77	3.13
Nb	2.88	3.82	1.96	2.20	4.50	2.12

Element	2j (High Fe-tholeiite) n = 4 Average	Variance	SD	2o (altered Fe-tholeiite n = 2 Average	Variance	SD
SIO_2	51.39	1.01	1.00	52.30	2.34	1.53
Al_2O_3	14.26	0.48	0.69	14.11	0.03	0.17
Fe_2O_3	16.12	1.27	1.13	12.80	3.33	1.83
MgO	5.64	0.88	0.94	4.92	0.61	0.78
CaO	8.54	2.64	1.63	11.31	0.39	0.63
Na_2O	1.99	0.47	0.69	1.87	0.03	0.18
K_2O	1.00	0.07	0.26	1.12	0.09	0.31
TiO_2	0.76	0.01	0.11	1.24	0.01	0.12
MnO	0.21	0.00	0.04	0.22	0.00	0.01
P_2O_5	0.09	0.00	0.01	0.12	0.00	0.04
Ba	225.60	6.6E+3	81.17	122.00	576.00	24.00
V	324.30	524.56	22.90	355.50	420.25	20.50
As	1.67	1.21	1.10	0.50	0.00	0.00
Co	57.62	30.30	5.50	42.70	19.36	4.40
Cu	73.34	4.4E+3	66.48	30.65	414.12	20.35

(table 5-1 continued)

Element	Average	Variance	SD	Average	Variance	SD
Cr	320.69	9.0E+3	94.99	50.20	408.04	20.20
Ni	91.70	451.56	21.25	61.50	12.25	3.50
Zn	131.80	466.16	21.59	88.50	110.25	10.50
Rb	32.24	168.20	12.97	50.05	197.40	14.05
Sr	117.94	739.26	27.19	141.35	1.5E+3	38.25
Y	16.55	6.46	2.54	24.05	0.00	0.05
Zr	48.83	9.07	3.01	83.10	127.69	11.30
Nb	2.44	1.73	1.32	3.95	1.32	1.15

	Breccia Fragments n = 15			metasomatized volc.	
Element	Average	Variance	SD	284	300
SiO_2	49.74	0.74	0.86	56.75	57.33
Al_2O_3	14.07	0.97	0.99	14.35	13.45
Fe_2O_3	14.31	2.37	1.54	9.15	8.91
MgO	7.04	3.67	1.92	5.63	9.00
CaO	9.22	0.78	0.88	8.82	5.60
Na_2O	1.60	0.07	0.27	3.51	2.82
K_2O	1.10	0.05	0.22	0.80	1.97
TiO_2	0.31	0.00	0.05	0.70	0.54
MnO	0.20	0.00	0.04	0.20	0.13
P_2O_5	0.12	0.01	0.10	0.08	0.25
Ba	244.33	5.7E+4	238.34	271.00	995.00
V	*	*	*	253.00	161.00
As	*	*	*	1.40	3.00
Co	*	*	*	23.70	24.70
Cu	358.10	2.7E+5	517.55	11.10	33.00
Cr	86.98	1.6E+3	40.23	215.80	890.40
Ni	117.58	394.03	19.85	86.00	142.00
Zn	52.85	47.17	6.87	91.00	101.00
Rb	86.98	1.6E+3	40.23	34.70	40.40
Sr	117.58	394.03	19.85	230.20	272.00
Y	25.05	12.07	3.47	23.00	16.40
Zr	52.85	47.17	6.87	60.90	103.80
Nb	14.18	1.21	1.10	5.30	6.00

	Gabbroic samples			Dyke Samples	
Element	306	174	112	190	330
SiO_2	51.81	48.95	54.81	48.20	47.58
Al_2O_3	12.27	10.84	14.01	15.56	14.85
Fe_2O_3	14.91	20.71	9.25	15.50	16.96
MgO	6.18	6.48	8.19	6.01	5.97
CaO	10.53	8.94	7.56	6.32	8.54
Na_2O	2.30	1.37	4.17	1.32	1.98
K_2O	0.41	1.11	0.95	2.95	0.89
TiO_2	1.28	1.28	0.67	3.21	2.51
MnO	0.22	0.26	0.14	0.24	0.18

(table 5-1 continued)

	306	174	112	190	330
P_2O_5 %	0.09	0.07	0.27	0.71	0.53
Ba	136.00	113.33	819.00	512.00	373.00
V	452.00	534.33	154.00	378.50	296.00
As	1.80	1.77	1.00	2.30	4.90
Co	29.70	68.00	30.50	54.20	57.90
Cu	68.00	419.67	87.00	59.50	56.00
Cr	25.30	163.17	719.40	82.65	91.00
Ni	111.00	228.00	234.00	69.00	109.00
Zn	132.00	122.00	142.00	150.00	116.00
Rb	14.80	92.90	30.30	342.60	19.50
Sr	196.30	106.50	425.60	370.05	423.20
Y	20.60	8.17	22.20	21.10	26.90
Zr	64.20	29.23	132.90	203.25	163.60
Nb	1.10	1.03	9.70	12.15	4.20

(*; no analysis)

the volcanics, and probably are not feeders to these flows.

The anomalously high-Fe concentration of the gabbroic sample 174 reflects iron oxide, pyrite and chalcopyrite mineralization, which clearly influences the relative amounts of other major elements. A simple re-normalization of the 174 analysis, after replacing the high Fe_2O_3 value (21 %) with a value representative of the volcanic average (15 %), results in major element chemistry similar to the volcanics. However, based on texture and mineralization 174 is considered to be a sample of the layered tholeiitic intrusion discussed in chapter 2 (Map 1).

Sample 306 has a similar texture to 174 (refer chap.2) and may also be related to the layered tholeiitic intrusion; however, the Jensen classification indicates that sample 306 is compositionally more similar to the volcanics than to sample 174. In addition the complex contact relationship, petrographic evidence of alteration (refer chap.2) and adjacent vein mineralization suggested that 306 is an altered volcanic as opposed to a gabbro.

5.3 Element Mobility

5.3.1 Gresens Calculations

Simple comparisons of the chemical composition of rocks subject to variable alteration are often misleading with respect to absolute gains and losses of elements associated with alteration. One reason for this complexity is that chemical analyses are expressed as percents so that absolute change in one or more elements alters the relative amounts of all other components. To express the true gains and losses of elements resulting from metasomatic processes Gresens (1967) proposed a method whereby a unique solution could be derived by either determination of the volume change or the assumption that at least one element remained immobile during the alteration. The general equation that describes the change x in component n in alteration of rock A to B is given by:

$$[f_v(gB/gA)c_n^B - c_n^A]100 = x_n$$

Where: f_v = the volume factor

gB = the specific gravity of the product

gA = the specific gravity of the starting composition

c_n^A = the concentration of the starting composition in percent of component n

c_n^B = the concentration of the product in percent of component n

x_n = gain or loss of component n in grams where the original content of component n in A is 100 g.

For a particular alteration sequence it is possible to estimate f_v, as suggested by Gresens (1967), on a plot of gains and losses versus f_v. Under this scheme a series of straight lines are produced, defined by each element, that show the gains and losses required to satisfy the above relationship for different volume factors. If a series of elements intersect the zero gain-loss line at a common value of f_v then it is likely that this is the correct volume factor and those elements that define it are immobile. Alternatively, if elements such as Al and Zr are known from independent criteria to be immobile, as has been suggested for rocks in the Temagami greenstone belt (Beswick and Soucie, 1978), then the value of f_v that satisfies the Gresens formula for x = 0 can be used.

5.3.2 Element Mobility in the Volcanics

5.3.2.1 Alteration of the High-Mg Tholeiites (2i), and the High-Fe Tholeiites (2j and 2k)

Before approaching the problem of deciphering alteration patterns amongst the volcanic rocks a datum or unaltered starting composition must be defined. For the purpose of this study it is desirable to define alteration or element mobility on a small scale where spatial relationships might be attributed to proximity to the breccia or intrusive contact. Other workers have considered element mobility in the Temagami greenstone belt, but these studies were conducted on a regional basis (Beswick and Soucie, 1978; Beswick and James, 1984; Brons, 1989).

Based on several criteria two samples (152, 342) were chosen and averaged to define least altered mafic volcanic. Sample 342 is a pillowed high-Mg tholeiite (2i) from an outcrop on highway 11 at grid location 290 SE, 900 SW. Sample 152 was taken near the breccia at grid location 340 SE, 130 SW from non-pillowed high-Mg tholeiite (2i). Petrographically these samples are typical examples of high-Mg tholeiite (2i) (refer chap. 2) except for the presence of well-defined primary plagioclase and a complete absence of biotite. The compositions of these two samples are

essentially the same with respect to all major and most trace elements. In the Jensen classification both samples plot at nearly the same point in the high-Mg tholeiite field (Fig. 5-1). Based on the presence of microscopic and outcrop scale primary textures and absence of extreme alteration these samples are considered an appropriate starting composition for the Gresens calculation. This starting composition or datum is meant to approximate the composition of basic volcanic rocks in this area, prior to hydrothermal alteration localized within and surrounding the breccia and intrusion. The starting composition does not represent a composition prior to earlier alteration such as sea water alteration, which may have altered the entire volcanic package. The analysis to follow assumes that, because the sampling area is small, the original or pre-alteration composition of volcanics was relatively homogeneous and that variations defined represent different degrees of alteration relative to this starting composition. It is also assumed that the difference in density between the starting composition and daughter are minimal and that exclusion of the density term from the Gresens relationship is relatively inconsequential.

As was suggested by Gresens (1967) a plot of gains and losses versus volume factor can be utilized to determine the

volume factor and the elements which have remained immobile during alteration. Rather than creating plots for every sample to determine the volume factor the method was carried out on a few samples to see if the volume relationship was consistent. Figure 5-2a is an example for a highly altered breccia fragment and it shows that some of the major elements including Si and Al intersect the zero gain-loss line near $f_v = 1$. Table 5-2 similarly lists the calculated value of f_v for $x = 0$ for Si, Al, Mn, and Zr. From these results it is apparent that Al Si and Mn are essentially immobile and that on average there is no significant net volume change associated with the alteration of most samples. Considering that alteration of the volcanics is weak it is not surprising that the volume has remained essentially constant.

The calculations have been expressed as a percentage gain or loss relative to the starting composition and then contoured to show spatial relationships. Several elements including Rb, Ba, Y, Cu, K, Na, Ca, Fe and Mg reveal systematic variations over the sampled area (Fig. 5-3 - 5-7). Other elements either display little variation or a lack of spatial dependence. The elements Rb, K and possibly Y behave similarly in that they are depleted in the north and enriched to the greatest degree within the mineralized

Figure 5-2a (page 172): Gresens diagram of gains and losses (g) versus the volume factor for an altered breccia fragment. The intersection of several lines near a volume factor of zero suggests that the alteration was not accompanied by a volume change and that the absolute amounts of these elements did not change during alteration.

Figure 5-2b (page 172): Gresens diagram calculated by use of the Gresens relationship and setting x = 0 (ie no loss or gain). Diagram represents data for individual samples 284, 300, 306 and an average of 3 breccia fragment analyses.

Figure 5-3a (page 173): Simplified geology of the breccia and adjacent rocks.

Figure 5-3b (page 173): Contoured results of the Gresens calculation for Y expressed as percentage gains and losses relative to the 'unaltered' parent.

Figure 5-4a (page 174): Contoured results of the Gresens calculation for Rb.

Figure 5-4b (page 174): Contoured results of the Gresens calculation for K.

Figure 5-5a (page 175): Contoured results of the Gresens calculation for Na.

Figure 5-5b (page 175): Contoured results of the Gresens calculation for Ba.

Figure 5-6a (page 176): Contoured results of the Gresens calculation for Ca.

Figure 5-6b (page 176): Contoured results of the Gresens calculation for Mg.

Figure 5-7a (page 177): Contoured results of the Gresens calculation for Fe.

Figure 5-7b (page 177): Contoured results of the Gresens calculation for Cu.

a

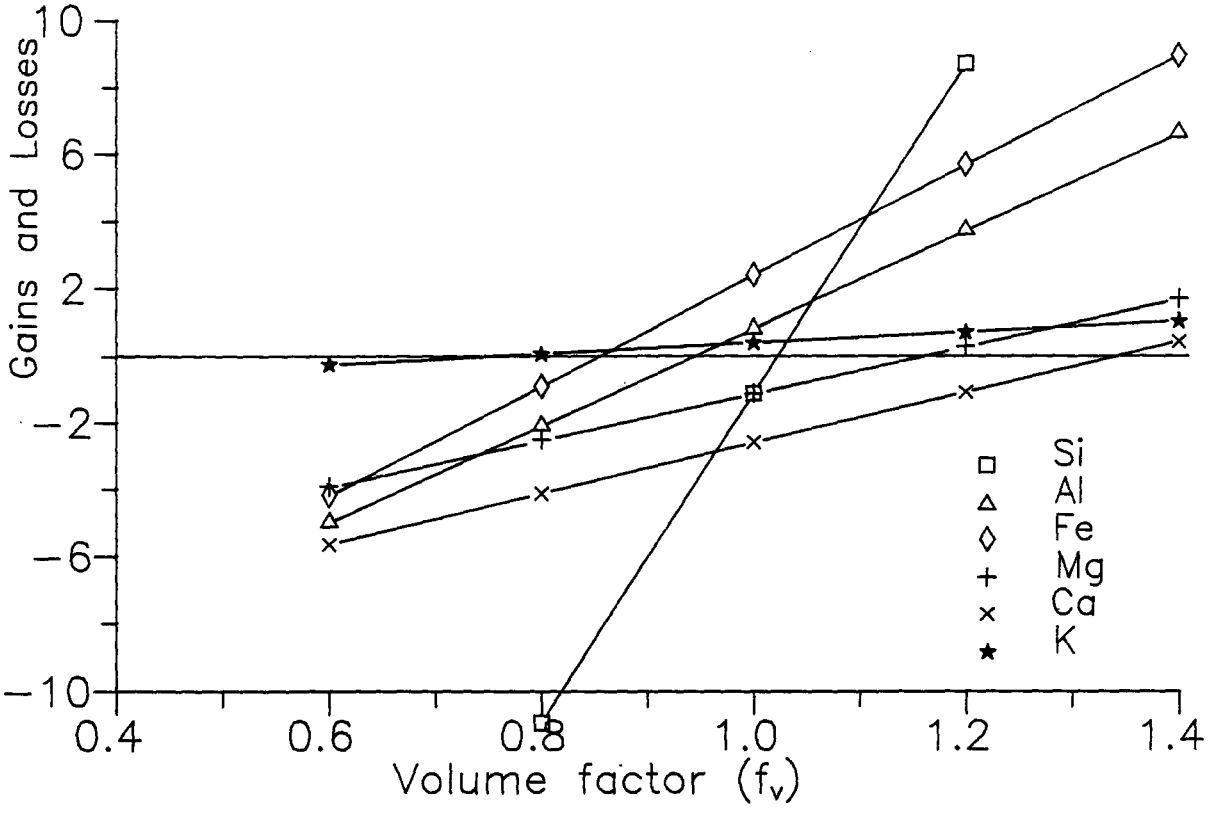
Gains and Losses
10
6
2
−2
−6
−10
0.4
0.6
0.8
1.0
1.2
1.4
Volume factor (f_v)
Si
Al
Fe
Mg
Ca
K

b

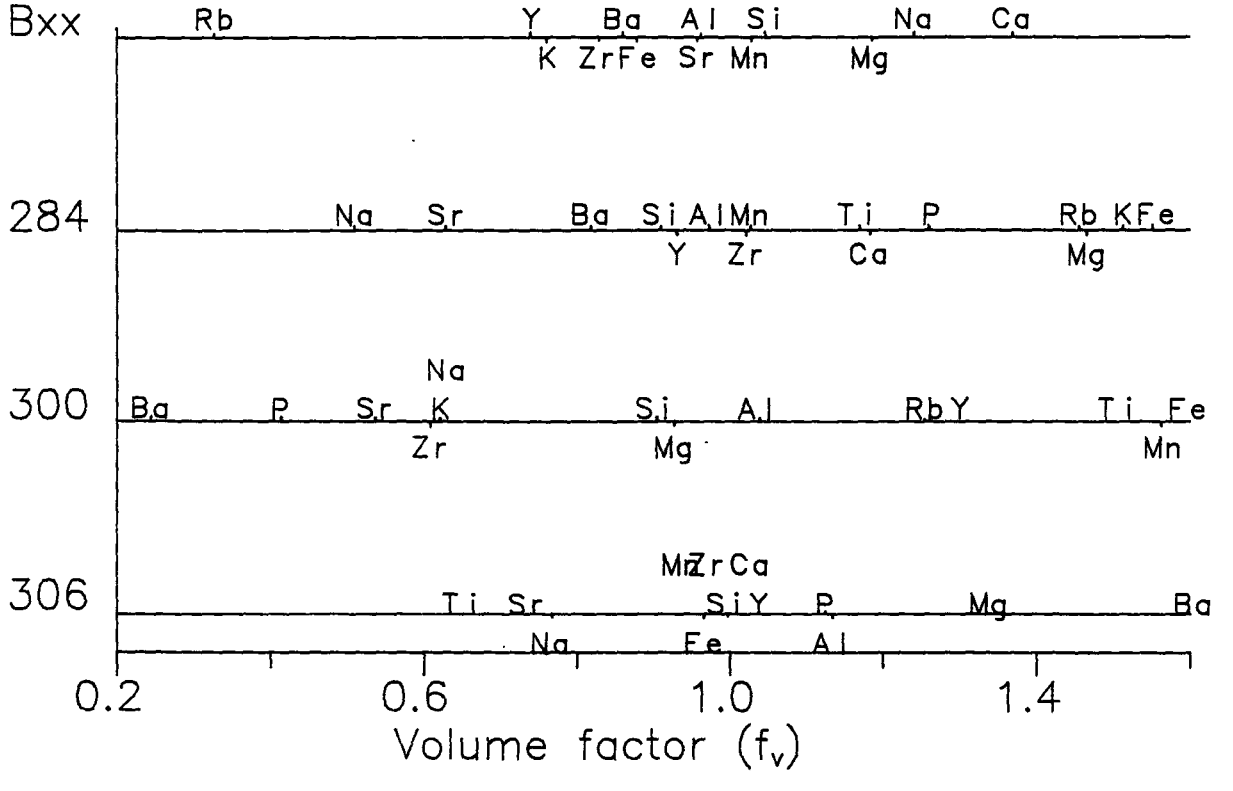
Bxx
Rb
Y Ba Al Si Na Ca
K Zr Fe Sr Mn Mg
284
Na Sr Ba Si Al Mn Ti P Rb K Fe
Y Zr Ca Mg
300
Na
Ba P Sr K Si Al Rb Y Ti Fe
Zr Mg Mn
306
Mn Zr Ca
Ti Sr Si Y P Mg Ba
Na Fe Al
0.2
0.6
1.0
1.4
Volume factor (f_v)

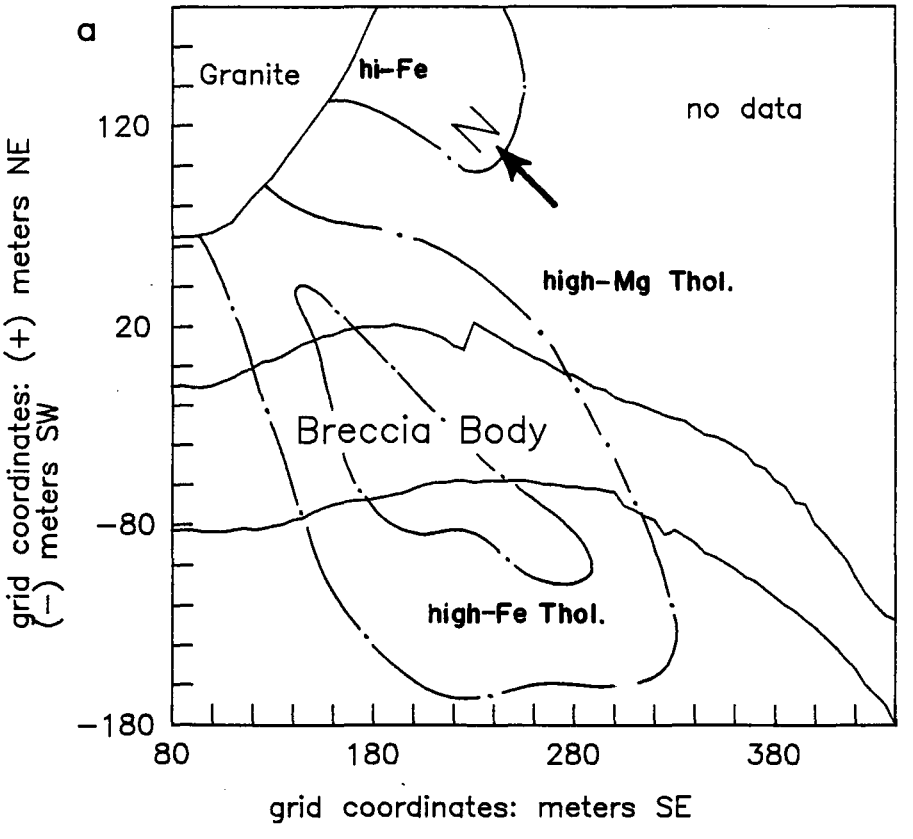
a
Granite
hi-Fe
no data
N
high-Mg Thol.
Breccia Body
high-Fe Thol.
120
20
-80
-180
80
180
280
380
grid coordinates: (+) meters NE
(-) meters SW
grid coordinates: meters SE

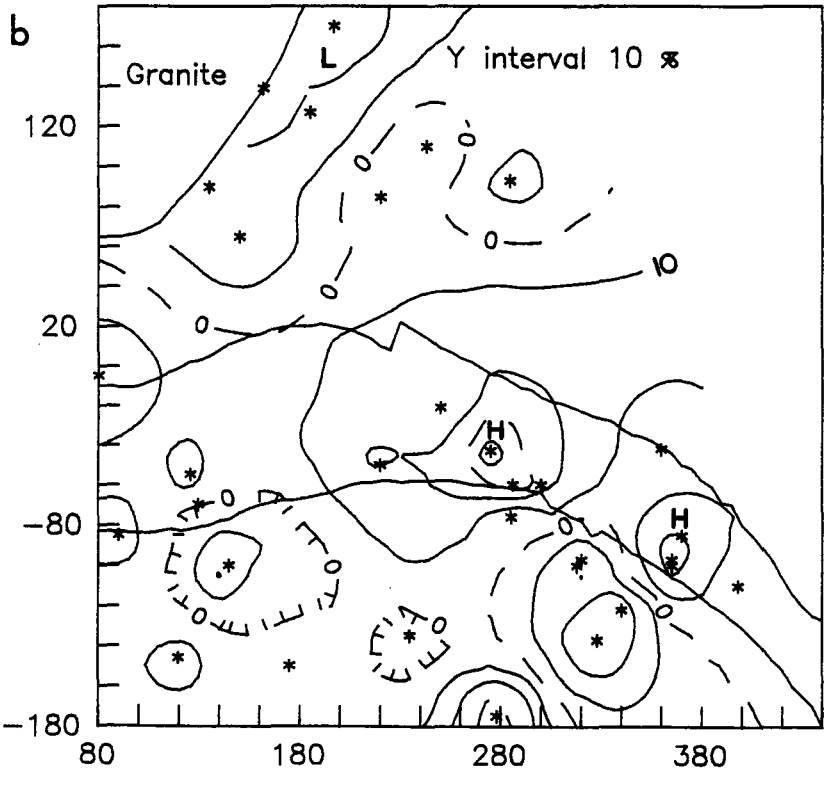
b
Granite
L
Y interval 10 %
H
H
0
10
120
20
-80
-180
80
180
280
380

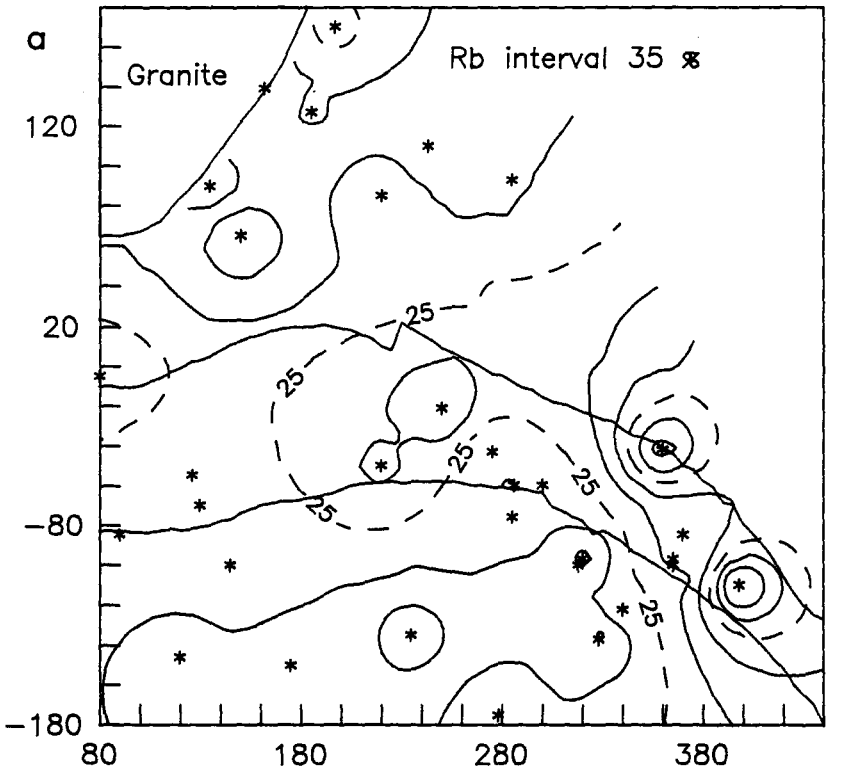
a
Granite
Rb interval 35 %
120
20
-80
-180
80
180
280
380
25
25
25
25
25
25

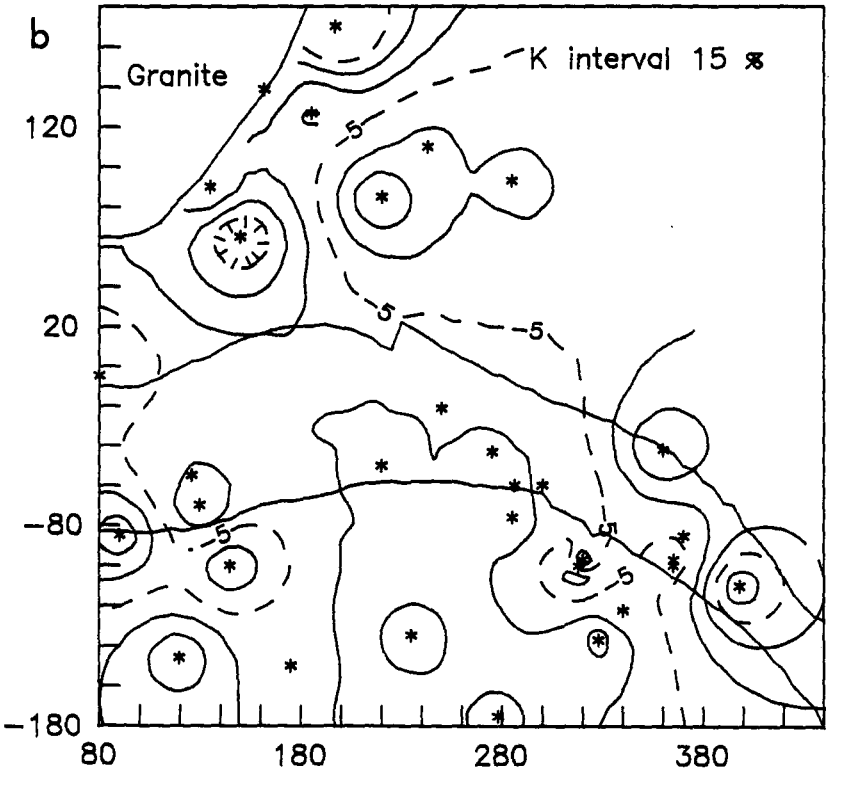
b
Granite
K interval 15 %
120
20
-80
-180
80
180
280
380
5
5
5
5
5
5

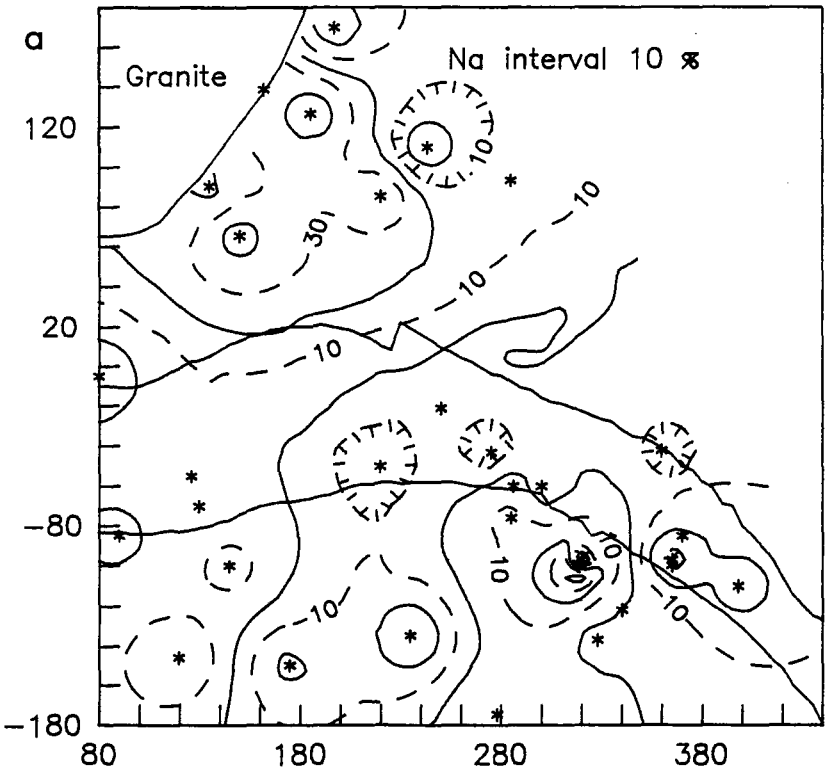
a
Granite
Na interval 10 %
120
20
-80
-180
80
180
280
380
10
30

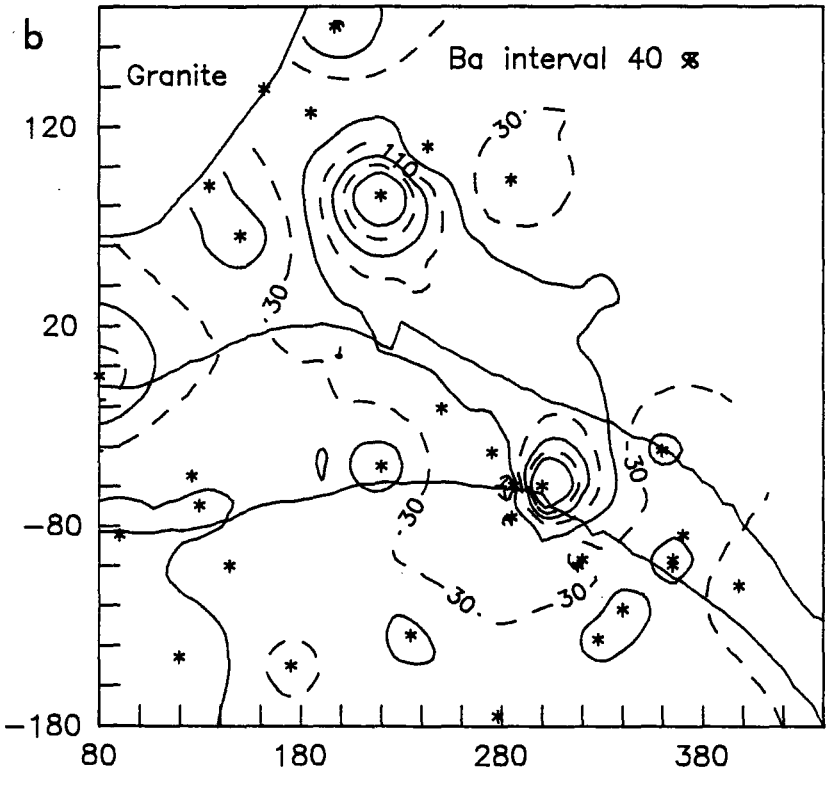
b
Granite
Ba interval 40 %
120
20
-80
-180
80
180
280
380
30
110

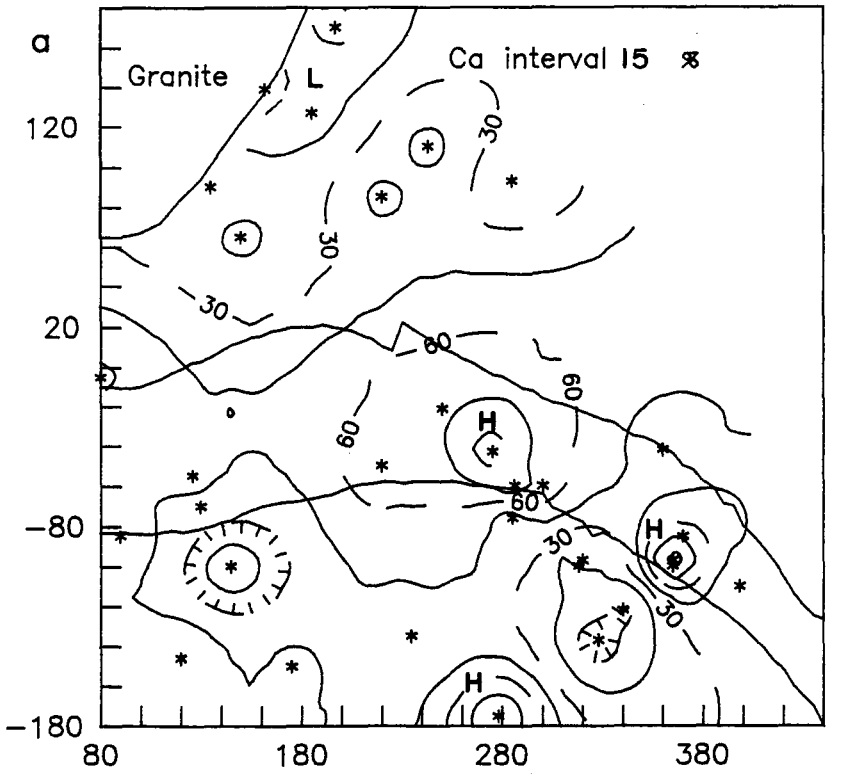
a
Granite
L
Ca interval 15 %
120
20
−80
−180
80
180
280
380
30
60
H
L

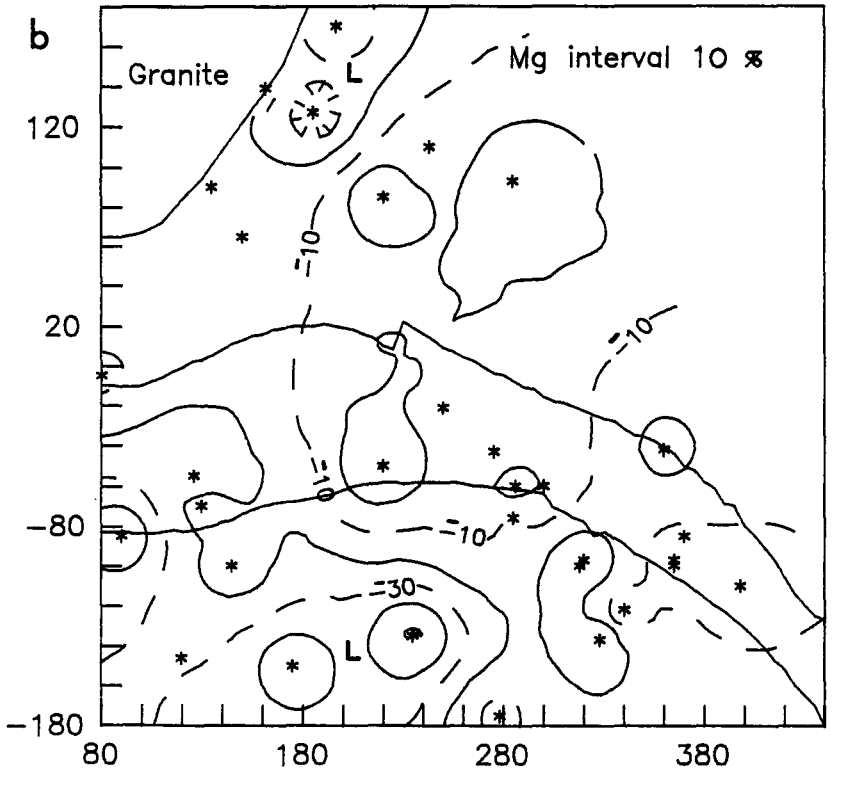
b
Granite
L
Mg interval 10 %
120
20
−80
−180
80
180
280
380
10
30
L

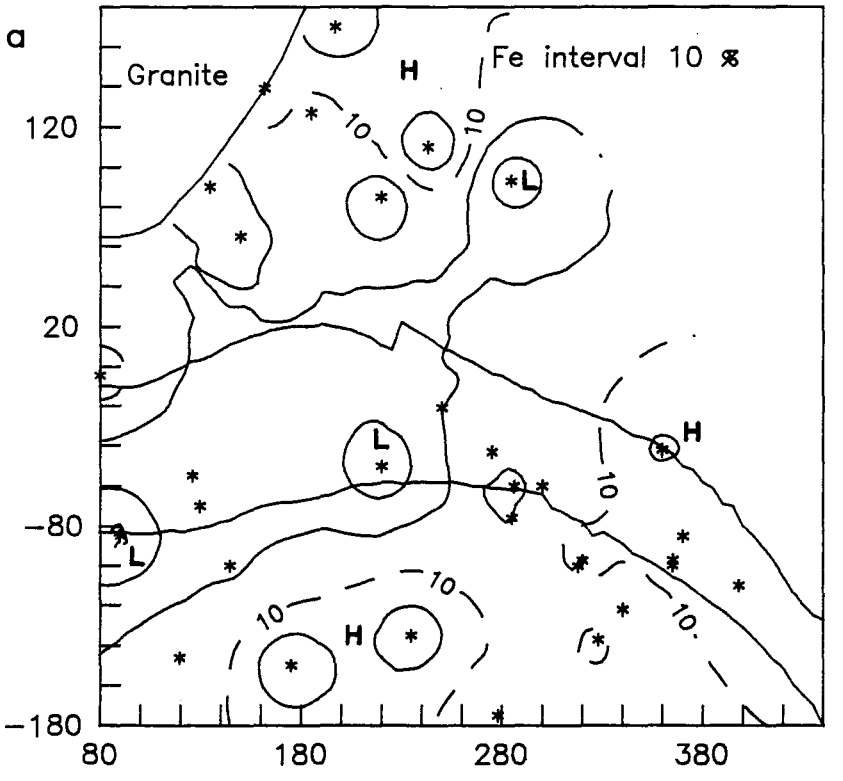
a
Granite
Fe interval 10 %
H
L
10
120
20
-80
-180
80
180
280
380

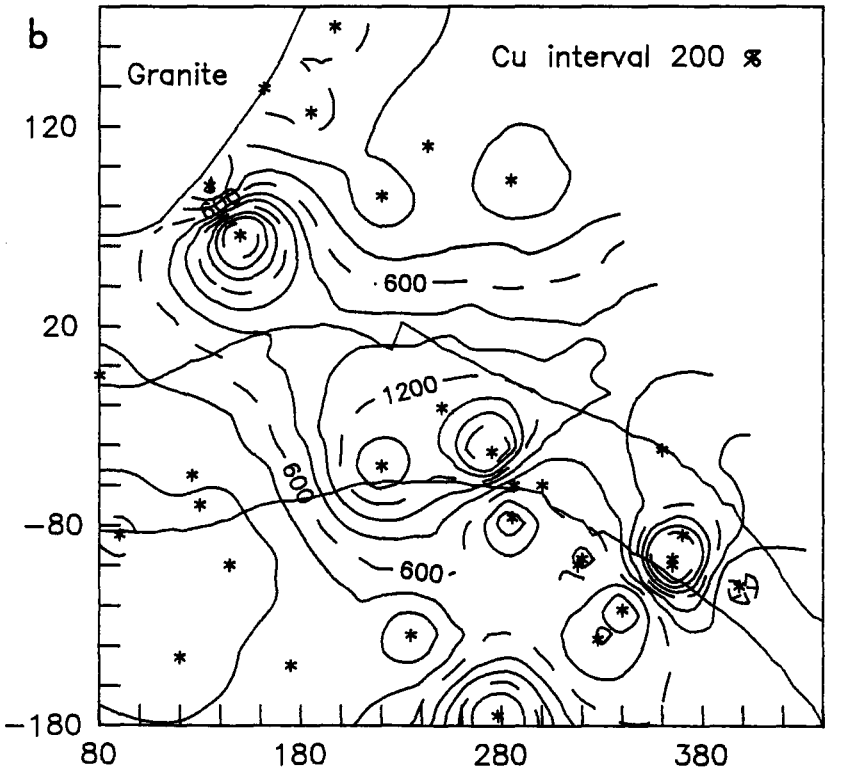
b
Granite
Cu interval 200 %
600
1200
120
20
-80
-180
80
180
280
380

TABLE 5-2

calculated values of fv when x = 0
(x is gain or loss in grams)

Sample	Type	Si	Al	Mn	Zr
89	2i	1.04	1.02	1.20	1.83
152	2i	1.04	0.99	1.20	1.44
233	2i	1.01	0.94	1.13	1.41
236	2i	1.00	0.96	0.95	1.10
238	2i	0.99	1.02	0.95	0.85
238	2i	1.01	0.98	1.06	1.22
136	2k	1.01	1.00	1.00	1.43
138	2k	0.97	0.98	0.82	1.25
247	2k	1.04	1.08	1.00	1.25
250	2k	1.04	1.00	0.78	1.43
133	2j	0.99	0.94	0.95	1.13
151	2j	1.04	0.89	0.86	1.31
153	2j	1.00	0.89	1.13	1.28
228	2j	1.04	0.99	0.90	1.33
241	2j	1.00	0.99	0.64	1.18
20	2o	1.03	0.96	0.78	0.84
265	2o	0.97	0.94	0.86	0.64
52f	Bxx. frag.	1.05	1.01	1.00	1.27
56f	Bxx. frag.	1.06	0.96	1.06	1.28
61f	Bxx. frag.	1.04	1.07	0.90	1.24
63f	Bxx. frag.	1.05	1.06	0.64	0.96
67f	Bxx. frag.	1.06	0.94	0.78	1.03
71f	Bxx. frag.	1.06	0.91	0.86	0.98
114f	Bxx. frag.	0.99	0.91	1.13	1.19
116f	Bxx. frag.	1.07	0.80	1.13	1.04
119f	Bxx. frag.	1.07	0.92	0.78	0.90
123f	Bxx. frag.	1.04	0.91	1.38	1.28
146f	Bxx. frag.	1.05	0.96	0.90	1.22
150f	Bxx. frag.	1.05	0.98	0.95	1.30
272f	Bxx. frag.	1.05	0.97	1.06	1.35
275f	Bxx. frag.	1.05	0.97	0.82	1.23
1344a	Bxx. frag.	1.03	0.98	0.90	1.21

(2i-high-Mg tholeiite; 2j,2k-high-Fe tholeiite;
2o-altered high-Mg tholeiite; bxx. frag.-breccia fragment)

breccia (Fig. 5-3,4). Rb in particular is only enriched within the breccia fragments, whereas K is also enriched in some of the surrounding volcanics. Na has a negative correlation with Rb, K and Y so that Na is conspicuously enriched adjacent to the intrusive contact and depleted within the mineralized breccia (Fig. 5-5). The inverse relationship between Ba and Ca is indicated by Ca enrichment in the 2o subdivision and in the central breccia, whereas Ba is depleted (Fig. 5-5b;5-6a). Magnesium is weakly enriched to the north of the breccia, within and adjacent to the breccia along the SW margin (Fig. 5-6b) and depleted south of the breccia. Iron is somewhat enriched in the extreme SW and NE borders of the area and is depleted within the NW end of the breccia (Fig. 5-7a). The distribution of Fe and Mg roughly correlates with the distribution of the high-Fe and Mg tholeiites defined previously (Map 2; Fig. 5-3). Copper distribution is erratic characterized by extreme highs in association with mineralized breccias and veins (Fig. 5-7b).

5.3.2.2 Alteration of Basalts Samples 284, 300, 306

These samples are investigated since they display features suggestive of intense alteration. Sample 284 is a highly bleached volcanic that contains vesicles and

hyaloclastite textures indicative of an extrusive origin (Plate 5-1a). The gain-loss versus f_v plot indicates that a volume factor of 0.95 should be adopted, assuming Al and Zr immobility (Fig. 5-2b). Sample 300, another altered volcanic sample, was bleached to a pale pinkish colour, and contained abundant myrmekitic textures suggestive of silicic and potassic alteration (Deer et al., 1983). Primary volcanic textures were lacking and field relationships did not show indisputable evidence that the precursor to this rock was a volcanic. A volume factor of 1 was obtained based on Al rather than Zr since Zr indicated a significant volume loss and a high degree of SiO_2 depletion, which is unlikely in an obviously silica-rich system with abundant quartz veining (Fig. 5-2b). Sample 306 is an amphibole-rich gabbroic sample in contact with fine-grained volcanics. Several elements including Si, Fe, Al, Mg and Zr indicated f_v values ranging between 0.9 and 1.1. Aluminium indicates a volume factor of 1.09 but because several elements clustered near $f_v = 1$ results have been calculated using both $f_v = 1.09$ and 1.0

Results from the calculations indicate that samples 284 and 300 were similarly altered while sample 306 shows contrasting alteration behaviour (Table 5-3). Significant changes for sample 284 include gains in Na, Sr, Nb and

possibly Si, and losses in Fe, K, P, Ti, Cu and Rb. Sample 300 shows significant gains in Si, Mg, Na, K, P, Ba, Sr, Zr and Nb and losses in Fe, Ti, Ca and Mn. Common features between 284 and 300 are gains in Na, Sr and Nb and losses in Fe and Ti. Sample 306 displays contrasting behaviour to 284 and 300 in that it shows gains in Si, Mg, Ca, Na, Ti, Mn, Cu, and Sr and losses of K, Ba, Rb and Nb.

5.3.3 Discussion of Results

5.3.3.1 Alteration of the Volcanics Near and Within the Breccia

One of the best defined relationships is the coupled enrichment of K and Rb centred around the mineralized portion of the breccia. The most likely mineralogical expression of this chemistry is the increased amount of biotite, which contains abundant K and Rb, noted within the fragments of the mineralized zone (Plate 4-8c). As noted in chapter 2, Brons (1989) defines a biotite zone within inner metamorphic contact aureole. Such biotite zones are relatively common in porphyry Cu-Mo deposits and in these systems are considered to represent the early potassic alteration halo (Titley, 1975; Carson et al., 1974; Cheney

TABLE 5-3

Gains and Losses expressed as a percentage relative to the parent (average of sample 152,342)

(oxides as percent trace elements in ppm)

Sample ->	284	300	306	306
volume factor ->	0.94	1.00	1.09	1.00
SiO_2	1.81	10.00	8.56	-0.60
Al_2O_3	0.13	0.37	0.00	-8.43
Fe_2O_3	-45.33	-43.07	4.05	-4.73
MgO	-6.17	60.43	20.31	10.16
CaO	-6.07	-36.22	30.98	19.93
Na_2O	93.05	65.88	47.76	35.29
K_2O	-31.38	80.73	-58.92	-62.39
TiO_2	-24.77	-37.93	60.68	47.13
MnO	3.89	-27.78	33.48	22.22
P_2O_5	-25.20	150.00	-1.71	-10.00
Ba	18.13	363.87	-30.76	-36.60
Cu	-73.11	-14.51	92.39	76.17
Rb	-34.59	-18.55	-67.41	-70.16
Sr	54.46	95.19	53.84	40.87
Y	1.68	-22.46	6.37	-2.60
Zr	-6.12	71.15	15.60	5.85
Nb	154.13	207.69	-38.39	-43.59

and Trammell, 1975). In their discussion of Archean and Proterozoic REE pegmatite granitic intrusions, Cerny and Meintzer (1988) refer to the biotitization of adjacent metabasalts as part of the process of granite exomorphism and that the formation of biotite indicates K outflow. They also mention that elements such as Rb can be expected to form subtle haloes in the country rocks. The inverse relation between Na and K-Rb is further suggestive of potassic alteration, which is essentially an exchange of K for Ca and Na (Beane, 1982). These features imply that biotite represents an introduced alteration phase associated with K-metasomatism like that apparent in many porphyry mineral deposits. In this study the alteration is centred on the breccia and in the satellite breccia to the north where it is locally intense (Plate 4-8d). Alteration was probably concentrated within the area of the breccia because of high permeability, and was most intense in the satellite breccia because of proximity to the intrusive. The presence of another biotite zone near Temagami North (Brons, 1989), is probably a reflection of hydrothermal and intrusive activity in that area (refer chap.2). Biotite is not only a replacement phase in volcanics, but is also common in the breccia and vein matrix where it forms partial selvages. The presence of biotite as a replacement mineral in the

volcanics and as a primary mineral in the quartz domains affirms that potassic alteration associated with intrusion and peak metamorphism was synchronous with vein and breccia formation.

The distribution of Fe and Mg variation is difficult to interpret. It is not known if the high-Mg tholeiites and high-Fe tholeiites, of which the Mg, Fe data are a reflection, are primary lithologic units or represent secondary alteration. The higher Fe and Ti content of the high-Fe tholeiites (2j,2k) is probably reflected in the presence of secondary biotite and Fe, Ti-rich amphibole (refer chap.2). Unfortunately these mineralogical differences could have been caused by either metasomatic activity or different primary lithologies.

Copper is difficult to interpret since isolated patches of mineralization are likely responsible for elevated Cu values. It is no surprise that Cu is highest within the mineralized zone, but from the Cu enrichments adjacent to the breccia it appears that the mineralizing fluids formed disseminated mineralization in wall rocks as well as in veins.

Ca shows uneven enrichment in a number of areas including unit 2o, which was distinguished from 2i by having a coarser texture and displaying probable metasomatic

textures (Plate 2-10b). Thin sections from this area revealed a greater proportion of epidote and carbonate veinlets as well as secondary quartz, and up to 20 % replacement of feldspar grains by sericite. These replacement and microveinlet textures indicate that fluids permeated this zone. The inverse correlation of Ba with Ca may be explained by fluid alteration since Ba might be released by alteration of feldspar and fractionated into the fluid phase.

5.3.3.2 Intensely Altered Samples

The significant addition of K to sample 300, the metasomatized volcanic, would seem to indicate K-metasomatism or potassic alteration (Lowell and Guilbert, 1970) similar to that found in porphyry Cu-Mo deposits. The significant decrease in Fe and increase in Na, however, do not adhere to the normal patterns of potassic alteration. The addition of K and Si and possibly the depletion of Fe, Ca, Ti and Mn are attributed to sericite alteration of feldspar, quartz replacement of amphibole and K-feldspar replacement as evidenced by myrmekitic textures (Deer et al., 1983; Plate 5-1b). An abundance of secondary carbonate may be a source of the strong Sr and Ba enrichment while

abundant apatite is likely a reflection of the enriched P. Biotite is not apparent, although it may have been replaced by chlorite.

Sample 284 is dominantly comprised of a fine-grained intergrowth of quartz and plagioclase, with less than 10 % hornblende, interupted by veinlets and amygdules filled with epidote and hornblende. The depletion of Fe, Mg and Ti is evidenced by the replacement of mafic minerals, and the increase in Na by the introduction of plagioclase. The apparent element mobility shown by sample 306, the gabbroic sample, is supported by several microscopic textures. The increased Si is apparent as extensive replacement of amphibole by quartz and quartz dominated microveinlets. Ca and Na enrichment may be expressed by the abundant plagioclase that extensively replaces amphibole. In addition the occurrence of epidote and carbonate in veinlets with quartz and chlorite may have contributed to Ca enrichment. Enriched Ti likely originates from the rimming of secondary carbonate grains with sphene. Because the alteration of 306 was so much different to that shown in other volcanics it is suggested that it may have been altered by fluids associated with the emplacement of the tholeiite intrusion rather than those associated with the Strathy-Chambers batholith.

5.4 Summary

The geochemical investigation of the volcanics and associated rocks reveals several features. Firstly the mapped volcanic subdivisions can be characterized chemically so that group 2i rocks classify as high-Mg tholeiites and 2j and 2k as high-Fe tholeiites. Analysis of the mafic dykes, which cut the breccia, indicate significant chemical contrasts with the volcanics, suggesting that there is no genetic affinity with the volcanics and that they probably belong to a later episode of basaltic magmatism. The two analyses of the gabbroic rocks suggest sample 174 is part of the tholeiitic intrusion and that the precursor to 306 may have been a volcanic rock altered by fluids associated with the tholeiitic intrusive. The bleached volcanic samples 284 and 300 behaved analogously with respect to several elements. Both samples are in very close contact with the underlying intrusives and not surprisingly they were affected in a similar manner by hydrous fluids that permeated these contact areas. A significant observation is that areas corresponding to the biotite zone (Brons (1989) experienced K and Rb metasomatism, or potassic alteration, analogous to that found in porphyry mineral deposits.

Potassic or biotite alteration was developed to the greatest degree in the brecciated volcanics often in accompaniment with mineralization.

CHAPTER 6

GEOCHEMISTRY OF INTRUSIVE ROCKS AND THOSE ASSOCIATED WITH THE STRATHY-CHAMBERS BATHOLITH

6.1 Introduction

Major element oxides, trace elements and rare earth elements (REE) were determined on a suite of intrusive rocks considered comagmatic with the Strathy-Chambers batholith. These rocks included: felsic porphyry dykes, granitic rocks, weakly mineralized granites (< 2% combined sulphides) and associated aplites and pegmatites. In addition to classifying these rocks study of the intrusive geochemistry was carried out to determine whether the local porphyritic dykes and granitic rocks were comagmatic, being linked by some process of crystal fractionation. The felsic dykes are known to cut the breccia, so if the granites and dykes are comagmatic then a relative time constraint can be put on the timing of breccia formation and mineralization. In addition

the cause and source of the hydrothermal activity that produced the breccia, veins and mineralization are not obvious, and there seems to be little perceptible textural or mineralogical variation of the granite over the immediate study area. It was considered important to recognize any spatially controlled chemical variation within the Strathy-Chambers batholith near intrusive-volcanic contact. To test for such variation samples were analyzed from a traverse that extended along highway 11, approximately perpendicular to the volcanic-intrusive contact (Fig. 6-1). Four samples of Strathy-Chambers batholith, from southern Best township and Chambers township were also analyzed in order to represent a more average composition (Fig 6-1). Samples of pegmatites and aplites were analyzed to gain insight into their formation since they likely evolved during the late stages of intrusive crystallization. Four samples of weakly mineralized granites were also analyzed to determine if these rocks displayed any compositional contrasts with adjacent unmineralized granitic rocks. Two fine-grained samples, of quenched granite, (refer chap.2 sec. 2.2.2) were also analyzed. Poor outcrop exposure made it difficult to interpret the field associations of these rocks, but it was hoped that the geochemistry could at least define whether or not they were of granitic affinity.

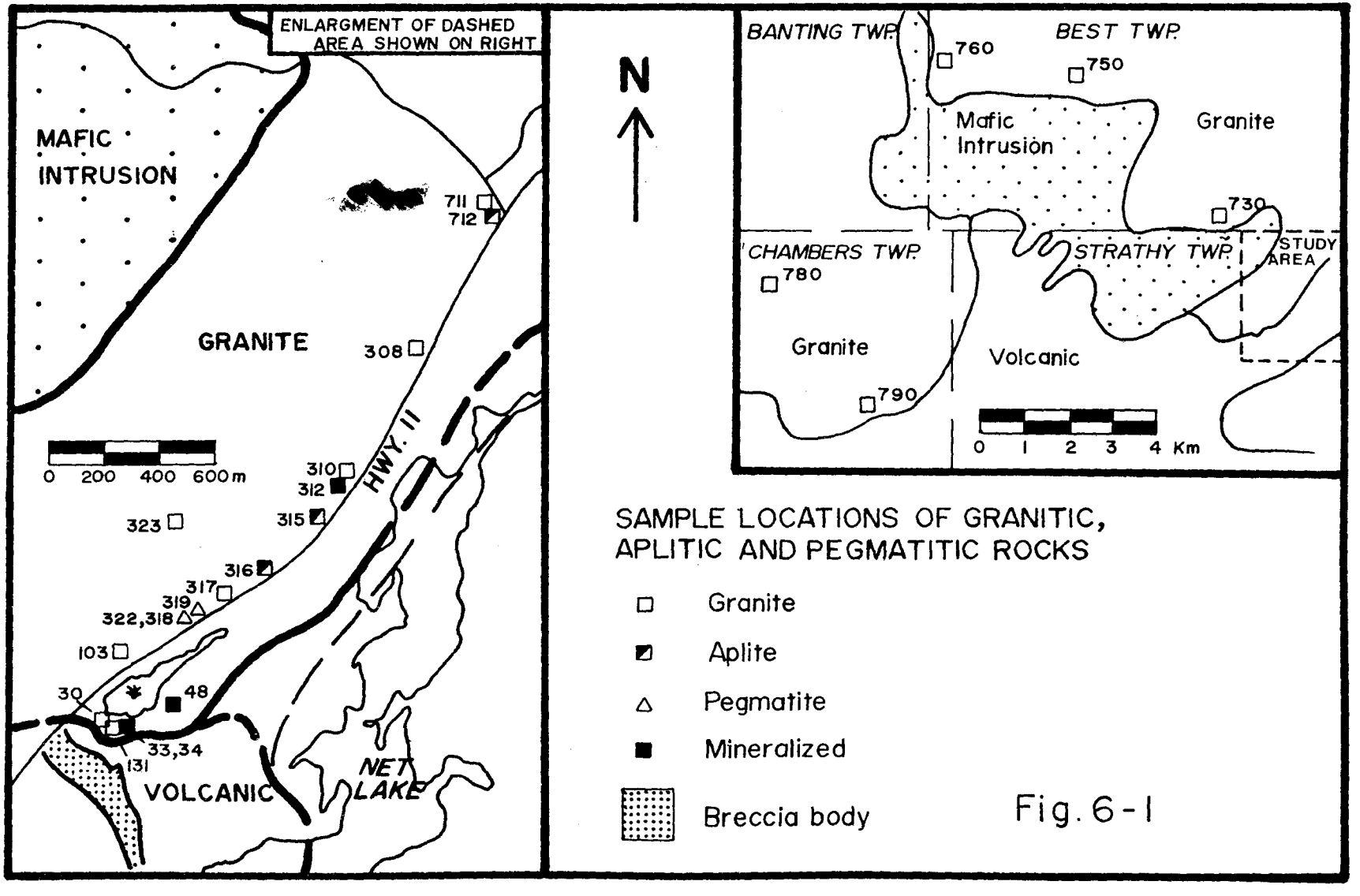
ENLARGMENT OF DASHED AREA SHOWN ON RIGHT
MAFIC INTRUSION
GRANITE
VOLCANIC
NET LAKE
HWY. 11
0 200 400 600m
711
712
308
310
312
315
323
316
317
319
322,318
103
30
48
33,34
131
N
BANTING TWP.
BEST TWP.
760
750
Mafic Intrusion
Granite
730
CHAMBERS TWP.
STRATHY TWP.
STUDY AREA
780
Granite
Volcanic
790
0 1 2 3 4 Km
SAMPLE LOCATIONS OF GRANITIC, APLITIC AND PEGMATITIC ROCKS
Granite
Aplite
Pegmatite
Mineralized
Breccia body

Fig. 6-1

Most of the results of the major and trace element results have been represented on Harker and ratio variation diagrams. Chemical data are also plotted against distance from the volcanic-intrusive contact to define any spatial dependence. Rare earth element (REE) results are plotted on chondrite normalized profiles as well as on Harker and concentration versus distance (dist.) diagrams.

Chemical variations defined on the various plots suggest the existence of a comagmatic suite extending between end members represented by the felsic dykes and some of the most Si-rich granitic rocks. In order to test the validity of this proposed relationship a semi-quantitative major element mass balance calculation was completed and supplemented by Raleigh fractionation models utilising the large ion lithophile elements (LIL), Rb, Sr and Ba. Variation of the light rare earth elements (LREE) also suggested fractionation of LREE-bearing phases, so this was also tested by mass balance calculations. As a further investigation of the validity of crystal fractionation, the europium anomalies were used to model the differentiation process.

6.2 Major Element Results

6.2.1 Classification

Using the normative mineral assemblages and the Streckeisen classification, (Streckeisen, 1973; Fig. 6-2b) most of the samples classify as either granodiorite or granite. If the trend from granodiorite to granite represents a comagmatic differentiation series, it would then correspond to the calk-alkaline granodiorite trend as defined by Lameyre and Bowden (1982). Dyke samples trend toward the granodiorite field while granites and mineralized granites lie mostly within the granite field. These results indicate different contact phase compositions as compared with the overall trondhjemite composition of the Strathy-Chambers batholith put forth by Fyon and Wheatley (1988), and Fyon et al. (1988) and the quartz monzonite composition suggested by Bennett (1978). In his study area, which comprises the east-west trending lobe of intrusive on the southwest shore of Net Lake, Brons (1989), classifies the Strathy-Chambers batholith as granodiorite with border phases of trondhjemite. According to the Streckeisen classification used in this study it would appear that some of the samples are more felsic than the average composition of the intrusive documented by others. Intrusive rocks are also plotted on an AFM diagram, which shows that the samples

follow a strong calk-alkaline trend that approaches the alkaline apex (Fig. 6-2a) (Carmichael et al., 1974). There is no compositional gap on the AFM plot, and the rocks of different lithologies overlap and lie along a tightly defined trend. The fields defined by the modified Peacock diagram (Cerny et al., 1988) do not extend to the region occupied by these samples, but extrapolation of the fields shows that the samples actually span all three (Fig. 6-3). The dykes occupy the tholeiitic and calk-alkaline region while the granitic rocks extend well into the alkaline field. On the basis of aluminium saturation (Shand, 1943) all samples classify as peraluminous, a feature compatible with ubiquitous normative corundum.

6.2.2 Harker Diagrams

Major elements are plotted as weight percent oxides against SiO_2 in figure 6-4,5. The SiO2 ranges from 63 % to 81 %, a large enough variation to justify using SiO2 as an index of differentiation. For the entire group of samples it is observed that the oxides of Al, Fe, Mg, Ca, Ti, and P all show a negative correlation with SiO_2, while K displays a positive correlation. Plots of Al_2O_3 and TiO_2 versus SiO_2 show very tightly constrained linear arrays with minor

Figure 6-2a (page 195): AFM plot of granitic and porphyritic samples. Line dividing fields between tholeiitic and calk-alkalic suites from Irvine and Baragar, 1971.

Figure 6-2b (page 195): Classification of granitic and porphyritic rocks. Field 1, granites; Field 2, granodiorites; Field 3 Tonalites (Streckeisen, 1973)

Figure 6-3 (page 196): Modified Peacock diagram (Cerny and Meintzer, 1985) of granitic and porphyritic rocks. Symbols same as for figure 6-2.

Figure 6-4 (page 197): Major element concentrations versus SiO_2 for granitic and porphyritic rocks. Symbols same as for figure 6-2.

Figure 6-5 (page 198): Major element concentrations versus SiO_2 for granitic and porphyritic rocks. Symbols same as for figure 6-2.

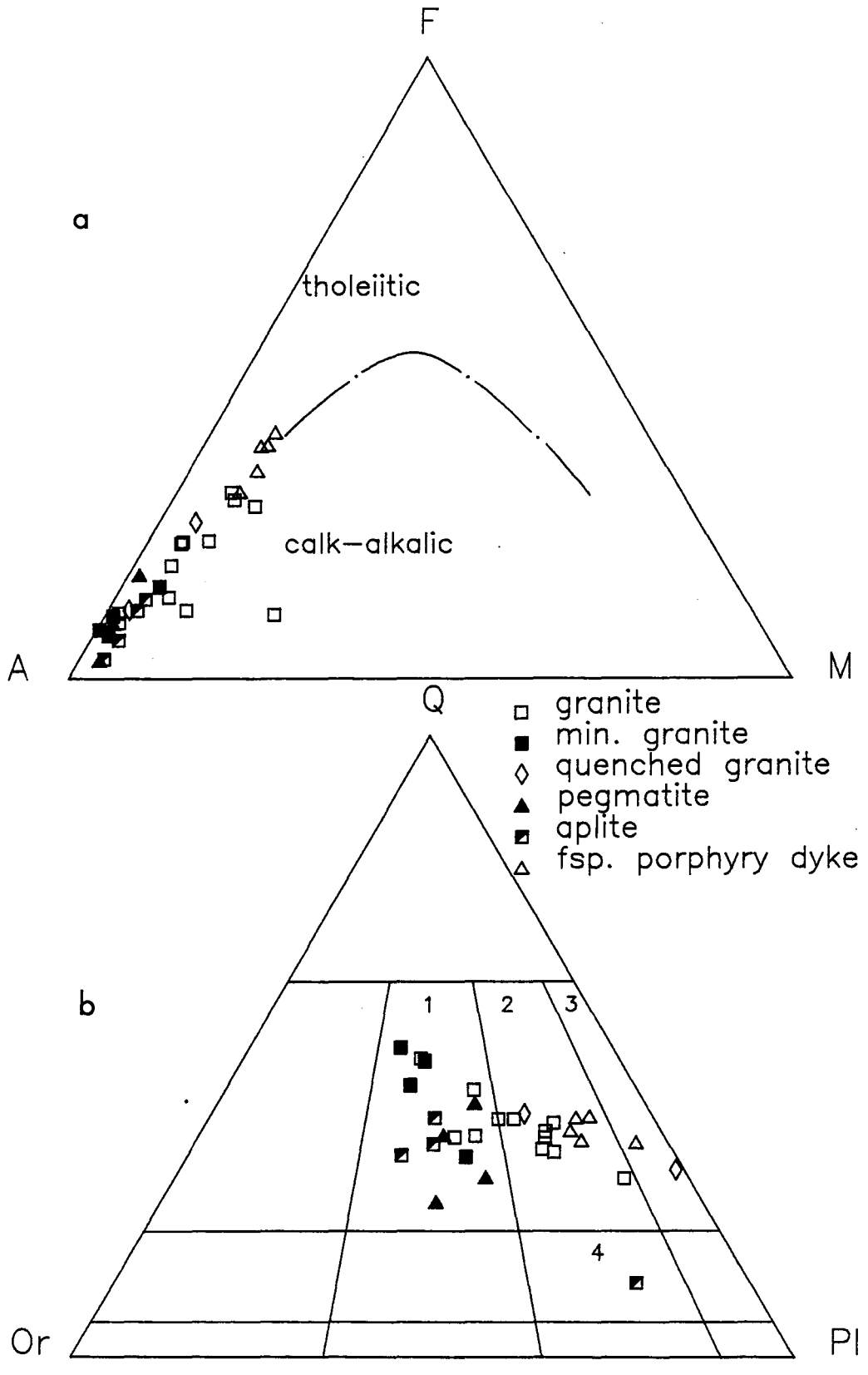
F
a
tholeiitic
calk–alkalic
A
M
Q
granite
min. granite
quenched granite
pegmatite
aplite
fsp. porphyry dyke
b
1
2
3
4
Or
Pl

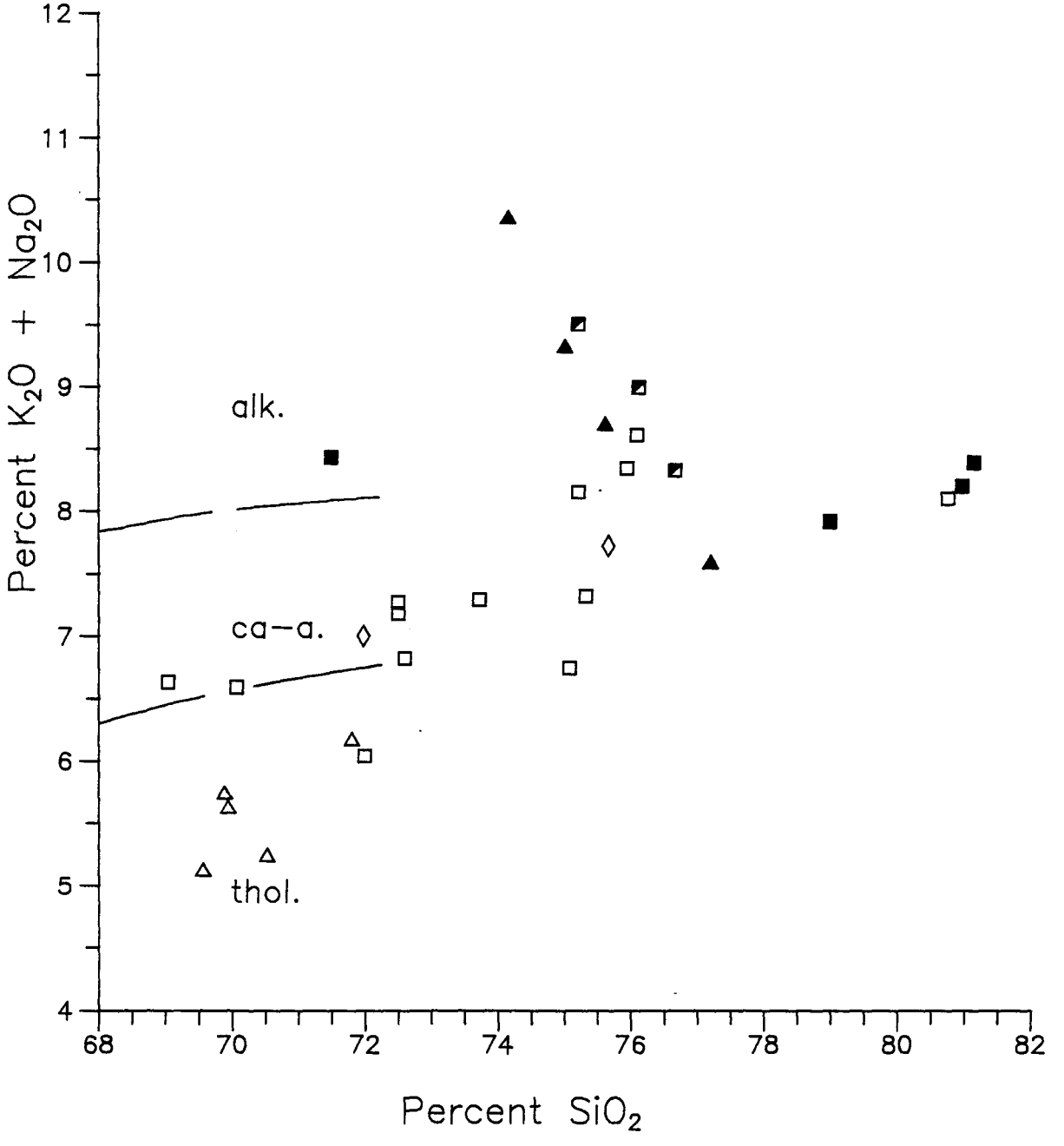
12
11
10
9
8
7
6
5
4
Percent $K_2O + Na_2O$
alk.
ca–a.
thol.
68
70
72
74
76
78
80
82
Percent SiO_2

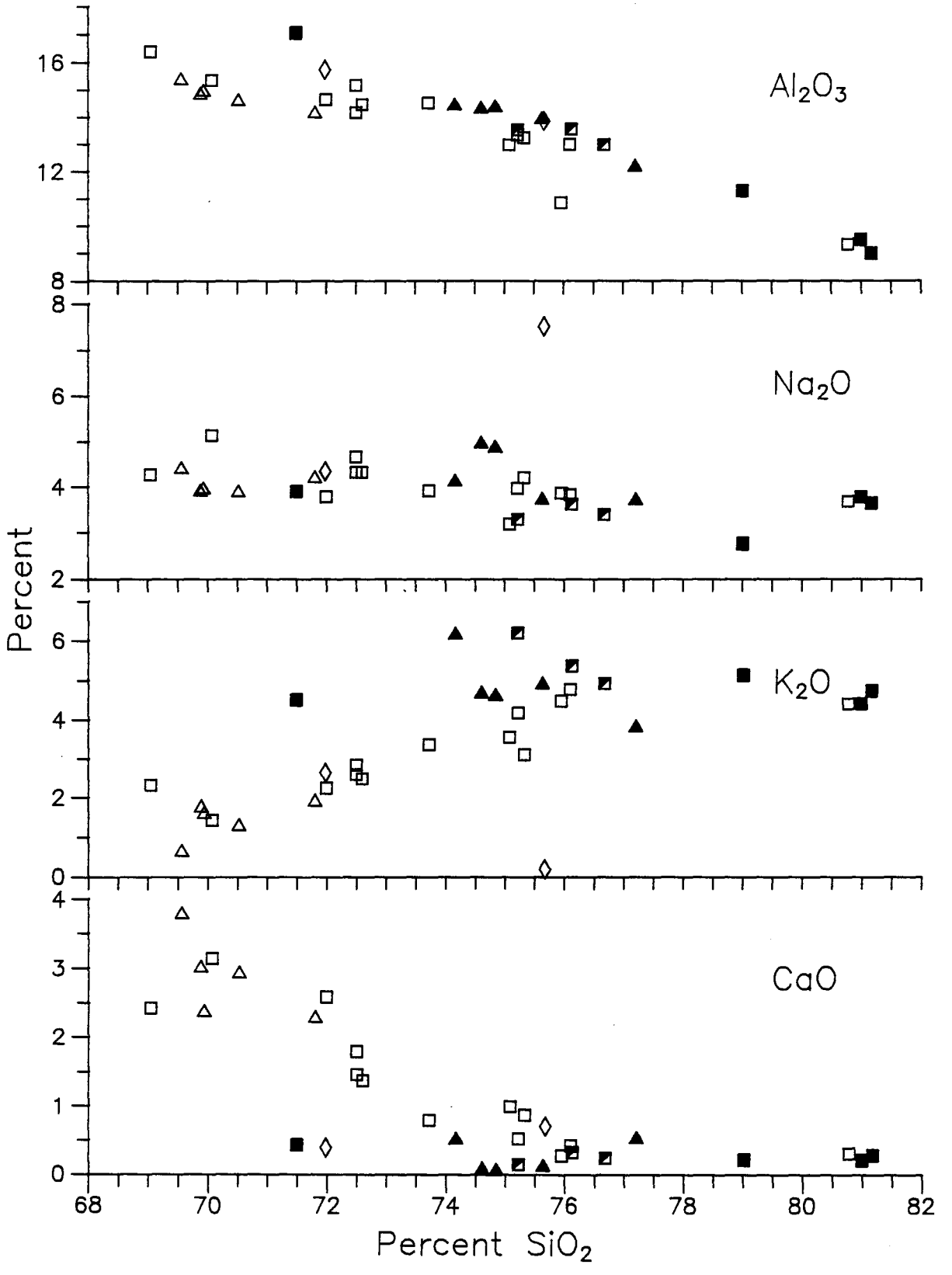
Al2O3
Na2O
K2O
CaO
Percent
Percent SiO2
16
12
8
6
4
2
0
3
1
68
70
72
74
76
78
80
82

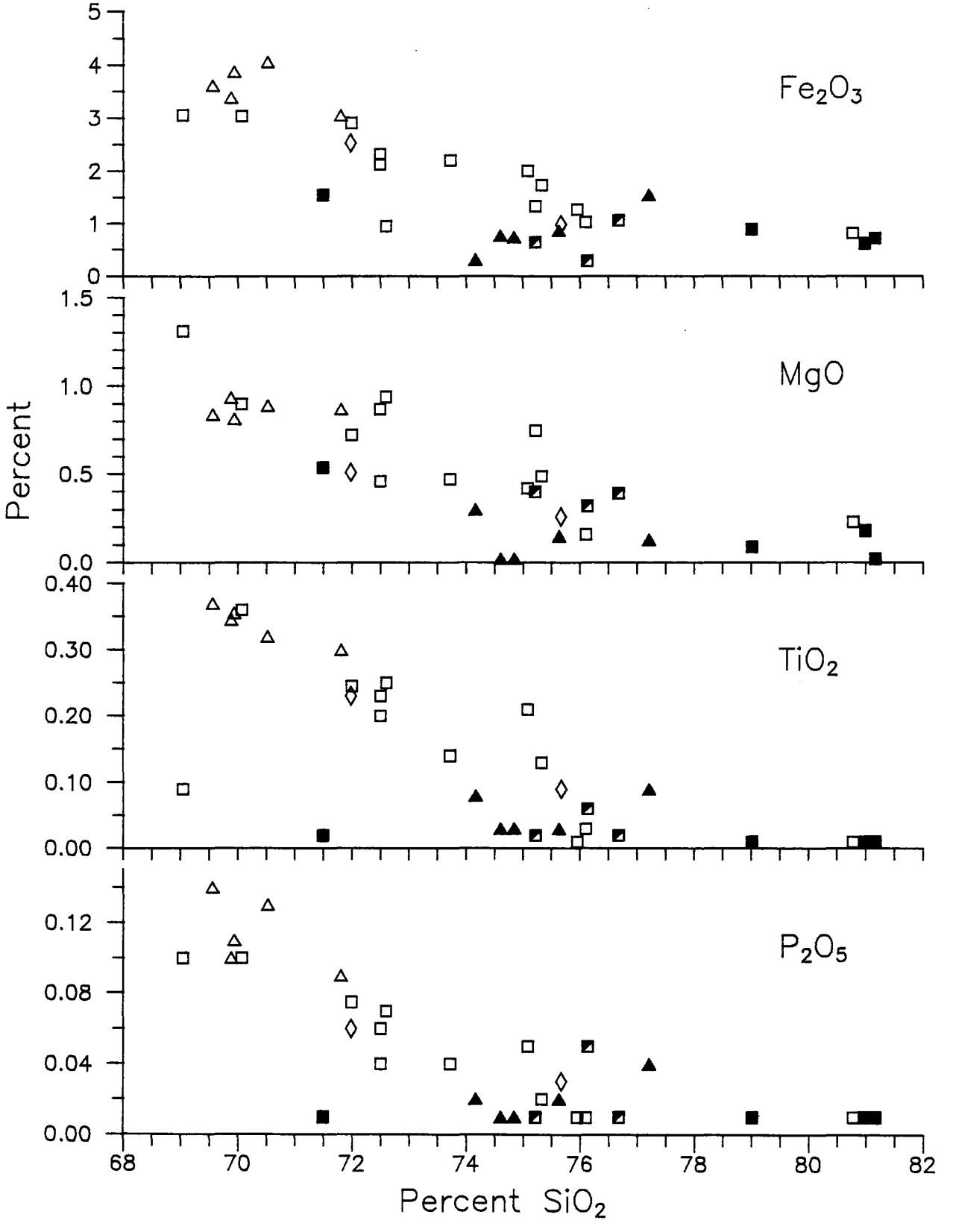
Fe2O3
MgO
TiO2
P2O5
Percent
Percent SiO2
5
4
3
2
1
0
1.5
1.0
0.5
0.0
0.40
0.30
0.20
0.10
0.00
0.12
0.08
0.04
0.00
68
70
72
74
76
78
80
82

overlap between granite and dyke samples. If it is assumed that Ca, Fe and Mg decrease with increasing differentiation, due to fractionation of minerals such as plagioclase pyroxenes and amphiboles, then the felsic dykes probably are the most primitive members of a differentiation sequence extending from the low-Si dykes to the Si-rich granites. Aplites and pegmatites generally posses an evolved character similar to the high-Si granites, but not surprisingly there is considerable scatter within the pegmatitic samples, likely owing to their coarse-grained texture.

Deviations from the linear trends are most evident in mineralized samples and aplites and pegmatites with greater than 75 % SiO_2. Relative to the trend defined by the granite samples, with the exception of sample 30, three of the four mineralized samples are comparatively enriched in SiO_2. Aplites and pegmatites are compositionally similar to high-Si granites; however, pegmatites show significant variation. The two quenched granites usually lie on trends with the other granitic rocks, however, they show anomalous behaviour in some elements. Sample 298, the high-Si aphanitic sample (refer chap.2), shows strong depletion in K, and enrichment in Na. Sample 290, the less Si-rich porphyritic sample, is markedly depleted in Ca. In later sections it is noted that the trace element concentrations

of these samples are also anomalous.

The Harker plots of major elements indicate an apparent comagmatic differentiation series between the dykes and Si-rich granites. The felsic dykes may represent a parental composition that evolved to one represented by the most Si-rich granites, through separation of feldspar, mafics, and accessories such as ilmenite, magnetite, zircon and sphene.

6.2.3 Major Elements as a Function of Distance From the Intrusive-volcanic contact (dist.)

The majority of intrusive samples were taken along a 3 km traverse along highway 11 (Fig. 6-1). This traverse is approximately perpendicular to the Strathy-Chambers-volcanic contact, beginning at the point nearest the breccia body and quartz vein system. The main reason for this sampling scheme was to test for the presence of any compositional variation within the granite as a function of the distance (dist.) from the contact at that point.

Oxide concentrations as a function of radial distance (dist.) from volcanic-intrusive contact, at the point nearest the breccia body, are plotted in figures 6-6 and 6-7. Line segments have been drawn between successive granite sample locations to clarify the general trends. The same

Figure 6-6 (page 201): Major element concentrations versus distance from the intrusive volcanic contact, opposite the breccia body. Line segments join granitic samples to better illustrate the variations. The two samples at 250 and 1200 m are distinct from the rest of granitic samples (see text). Symbols same as for figure 6-2.

Figure 6-7 (page 202): Major element concentrations versus distance from the intrusive-volcanic contact, opposite the breccia body. Symbols same as for figure 6-2.

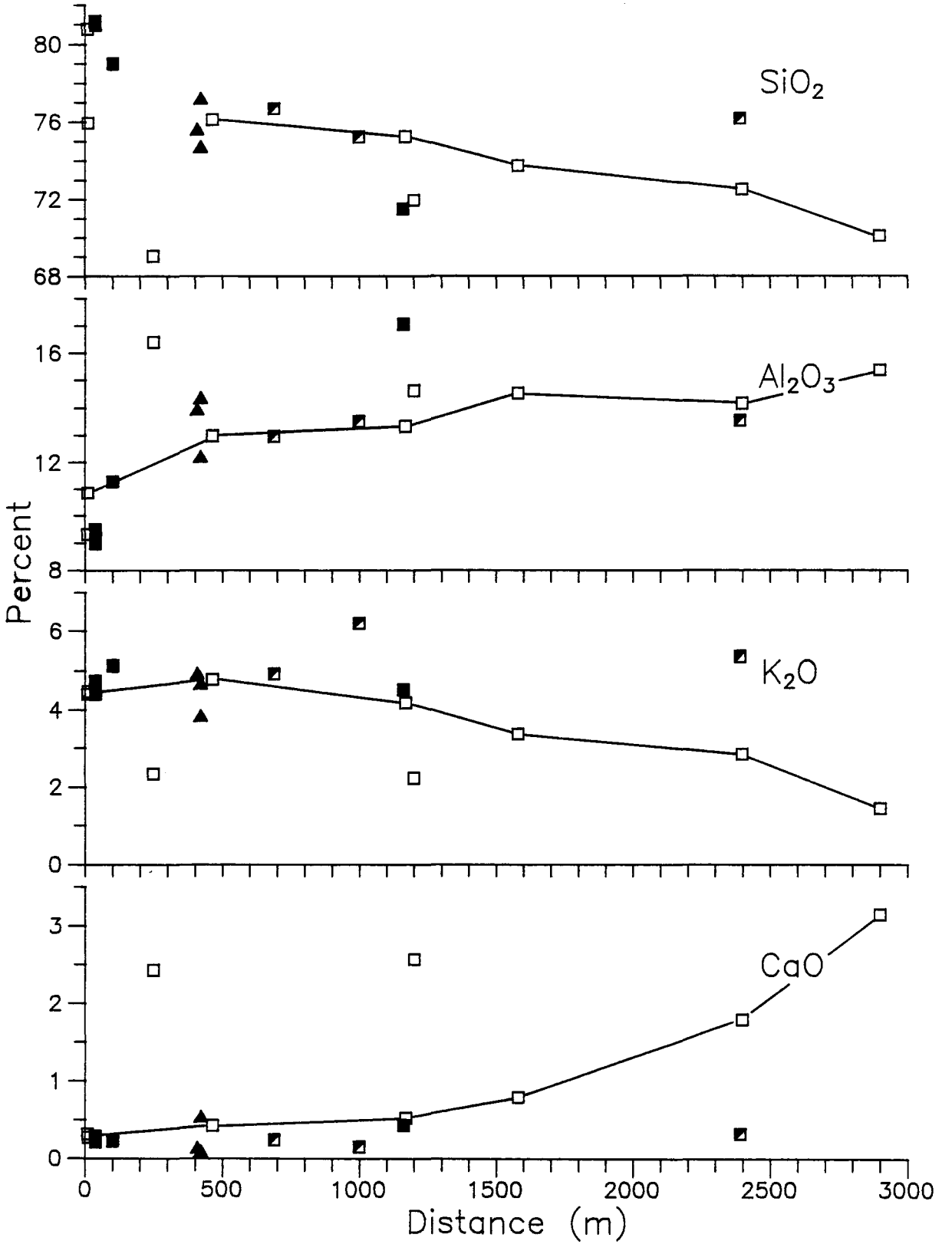
80
76
72
68
SiO_2
16
12
8
Al_2O_3
Percent
6
4
2
0
K_2O
3
2
1
0
CaO
0
500
1000
1500
2000
2500
3000
Distance (m)

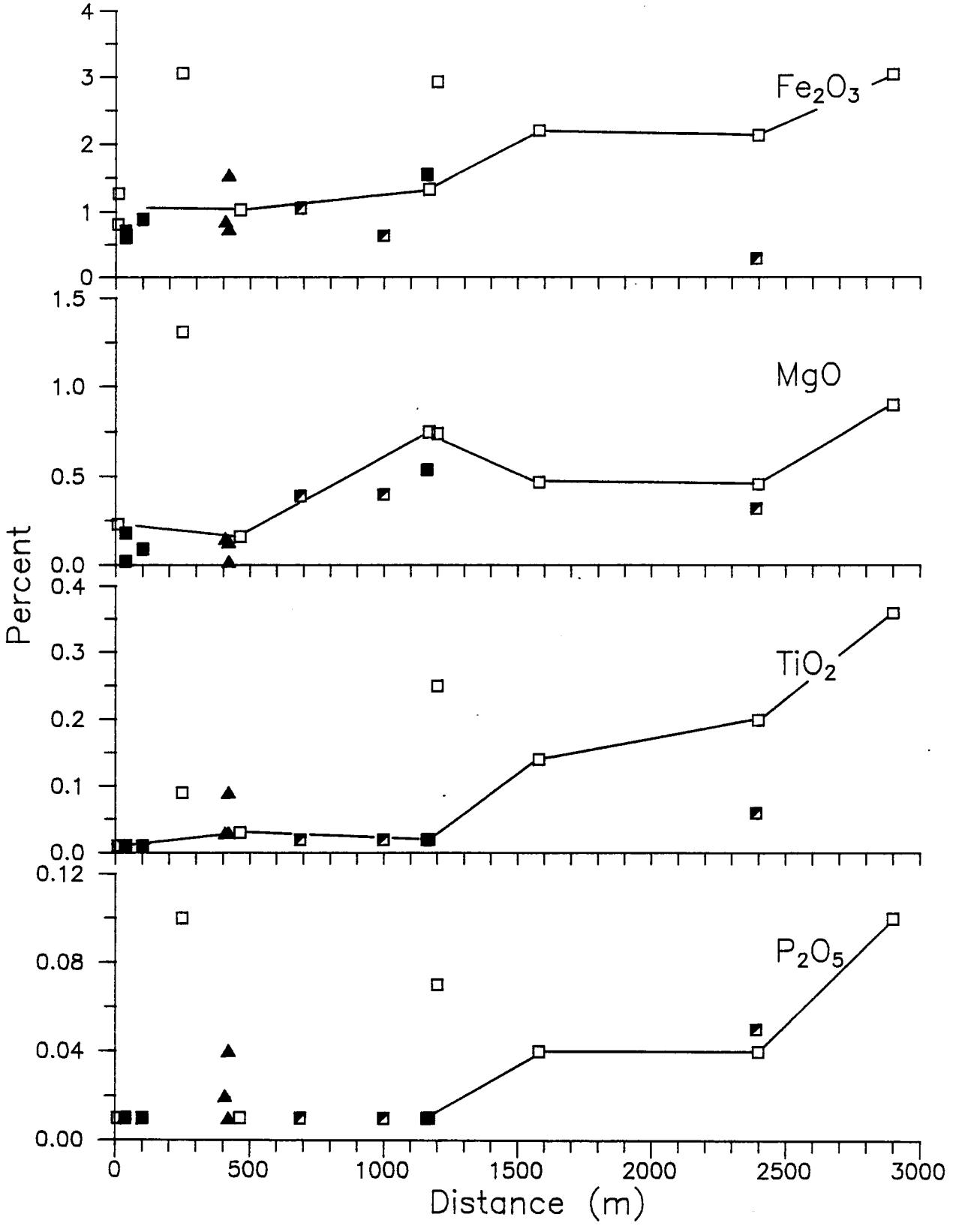
Fe2O3
MgO
TiO2
P2O5
Percent
Distance (m)
0
500
1000
1500
2000
2500
3000

groups of rocks are also shown without the dykes, which for obvious reasons do not fit under such a scheme. The first significant feature is a dependence of major element abundances on distance from the contact. Secondly it is obvious that samples 103 and 323 do not plot along the trend lines defined by the granites. The latter sample of buff coloured granite was taken approximately 300 m NW of the traverse line, whereas 103 was taken from the most southerly outcrop on highway 11 south of a transition from pink to buff coloured granite (Fig. 6-1). According to Bennett's map (1978), sample 323 and possibly 103, lie to the north of an inferred fault, which is not exposed adjacent to the samples, but is in the road cut approximately 2 km to the northeast on highway 11 (Map 1; Fig. 6-1). Alternatively these two samples may represent a different phase of the intrusive that was emplaced or evolved at a different time. In either case they will not be included in the discussions of the concentration versus dist. plots.

Oxides versus dist. plots exhibit moderate to well defined correlations that suggest a relationship between degree of differentiation and dist. In particular the oxides of Al, Ca, Fe, Mg and Ti are depleted towards the contact, whereas Si and K are enriched. Mineralized granites, likely by no coincidence, occur primarily adjacent

to the contact and because they occur only in close proximity (Fig. 6-1) to the contact it is not possible to observe any compositional dependence on dist. As already noted on the Harker plots the mineralized granites seem to have major element compositions very similar to adjacent unmineralized granites.

Three aplite samples indicate a lack of any spatial-compositional dependence. Compared to the host granites the aplites have major element compositions, except for Al, more similar to the most evolved granites.

Pegmatites are exposed within a restricted zone (Fig. 6-1) within the granite, so, as with the mineralized granites, no spatial dependencies can be defined. The relationship of the pegmatites to the host granites is not obvious because of the few samples and large compositional variation; nevertheless, the pegmatites seem to have major element compositions similar to the host granites.

6.3 Trace Element Results

Trace element analysis of Ba, V, Cr, Ni, Pb, Zn, Rb, Sr, Y, Zr, and Nb was conducted by X-ray fluorescence (XRF) (appendix A). Instrumental neutron activation analysis (INAA) was used for the determination of As, Co, Th, U, Sc,

Cs, Au, Sb, W, Mo, Hf, Ta and Cl concentrations (appendix A). Details of the analytical procedures, results and precision of results are given in the appendices A, B and C.

6.3.1 Harker Diagrams

The trace element data are graphically represented on Harker plots shown in figures 6-8 through 6-10. Strontium, Ba, Zr and Sc correlate negatively, while Th, U and Ta correlate positively with SiO_2. The Sr plot is very similar to CaO versus Si in that the trend is well defined with dyke and granitic samples overlapping and the trend flattens with increasing Si. The Ba versus Si trend is more complex, and indicates that Ba initially increases but subsequently decreases relative to Si. Zirconium and Hf both decrease against Si with significant scatter in the high-Si samples. The similar depletion of Zr and Hf suggests zircon fractionation. Sc also shows depletion against SiO_2. Sc is known to partition into pyroxenes, amphiboles and sphene (Henderson, 1986), so it is possible that at some period one or more of these phases precipitated from the parental magma. Although the trend is weak Ta appears to increase with increasing Si. It has been suggested that because of the high ionic potential of Ta and Nb they should form oxide

Figure 6-8 (page 206): Trace element concentrations versus SiO_2 for granitic and porphyritic rocks. Symbols same as for figure 6-2.

Figure 6-9 (page 207): Trace element concentrations versus SiO_2 for granitic and porphyritic rocks. Symbols same as for figure 6-2.

Figure 6-10 (Page 208): Trace element concentrations and trace element ratios versus SiO_2 for granitic and porphyritic samples. Symbols same as for figure 6-2.

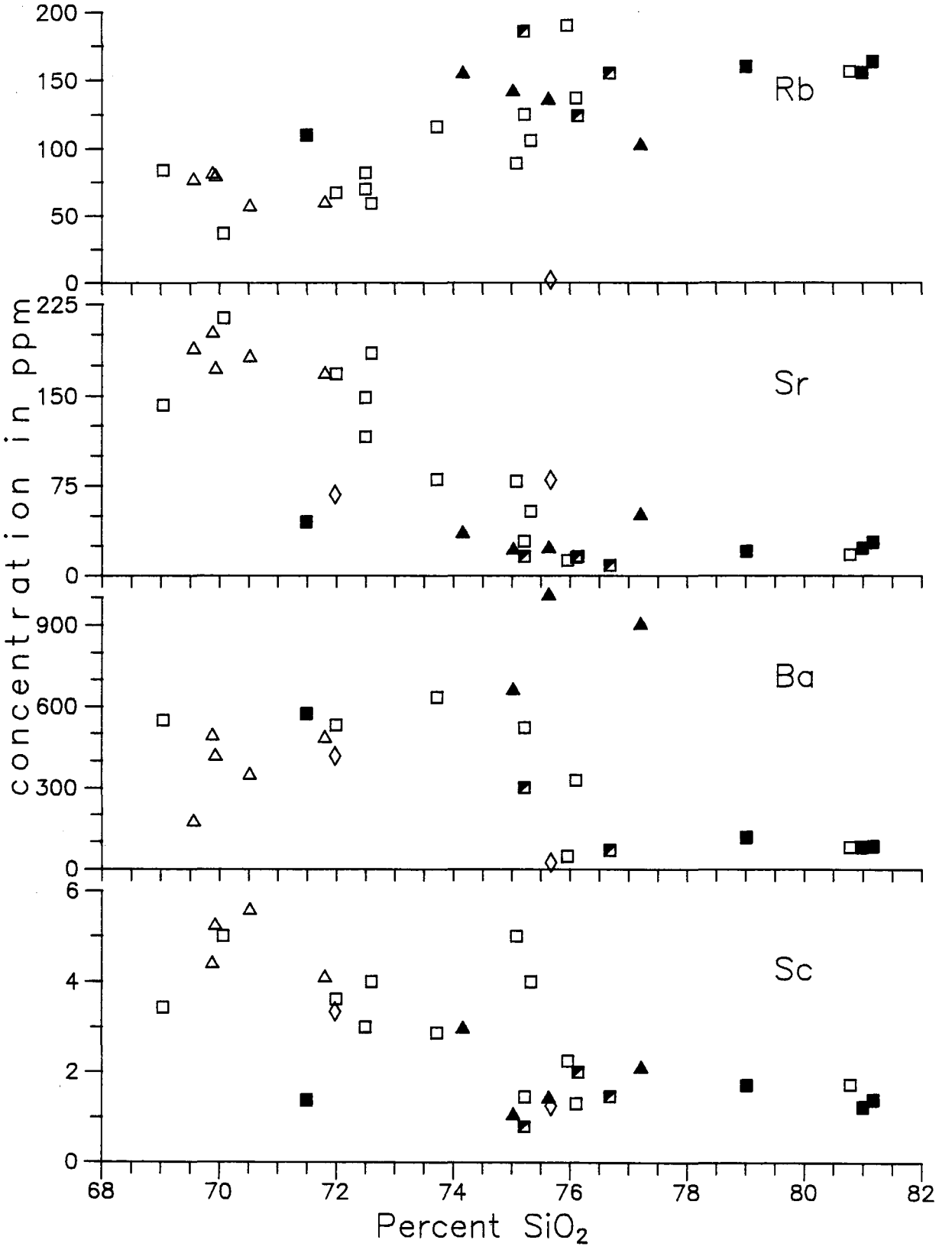
Rb
Sr
Ba
Sc
concentration in ppm
Percent SiO_2
200
150
100
50
0
225
150
75
0
900
600
300
0
6
4
2
0
68
70
72
74
76
78
80
82

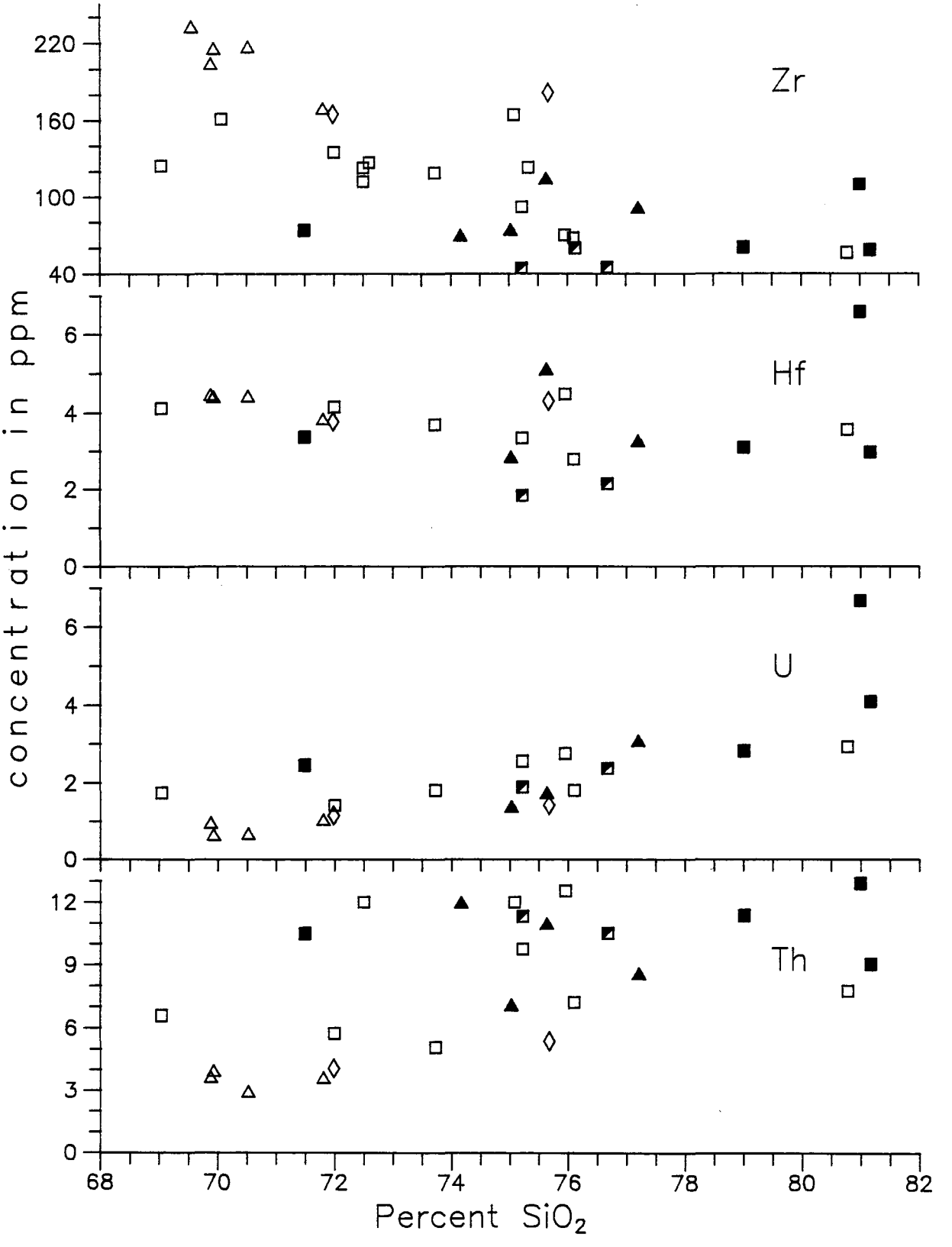
Zr
Hf
U
Th
concentration in ppm
Percent SiO_2
220
160
100
40
6
4
2
0
12
9
3
68
70
72
74
76
78
80
82

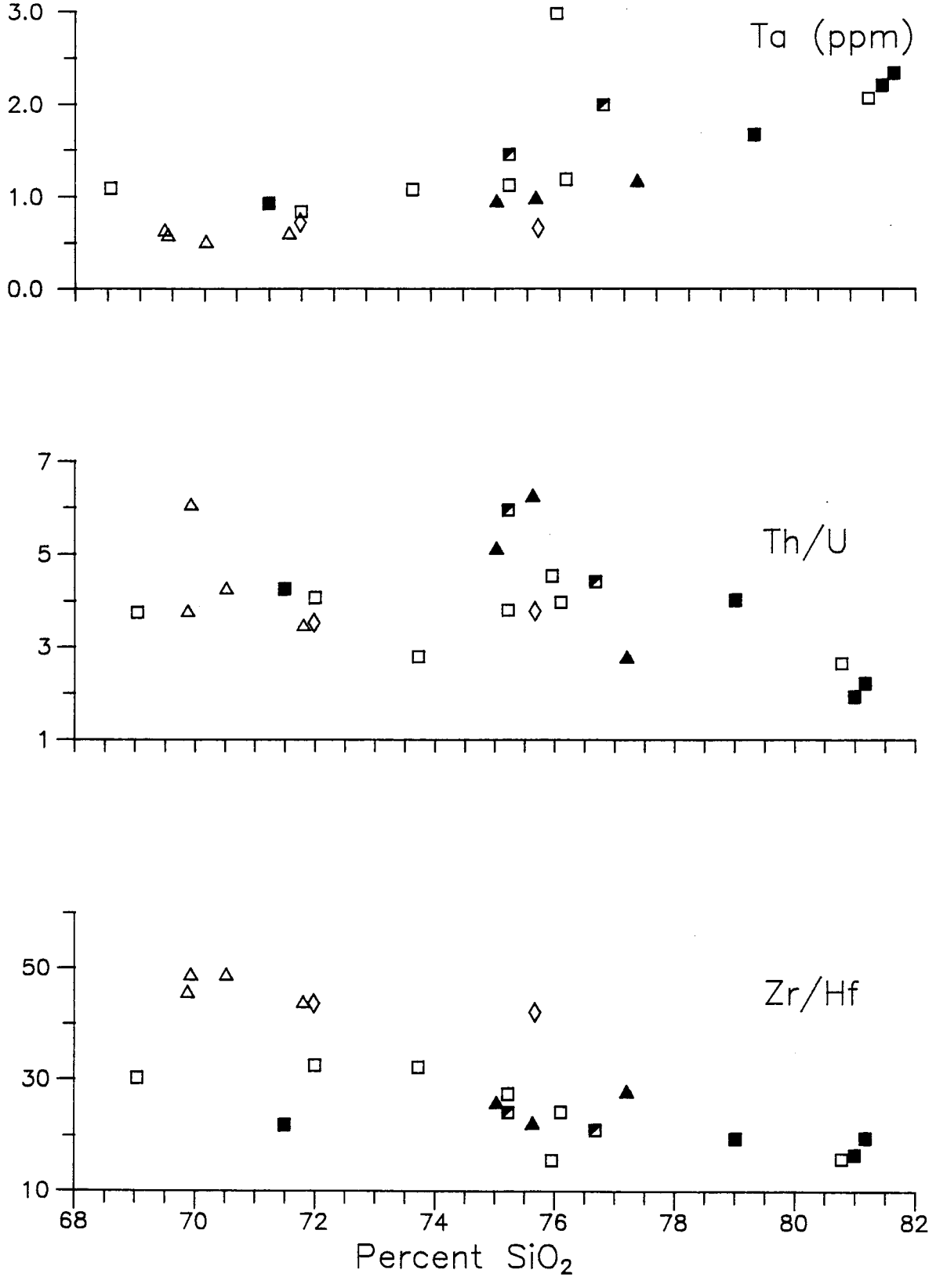
3.0
2.0
1.0
0.0
Ta (ppm)
7
5
3
1
Th/U
50
30
10
Zr/Hf
68
70
72
74
76
78
80
82
Percent SiO_2

complexes such as $(NbO4)^{3-}$ and $(TaO4)^{3-}$, and concentrate in residual melts (Taylor, 1965; Cerny et al., 1988; Strong, 1988). Unfortunately the parallel behaviour of Ta and Nb cannot be examined here since Nb results are near the limit of detection. Th and U increase with Si a feature common to differentiated granitic rocks, such as those in the Sierra Nevada (Dodge et al., 1982). The consistent Th/U ratio of 3-4 noted for the granites and dykes is similar to the global average of approximately 4, for granodiorites (McKelvey, et al., 1955). The mineralized samples are characterized by lower ratios suggestive of U enrichment (Fig. 6-10). This feature is probably related to the tendency of U to become oxidized and partitioned into the aqueous phase (McKelvey, et al., 1955). Not unlike the situation described by Chatterjee et al. (1983) in the South Mountain batholith, the U enrichment could be caused by an aqueous fluid that was also responsible for the enrichment of Rb and Ta.

The two quench samples generally lie on the differentiation trend defined by granites, although as with the major elements there are some deviations. Sample 298, the aphanitic Si-rich sample, shows depletion in Ba and Rb and enrichment in Na, and to a minor extent, Sr. The observation that Ba and Rb are compatible in K-feldspar and

Na and Sr in plagioclase, suggests that plagioclase has replaced K-feldspar. Sample 290, the plagioclase porphyritic sample, is depleted in Ca and Sr, which may be a chemical reflection of the extensive replacement of plagioclase phenocrysts by sericite (refer chap.2).

6.3.2 Trace Elements as a Function of dist.

Like the major elements the trace elements for the most part show a strong correlation with dist. (Fig. 6-11,12). Within the granitic rocks, the large ion lithophile elements (LIL) ,Rb, Sr and Ba show well defined trends. Sr and Ba decrease toward the contact whereas Rb increases. The LIL concentrations of mineralized granites are essentially equivalent to adjacent unmineralized granites a feature also noted with the major elements. The concentrations of LIL elements in the aplites differs significantly from the enclosing granites and are more like the samples nearest the contact. The Rb versus dist. and K_2O versus dist. plots show that major and LIL elements behave similarly in aplites (Fig. 6-6,11). Trace elements show much more variation in pegmatites than the enclosing granites, but as with the major elements Rb and Sr concentrations are similar to the host granites.

Figure 6-11 (Page 211): Trace element concentrations versus distance from the intrusive-volcanic contact, opposite the breccia body. As with the major element versus distance diagrams the samples at 250 and 1200 m contrast with the other adjacent granitic samples. Symbols same as for figure 6-2.

Figure 6-12 (Page 212): Trace element concentrations and trace element ratios versus distance from the intrusive-volcanic contact, opposite the breccia body. Symbols same as for figure 6-2.

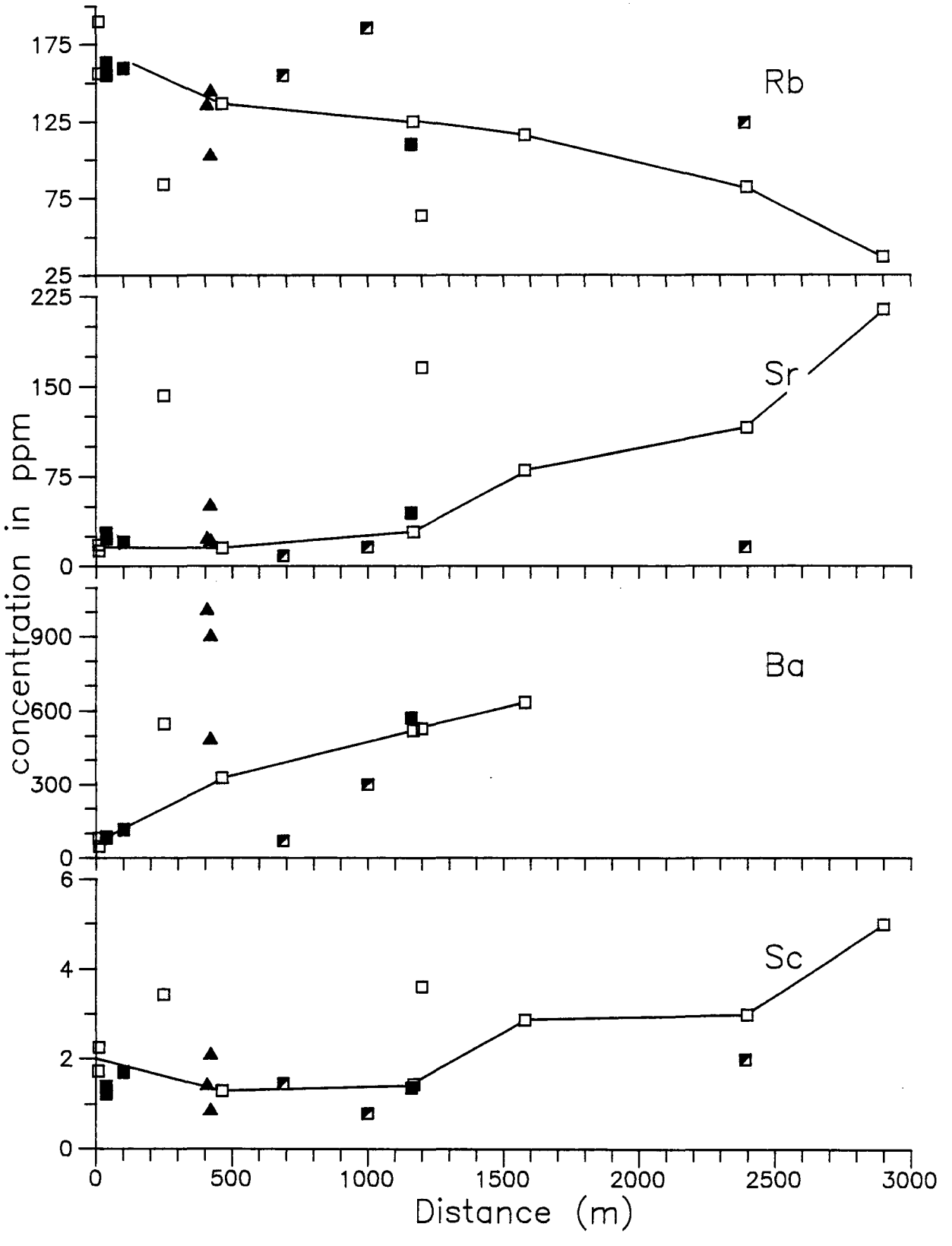
Rb
Sr
Ba
Sc
concentration in ppm
Distance (m)
175
125
75
25
225
150
75
0
900
600
300
0
6
4
2
0
0
500
1000
1500
2000
2500
3000

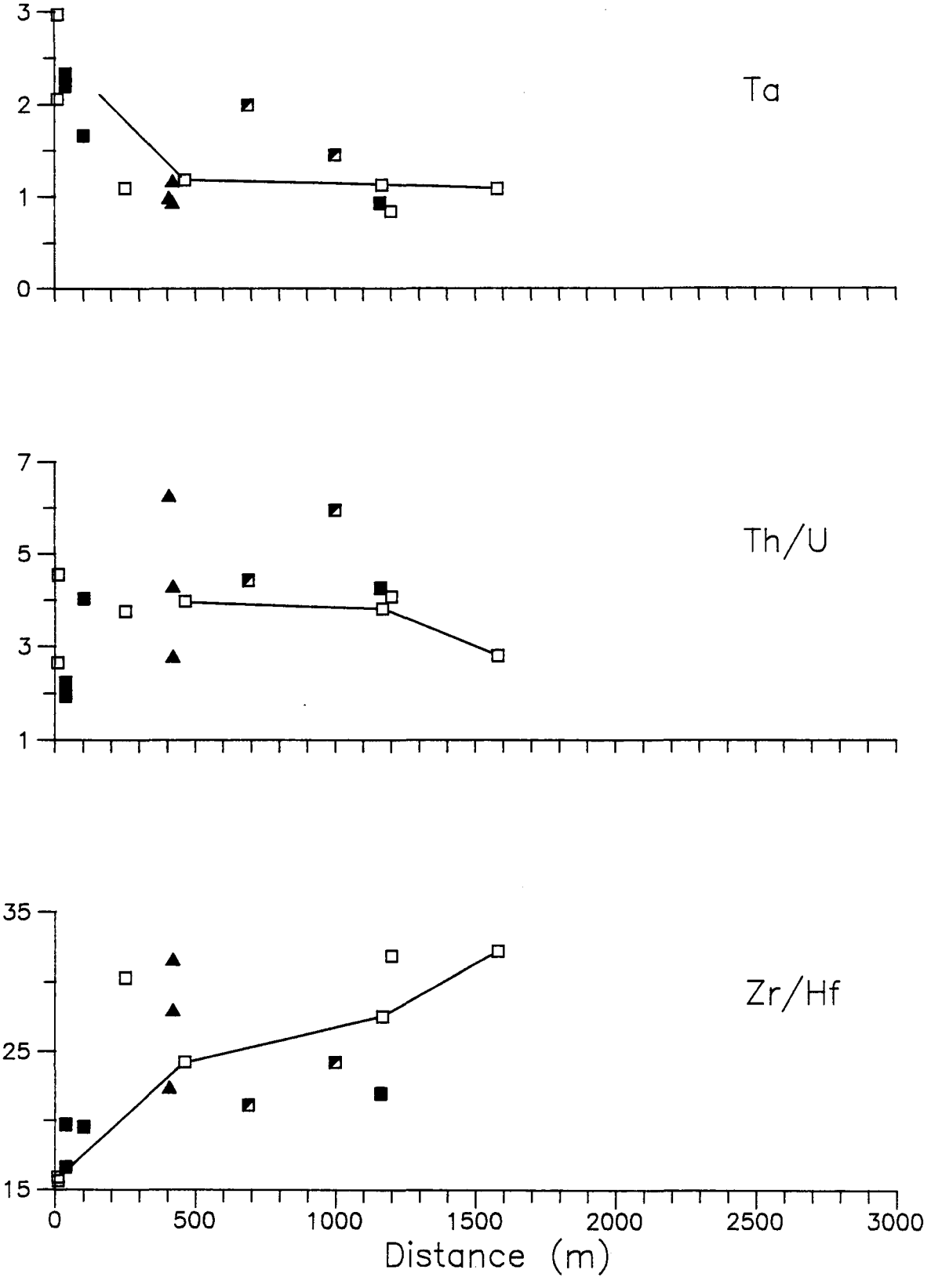
3
2
1
0
Ta
7
5
3
1
Th/U
35
25
15
Zr/Hf
0
500
1000
1500
2000
2500
3000
Distance (m)

The Zr and Hf concentrations of granites decrease in concentration with decreasing dist., but adjacent to the contact Hf displays an apparent increase relative to Zr. The behaviour of Zr and Hf is most obvious on the Zr/Hf versus dist. plot where a decrease in this ratio is clearly evident (Fig. 6-12). A decreasing Zr/Hf ratio with simultaneous decrease in Zr has been attributed to zircon fractionation in other similar studies (Taylor, 1965; Whalen, 1980; Tindle and Pearce, 1981). Zirconium and Hf are too variable in the mineralized granites, aplites and pegmatites to make any consistent comparisons between the concentrations in these rocks and the host granites. The Zr/Hf ratios of mineralized samples are similar to their hosts unlike the aplites, which, as was the case with the majors, have a higher Zr/Hf ratio.

The relationship of Th and U to dist. is unclear. Neither Th nor U concentrations vary significantly in granites and it would appear that these elements do not vary with distance from the contact. The U, Th concentrations of the mineralized granites and pegmatites, and Th in aplites, do appear to be enriched relative to the host granites.

Sc concentrations of the granitic rocks show an irregular decrease toward the contact with a possible increase very near the contact. Considering the scatter,

the mineralized granites and pegmatites appear to have Sc concentrations similar to their host granites. The concentrations in aplites are more ambiguous, but seem to be more like those granites near the contact. The behaviour of Sc mimics the major transition elements, suggesting that Sc may substitute for elements such as Fe^{2+} and Zr in fractionating phases (Taylor, 1965).

6.4 Rare Earth Elements

6.4.1 Chondrite Normalized REE Profiles

Thirty-two samples were analyzed for La, Ce, Sm, Eu, Tb, Yb, and Lu by INAA. The suite is divided into seven groups, distinguished by chondrite normalized REE patterns and other trace and major elements (Fig. 6-13 - 6-15; Chondrite normalization factors from Evensen et al., 1978). Group 1 rocks are granitic and have a the least evolved signature as expressed by the major and trace elements. These samples were collected from localities well within the Strathy-Chambers batholith and probably represent average batholith composition. Group 2 rocks are also granitic and have a differentiated signature intermediate between groups 1 and 3. Rocks of group 3 represent the most evolved

Figure 6-13a (page 215): Chondrite normalized REE diagram for groups 1,2 and 8.

Figure 6-13b (page 215): Chondrite normalized REE diagram for groups 3 and 4.

Figure 6-14a (page 216): Chondrite normalized REE diagram for group 5 - pegmatites and aplites.

Figure 6-14b (page 216): Chondrite normalized REE diagram for group 7 and the two quenched granite samples 290 and 298.

Figure 6-15a (page 217): Composite chondrite normalized REE diagram of the averages for groups 1-8.

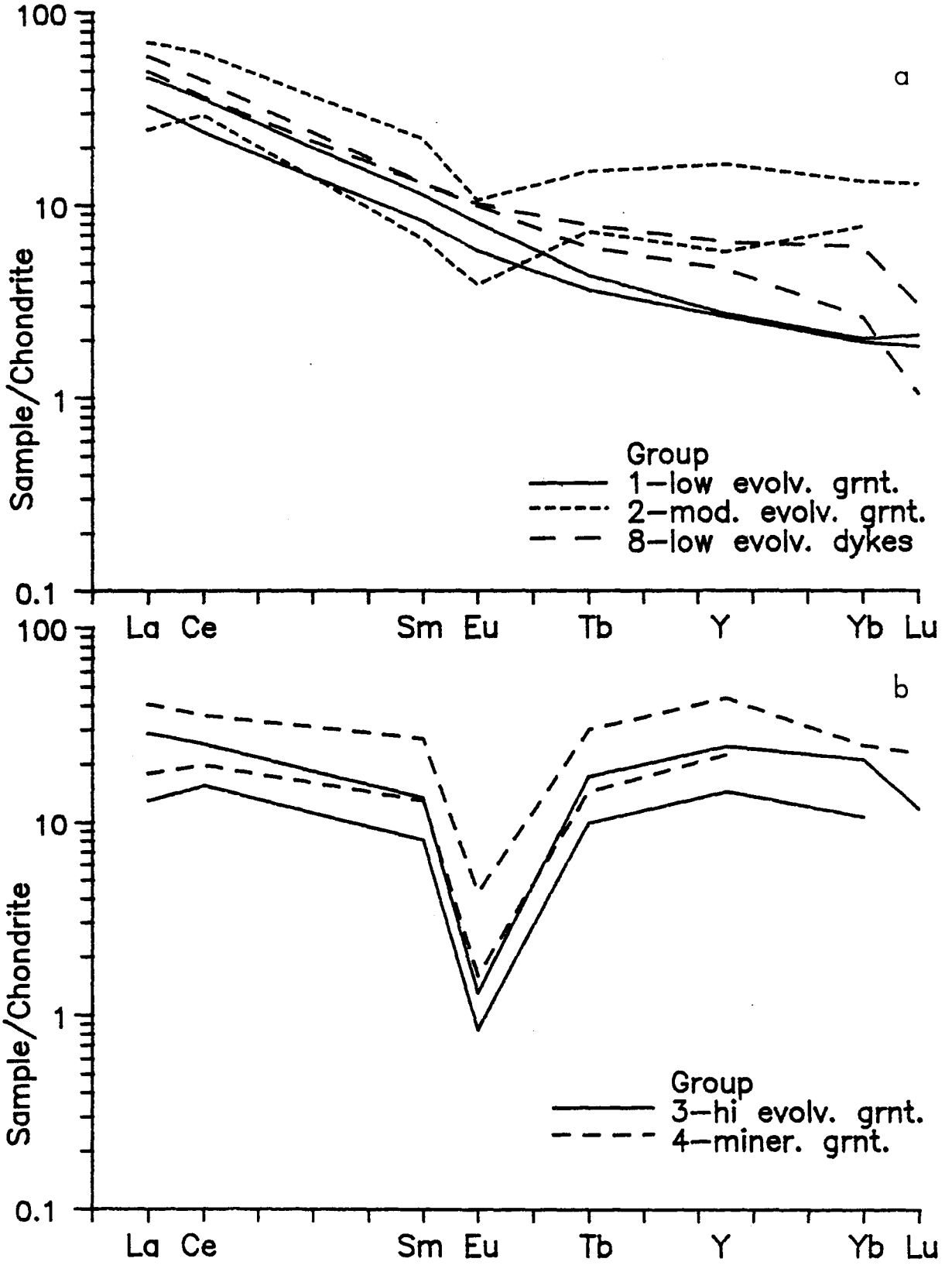
100
10
1
0.1
Sample/Chondrite
a
Group
1—low evolv. grnt.
2—mod. evolv. grnt.
8—low evolv. dykes
La Ce Sm Eu Tb Y Yb Lu
b
Group
3—hi evolv. grnt.
4—miner. grnt.

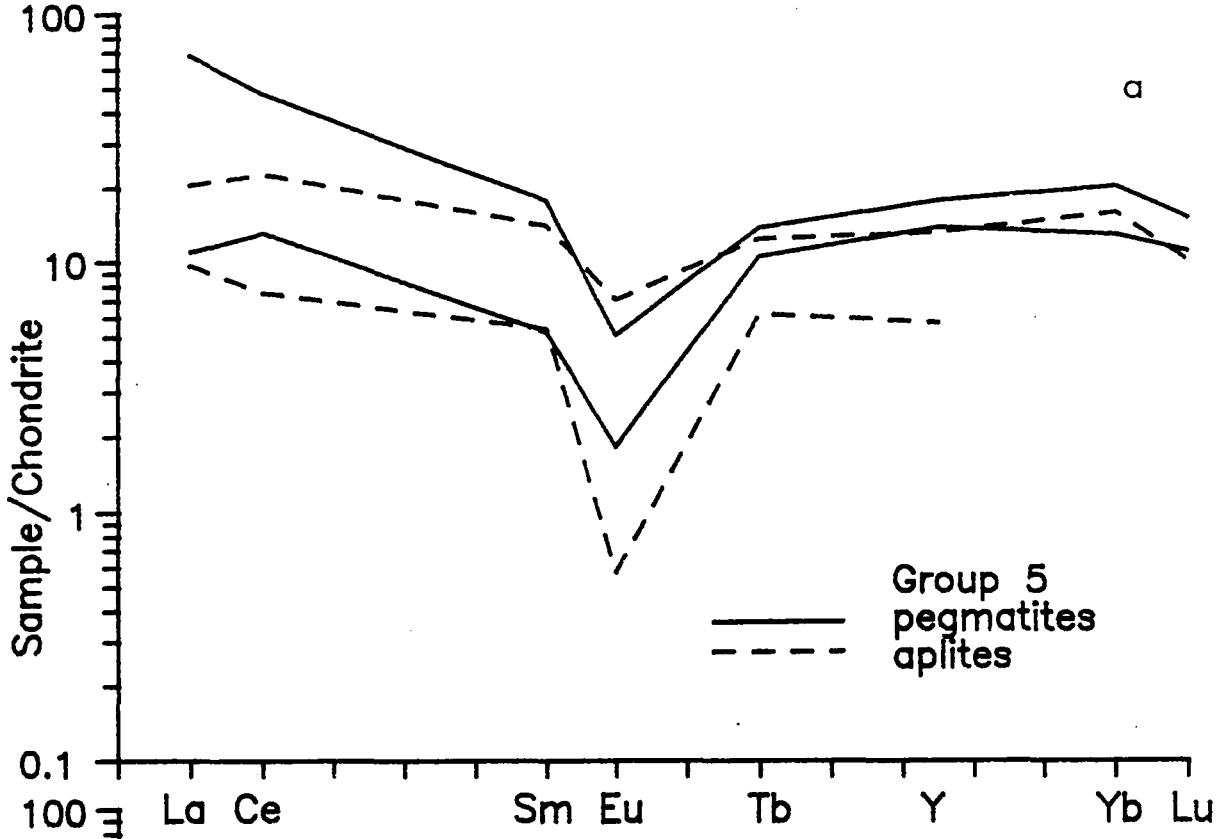
100
10
1
0.1
Sample/Chondrite
a
Group 5
pegmatites
aplites
La Ce
Sm Eu
Tb
Y
Yb Lu

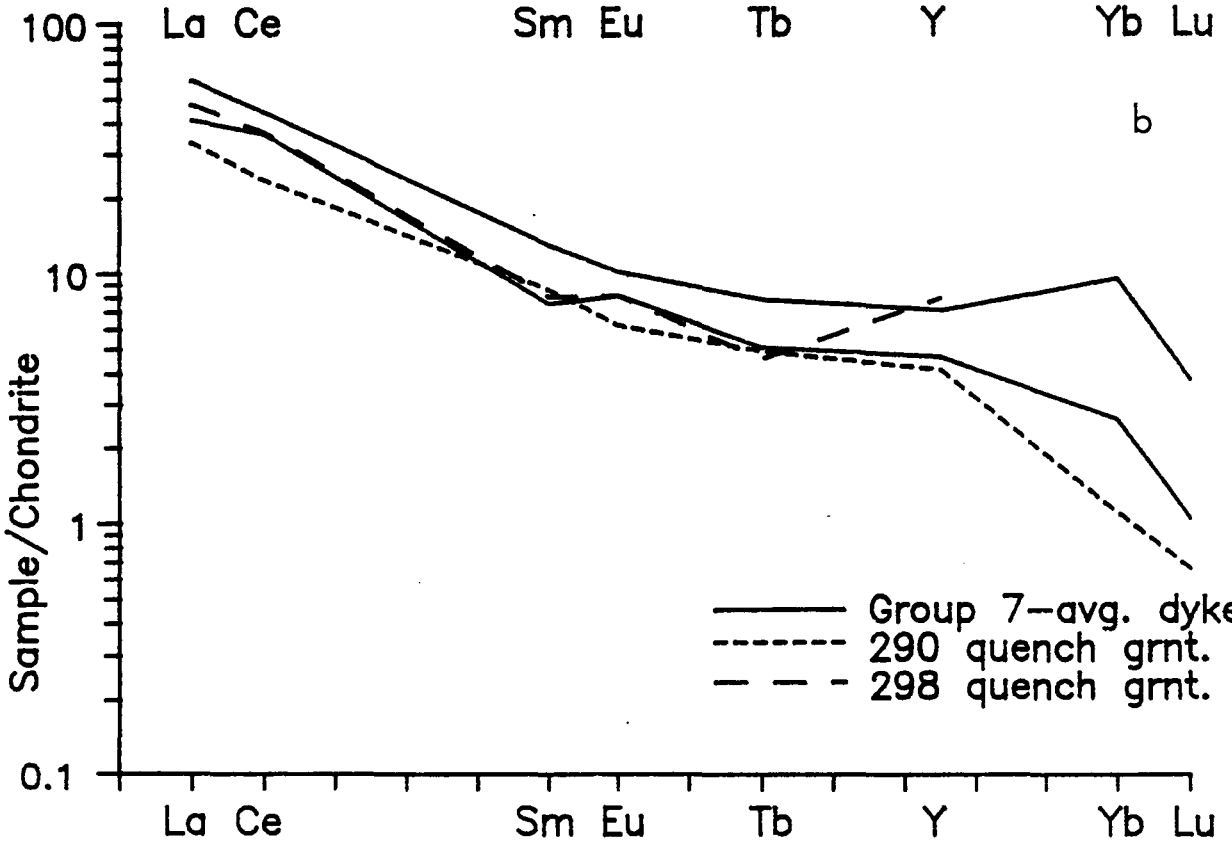
100
10
1
0.1
Sample/Chondrite
b
Group 7--avg. dykes
290 quench grnt.
298 quench grnt.
La Ce
Sm Eu
Tb
Y
Yb Lu

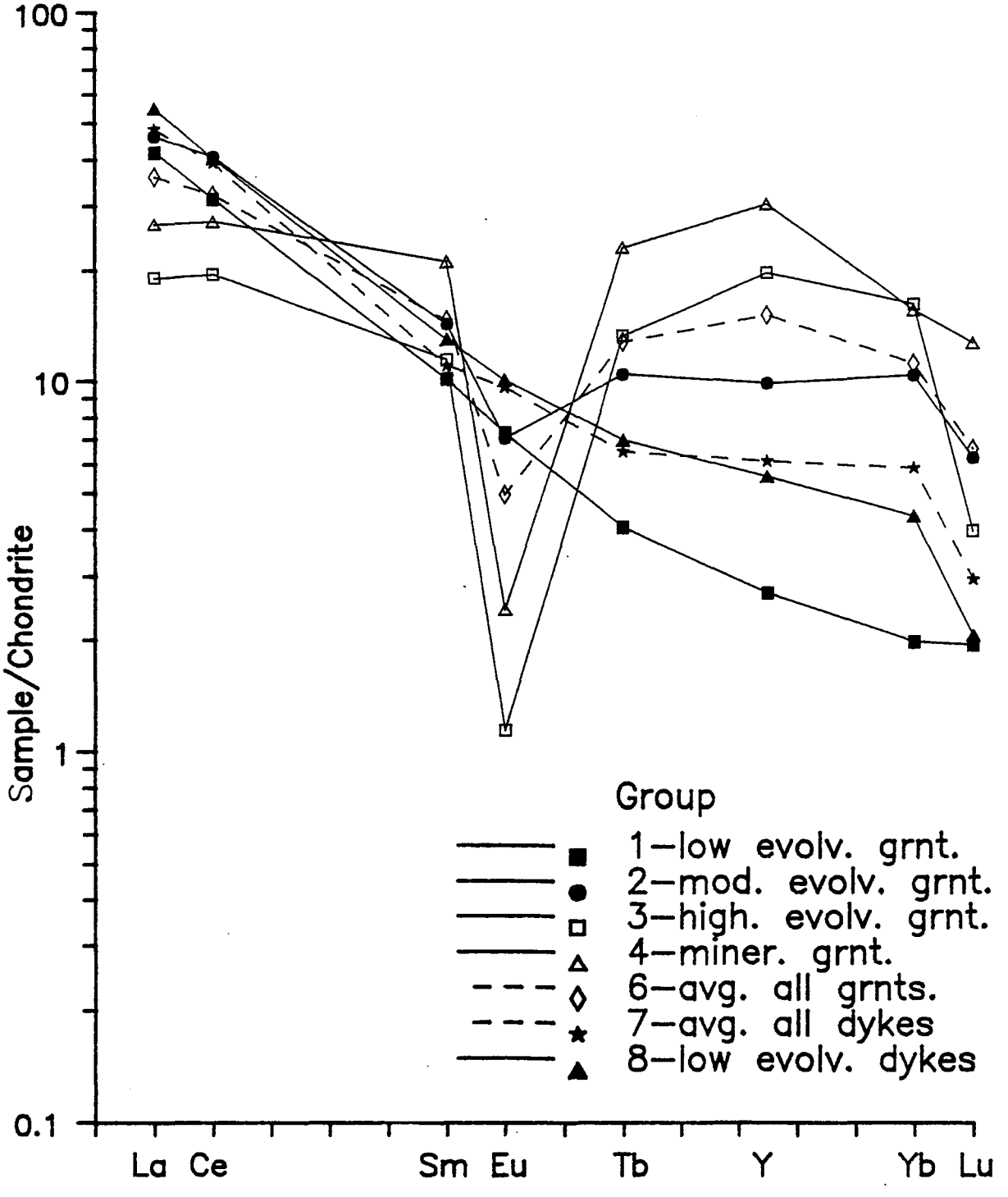
100
10
1
0.1
Sample/Chondrite
La
Ce
Sm
Eu
Tb
Y
Yb
Lu
Group
1—low evolv. grnt.
2—mod. evolv. grnt.
3—high. evolv. grnt.
4—miner. grnt.
6—avg. all grnts.
7—avg. all dykes
8—low evolv. dykes

granites that are located near the intrusive-volcanic contact. Group 4 samples are mineralized granites, group 5 are aplites and 6 pegmatites, while group 8 contains the 2 most primitive felsic dykes. Referring to the chondrite plots in figures 6-13,14,15 and table 6-1, the three primary features that distinguish groups are the LREE contents, the Eu anomalies and the HREE. In general, the least evolved samples have higher abundances of LREE (table 6-1). The HREE increase with increased differentiation as shown by the various calculated averages and the chondrite plots (table 6-1; Fig. 6-15). The Eu anomaly (Eu^*/Eu) decreases with increased differentiation and ranges from 1 to 0.06. A further indication of fractionation is the La/Yb ratio or LREE/HREE, which decreases with differentiation (table 6-1; Fig. 6-15). To test the consistency of the REE as indicators of differentiation table 6-2 ranks the various groups in order of differentiation based on these four REE criteria. The results show that categorization of groups from most primitive to most evolved, based on REE characteristics produces results consistent with the major and trace element indices of differentiation. In summary, evolution from primitive to the most evolved samples generates a LREE decrease by a factor of about 2, a HREE increase by a factor of about 4, a europium anomaly decrease

TABLE 6-1

REE Concentrations and REE Ratios of Groups 1-8

GROUP	Total REE [of those analysed]	AVG LREE [La,Ce,Sm]	AVG LREE [La,Ce]	AVG HREE [Yb,Lu]	AVG HREE [Tb,Y,Yb,Lu
1	54.71	15.89	22.67	0.28	1.60
2	86.57	21.58	30.57	1.27	5.29
3	74.47	9.46	12.87	2.07	11.50
4	109.60	13.58	17.93	2.16	17.17
5	55.05	9.26	12.78	1.54	6.75
6	74.94	16.49	23.27	1.29	6.25
7	67.95	17.67	25.34	0.54	3.54
8	75.75	20.58	29.38	0.57	3.28

GROUP	AVG HREE [Y,Yb]	LREE/HREE La,Ce,Sm/ Tb,Y,Yb,Lu	LREE/HREE La,Ce/Yb,Lu	LREE/HREE La/Yb	Eu/Eu*
1	3.05	10.46	18.91	21.27	0.92
2	10.17	4.65	7.20	5.65	0.64
3	22.54	1.28	2.09	1.24	0.07
4	33.44	1.30	2.45	1.42	0.10
5	13.08	1.81	4.23	1.81	0.32
6	12.13	4.87	8.18	7.75	0.55
7	6.87	7.18	16.40	14.41	1.16
8	6.32	7.68	17.57	14.61	0.98

Group descriptions

1: least evolved granites, very small range:730,750,760
2: moderately evolved granites:790,780,711,103,323
3: highly evolved granites:30,131,317
4: mineralized granites:312a,33,34,48b
5: pegmatites and aplites
6: average of all granites
7: average of all feldspar porphyry dykes
8: least evolved dykes:302,320

(Eu/Eu* is the ratio of the Eu concentration over the calculated concentration, assuming no Eu anomoly. The values were determined by interpolating between Sm and Tb concentrations)

TABLE 6-2

Ranking in Order of Degree of Differentiation
Based on REE Criteria

GROUP	AVG LREE [La,Ce]	GROUP	AVG HREE [Y,Yb]	GROUP	Eu/Eu*	GROUP	LREE/HREE La/Yb
2	30.57	1	3.05	8	0.98	1	21.27
8	29.38	8	6.32	1	0.92	8	14.61
1	22.67	2	10.17	2	0.64	2	5.65
4	17.93	5	13.08	5	0.32	5	1.81
3	12.87	3	22.54	4	0.10	4	1.42
5	12.78	4	33.44	3	0.07	3	1.24

	Least----------				----------Most evolved
AVG LREE [La,Ce]	2	8	1	4	3	5
AVG HREE [Y,Yb]	1	8	2	5	3	4
Eu/Eu*	8	1	2	5	4	3
LREE/HREE La/Yb	1	8	2	5	4	3

Group descriptions

1: least evolved granites very small range:730,750,760
2: moderately evolved granites:790,780,711,103,323
3: highly evolved granites:30,131,317
4: mineralized granites:312a,33,34,48b
5: pegmatites and aplites
6: average of all granites
7: average of all dykes
8: least evolved dykes:302,320

from 1 to 0.06 and a La/Yb ratio that decreases by a factor of 20.

The REE geochemistry of the quench samples appears to be most similar to the dykes and perhaps group 2 samples. The obvious contrast between the quench samples and the rest of the suite is that both quench samples have very low HREE concentrations.

6.4.2 Rare Earth Elements as a Function of dist.

Plots of REE against dist. are similar to plots of the major and trace elements in that there is a strong relationship between the element concentrations and the distance from the volcanic-intrusive contact (Fig. 6-16 -6-18). Granitic rocks are depleted in the LREE toward the contact while the HREE are enriched. The Eu anomaly decreases toward the contact as does the La/Yb ratio (Fig. 6-18). With the exception of one sample, the mineralized granites have similar LREE abundances to the adjacent unmineralized granites, but the Sm, Tb and HREE concentrations appear to be relatively enriched. The Eu contents of mineralized granites, like the major and LIL elements, are similar to the adjacent unmineralized granites. Aplite samples have LREE contents that are much

Figure 6-16 (page 222): Concentrations of the LREE-MREE, versus distance from the intrusive-volcanic contact, opposite the breccia body. Symbols same as for figure 6-2.

Figure 6-17 (page 223): Concentrations of the MREE-HREE, versus distance from the intrusive-volcanic contact, opposite the breccia body. Symbols same as for figure 6-2.

Figure 6-18 (page 224): Ratio of La/Yb (LREE/HREE) and the Eu anomaly versus distance from the intrusive-volcanic contact, opposite the breccia body. Symbols same as for figure 6-2.

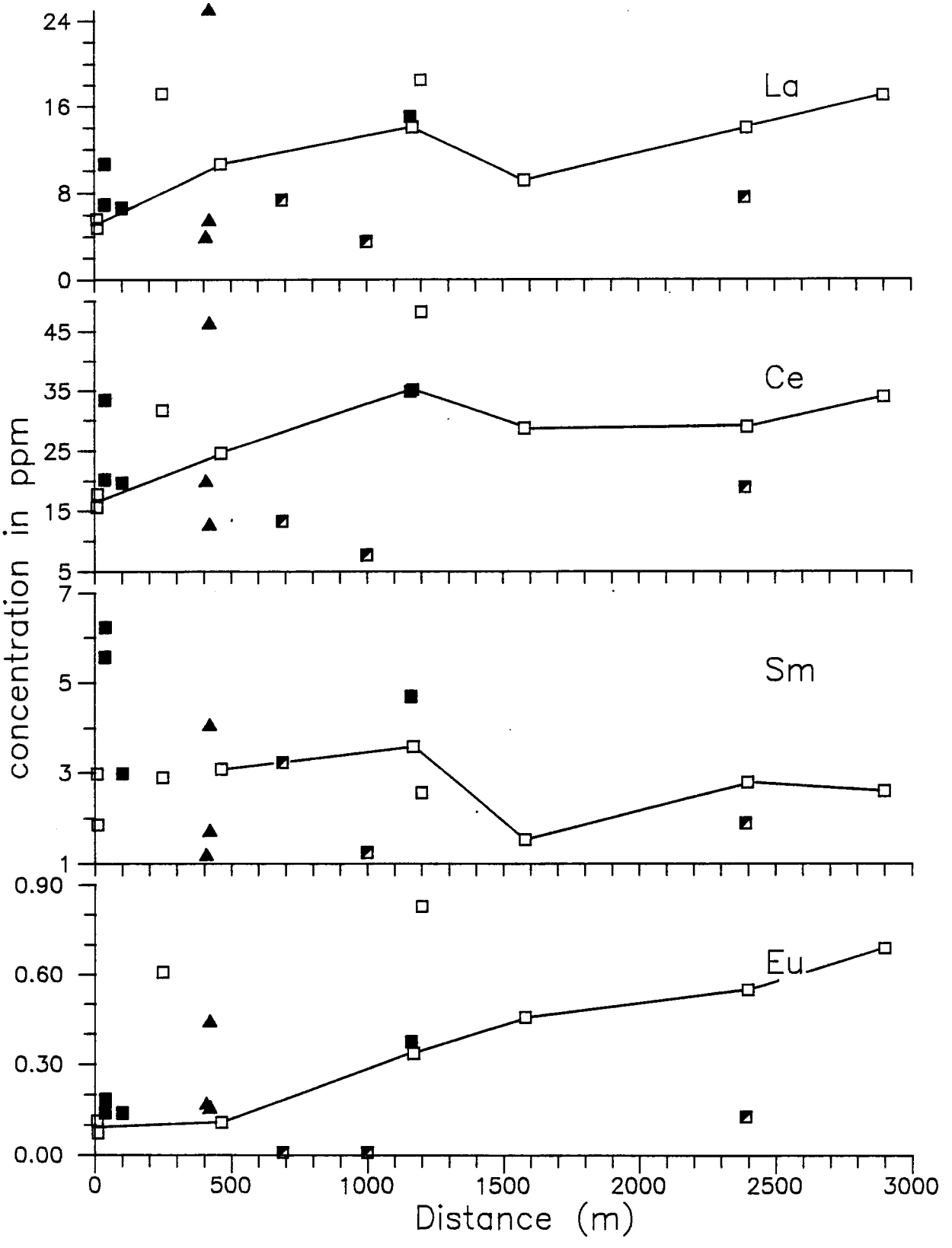
La
Ce
Sm
Eu
concentration in ppm
Distance (m)
24
16
8
0
45
35
25
15
5
7
5
3
1
0.90
0.60
0.30
0.00
0
500
1000
1500
2000
2500
3000

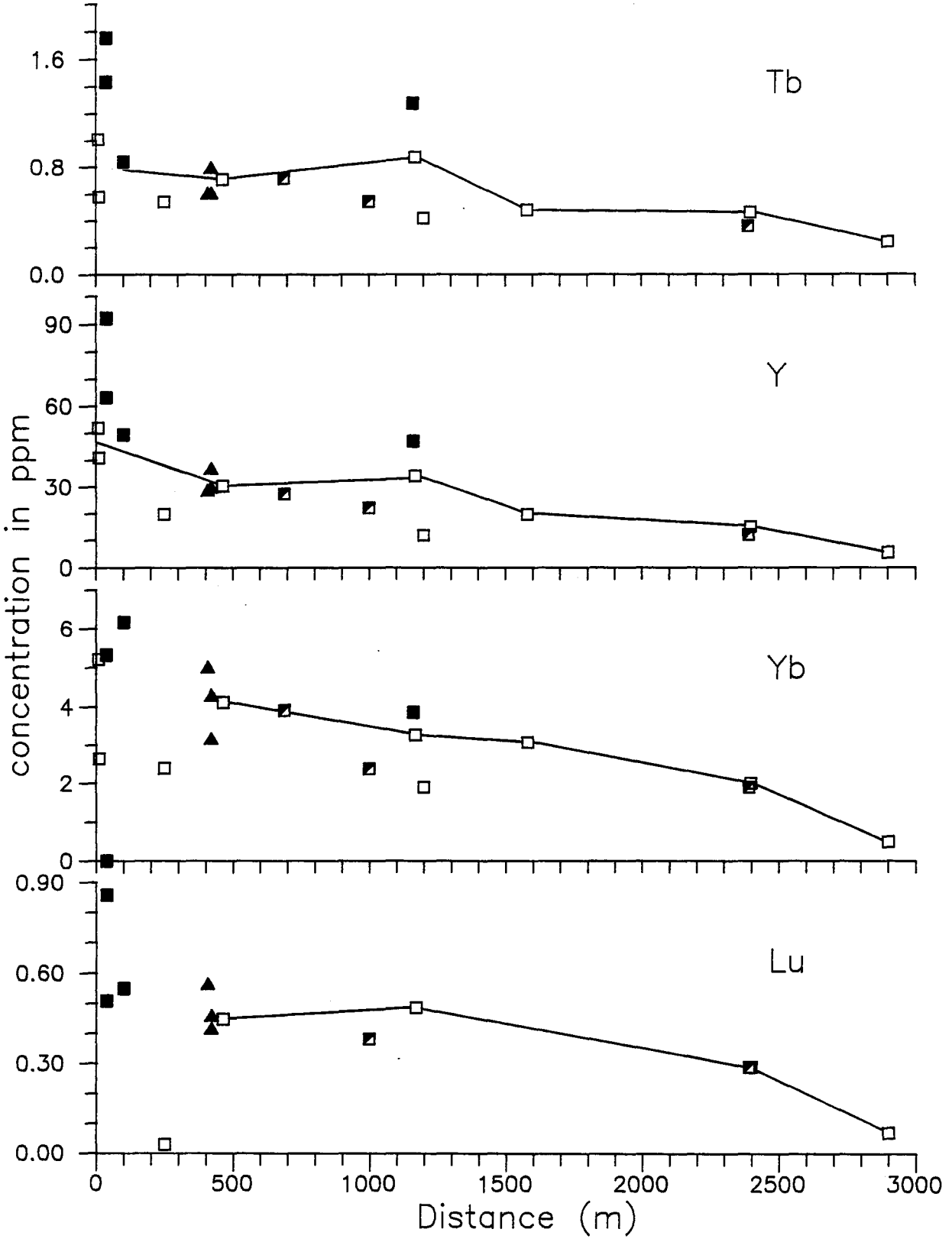
Tb
Y
Yb
Lu
concentration in ppm
Distance (m)
1.6
0.8
0.0
90
60
30
0
6
4
2
0
0.90
0.60
0.30
0.00
0
500
1000
1500
2000
2500
3000

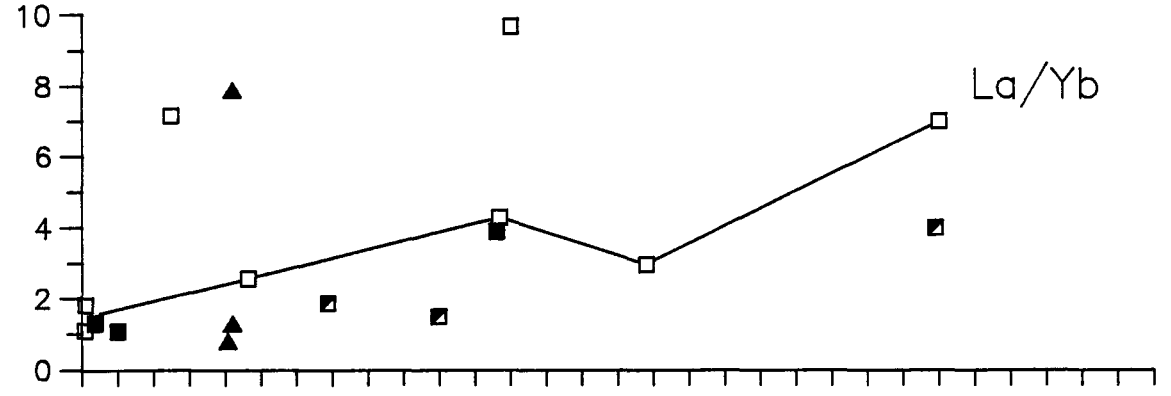
10
8
6
4
2
0
La/Yb

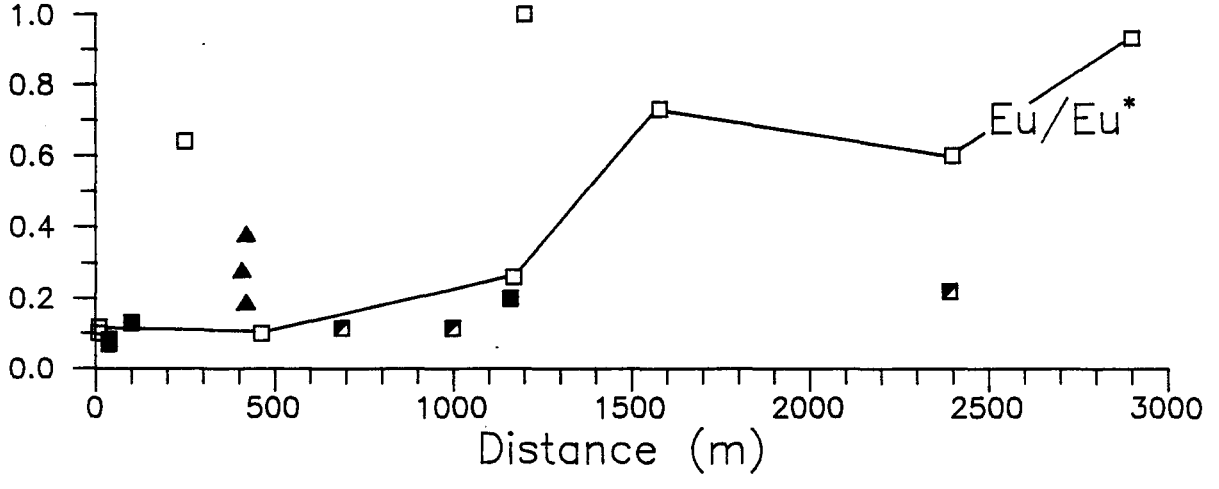
1.0
0.8
0.6
0.4
0.2
0.0
Eu/Eu*
0
500
1000
1500
2000
2500
3000
Distance (m)

lower than the host granites and more similar to granites nearest the contact. The HREE concentrations of aplites are very similar to the host granites. Pegmatites have highly variable LREE and middle REE (MREE) contents and thus it is impossible to define any relationship between the concentrations in the pegmatite versus the host granite. In contrast the HREE contents of pegmatites are similar to the host granites.

In summary it is clear that the REE show comparable fractionation trends to other trace and major elements. During differentiation LREE and Eu were depleted while the HREE were enriched in the more evolved rocks. The partitioning of LREE in the formation of mineralized granites and aplites is similar to that of the major and trace elements. Aplites crystallized with major, trace and LREE abundances different from their host rocks and characteristic of the more evolved rocks near the contact. The HREE abundances of aplites are, however, very similar to the host granites. Mineralized granites evolved with major, trace and LREE abundances similar to adjacent unmineralized granites. The HREE behaved as incompatible elements becoming enriched in the most differentiated granites. Heavy REE and U enrichment of mineralized granites suggests that these rocks were affected by aqueous fluids enriched in

these constituents.

6.5 Geochemical Modelling of Chemical Variation Amongst Intrusive Rocks

6.5.1 Introduction

From the results discussed thus far it is suggested that the compositional variation observed represents a magmatic series formed by differentiation of a parent composition. In general the primitive end member of the differentiation series includes the felsic dykes and some of the most mafic granitic rocks that are relatively high in Al, Ca, Sr, Fe, Mg, Ti, Zr and low in Rb and K. The differentiated end member is represented by mineralized and non-mineralized granites that are characterized by low Al, Ca, Sr, Fe, Mg, Ti, Zr and high Rb and K. With increased differentiation, REE generally show a decrease in LREE, enrichment in HREE, decreasing Eu anomalies and a decrease in the LREE/HREE ratios. It has also been established that there is a strong spatial dependence of composition, defined by a more evolved character toward the volcanic-intrusive contact. Physical evidence such as the increased frequency of aplites and pegmatites towards the contact suggest that

the magma was also supersaturated in H_2O and volatile components in the vicinity of the contact. This physical and chemical evidence suggests that the intrusive phase, in the region of the contact, represents the apical portion of a hydrous differentiated magma chamber. In an attempt to solidify the argument that favours the development of chemical zonation via a process of crystal fractionation several semi-quantitative models will be illustrated in the following sections. The models are semi-quantitative because the necessary geochemical and petrological information is incomplete. Definite conclusions based on these models are not possible, but results indicate that the proposed models are geologically reasonable.

6.5.2 Possible Differentiation Processes

It has been implied by major, trace and rare earth elements that there is a comagmatic series between felsic dykes and evolved granites, where the dykes represent a parent liquid and the evolved granites a residual liquid after differentiation. Several processes of differentiation may have occurred, but as an initial assumption it will be assumed that crystal fractionation was the relevant process. An extreme version of this model implies that each end

member represents a true magmatic liquid, a very unlikely situation in granitic systems (Wright and Doherty, 1970; Tindle and Pearce, 1981). It is more plausible that end members are mixtures of both liquid and cumulate phases. Before testing the crystal fractionation model other possible causes of the chemical variation will first be considered.

Contamination of the magma by enclosing country rocks is one possible cause for chemical variation. Brons (1989), Bennett (1978) and Fyon et al. (1988) all mention the presence of border phases that probably indicate local contamination by the enclosing volcanics. In the intrusive breccia zone volcanic blocks are incorporated in breccias, but they do not appear to be extensively digested by the intrusive. Even if digestion in the contact zone was significant the result could not have led to the observed zonation and indeed for most of the elements contamination would have led to zonation in the opposite spatial sense (table 6-3).

Vapour-Fluid phase transfer Vapour phase, or hydrothermal fluid transfer is cited in some studies as a process leading to chemical zonation of REE and other elements in granitic rocks (Flynn and Burnham, 1978: Muecke and Clarke, 1980). There is evidence of hydrothermal

TABLE 6-3

Contamination Hypothesis

[Contamination ---> volcanic + Group 1 or 2 = group 3]
(volc. + least evolv. grnt.= evolv. grnt.)

	Volcanic [average]	Group 1	Group 2	Group 3	Accept or reject hypothesis
SiO_2	58.44	71.72	72.79	77.61	reject
Al_2O_3	13.64	15.00	14.28	11.05	reject
Fe_2O_3	10.57	2.10	2.37	1.04	reject
MgO	4.14	0.90	0.68	1.10	accept
CaO	6.04	1.99	1.73	0.33	reject
K_2O	1.73	2.18	2.82	4.56	reject
TiO_2	0.79	0.28	0.18	0.02	reject
P_2O_5	0.12	0.08	0.06	0.01	reject
Ba	342.50	*	215.60	152.67	reject
Rb	71.43	55.33	85.64	160.93	reject
Sr	146.47	182.67	111.95	15.40	reject
Y	22.07	5.43	18.54	41.10	reject
Zr	103.63	137.00	131.75	64.73	reject

(* no analysis)

activity outside the granite, in the form of veins and breccia, and within the granite as pegmatites and aplites. Aside from these features there are no obvious signs of intense pervasive alteration other than the replacement of biotite by chlorite and weak saussuritization of feldspars. It has been suggested that uniform variation among the elements Rb, Sr and Ba, which are normally considered susceptible to alteration, can be used as evidence against volatile transfer processes (Whalen, 1983). In the rocks of this study variation of these elements is uniform except for the quench rocks which do show element mobility, but because they probably only reflect very local conditions they are not deemed important in the larger context. Pegmatites and aplites likely formed by processes of volatile and fluid transfer, but again these features are not volumetrically important. The lack of evidence for pervasive alteration and the fact that most elements display linear variations is probably ample evidence against vapour or fluid phase transfer as the major process of creating compositional zonation.

Restite Unmixing Restite unmixing is a process whereby refractory crystalline residue is separated from a magma to produce chemical variation. Such magmas are thought to be derived by partial melting of source rocks, which have

incorporated a refractory residue (White and Chappel, 1977). Two lines of evidence indicative of restite unmixing includes linear variations of chemical constituents against Si, and identification of a restite phase (White and Chappel, 1977). The Si variation diagrams from this study do not display obvious curved or straight line relationships, with possibly the exception of Ba, probably due to the relatively small number of samples and relative scatter of data. Because of this problem linear compositional trends were not used to recognise this type of fractionation process. Whalen (1983) and Mittlefehldt and Miller (1983) suggest that the process of restite unmixing cannot result in enrichments or depletions of trace element components to a degree larger than allowed by the bulk distribution coefficient (i.e. $K_x = [X]_{solid}/[X]_{liquid}$). As an example it is evident that Sr concentration, in extremes of differentiation from dykes to mineralized granites, ranges by a factor of ten, which is approximately equal to the sum of distribution coefficients for plagioclase and K-feldspar (Arth, 1976). However, the partition coefficients for elements such as Sr vary widely in the literature so, in general partition coeficient data is too variable to discount restite unmixing. Although the chemical data appear inconclusive, physical evidence in the apparent lack

of a restite phase may be the most important evidence against the restite unmixing model.

Thermo-gravitational diffusion (TGD) Thermo-gravitational diffusion is a process described extensively by Shaw et al. (1976) and Hildreth (1979, 1981), whereby chemical zonation in high-Si magmatic systems is attributed to liquid state processes, namely diffusion and convective circulation. In the majority of studies TGD is applied to Si-rich volcanic systems that are deficient in phenocryst phases. Indeed, one of the reasons for appealing to the process of TGD was to explain the existence of compositional zonation in silicic tuffs, that apparently lacked sufficient phenocrysts to account for the zonation by processes such as crystal fractionation (Hildreth, 1979,1981). Application of TGD to granitic systems is less common in the literature since zonation can often be explained by more conventional means. In his study of the Ackley City batholith Whalen (1983) does not discount TGD as a process that may create zonation, but he also points out that the variation can be modeled by fractional crystallization. Ludington (1981) applied the concept of TGD to the Redskin granite, basing most of his arguments on the similarities between chemical enrichments in his data and Hildreth's data from the Bishop Tuff. These chemical enrichments represent the

concentration of an element in the most evolved samples divided by the concentration of that element in the least evolved samples of the suite. Hildreth suggests that lithophile elements such as Nb, Ta, As, Sb, Mo, W, Th, and U are highly susceptible to complexing and are preferential enriched upward in a magmatic system. Hildreth also argues that in the Bishop tuff elements such as Mg, P, Sr, Ba, and Eu are depleted too severely to be explained by crystal fractionation alone. Volatile phases such as F, Cl and Mn are highly enriched in the Bishop tuff but not so in the Redskin granite, a feature Ludington (1981) attributes to aqueous phase transport and depletion. Comparison of the results from Temagami to those from the Bishop tuff and Redskin granite reveal remarkable similarities, but also some important differences (Fig. 6-19). Increased Na and Rb with decreasing K are two features thought to be characteristic of TGD-influenced systems (Ludington, 1981), but the Temagami data clearly do not follow this pattern since K increases markedly while Na is marginally depleted. Enrichments of Sc and Mg in the Bishop tuff also contrast with the results of this study, but as Ludington suggests these elements may have been fractionated by aqueous fluids. The REE behaviour of the Temagami and Bishop data are similar, although Y and Yb are more enriched in the Temagami

Figure 6-19 (page 234): Comparison of enrichment factors for data from Temagami, the Bishop Tuff (Hildreth, 1981) and the Ackley City batholith (Whalen, 1983). The factors are calculated by dividing the concentrations of the least evolved rocks into the most evolved rocks of the proposed differentiation sequence.

Figure 6-20a (page 236): Comparison of Y versus Zr variation for Temagami samples to trends defined by the Bishop Tuff (Hildreth, 1981). Symbols same as for figure 6-2.

Figure 6-20b (page 236): Comparison of Sr versus Rb variation for Temagami samples to trends defined by the Bishop Tuff (Hildreth, 1981). Symbols same as for figure 6-2.

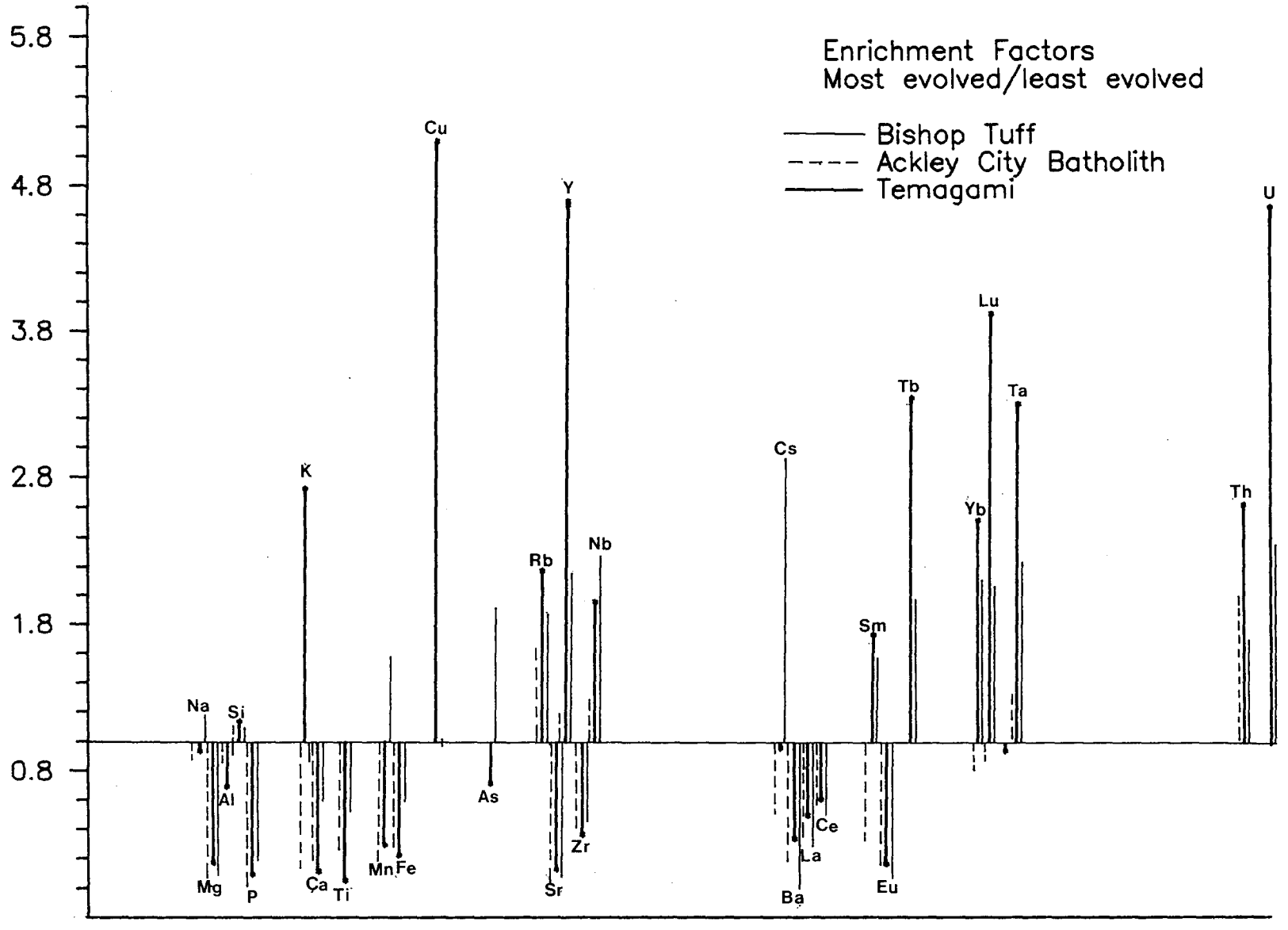
Enrichment Factors
Most evolved/least evolved
Bishop Tuff
Ackley City Batholith
Temagami
5.8
4.8
3.8
2.8
1.8
0.8
Na
Si
Al
Mg
P
K
Ca
Ti
Mn
Fe
Cu
As
Rb
Y
Nb
Sr
Zr
Cs
Ba
La
Ce
Sm
Eu
Tb
Yb
Lu
Ta
Th
U

samples. Light REE depletion noted in the Bishop tuff, Redskin granite, and in this study, was considered problematic by Ludington (1981), but subsequent studies have suggested that crystal fractionation of LREE-bearing phases such as monazite or allanite can account for LREE depletion (Anderson and Cullers, 1978; Tindle and Pearce, 1981; Mittlefehldt and Miller, 1983). In addition to the comparison of enrichment data, variation diagrams such as Rb versus Sr and Y versus Zr show strong similarity to the Bishop tuff data (Fig. 6-20a,b). The similarities are numerous, although an extensive comparative study of documented differentiated granitic systems might also reveal many like similarities. In addition the concept of TGD has since been challenged by Micheal (1983), who suggests that the Bishop tuff could have evolved through a process of fractional crystallization. It cannot be proven that TGD has influenced the zonation in the Strathy-Chambers batholith and therefore it is only noted that there are great similarities between the Temagami data and data considered by other authors to have resulted from TGD.

The above discussions have summarized some of the possible mechanisms by which chemical zonation could arise in a granitic system. Limitations in the data base have not permitted the elimination of all the models; however, none

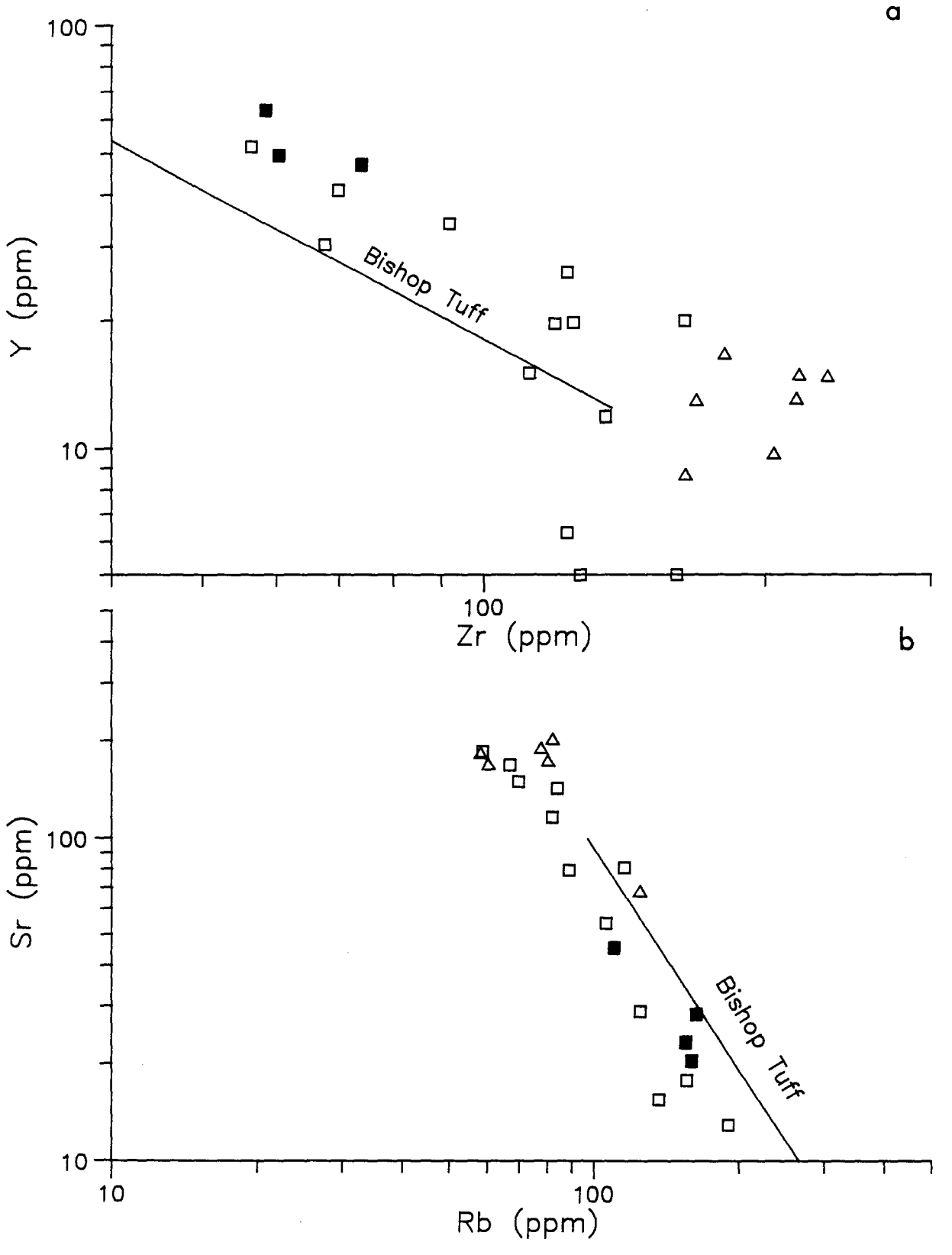
a
100
10
Y (ppm)
Bishop Tuff
100
Zr (ppm)
b
100
10
Sr (ppm)
Bishop Tuff
10
100
Rb (ppm)

of those discussed are thought to be as likely to produce the zonation as are mechanisms related to fractional crystallization.

6.5.3 Major Element Modelling

Fractional crystallization models attempt to describe a process whereby crystallizing phases extract elements from a liquid (e.g. magma) to produce a compositionally new liquid and a cumulate phase. In the following model calculations the initial liquid or parent magma is represented by the most mafic composition of the magmatic series or by some hypothetical composition. The daughter composition is represented by the most felsic or evolved member in the magma series. In summary the model follows the relation:

$$\text{parent} = \text{crystals} + \text{daughter}$$

In situ fractional crystallization as described by Tindle and Pearce (1981) takes the parental liquid to have a composition equal to the average of the magmatic series under investigation. From this average composition, differentiation proceeds to develop two extreme compositions that correspond to the primitive, or parent and most evolved

end members of the series. This model addresses the often cited problem of not being able to identify the cumulate rocks in the field. A major criticism of crystal fractionation within granitic systems is that the high viscosity of these magmas precludes crystal settling (Rice,1981). In answer to this problem processes such as filter pressing and flow differentiation have been suggested as a means of crystal liquid separation (Rice, 1981).

The employment of a crystal fractionation model to the present study has several limitations. Firstly, the compositions of the fractionated mineral species are unknown. Secondly, in the Strathy-Chambers batholith the primary mafic mineral assemblage has been replaced and altered by postmagmatic processes. Keeping these problems in mind it is still reasonable to attempt modelling fractional crystallization using appropriate mineral compositions from published analysis for both primary and secondary minerals. Use of secondary mineral compositions assumes that the bulk composition of the rock did not vary due to secondary processes and that secondary minerals represent replacements of primary phases. Model results mainly test whether chemical variation can be accounted for by separation of a reasonable proportion of various mineral cumulates, and do not claim high accuracy with respect to

proportions of specific minerals crystallized. With the exception of opaques, only observed phases were used in the model. Chlorite, although present, was not used as a model phase; rather biotite and hornblende were used since chlorite replaces these probable primary phases. Clinozoisite was employed since it represented an alteration product of primary minerals such as feldspar. Fyon and Wheatley (1988) have suggested that epidote may be a primary phase in the Strathy-Chambers batholith, which implies that use of clinozoisite in the model might not be entirely hypothetical. The parental liquid was defined as the average composition of three of the least evolved dyke samples (113,302,320), while the residual or evolved composition was defined by the average of three highly evolved granite samples (30,131,317).

The actual computation of the model was done by a computer program that follows a least squares mixing calculation as described by Bryan et al. (1969), Bryan (1969) and Chayes (1968). The information required for the computation include, the parent and daughter compositions, the fractionating minerals and their compositions. In general the model calculation subtracts various combinations of minerals from the parent composition to eventually produce a residual liquid that is as close as possible to

the daughter composition. The difference in a particular element between the actual daughter and the calculated daughter composition is termed the residual. The sum of squares of the residuals for all the elements is a measure of the model success. In the present study there are very few constraints as to minerals involved and their compositions so that many mineral combinations all produce similar results in terms of the residuals. A summary of some of the most successful results are tabulated in table 6-4.

One significant problem with the model is that the residuals for K_2O are a large contributor to the total sum of residuals squared. This indicates that the increase in K_2O may be too great to be explained by simple fractionation of K-free phases. Such a problem was cited by Bateman and Chappel (1979) in their study of compositional zonation in the Tolumne intrusive of California. They suggested that enrichment of K could be augmented by aqueous phases enriched in K. If this were the case at Temagami then it might be expected that the modal abundance of muscovite, biotite and secondary feldspar should increase along with K. Detailed study of the model mineralogy was not conducted, but inspection of thin sections revealed that interstitial microcline was ubiquitous and that biotite was often

TABLE 6-4

Results of Major Element Modeling

fract. min.	1 Wt% of	cum.min.	2 Wt% of	cum.min.	3 Wt% of:	cum.min.	4 Wt% of:	cum.min.
Plag.	16.0	48.8	15.7	49.5	15.8	48.2	14.9	43.6
Clinozoi.	10.9	33.2	10.7	33.8	11.0	33.5	10.4	30.4
Hrnblnd	3.5	10.7	3.6	11.4	3.5	10.7	3.8	11.1
Sphene	0.3	0.9	0.2	0.6	0.0	0.0	0.0	0.0
Magnetite	1.9	5.8	1.3	4.1	1.6	4.9	0.0	0.0
Biotite	0.0	0.0	0.0	0.0	0.0	0.0	4.2	12.3
Ilmenite	0.0	0.0	0.0	0.0	0.7	2.1	0.7	2.0
Apatite	0.2	0.6	0.2	0.6	0.2	0.6	0.2	0.6
Total % Cumulate	32.8		31.7		32.8		34.2	
Sum of residuals	0.86		0.72		0.66		0.47	

fract. min.	5 Wt% of	cum.min.	6 Wt% of	cum.min.	7 Wt% of:	cum.min.
Plag.	15.6	47.6	15.8	49.8	16.0	48.8
Clinozoi.	10.8	32.9	11.1	35.0	10.9	33.2
Hrnblnd	3.5	10.7	3.5	11.0	3.5	10.7
Sphene	0.0	0.0	0.0	0.0	0.3	0.9
Magnetite	1.2	3.7	1.9	6.0	1.9	5.8
Biotite	1.2	3.7	0.0	0.0	0.0	0.0
Ilmenite	0.6	1.8	0.0	0.0	0.0	0.0
Apatite	0.2	0.6	0.2	0.6	0.2	0.6
Total % Cumulate	33.1		32.5		32.8	
Sum of residuals	0.59		0.91		0.88	

[First column is amount of mineral in percent subtracted from initial 100 percent liquid. Second column is recalculation to 100 percent cumulate minerals]

enriched near the contact and in the adjacent volcanics (refer chap.5). The proportion of muscovite did not, however, show any definite correlation with K concentration. The omission of K_2O from the model calculation produced better results (Table 6-4). Another important feature of the modelling is that the calculated percent cumulate is low, and within values obtained in other similar studies (Anderson and Cullers, 1978; Bateman and Chappel, 1979; Tindle and Pearce, 1981; Mittlefehldt and Miller, 1983; Whalen, 1983). Accepting that some of the fractionating phases used in the model are likely secondary minerals, the proportions of different minerals in the cumulate are also geologically reasonable.

With the possible exception of K the results of the major element modelling indicate that chemical variations can be explained by subtraction from a parent liquid of a cumulate phase comprised of some or all of the minerals: plagioclase, clinozoisite-epidote, biotite, hornblende, ilmenite, magnetite, sphene, and apatite. Use of epidote in place of clinozoisite produced similar results with slightly higher residuals. Fyon and Wheatley (1988) mention that apatite and zircon occur as inclusions in plagioclase hornblende and biotite and that sphene forms inclusions in plagioclase and femic minerals. These textures may indicate

that the minor constituents may have been entrapped and then fractionated along with the more predominant minerals. Fyon and Wheatley (1988) also mention that plagioclase hornblende and biotite are all altered and replaced by epidote and clinozoisite; substantiating the use of these two secondary minerals in the model.

6.5.4 Trace Element Modelling

Rubidium, Sr and Ba are particularly useful in modelling crystal fractionation processes since they are concentrated in the major rock forming minerals found in granites. The Raleigh crystal fractionation model as described by McCarthy and Hasty (1976) is illustrated by the relation:

$$C_l/C_0 = F^{(Da-1)}$$

Where: C_0 = concentration of element a in the original melt

C_l = concentration of element a in the residual melt

F = weight fraction of melt remaining

D_a = bulk distribution coefficient for element a

$D_a = K_{ai}X_{i,}$ where K_{ai} = distribution coefficient for element a in mineral i, x_i = weight fraction of phase i

In the plutonic environment the type of crystallization lies somewhere between equilibrium crystallization and Raleigh fractional crystallization (Tindle and Pearce, 1981; Lynch and Pride, 1983; Whalen, 1983). Physical evidence for Raleigh fractionation is suggested by the presence of zoned plagioclase in some samples. A significant problem with models that utilize these particular elements is the significant disagreement on the distribution coefficients applicable to different geological circumstances. Even though there are significant limitations in applying the model to this study, it is useful to supplement and check the major element results. An effective method of illustrating the model, as proposed by Tindle and Pearce (1981), is shown in figure 6-21, where mineral vectors are used to depict element variation resulting from fractionation of different minerals. These vectors were constructed from the Raleigh equations and the distribution coefficients proposed by Arth (1976) and Condie (1978). The parent composition was defined as dyke sample 56 rather than

Figure 6-21: Ba versus Sr, Ba versus Rb and Sr versus Rb variation diagrams for granitic and porphyritic samples. Dotted lines indicate possible differentiation trends caused by the fractionation of different mineral phases. The vectors on the right show the theoretical effects on a melt composition of crystallizing mineral phases, assuming Rayleigh fractionation. Amphiboles would likely have similar fractionating characteristics with clinopyroxene. The first tics correspond to 75% original melt remaining the second, when shown, indicate 50% liquid remaining. Method and distribution coefficients from Tindle and Pearce (1981). Abbreviations: Bio-biotite; plag-plagioclase; cpx-clinopyroxene; K-fsp-potassium feldspar.

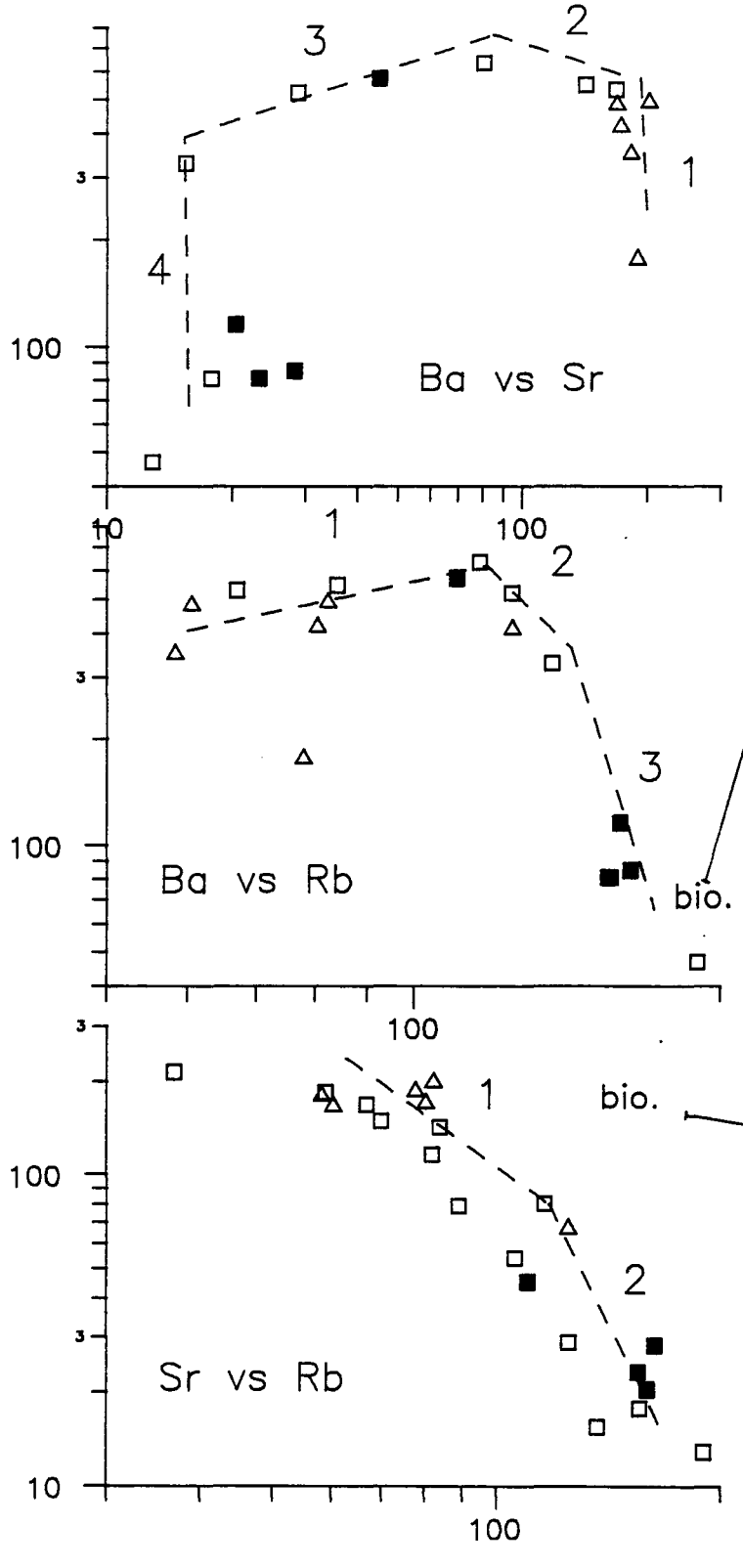
3
2
1
4
100
Ba vs Sr
10
1
100
2
3
100
Ba vs Rb
100
1
bio.
100
2
Sr vs Rb
10
100

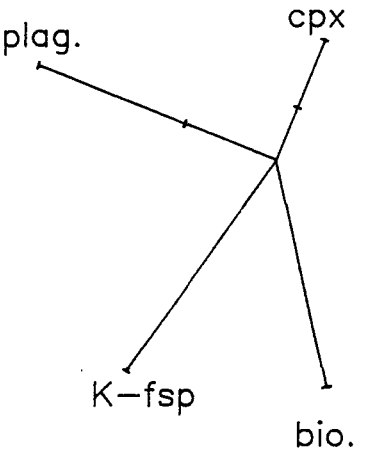
plag.
cpx
K–fsp
bio.

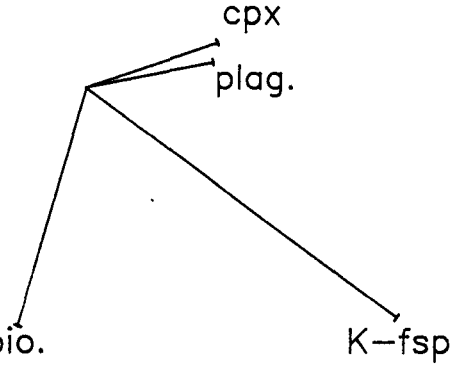
cpx
plag.
bio.
K–fsp

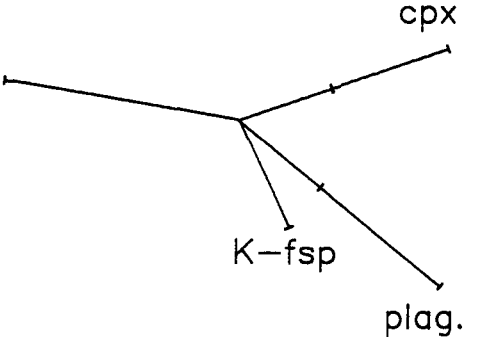
cpx
K–fsp
plag.

the three sample average used for the major element modelling, since there was considerable variation in LIL elements amongst the dykes. The three log plots of data (Fig. 6-21) show prominent inflections in the data arrays. These inflections were also noted by Tindle and Pearce (1981) who suggested that they represent stages during magma differentiation during which different minerals were crystallizing and fractionating. The limited data make the definition of these individual trends difficult with the Temagami data, but probable trends are outlined. Vector additions for each diagram suggest that all four proposed phases influenced the trace element variations. Trend 1 on the Ba versus Rb plot appears to be primarily controlled by plagioclase fractionation, while trends 2 and 3 appear to be controlled by K-feldspar. The poorly defined trend 1 on the Ba versus Sr plot could be controlled by plagioclase and clinopyroxene. Clinopyroxene is here substituted for hornblende, but the behaviour of amphiboles would be somewhat similar. Trends 2 and 3 appear to be controlled by plagioclase and K-feldspar. Trend 4 is difficult to model since it would require an unreasonably large fraction of both K-feldspar and biotite. Trend 1 of the Sr versus Rb plot is best defined by plagioclase and minor clinopyroxene, while trend 2 is probably controlled by K-feldspar and minor

biotite. Detailed results of the trends, the likely phases that cause them and the phase proportions are listed in table 6-5. The sum of the results indicate that the trend from dykes to granites was controlled primarily by fractionation of plagioclase and a mafic phase, such as pyroxene or amphibole, that has a low partition coefficient for Rb, Sr, and Ba. The trends that extend between granites to evolved granites and mineralized granites appear to be controlled by K-feldspar and minor biotite. This last conclusion conflicts with those based on the major element results discussed previously, which suggest K-feldspar was not a fractionating mineral. Closer inspection of K_2O variation reveals that it does increase until about 76 % SiO_2 beyond which it remains constant (Fig. 6-4). In addition the normative modal abundance of orthoclase increases with differentiation except for the most evolved samples which may show a minor decrease. The LIL variations indicate that K-feldspar was not the dominant fractionating phase until possibly the latter stages, represented by the interval between moderately evolved granites and the most mineralized and most differentiated granites. In a very similar situation Tindle and Pearce (1981) considered that the LIL elements might have been strongly controlled by magmatic fluids which might be expected to migrate towards

TABLE 6-5

Results of Trace element modeling
(refer to Fig.6-21)

Stages	Plot Ba v Sr	Plot Ba v Rb	Plot Sr v Rb
1	0.6 Cpx	-	0.87 Cpx
	0.9 Plag	0.5 Plag	0.6 Plag
	-	0.98 Ksp	-
2	-	-	0.98 Bio
	0.6 Plag	0.97 Plag	-
	.98 Ksp or Bio	0.85 Ksp	0.75 Ksp
3	-	0.98 Bio	-
	0.5 Plag	-	-
	0.8 Ksp	0.7 Ksp	-
4	unreasonable	-	-
	proportion of	-	-
	Ksp + Cpx or Bi	-	-

(Proportions refer to weight fraction of original liquid remaining.)

abreviations: Cpx-clinopyroxene; Plag-plagioclase; Ksp-potassium feldspar; Bio-biotite

the top of the magma body. This suggestion is analogous to that of Bateman and Chappel (1979) in their study of the Tolumn intrusive, in which they suggested K enrichment by an aqueous fluid. In light of these trends it would appear that the evolved rocks may have lost K, Rb, Sr and Ba to an aqueous fluid. Alkali transport via magmatically derived aqueous fluids has several advantages in the larger geological context. In previous chapters mention was made of the distinctive plagioclase selvages that rimmed a large proportion of the breccia fragments and the minor K-feldspar occurring in veinlets. In isolated pockets of breccia and in veins very near to the volcanic-intrusive contact, vein selvages and breccia matrix material were comprised of medium to fine-grained felsic material thought to be largely K-feldspar. It is reasonable to assume that the components in the hydrothermal solution that precipitated the quartz and feldspar were derived from the aqueous phase exsolved from the differentiated magma. The apparent depletions in Ca, Al, Ba, Sr, Rb and possibly K in the most evolved samples and those closest to the supposed magma chamber roof would then be attributed to aqueous phase transport and re-precipitation in the breccia and adjacent vein systems.

6.5.4.1 Mass Balance Calculations

It was previously proposed that the well defined variation of Zr and Zr/Hf with Si resulted from zircon fractionation. It is difficult to verify if zircon was a fractionating phase, but an indication might be obtained by calculating if the variation can be accounted for by separation of a reasonable proportion of zircon from the parental magma. The calculation is analogous to the equations used in the least squares mixing program for the major element modelling, following the relation:

$$X(\text{parent}) - (X_i)(Y_i) = X(\text{daughter})$$

Where: X(parent) and X(daughter) are the concentrations of ZrO_2 in the parent and daughter respectively.

X_i = the weight proportion of ZrO_2 in zircon ($ZrSiO_4$)

Y_i = the weight proportion of zircon fractionated (subtracted) from the parent to produce the observed zircon content of the daughter.

(the composition of parent and daughter are the same as those used in the major element modelling)

For zirconium fractionation to cause the observed variation 0.02% zircon would have to be removed from the parent melt. This amount is not unreasonable as suggested by the results of other studies, (Tindle and Pearce, 1981; Cullers and Graf, 1984; Dodge et al., 1982; Whalen, 1983) although zircon fractionation may conflict with the REE data. The possibility of zircon fractionation is supported by the conclusions of Cerny et al. (1985) who suggests that Zr has a very low solubility in peraluminous melts and is likely to form Zr-bearing minerals such as zircon.

6.5.5 REE Variation

In earlier discussions several features of the REE were noted to vary with increased differentiation including a decrease in LREE, increased HREE, a decrease in the HREE/LREE ratio and an increase in the magnitude of the negative Eu anomaly. Such variations are relatively common in the literature where differentiated suites of intermediate to felsic igneous and volcanic rocks have been investigated (Anderson and Cullers, 1978; Hildreth, 1981; Tindle and Pearce, 1981; Miller and Mittlefehldt, 1982; Lynch and Pride, 1983; Mittlefehldt and Miller, 1983; Whalen, 1983). With the exception of Hildreth (1981) the

above authors propose that the LREE are depleted by fractionation of minor phases such as allanite and monazite. The Temagami data indicate monazite was not a fractionating phase since there is no correlation between LREE and Th, which substitutes into monazite, and because monazite was not observed in any of the samples. Allanite on the other hand is documented in the intrusive rocks (Bennett, 1978). Published analyses of allanite may contain trace amounts of Th and U, but it will be assumed that the Temagami allanites were low in these elements or that other factors were more important in controlling Th and U. The possibility of allanite fractionation was tested by a simple mass balance calculation like that performed for zircon. As in the major element modelling parent and daughter compositions are calculated averages of samples thought to be representative. Using the allanite analysis number 11 from Deer et al. (1986) the calculation indicates that precipitation of 0.015 % allanite from the parent is required. This figure is reasonable when compared to the results of Tindle and Pearce (1981) for the Loch Doon pluton, where they calculated 0.05 % allanite fractionation. Assuming that allanite is the cause of LREE fractionation it is useful to note from tables 6-1,2 and figure 6-15, how La and Ce vary with differentiation. Table 6-2 indicates that La and Ce

increase from groups 1 to 8, suggesting that the LREE increase with differentiation. From groups 2 to 8 the LREE concentrations remain fairly constant but from groups 2 to 3 the LREE concentrations diminish. It would appear from these findings that the LREE initially behaved as incompatible species and that fractionation of allanite did not ensue until magmas reached a level of differentiation beyond that represented by group 2. This initial enrichment of LREE and subsequent depletion after reaching a certain level of differentiation is also noted in Anderson and Cullers (1978) analysis of the Wolf River batholith and the investigations of the Loch Doon pluton by Tindle and Pearce (1981). In both of these studies the authors suggest that REE containing phases such as monazite and allanite fractionated the LREE during the latter stages of magma evolution.

The HREE elements show a straightforward variation of increasing concentration with differentiation (Fig. 6-13 - 6-15; table 6-1,2). With the absence of a concentrating phase, HREE enrichment may be expected owing to incompatibility with most rock-forming minerals. According to Cullers and Graf (1984) HREE should be enriched in the upper portions of silicic magma chambers since they form complex ions more readily than the LREE. Zircon

fractionation is somewhat incompatible with the HREE pattern since zircon fractionates HREE over LREE, although if fractionation was only minor the effect might be minimal.

The chondrite plots and tables 6-1,2 show that the magnitude of the negative Eu anomaly increases with differentiation. Europium^{2+}, as opposed to Eu^{3+}, behaves geochemically like Sr (Philpotts and Schnetzler 1970), relative to other REE and it is this property that leads to Eu depletion during feldspar fractionation. A Raleigh fractionation model can be employed to model the variation of Eu in much the same manner as for the LIL elements. In the method proposed by Noble et al. (1979) the Raleigh equation can be manipulated to produce an analogous expression:

$$Eu/Eu^{*} = F^{(Deu - Deu3+)}$$

Where: Eu = concentration in the residual liquid

Eu^{*}= concentration of Eu in an unfractionated, but otherwise identical residual liquid, as inferred from concentrations of the other REE in the liquid

Deu= the distribution coefficient observed or inferred for total Eu

Deu^{3+}= the distribution coefficient for Eu, as inferred from the concentrations of the other REE in associated crystalline and glass phases

F= weight fraction of residual liquid remaining after fractionation.

The application of this model requires that an estimate of ($Deu-Deu^{3+}$) be made. Noble et al. (1979) concludes that values ranging from 1.5 to 3.0 are consistent for the distribution of Eu between Ca-poor feldspar and subalkaline silicic melts, but that values < 1 are preferred for peralkaline magmas (Barberi et al., 1975) and values as high as 8.0 for very silicic subalkaline magmas of the Bishop tuff (Hildreth, 1977). For this study it is not possible to apply a well constrained value of ($Deu-Deu^{3+}$) and only range can be assumed based on the silicic subalkaline nature, and the Ca-poor plagioclase in the Strathy-Chambers batholith (refer chap.2). For the purposes of the discussion a range of 1.3 to 5.0 is used to calculate corresponding degrees of fractionation (F). Resulting values of F indicate how much feldspar must be separated from the parent to derive the observed Eu anomaly for a given sample. Results in table 6-6 indicate that the less evolved rocks of group 1 and 8

TABLE 6-6

Calculation of The Europium Anomoly

Determination of the Europium anomoly from the relationship: $Eu/Eu^{*} = F^{(Deu - Deu+3)}$ (see text)

Fraction of liquid remaining (F) after fractional crystalization, calculated for selected values of Eu/Eu^{*} and (Deu - Deu+3)

Anomoly of Group (avg.)	Eu/Eu^{*}	(Deu - Deu+3)			
		1.0	1.3	2.0	3.0
3	0.060	0.060	0.115	0.245	0.391
4	0.100	0.100	0.170	0.316	0.464
	0.300	0.300	0.396	0.548	0.669
5	0.500	0.500	0.587	0.707	0.794
2	0.600	0.600	0.675	0.775	0.843
	0.800	0.800	0.842	0.894	0.928
1	0.900	0.900	0.922	0.949	0.965
8	1	1	1	1	1

require 0 and 8 % fractional crystallization to produce the corresponding anomalies of 1.0 and 0.9. The moderately evolved granitic rocks of group 2 have an average anomaly of 0.6 require 32.5 and 10 % fractional crystallization for ($Deu-Deu^{3+}$) values of 1.3 and 5.0. The highly evolved granites of group 3 would demand 87 and 43 % fractional crystallization of feldspar to produce an average anomaly of 0.06 for the same values of ($Deu-Deu^{3+}$). The mineralized rocks that comprise group 4 have an average anomaly of 0.10 which would be produced by 83 and 37 % fractional crystallization. Application of the model, which assumes magmatic fractionation, to aplitic rocks and especially pegmatites is not appropriate since processes transitional between magmatic and hydrothermal may have been important in their formation.

The Eu fractionation model suggests that the proportions of feldspar needed to fractionate the Eu is reasonable in most cases. Predictions of greater than 80 % fractional crystallization when using a ($Deu-Deu^{3+}$) value of 1.5 are unreasonable, however, without more precise estimates of ($Deu-Deu^{3+}$) these results are difficult to interpret.

6.5.6 REE Distribution Amongst Mineralized Granites,

Aplites and Pegmatites

The REE content of mineralized granites generally indicate that the LREE and HREE are similar to the host granites, whereas Sm, Tb and Y are enriched relative to their host granites (Fig. 6-16,17). The reason for this apparent enrichment is difficult to resolve, but it has been found that Sm concentrates in sulphides such as galena (Cullers and Graf, 1984). From the Cu and Mo data (appendix B) it is likely that the mineralized samples contain small amounts of sulphides allowing for the possibility that some of the REE have been concentrated in these sulphides. However the argument for sulphide enrichment is weakened by the fact that mineralized sample 48 contains the greatest concentrations of Cu and Mo and the lowest concentrations of Sm, Tb and Y of the mineralized samples. An alternative idea is based on the assumption that mineralization of these granitic rocks took place by interaction with saline metal bearing fluids. The partitioning behaviour of the REE in hydrous vapours and saline solutions is not well understood, but there is some consensus that the HREE are preferentially fractionated into these phases due to their tendency to form complex ions (Dodge, 1979; Bowden and Whitley, 1979; Cullers and Graf, 1984). How the mineralized granites obtained

their unique REE character is difficult to determine but the fact that they are distinct is in itself of importance. This tendency for HREE to concentrate in hydrous solutions may have some bearing on the apparent HREE depletion of the quench rocks discussed earlier. The very nature of the quench texture implies loss of an exsolved hydrous phase, which presumably could have carried the HREE plus the other depleted elements.

Aplitic rocks have LREE contents lower than the host rocks, but similar to the most evolved samples, and HREE concentrations similar to the enclosing granites (Fig. 6-16,17). This parallels the observation made earlier that the aplites had trace and major element concentrations distinct from the host and more like the most evolved samples. These features are much like those documented by Taylor and Gorton (1977) and Mittlefehldt and Miller (1983) in their comparisons of aplitic rocks to their host granites. The circumstances at Temagami suggest that the aplites represent a residual liquid with LREE profiles acquired through a process of differentiation like that experienced by the evolved granites. The fine-grained texture and abundant graphic intergrowths suggests that the aplites crystallized in the presence of an aqueous phase (Jahns and Burnham, 1969) and that the marginal aphanitic

phases represents a quench texture resulting from a loss of hydrous fluid (Lynch and Pride, 1983). One interpretation of the HREE is that during the evolution of these residual liquids equilibrium between the host granites and HREE was maintained by the presence of hydrous fluids.

Pegmatites have LREE concentrations that are variable but HREE concentrations that are very similar to their host rocks (Fig. 6-16,17). Referring to the major element analysis it is apparent that the pegmatites have major element compositions that are surprisingly similar, given the coarse-grained texture, to their host granites. This implies that the modal mineral assemblages are in turn similar to the host granites. If the HREE are hosted in the various rock forming minerals such as feldspars, biotite and amphiboles then it is not surprising that the HREE contents of pegmatites and adjacent granites are equivalent. The similarity in HREE content of host and pegmatite suggests that the fluids or vapours that formed the pegmatites were in equilibrium with the enclosing magma, and were locally derived. The LREE variability of pegmatites with respect to the host might be related to the fact that LREE are hosted in proportionately minor phases such as allanite. Non-representative sampling or fractionation during precipitation could easily account for the variability of

LREE concentrations within the pegmatites.

6.6 Conclusions

The investigation provided evidence that supports the hypothesis that chemical variation observed amongst the intrusive rocks arose by fractional crystallization. It is proposed that the felsic dykes represent the most primitive member of the differentiation series and mineralized granites and granites adjacent to the volcanic-intrusive contact are the most differentiated. Aqueous fluids were at least in part responsible for mobilization of Si, Al, Ca, K, Rb, Sr, and Ba in the most differentiated rocks. These aqueous fluids are probably the hydrothermal fluids that pervaded the breccia and veins where they precipitated these components as feldspar and other hydrothermal minerals.

The degree of differentiation was greatest near the intrusive-volcanic contact opposite the breccia. This area of the intrusion probably represents what was the roof or cupola atop a progressively differentiating magma chamber that subsequently evolved to produce the hydrothermal system responsible for veining and brecciation.

CHAPTER 7

GEOCHEMISTRY OF VEINS AND BRECCIA QUARTZ

7.1 Introduction

Forty eight samples of quartz material were analyzed for Au, As, Sb, and W and from this group a smaller number were analyzed for U, Th, and Cl. Samples were taken to represent eight different groups of quartz defined as: unmineralized veins, mineralized veins, feldspar-bearing veins, unmineralized breccia, mineralized breccia, unmineralized feldspar-bearing breccia, mineralized feldspar-bearing breccia and granite hosted veins. Mineralization refers to areas where combined sulphides, mainly chalcopyrite and molybdenite, account for at least 1 % of the vein or breccia. In most cases mineralization consists of chalcopyrite and molybdenite, in similar proportions, as selvages on breccia fragments and vein walls. The style and concentration of mineralization in veins and breccias are very similar. As mentioned

previously feldspar-bearing veins and breccias are rarely mineralized and the significant mineralization is exclusively in the feldspar deficient veins and breccias. In addition to the quartz, sulphide separates were extracted from seven of the most heavily mineralized samples and these were analyzed for Au, As, Sb, W and for sulphur isotope ratios.

The objective of the quartz study was to test if the concentration of various elements differed amongst these various quartz groups. The recognition of differences would be suggestive of compositionally different hydrothermal fluids. In addition analyses were intended to define the areal extent of mineralization beyond what was visible at the outcrop scale. The determination of Au was deemed important because of possible genetic implications for gold occurrences such as those near Arsenic lake and along the NLVL zone of deformation. Sulphur isotope determinations were intended to test whether the metallization was magmatically derived or whether non-magmatic sources of sulphur played a role in mineralization.

7.2 Quartz Geochemistry

7.2.1 Sample Preparation

Samples consisted of at least 300 g of quartz granules, free from impurities. Volcanic fragments, sulphide particles and limonite stained grains were separated by hand from coarsely crushed vein and breccia matrix material. The quartz was rinsed in distilled water and then crushed and sieved through 150 mesh bolting cloth in preparation for analysis. Analyses were performed on 1.2 g portions of the original sample by instrumental neutron activation analysis (appendix A). Because the samples were relatively pure quartz, matrix background, compared to that usually encountered with rock samples, was extremely low. This resulted in high signal to background ratios allowing for the determination of very low concentrations.

7.2.3 Results of the Quartz Analysis

A problem in the interpretation of the quartz analysis is that the host phases of the elements analyzed is uncertain. The various elements may occur as microscopic mineral particles or perhaps within fluid inclusions. If they are in fluid inclusions the abundance data is more likely to be representative of the original hydrothermal fluids than if the elements are within mineral particles. Unfortunately there is no simple method to ascertain the host of the various elements in the quartz suite. However,

it is still useful to determine whether or not fluids that precipitated the different quartz types were compositionally different in terms of the elements analyzed. Evidence presented previously suggests that all the veins and breccias formed synchronously; however, the heterogeneity of mineralization suggests that the fluids in breccias and veins may have differed in composition.

The results in table 7-1 indicate that there is very little distinction between quartz groups based on elemental abundances. The most obvious, and not unexpected relationship is that mineralized veins and breccias are higher in Au, Mo and possibly in As and Sb. Another feature is that W is higher in breccia samples than in vein samples. Interelement correlations are very weak, except for U-Th and As-Sb in quartz (table 7-2).

The quartz data can be illustrated by contouring element concentrations to show spatial relationships with the breccia zone and the intrusive-volcanic contact. Sample coverage is limited by outcrop exposure so that the highest density of data is from the area immediately surrounding the breccia. The spatial variation of the seven elements analyzed are contoured at appropriate intervals and are shown in figures 7-1 - 7-4. Chlorine does not correlate with the other elements and has a somewhat complex distribution (Fig. 7-1b). Molybdenum is concentrated in the

TABLE 7-1

Element Concentrations Separated According to Quartz type

(all concentrations except for Au (ppb) are in ppm)

	Unmineralized Veins			Mineralized Veins			Feldspar-bearing Veins		
	average	std.dev.	n	average	std.dev.	n	average	std.dev.	n
Au	0.54	0.42	6	6.96	14.55	18	0.41	0.29	3
As	0.18	0.07	6	0.27	0.47	18	0.18	0.07	3
Sb	0.02	0.00	6	0.03	0.01	18	0.01	0.01	3
W	0.06	0.05	6	0.03	0.02	18	0.03	0.01	3
Mo	1.25	1.87	6	8.68	11.61	18	0.87	1.06	3
Cl	312.50	142.02	4	515.71	305.51	7	*	*	0
U	0.01	0.01	6	0.02	0.02	16	0.02	0.01	3

	Unmineralized Breccia			Mineralized Breccia			Feldspar-bearing Breccia		
	average	std.dev.	n	average	std.dev.	n	average	std.dev.	n
Au	0.86	0.72	5	3.18	4.97	7	0.38	0.24	5
As	0.29	0.11	5	0.29	0.23	7	0.20	0.02	5
Sb	0.02	0.01	5	0.01	0.00	7	0.01	0.00	5
W	0.24	0.22	5	0.04	0.02	7	0.11	0.09	5
Mo	0.86	1.03	5	38.95	39.03	7	0.19	0.23	5
Cl	436.67	142.91	3	370.00	205.33	5	352.50	134.61	3
U	0.02	0.01	5	0.01	0.01	6	0.02	0.00	5

	Mineralized Feldspar-bearing Breccia		Granite Hosted Vein		
		n	average	std.dev.	n
Au	0.37	1	0.71	0.69	3
As	0.39	1	0.43	0.35	3
Sb	0.04	1	0.02	0.02	3
W	0.05	1	0.08	0.00	3
Mo	0.50	1	0.32	0.26	3
Cl	160.00	1	403.33	250.91	3
U	0.02	1	0.07	0.06	3

(* no analysis)

Table 7-2

Correlation coefficients for quartz and sulphide analyses

R-squared values for quartz analyses

	Au	As	Sb	W	Mo	Cl	U
Th	0.0534	0.2862	0.4254	0.1114	0.0863	0.3401	0.8706
U	0.0918	0.3286	0.3848	0.0030	0.0976	0.3234	
Cl	0.1000	0.1034	0.0100	0.1068	0.3387		
Mo	0.1487	0.1068	0.0610	0.1175			
W	0.0590	0.0722	0.0253				
Sb	0.2508	0.7095					
As	0.1175						

R-squared values for sulphide concentrate analyses

	Au	As	Sb	W
Mo	0.0768	0.1082	0.4783	0.1300
W	0.0480	0.4104	0.0843	
Sb	0.3578	0.4941		
As	0.2298			

central and SW end of the breccia and to a minor extent at grid location 260 SE, 300 SW (Fig. 7-2a). These areas are known to be mineralized with molybdenite. Gold is concentrated at the SE end of the breccia and SW as far as the exposure of veins 300 m SW of the grid baseline (Fig. 7-3a). This area of elevated Au is evident in the field as a zone of prominent mineralization. The high Au contours at 360 SE, 950 SW are caused by a single high value and therefore may not be reliable. The distribution of As is comparable to Au (Fig. 7-3b), and similar to Sb, (Fig. 7-2b) although there is uncertainty in the Sb data since most analyses were near the detection limit. Tungsten displays a more limited extent of enrichment that centres on and does not extend much beyond the breccia margin (Fig. 7-4a). Uranium like Sb occurs in concentrations near detection, however, results indicate an enrichment roughly coincident with the mineralized zone (Fig. 7-4b;Map 2).

7.3 Geochemistry of Sulphide Separates

7.3.1 Sample Preparation

Chalcopyrite and molybdenite mineral fractions were obtained by heavy liquid separation using 1,1,2,2 tetrabromoethane (ρ = 2.967). Pyrite, present only in trace

Figure 7-1a (page 269): Map of the breccia body, granite contact and grid coordinate system.

Figure 7-1b (page 269): Contour map of Cl concentrations for vein and breccia quartz. H, and L refer to areas of relative high and low concentrations. Open circles are sample locations.

Figure 7-2a (page 270): Contour map of Mo concentrations for vein and breccia quartz. H, and L refer to areas of relative high and low concentrations. Open circles are sample locations.

Figure 7-2b (page 270): Contour map of Sb concentrations for vein and breccia quartz. H, and L refer to areas of relative high and low concentrations. Open circles are sample locations.

Figure 7-3a (page 271): Contour map of Au concentrations for vein and breccia quartz. H, and L refer to areas of relative high and low concentrations. Open circles are sample locations.

Figure 7-3a (page 271): Contour map of As concentrations for vein and breccia quartz. H, and L refer to areas of relative high and low concentrations. Open circles are sample locations.

Figure 7-4a (page 272): Contour map of W concentrations for vein and breccia quartz. H, and L refer to areas of relative high and low concentrations. Open circles are sample locations.

Figure 7-4b (page 272): Contour map of U concentrations for vein and breccia quartz. H, and L refer to areas of relative high and low concentrations. Open circles are sample locations.

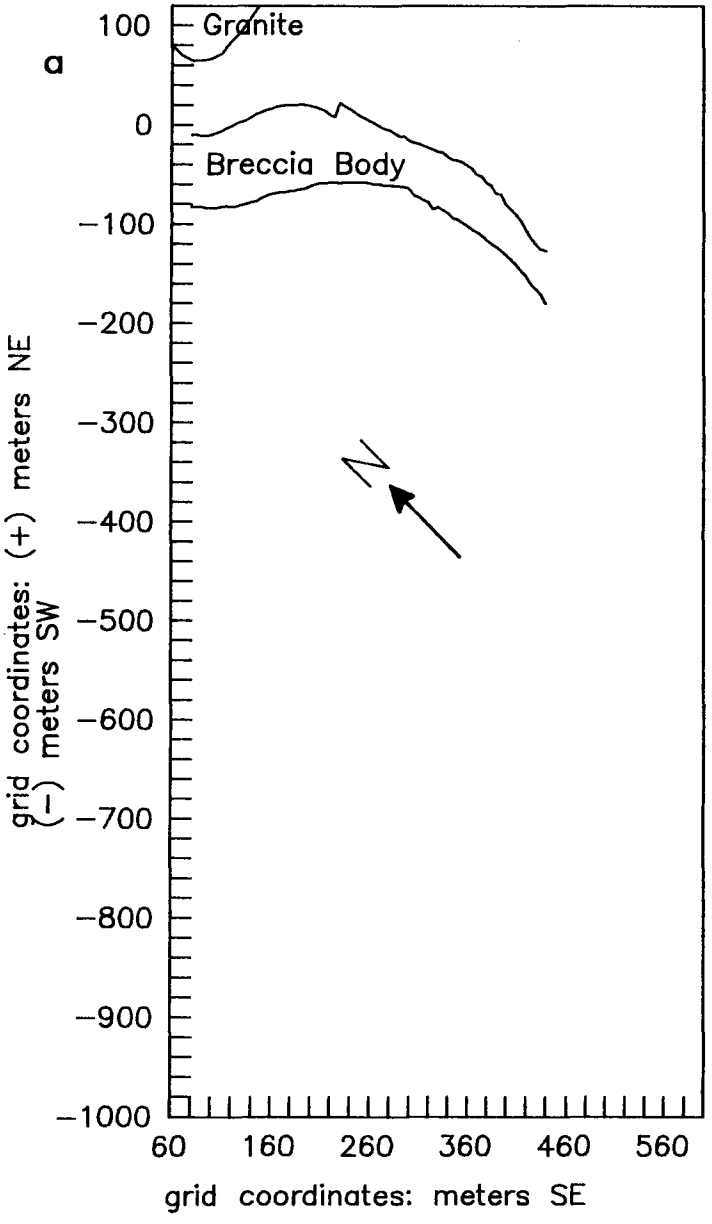
a
Granite
Breccia Body
N
100
0
−100
−200
−300
−400
−500
−600
−700
−800
−900
−1000
60
160
260
360
460
560
grid coordinates: (+) meters NE
(−) meters SW
grid coordinates: meters SE

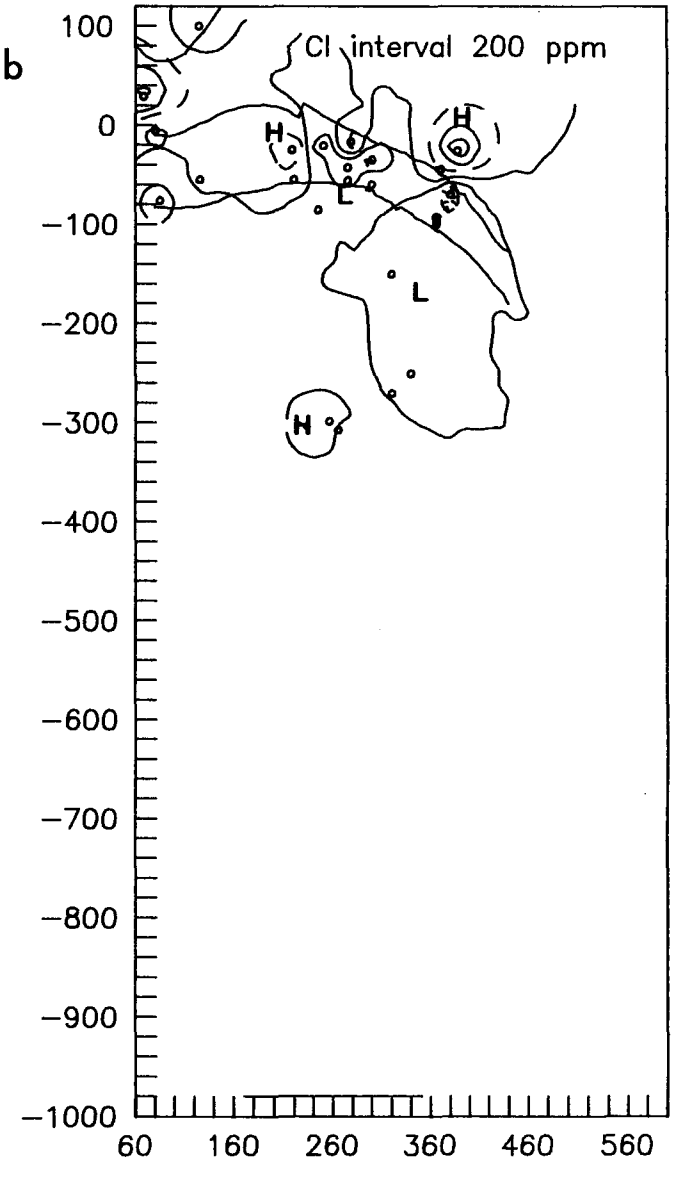
b
Cl interval 200 ppm
H
H
H
L
L
100
0
−100
−200
−300
−400
−500
−600
−700
−800
−900
−1000
60
160
260
360
460
560

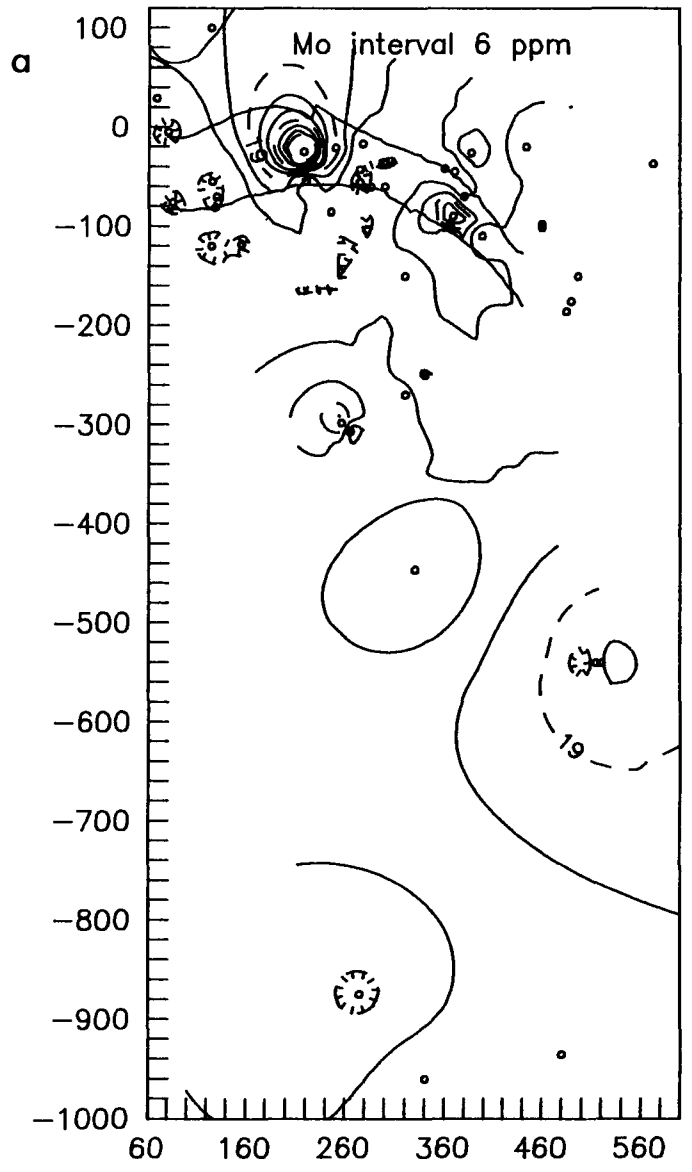
a
Mo interval 6 ppm
100
0
-100
-200
-300
-400
-500
-600
-700
-800
-900
-1000
60
160
260
360
460
560
19

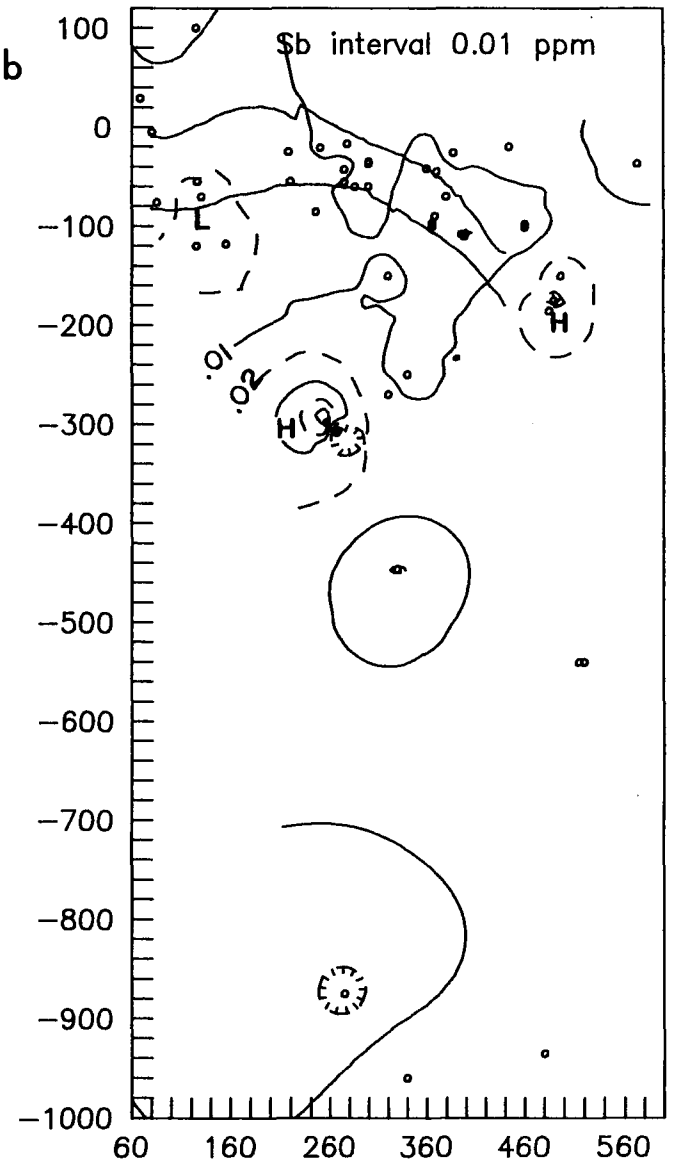
b
Sb interval 0.01 ppm
100
0
-100
-200
-300
-400
-500
-600
-700
-800
-900
-1000
60
160
260
360
460
560
L
H
.01
.02
H

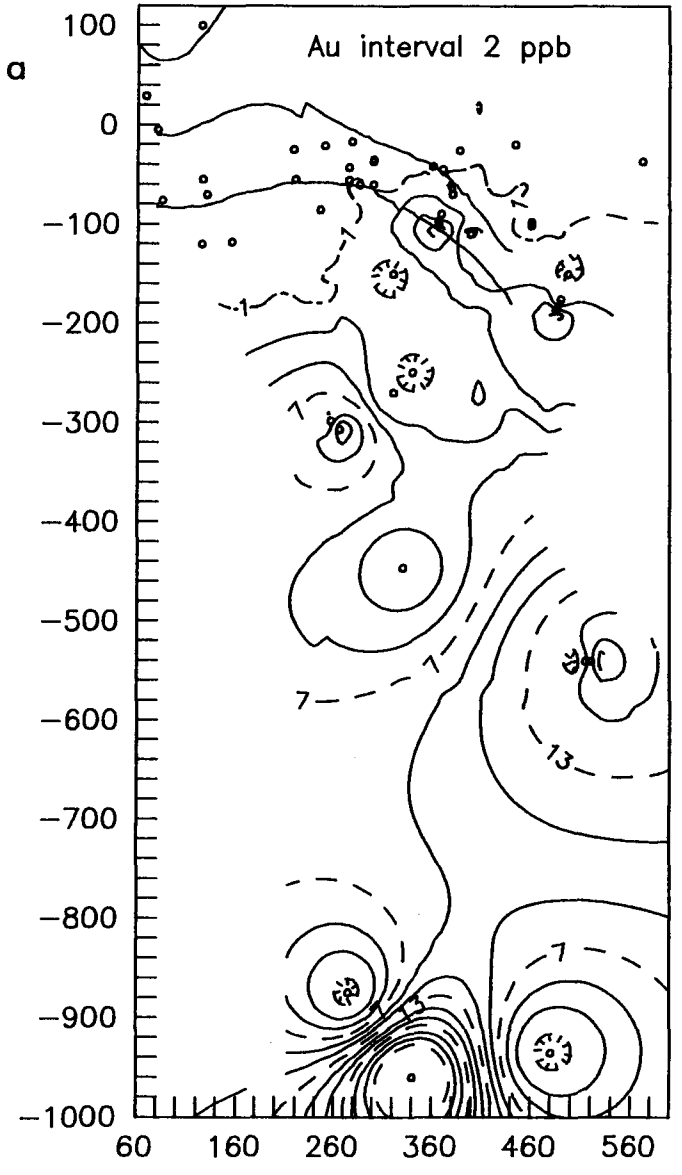
a
Au interval 2 ppb
100
0
−100
−200
−300
−400
−500
−600
−700
−800
−900
−1000
60
160
260
360
460
560
-1
7
13

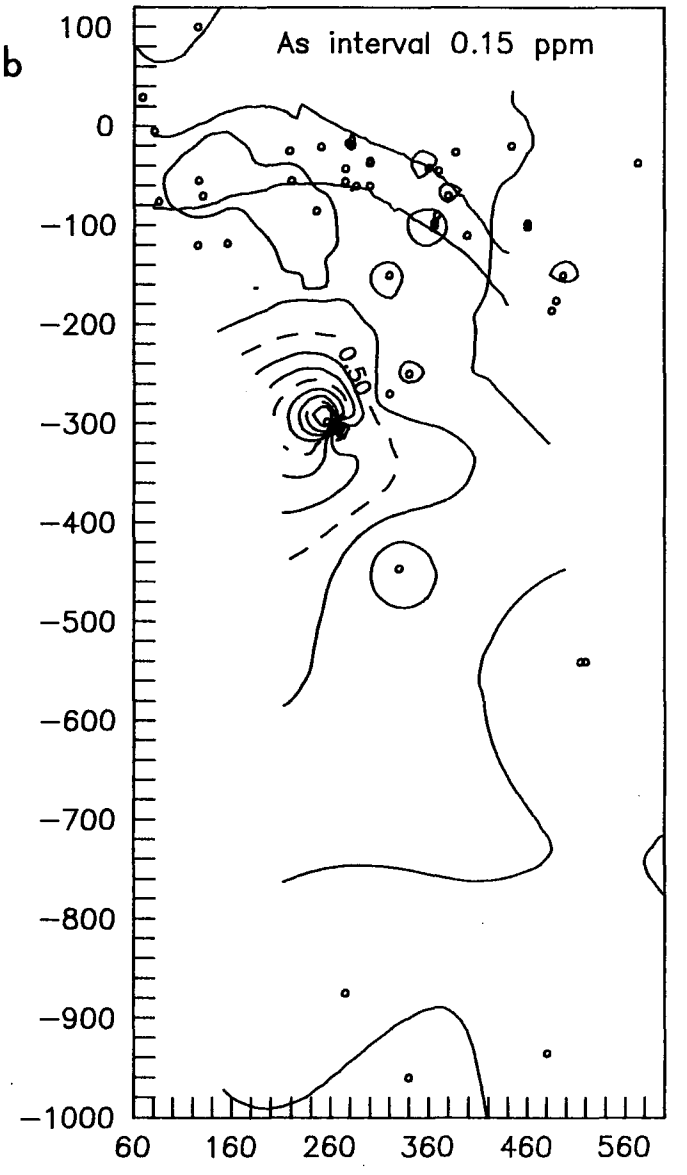
b
As interval 0.15 ppm
100
0
−100
−200
−300
−400
−500
−600
−700
−800
−900
−1000
60
160
260
360
460
560
0.50

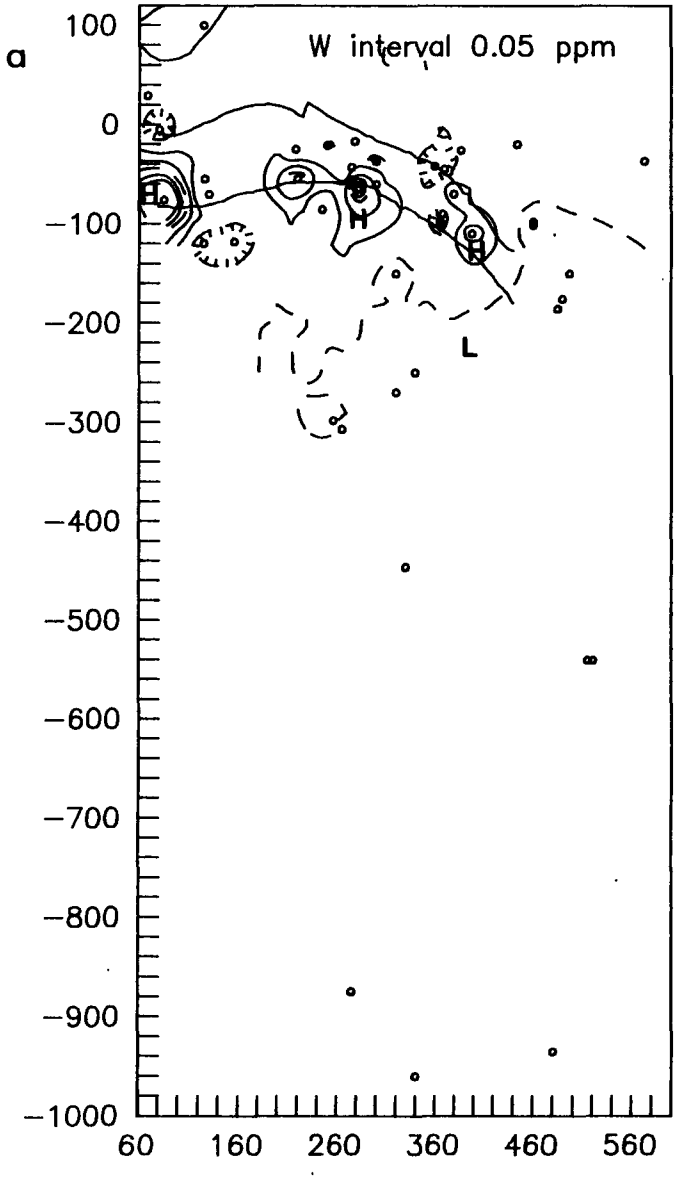
a
W interval 0.05 ppm
100
0
−100
−200
−300
−400
−500
−600
−700
−800
−900
−1000
60
160
260
360
460
560
H
H
H
L

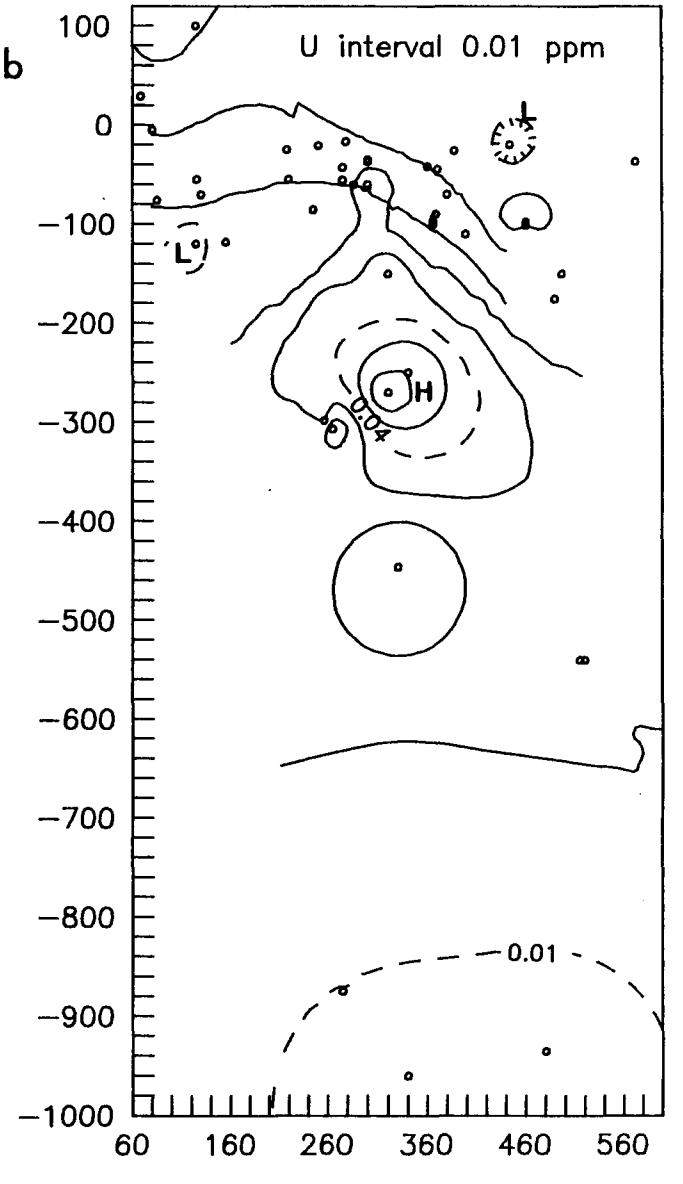
b
U interval 0.01 ppm
100
0
−100
−200
−300
−400
−500
−600
−700
−800
−900
−1000
60
160
260
360
460
560
L
H
0.04
0.01

amounts could not be separated and it therefore comprises a trace constituent in all samples. The mineral concentrates of chalcopyrite and molybdenite were of varying purity with most containing not more than 10 volume percent of the other sulphide. In a few samples the heavy liquid did not efficiently separate the sulphides from the gangue mineralogy and therefore some contain high proportions of gangue minerals. Samples of the gangue material analyzed by X-ray diffraction revealed that the gangue impurities were dominantly quartz, clinochlore, and traces of hematite and sphalerite. Samples of the nearly pure sulphide separates and of gangue were analyzed by INAA by the same method used for the quartz samples (appendix A).

7.3.2 Results of the Sulphide Analysis

Results listed in table 7-3 reveal that concentrations of the four elements analyzed are much higher than in the quartz. Because of higher matrix interferences several samples were below detection limits for As and Sb. The relatively poor precision, determined by duplicate analyses, is likely a result of sample heterogeneity. Gold concentrations range from 0.5 ppm to 8.0 ppm, averaging 3.2 ± 3.4 ppm, in chalcopyrite concentrates, and 0.1 to 3.8, averaging 1.1 ± 0.8 ppm, in molybdenite concentrates, indicating higher gold contents in chalcopyrite by approximately three times. This latter statement is,

TABLE 7-3

Results from Sulphide Separates
(All results in ppm)

Sam.	Main Sulphide	Prop. Gangue	cpy:mo	Gangue Minerals	Au	As	Sb	W
76a	mo	0.1	0:1	qtz, Fe-ox	0.9	*	*	21
181a	cpy	0.6	9:1	qtz, cl, sp	5.6	*	*	5.8
187a	mo	0.1	0:1	qtz	0.1	6	*	1.4
187b	mo	0.0	0:1	-	0.6	15	*	11
188a	cpy	0.1	1:0	cl	0.5	570	*	*
188b	cpy	1.0	1:0	qtz	1.2	260	3.9	20
192	cpy	0.1	1:0	qtz, htt	8.0	440	3.1	7.3
225a	mo	0.7	1:2	qtz, htt	1.3	8	1.2	7.5
225b	mo	0.7	1:2	qtz	2.3	*	*	30
256	mo	0.0	0:1	-	1.7	*	*	35
286a	cpy	0.7	9:1	qtz, cl	0.5	37	*	8.8
286b	mo	0.1	0:1	qtz	3.8	*	*	38

(* below detection)
(abbreviations: qtz=quartz; Fe-ox=iron oxide possibly limonite cl=chlinochlore; sp=sphalerite; htt=hematite)
(All mineral determinations by XRD)

however, thrown into doubt by more detailed inspection of the results. Sample pairs designated by 188a and 188b are taken from the same sample and therefore represent immediately adjacent sulphides and gangue. Sample 188a is 90 % chalcopyrite, while 188b the portion that floated on the heavy liquid is the dominantly quartz fraction. The Au results indicate that the quartz fraction contains more than twice the concentration of Au as the chalcopyrite portion. Similarly the molybdenite concentrates 225a and 225b contain 70 % gangue of mainly quartz and minor hematite and yet they have Au concentrations as high or higher than samples with very little gangue. The association of Au with either chalcopyrite or molybdenite is also somewhat ambiguous as samples 286a and 286b, coexisting chalcopyrite and molybdenite respectively, both contain relatively high concentrations of Au. Although dispersions are high average values favour a stronger association of Au with chalcopyrite

Arsenic and Sb are below detection in several samples, but in general the highest As values occur in chalcopyrite concentrates (Table 7-3). With the exception of sample 188b, which is a gangue sample, W is highest in molybdenite concentrates averaging 20.5 ppm as compared with 10.6 ppm in chalcopyrite. Strong interelement correlations are not evident for the entire sulphide data base as seen in table 7-2. The strongest correlations are for Sb-As where r =

0.49, however for molybdenite concentrates alone a moderately strong Au-W association with r = 0.78 (Fig. 7-5) is observed.

7.3.3 Discussion of the Quartz and Sulphide Results

It is likely that Mo and Cu occur in particulate molybdenite and chalcopyrite; however, the other elements, in particular Cl, could be hosted in fluid inclusions. Regardless of the mode of occurrence, it was considered that analysis of these purified quartz samples would be more useful in differentiating genetically different quartz populations and recognizing spatial variations of mineralized fluids than analyzing all of the vein material, including sulphides.

Results displayed in table 7-1 indicate that there are few discernable compositional differences between the various quartz populations except that mineralized samples show higher concentrations of Au and Mo. This may either mean there are mineral inclusions in the samples, or that fluids, hosted in fluid inclusions have different compositions. The spatial distribution of Au, As and Mo verify that mineralization is concentrated in or adjacent to the breccia and that it diminishes in intensity southwestward.

Figure 7-5: Au versus W concentration plot for samples of chalcopyrite and molybdenite concentrate. Straight line fit is for molybdenite samples only.

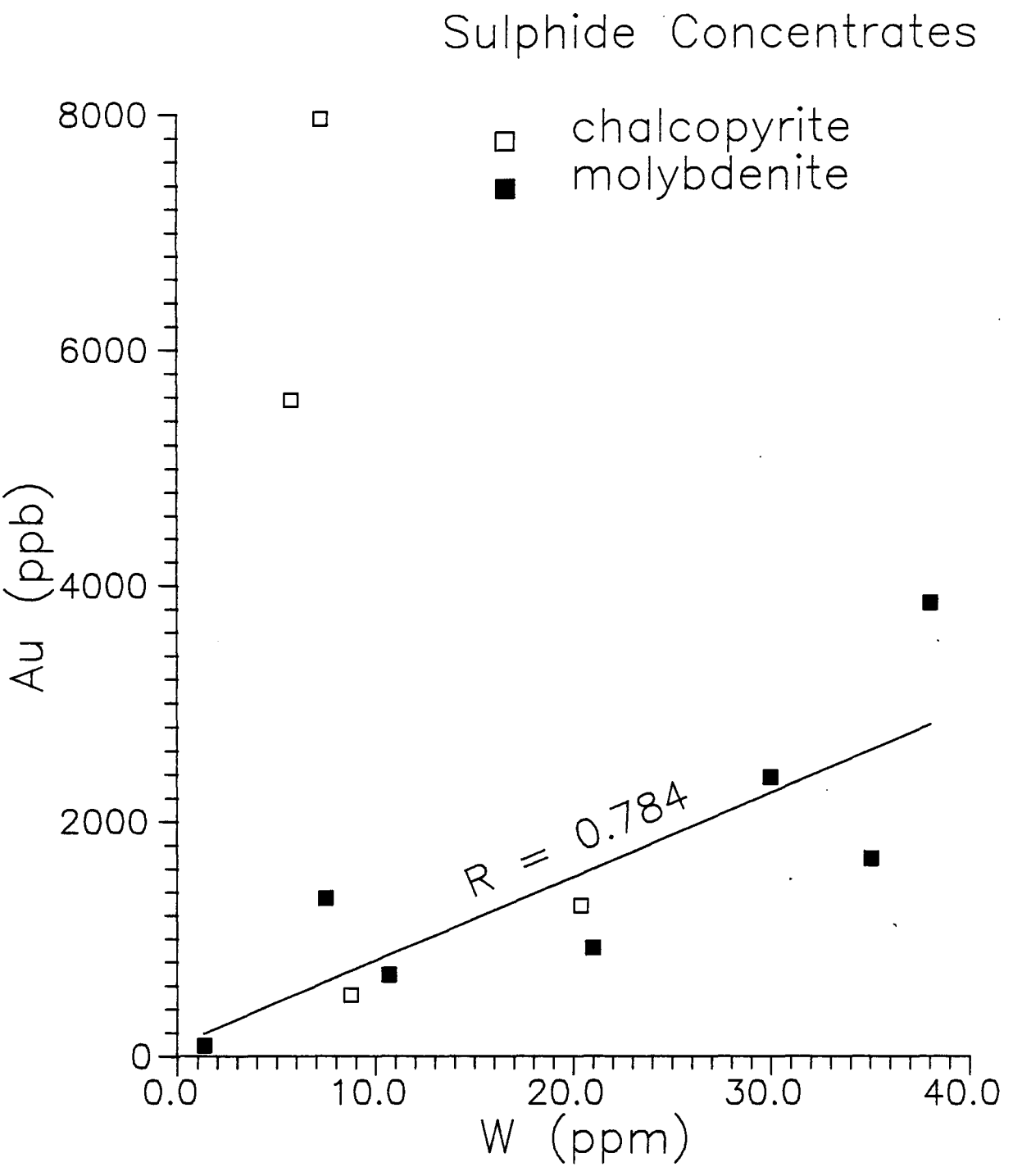
Sulphide Concentrates
chalcopyrite
molybdenite
8000
6000
4000
2000
0
Au (ppb)
R = 0.784
0.0
10.0
20.0
30.0
40.0
W (ppm)

The higher concentration of W within the breccia samples may be a feature which is more informative with respect to hydrothermal processes. As discussed in chapter 4 the proportion of selvage feldspar in the breccia and in veins close to the breccia implied that fluids which precipitated feldspar were close to the igneous-hydrothermal source. Similarly the higher concentration of a granophile element such as W (Strong, 1988), in the breccia might also be an indication that the breccia is centred on and above a source of magmatically derived hydrothermal fluids.

The two areas where U concentrations are highest correspond to a granite hosted vein and a group of veins that have unique mineralogies that include magnetite and hematite in excess of sulphides (refer chap.4). It is well established that U is often associated with hematite in U-bearing veins and that the precipitation of U oxide minerals is strongly controlled by the oxidation state of the fluids and wall-rocks (McKelvey et al., 1955). In light of these factors the association of U with these particular veins suggests that the U was controlled by the O_2 fugacity of late stage fluids (refer chap.4). The reason for the high concentration of the U in the granite-hosted vein is uncertain since only one sample from this type of vein was analyzed. Perhaps this high concentration of U was also influenced by transitions in the O_2 fugacity or cooling

influenced by the proximity of the volcanic-intrusive contact.

Chlorine highs coincide with breccias and veins with high proportions of feldspar selvage, while low concentrations coincide with feldspar deficient and mineralized zones. The association of Cl with feldspar abundance suggests that Cl was another element along with Na, Ca, Al and Si that was carried in the hydrothermal fluid (refer chap.4). In earlier discussion (chap. 4) it was suggested that one of the contributing factors to sulphide precipitation was the loss of metal complexing components such as Cl in the formation of feldspar and other hydrothermal minerals. It is plausible that, if the Cl data is representative of the hydrothermal solution, the inverse relationship of Cl with mineralization indicates the fluid had low concentrations of Cl in mineralized zones.

In the sulphide separates there is some indication that Au is preferentially associated with chalcopyrite over molybdenite although some evidence suggests that Au may be hosted in the gangue at sulphide grain boundaries. Except for the positive correlation of Au with W in molybdenite separates no significant interelement relationships were identified. Possibly the most important result of the analysis was that Au was occasionally present in high concentration (ppm levels), which might have some relevance

to the development of Au mineralization in areas to the south.

7.4 Sulphur Isotopes

7.4.1 Sulphur Isotope Systematics

Fractionation of the sulphur isotopes ^{32}S and ^{34}S, expressed as $\delta^{34}S$, can arise by a variety of means, but two processes are usually most important: 1) biologic fractionation by the reduction of seawater sulphate to produce H_2S, which is enriched in ^{32}S; 2) isotopic exchange between sulphur bearing ions (e.g. HS^{1-}, S^{2-}, SO_4^{2-}) molecules and solids by which ^{34}S is generally concentrated in compounds having the highest oxidation state of S, or greatest bond strength (Bachinski, 1969). This later process is the basis of the method of geothermometry described by Ohmoto and Rye, (1979), where isotopic fractionation between co-precipitating mineral pairs is temperature dependent. The definition of meteoritic sulphur isotopic composition as $\delta^{34}S = 0$ leads to the generalization that sulphur derived from the mantle sources has $\delta^{34}S$ values near 0. Sulphides that contain biogenic S derived by reduction of sulphate usually have negative and highly variable $\delta^{34}S$ values.

7.4.2 Sulphur Isotope Results

Sulphur isotope analysis were carried out at the laboratories of Dr. H.G. Thode at McMaster university. Results shown in table 7-4 indicate that in general the results of both chalcopyrite and molybdenite concentrates lie near zero, but that the uncertainty as determined by duplicate analysis is high. Although the uncertainty is high it is useful to calculate the temperature of crystallization, using averages for chalcopyrite and molybdenite concentrates, and the equilibrium isotopic fractionation relationships described by Ohmoto and Rye (1979). Such a calculation gives a temperature of 1000°C, which is too high based on results of this study and the conditions thought to prevail in this type of mineralizing environment (White et al., 1981). The reason for this extreme result is very likely related to the uncertainty in $\delta^{34}S$ measurements, however, it may also be that molybdenite chalcopyrite did not crystallize in equilibrium. A $\delta^{34}S_{Mo\text{-}Cpy}$ required for a more reasonable temperature of 500°C is 0.84 as compared to 0.30 calculated for the actual data. Noting that the uncertainty may be > 1.0‰ it is clear that the precision is too low to allow a reasonable temperature estimate.

The isotope results herein are similar to that compiled

Table 7-4

Sulphur Isotope Results for Molybdenite and Chalcopyrite Concentrates

Sample No.	Mineral	$\delta^{34}S$	difference between Duplicate analysis	Average of Duplicates
76a	mo	-0.5		
76b	mo	1.0	1.5	-0.2
181	cpy	0.3		
187a	mo	-0.2		
187b	mo	0.2	0.4	0.0
188a	cpy	-0.3		
192a	cpy	0.3		
192b	cpy	-0.5	0.8	-0.1
225b	mo	0.4		
256	mo	0.4		
286b	mo	0.4		
Average for molybdenite		0.28		
Average for chalcopyrite		-0.03		
$\Delta\delta^{34}S_{(MoS_2-CuFeS_2)}$		0.30		

from porphyry copper deposits by Ohmoto and Rye (1979). In their study they interpreted the near 0 values of $\delta^{34}S$ as an indication that the sulphur of porphyry deposits was derived largely from igneous sources, either as magmatic fluids or by dissolution of magmatic sulphides. In their overview of porphyry copper deposits Beane and Titley (1981) suggest the similarity of sulphur isotope values between porphyry deposits indicates that deposits of this type were formed under conditions of similar sulphur source, temperature, pH and fO_2. Although the mineralizing system considered in this study is not like an ideal porphyry system, the isotopic results do confirm the other geologic evidence that favours an igneous sulphide source and mineralization temperatures in the region of 475-650^{0}C. It is also possible that sulphur might have been derived from the volcanic pile, although it is not considered likely. If such were the case the isotopes ratios would be near zero as well and it would not be possible to differentiate if sulphur was derived from a plutonic or volcanic source.

CHAPTER 8

MODEL SUMMARY AND CONCLUSIONS

8.1 Emplacement of the Batholith

There are several indications that the Strathy-Chambers batholith was emplaced at a relatively shallow depth. The general statement that intrusions associated with mineral deposits often intrude to depths of less than 10 km and most commonly to less than 2 km (Burnham and Ohmoto, 1980) may be relevant to the Temagami situation. Geologic evidence for shallow emplacement is provided by the existence of miarolitic pegmatites (Lynch and Pride, 1983) and brittle behaviour of the volcanics in the intrusion breccia (Burnham, 1985; Cerny and Meintzer, 1988). Quantitative evidence is provided by pressure dependencies of amphibole chemistry, which indicate levels corresponding to less than 4 kb (15 km), but more likely 2 kb (7.5 km) (Brons, 1989). It has also been suggested by Fyon and Wheatly (1988),on the

basis of perthite textures that crystallization occurred below 5 kb fluid pressure. The ability of the magmas to intrude to these relatively shallow levels is likely related to the initial water content and presence of solidus-depressing elements such as F, B and Li (Strong, 1988; Manning, 1982). The presence of both biotite and hornblende in the Strathy-Chambers intrusive indicates the magma would have contained less than half the water content of a muscovite-bearing granitic melt (Strong, 1988). The biotite-hornblende melt would intersect the pressure dependent water saturated solidus at a shallower level than a muscovite-bearing melt, which becomes saturated at depths greater than 10 km (Strong, 1988). This may explain why biotite and hornblende bearing magmas are commonly associated with subvolcanic porphyry-type mineral deposits, which occur at shallow crustal levels (Strong, 1988).

The Strathy-Chambers batholith intrudes the volcanics in the study area as two lobes, which envelop a NE trending salient of volcanics. Several features such as the intrusion breccia, contact relations with elevation contours, intrusive exposures west of Temagami North and the intrusive related alteration on the west shore of Net Lake, suggest that the volcanic intrusive contact is very shallow. The width of the metamorphic aureole, as defined by Brons

(1989), also suggests that the volcanic salient is relatively thin and dips shallowly. The salient, particularly the area centred on the breccia, is viewed as a shallow sub-horizontal roof zone with an undulating surface creating potential fluid traps. Directly opposite the breccia the contact has a protuberance, that if considered in cross section might very well be the cupola that acted as the fluid reservoir, responsible for the formation of the breccia (Map 1;Fig. 4-12).

8.2 Crystallization of the Intrusive

After, and likely during, the emplacement of the Strathy-Chambers batholith, differentiation began as evidenced by the progressive depletion of, Al, Fe, Mg, Ca, Ti, P, Sr, Ba, Zr, Sc and enrichment of Si, K, Th, U, and Ta, toward the roof zone or cupola. Rare earth element results also indicate progressive differentiation toward the roof as shown by depletion in LREE, increasing negative Eu anomaly and increasing HREE concentrations. The semi-quantitative modelling of fractional crystallization based on major, trace element and REE variations confirms that subtraction of mineral phases from a parental liquid, approximated by the porphyry dykes, can explain

compositional variations. Differentiation, owing to the high viscosity of the melt, was likely by a combination of processes including crystal settling, flow differentiation and filter pressing. Some elements (K, Rb, Sr, Ba) do not conform to the crystal fractionation model for highly evolved samples and it is likely that they partitioned into late stage hydrous fluids.

8.3 Transition from Magmatic to Hydrothermal Processes

The formation of a separate aqueous volatile phase, essential to the development of mineralization, is largely dependent on the solubility of H_2O in the melt, which in turn is mostly dependent on pressure (Burnham, 1979). Once the melt has become saturated further cooling and crystallization causes additional water and incompatible elements to separate from the residual melt by a process commonly called second, or retrograde boiling (Burnham, 1979). The residual melt and aqueous phase become progressively enriched in elements incompatible with the solid phases. Several elements may be partitioned into the aqueous phase to the point where the hydrothermal fluid approaches the composition of a hydrous alkali silicate melt (Kovalenko et al., 1974; Glyuk, and Anfiligov, 1974).

Fluids such as these may have extremely high solubilities for Mo (> 10 wt. % MoS_2; Isuk, 1976).

The most significant evidence in Temagami for late stage separation of hydrous phase is provided by the existence of miarolitic pegmatites, aplites, pegmatoids and granophyric textures within a short distance of the roof zone. Pegmatites of the type documented at Temagami are often found in the cupolas of shallow, epizonal subvolcanic intrusives (Ginsburg et al., 1979). Together with associated aplites and presence of graphic textures such pegmatites are considered to arise as late stage differentiates that form in the presence of a separate aqueous phase (Jahns and Burnham, 1969). The occurrence of vein dykes and breccias with both quartz and igneous matrix are considered to record the transition from predominantly igneous to predominantly hydrothermal processes (White et al., 1981).

8.4 Fluid Pressure

As suggested by Burnham and Ohmoto (1980), emplacement of an intrusion is characterized by cooling, which begins at the contact with wall rocks and proceeds inward from the walls of the magma chamber. This marginal zone becomes

water saturated and crystallizes, creating a rind or carapace that inhibits transfer of fluids from the isolated interior (Burnham and Ohmoto, 1980). The carapace acts as an impervious trap in which exsolved aqueous fluids derived through second boiling are accumulated.

The transformation from H_2O-saturated melt to crystals + volatile phase involves a change in volume that produces internal pressure (Burnham, 1979). This vertical pressure or stress, which would have developed beneath the site of the Temagami breccia, overprinted or interacted with the existing regional stress field, which was characterized by a N-S compression (Fyon et al., 1988).

8.5 Failure and Brecciation

Failure of the roof rocks occurs when the tensile strength of the rocks is exceeded by internal pressure developed by the exsolved fluid. Such brittle response of roof rocks is not considered possible at depths greater than 8-10 km (Burnham, 1985). The expression of these tensile fractures at Temagami are the orthogonal joint sets that pervade the volcanic host and the breccia itself. The most convincing evidence that these joints were the surface of failure is the fact that the orthogonal pattern of joints

are essentially aligned with the often tabular fragments within the breccia. The set 1 joints, which trend 038^0, likely developed in response to more regional tensile stresses related to the same stress regime responsible for the veins and the 069^0 shear. Set 2 joints (Az 116^0) are thought to have resulted from the vertical stress component developed by fluid pressures. Development of these joint sets after solidification , as evidenced by their cross cutting the breccia, implies that similar stresses again built up, but were insufficient to cause re-brecciation. Continued stress is also indicated by the feldspar porphyry dykes, some of which postdate the breccia and intrude along structures occupied by the breccia.

The initial failure caused by resurgent boiling may have been an important process in brecciation, but subsequent decompression was likely the main source of energy responsible for brecciation (Burnham, 1979). Fluid streaming that may occur in response to decompression does not seem to have occurred at Temagami since fragments are not abraded nor is there a rock flour matrix component. The degree of fragmentation is highly variable throughout the breccia and distinct zones of incipient breccia grading into pervasive breccias have been identified. Well aligned arrays of tabular fragments and interlocking fragments

suggest that brecciation was passive and fragment transport and mixing was minimal. Textures also indicate that the brecciation was a single stage process.

The general attitude of quartz veins in and adjacent to the breccia is close to the average of the regional trend (071/85NW); however, veins near the breccia are much more variable in their orientations compared to veins greater than a hundred or more meters away from the breccia. This supports the concept that in the vicinity of the breccia the regional stress field was modified to one dominated by vertically directed stress. It also suggests, as does the mineralogy and field relationships, that veins were precipitated at the same time, and from the same fluids, as the breccia matrix.

The dominant trend of veins parallels the 069^0 shear zone on the east shore of Net Lake and is considered to have developed in response to the same stress regime. Kinematic indicators and tensional structures associated with veins demonstrate that they were related to sub-horizontal sinistral shearing. Most of the mineralized veins appear to coincide with a zone of brittle strain, characterized by higher joint densities, suggesting that vein mineralization was favoured by increased permeability.

8.6 Metamorphism and Alteration of Volcanics

The mineral assemblage characteristic of the inner zone of the contact aureole is defined by the hornblende-hornfels facies assemblage, ferro-hornblende + actinolite + epidote + plagioclase + quartz + ilmenite + apatite + magnetite ± chlorite ± sericite ± biotite ± microcline (Brons, 1989). Detailed investigations of the metamorphic assemblages within the volcanic rocks by Brons (1989) suggest that the peak metamorphic conditions near the intrusive contact were between 475°C and 550°C, with $X(CO_2) \leq 0.10$ and the fo_2 between 10^{-16} and 10^{-22} bars.

Alteration of primary and metamorphic minerals in the volcanics to biotite, muscovite and minor K-feldspar is prevalent in a zone within the inner metamorphic contact aureole. These alteration minerals are concentrated in and around the breccia and they are thought to represent K-silicate alteration similar to that associated with porphyry mineral deposits. K and Rb metasomatism in and adjacent to the breccia, as determined by Gresens calculations, is likely a reflection of these alteration minerals.

8.7 Vein and Breccia Mineral Assemblages

Plagioclase selvages on breccia fragments and vein walls occur in restricted zones within the breccia and in veins adjacent to feldspar-bearing breccias (Map 2). The feldspar is thought to have precipitated from the hydrous magmatic fluid, which, upon brecciation, was released from the cupola atop the magma chamber. One indication of the existence of such a fluid source is that some of the components needed to form feldspar, namely K, Ca, and Al are notably depleted in the most differentiated and apical samples in the Strathy-Chambers intrusive. Feldspar is concentrated in restricted zones within the breccia having a higher proportion of matrix, and in veins near the breccia. This may indicate that the components of feldspar were depleted from the hydrothermal solution before being channelled into more distant veins and that permeability might have encouraged feldspar accumulation in the breccia. Other silicates that occur in the veins and breccias are epidote, sericite, biotite, chlorite, hornblende and quartz. The greatest concentrations of these minerals is in mineralized zones where wall rocks are moderately to highly recrystallized.

The opaque mineral assemblages are like those associated with the K-silicate assemblage of porphyry deposits, considered to represent fluid temperatures between

400°C and 600°C (White et al., 1981). The paragenesis of opaque minerals indicates that the hydrothermal fluids experienced a decrease in fs_2 and an increase in fo_2.

Mechanisms of precipitation of sulphides may be reflected in the antipathetic relationship between mineralization and feldspar, the correspondence of wall-rock alteration with mineralization and the association of mineralization with small breccia fragments. The alteration-mineralization association suggests that fluid wall-rock interaction caused precipitation of sulphides and that feldspar selvages insulated fresh rock from hydrothermal fluids. The association of small fragments (increased surface area) and mineralization indicates that the fluid/rock ratio was important or that other conditions affecting mineralization differed between breccias of different textures.

The mineral assemblages found in both the veins and the breccias included all the essential minerals of the hornblende-hornfels facies mineral assemblage. This suggests that veins and breccias were formed during peak metamorphism, which is in agreement with other geologic indicators.

8.8 Conclusions

The Strathy-Chambers batholith intruded into the greenstone at a depth of about 7 to 10 km. Differentiation by processes dominated by crystal fractionation led to the development of a zoned magma chamber the top of which was below the present breccia body. Pressure dependant volatile saturation of the granitic melt and release of fluids through second boiling led to collection of a hydrous fluid phase within a crystalline rind or carapace. This saline fluid was enriched in the components that eventually precipitated as plagioclase, molybdenite and chalcopyrite in both the breccia and vein systems. The vertical fluid pressure eventually exceeded the tensile strength of the volcanic roof rocks resulting in the development of joint sets. This failure caused decompression and further exsolution of fluids which further promoted brecciation. Textures in the breccia indicate that brecciation was passive without fluid streaming and occurred as a single event. Veins that occur adjacent to the breccia and in a broad zone south of the breccia formed synchronously with the breccia, but their orientation was controlled by the shear stress reflected in the 069^0 sinistral shear zone.

Within the inner contact metamorphic aureole, K-silicate alteration is centred on the breccia and expressed

mineralogically by the development of biotite and K-feldspar. Mineral assemblages characteristic of the contact metamorphic assemblage also occur in the veins, indicating the breccia and veins coincided with peak metamorphism, where temperatures ranged from 475^{0}C to 550^{0}C and pressures 2kb-4kb (Brons, 1989). Sulphide mineralization was likely dependent on fluid wall rock interaction that was enhanced by high fluid/rock ratios and the absence of feldspar selvage mineralization.

On the basis of hydrothermal mineralogy and the proposed genesis, the formation of the breccia and veins coincided with the later stages of emplacement of the Strathy-Chambers batholith. It is also argued that the stress regime that determined the orientation of the 071^0 veins also caused the development of the 069^0 shear zone, which like the NLVL deformation zone cuts the outer zone of the Strathy-Chambers. This apparent conflict may be explained by considering that the shear stresses that produced the 069^0 and possibly the NLVL structures were a result of stresses caused by intrusion. During and after solidification of the outer margins of the batholith these stresses resulted in the development of shear structures such as the 069^0 shear, which truncated the outer margins of the batholith. Lower grade mineral assemblages identified

in these zones (Brons, 1989) do not necessarily represent the equilibrium conditions at the beginning of their formation, but rather the conditions that prevailed after protracted hydrothermal activity along these major fluid conduits. In summary it is proposed that the processes of intrusive emplacement, contact metamorphism, breccia and vein formation and the development of shear zones, and associated alteration were all interrelated and part of overlapping and continuous processes.

References

Allman-Ward, P., Halls, C., Rankin, A., and Bristow, C.M. 1982. An intrusive hydrothermal breccia body at Wheal Remfry in the western part of the St. Austell granite pluton, Cornwall, England. In Metallization Associated with Acid Magmatism. Edited by A.M. Evans. John Wiley and Sons Ltd., New York, pp. 1-28.

Anderson, E.M. 1936. The dynamics of the formation of cone sheets, ring dykes and cauldron subsidences. Royal Soc. Edinburgh Proc., v. 56, pp. 128-157.

Anderson, E.M. 1951. The dynamics of faulting and dyke formation with applications to Britain. Oliver and Boyd, Edinburgh, 206 p.

Anderson, J.L., and Cullers, R.L. 1978. Geochemistry and evolution of the Wolf river batholith, a late precambrian rapakivi massif in north Wisconsin, U.S.A. Precambrian Research, v. 7, pp. 287-324.

Arth, J.G. 1976. Behavior of trace elements during magnetic processes, a summary of theoretical models and their applications. J. Res. U.S. Geol. Surv., v. 4, pp. 41-47, illus. (incl. tables).

Atkinson, W.W.,Jr., Kaczmarowski, J.H., and Erikson, A.J.,Jr. 1982. Geology of a skarn-breccia orebody at the Victoria mine, Elko County, Nevada. Econ. Geol., v. 77, pp. 899-918.

Bachinski, D.J. 1969. Bond strength and sulfur isotopic fractionation in coexisting sulfides. Econ. Geol., v. 64, pp. 56-65.

Barberi, F., and others. 1975. A transitional basalt-pantellerite sequence of fractional crystallization, the Boina Centre (Afar Rift, Ethiopia). J. Petrol., v. 16, pp. 22-56.

Barlow, A.E. 1907. Second Edition of a Report on the Geology and Natural Resources of the Area Included by the Nipissing and Timiskaming Map-Sheets. Can. Geol. Surv., Rept. No. 962, 303 p.

Barnes, H.L. 1979. Solubilities of ore minerals. In Geochemistry of hydrothermal ore deposits, 2nd ed. Edited by H.L. Barnes. John Wiley and Sons, New York, pp. 404-460.

Bateman, Paul C., and Chappell, Bruce W. 1979. Crystallization, fractionation, and solidification of the Tuolumne Intrusive Series, Yosemite National Park, California. Geol. Soc. of Amer. Bulletin, v. 90, pp. 465-482.

Beane, R.E. and Titley, S.R. 1981. Hydrothermal Alteration and Mineralization. Part II, pp. 235-269. In Econ. Geol., 75th Anniv. Vol., Edited by B.J. Skinner. 964 p.

Beane, Richard E. 1982. Hydrothermal alteration in silicate rocks; Southwestern North America. In Advances in Geology of Porphyry Copper Deposits, Southwestern North America. Edited by S.R. Titley.

Bennett, G. 1978. Geology of the Northeast Temagami area, District of Nipissing. Ont. Geol. Surv. Rep., No. 163, 128 p.

Beswick, A.E., and Soucie, G. 1978. A correction procedure for metasomatism in an Archean greenstone belt. Precambrian Research, v. 6, pp. 235-248.

Beswick, A.E., and James, R.S. 1984. The metamorphic mineralogy and chemical alteration of the Temagami greenstone belt. Sudbury-Timmins-Algoma Minerals Project 4B, G.S.C. Open File Report 1091.

Blecha, Matthew. 1974. Batchawana Area - A Possible Precambrian Prophyry Copper District. CIM Bulletin, pp. 71-76.

Bowden, P., and Whitley, J.E. 1974. Rare-earth patterns in peralkaline and associated granites. Lithos, V. 7, pp. 15-21.

Brons, David J. 1989. Stratigraphy And Metamorphism of Mafic Volcanic Rocks Near Arsenic Lake, Temagami, Ontario. Unpubl. M.Sc. thesis, Laurentian Univ., Sudbury, Ont., 146 p.

Bryan, W.B., Finger, L.W., and Chayes, F. 1969. Estimating proportions in petrographic mixing equations by least squares approximation. Science, v. 163, pp. 926-927.

Bryan, W.B. 1969. Some applications of linear least squares calculations to petrographic problem (abs.).Amer. Geophys. Union Trans., v. 50, pp.354.

Burnham, C.W. 1979. Magmas and hydrothermal fluids. In Geochemistry of hydrothermal ore deposits. Edited by H.L. Barnes. New York, Whiley, pp. 71-136.

Burnham, Wayne C., and Ohmoto, Hiroshi. 1980. Late stage processes of felsic magmatism. In Granitic magmatism and related mineralization. Edited by S. Ishihara, and S. Takenouchi.

Burnham, C.W. 1981. Physicochemical constraints on porphyry mineralization. In Relations of tectonics to ore deposits in the southern cordillera. Edited by W.R. Dickinson, and W.D. Payne. Geol.Soc. Arizona Digest, v. 14, pp. 71-77.

Burnham, C. W. 1985. Energy Release in Subvolcanic Environments: Implications for Breccia Formation. Econ. Geol., v. 80, pp. 1515-1522.

Burnham, C.W. 1983. Deep submarine pyroclastic eruptions. Econ. Geol., Mon. 5, pp. 142-148.

Carmichael, I.S.E., Turner, F.J., and Verhoogen, J. 1974. Igneous Petrology. McGraw-Hill Book Co., New York,739 p.

Carson, D.J.T., Jambor, J.L., Ogryzlo, P., and Richards, T.A. 1976. Bell Copper: Geology, geochemistry and genesis of a supergene-enriched, biotized porphyry copper deposit with a superimposed phyllic zone. In Porphyry deposits of the Canadian Cordillera. Edited by Sutherland A. Brown. Canadian Institute of Mining and Metallurgy, Spec. Vol. 15, pp. 245-263.

Cerny, P. 1982. Anatomy and Classification of Granite Pegmatites. In Granitic Pegmatites in Science and Industry. Edited by P. Cerny.

Cerny, P. 1985. Pegmatite Studies; means and objectives (abstr.).Annual Report - Centre for Precambrian Studies, University of Manitoba, 1984, pp. 66-67.

Cerny, P., Meintzer, R.E., and Anderson, A.J. 1985. Extreme Fractionation in Rare-Element Granite Pegmatites: Selected Examples of Data and Mechanisms. Can. Mineral., v. 23, pp. 381-421.

Cerny, Petr, and Meintzer, Robert E. 1988. Fertile granites in the Archean and Proterozoic fields of rare-element pegmatites; crystal environment, geochemistry and petrogenic relationships. In Recent Advances in the Geology of Granite-Related Mineral Deposits. Edited by R.P. Taylor et al. Special Volume - Canadian Institute of Mining and Metallurgy, 39, pp. 170-207, illus. incl. 4 tables, geol. sketch maps, 220 ref. Meeting: Sept. 1985, Halifax, NS, Canada.

Chatterjee, A.K., Strong, D.F., and Muecke, G.K. 1983. A multivariate approach to geochemical distinction between tin-specialized and uranium-specialized granites of southern Nova Scotia. Can. J. Earth Sci., v. 20, pp. 420-430.

Chayes, F. 1968. A least squares approximation for estimating the amounts of petrographic partition products. Mineralog. et Petrog. Acta, v. 14, pp. 111-114.

Cheney, E.S., and Trammell, J.W. 1975. Batholiithic ore deposits (abst.).Econ. Geol., v. 70, pp. 1318-1319.

Condie, K.C. 1978. Geochemistry of Proterozoic granatic plutons from New Mexico, U.S.A. Chem. Geol., v. 21, pp. 131-149.

Deer, W.A., Howie, R.A., and Zussman, J. 1983. An Introduction to the Rock Forming Minerals. Longman Group Ltd., 528 p.

Deer, W.A., Howie, R.A.,and Zussman, J. 1986. Orthosilicates: in the collection of Rock-forming minerals, 2nd ed. Longman Group, London, United Kingdom, 1A, 919pp., illus. incl., 79 tables, anal., scattered ref. First edition 1961.

Dodge, F.C.W., Millard, Jr. H.T., and Elsheimer, H.N. 1982. Compositional Variations and Abundances of Selected Elements In Granitoid Rocks and Constituent Minerals, Central Sierra Nevada Batholith, California. United States Geol. Soc., Geol. Soc. Prof. Paper, No.1248, pp. 24, 48 ref.

Dodge, F.C.W. 1979. The Uyaijah ring structure, Kingdom of Saudi Arabia. U.S. Geol. Surv. Prof. Paper 774-E, 17 p.

Einaudi, M.T. 1982. General features and origin of skarns associated with porphyry copper plutons, southwestern North America. In Advances in Geology of Porphyry Copper Deposits , Southwestern North America. Edited by S.R. Titley. Tucson, Univ. Ariz. Press, Chapter 8.

Evensen, N.M., Hamilton, P.J., and O'Nions, R.K. 1978. Rare-earth abundances in chondritic meteorites. Geochim. Cosmochim. Acta, v. 42, pp. 1199-1212.

Flynn, R.T., and Burnham, C.W. 1978. An experimental determination of rare earth partition coefficients between a chloride containing vapor phase and silicate melts. In Proceedings of the International Conference on experimental trace element goechemistry.

Fyon, J.A., and Crocket, J.H. 1986. Exploration potential for base and precious metal mineralization in part of Strathy Township, Temagami area. Ont. Geol. Surv., Open File Report 5591, 46 p.

Fyon, J.A., and O'Donnell, L. 1987. Metallogenic studies in the Temagami greenstone belt, District of Nipissing; In Summary of Field Work and Other Activities 1987. Ont. Geol. Surv., Misc. Paper 137, pp. 190-197.

Fyon, J.A., and Wheatley, K.J. 1988. Petrographic characteristics of Archean granitoid rocks; In Summary of Field Work and other Activities. Ont. Geol. Surv. Misc. Paper 141, pp. 381-383.

Fyon, J.A., Hrabi, R.B., and Maitland, W.M. 1988. Relationships between lithological, alteration, and structural features and precious-metal occurrences in the Temagami greenstone belt, District of Nipissing; In Summary of Field Work and Other Activities 1988. Ont. Geol. Surv., Misc. Paper 137, pp. 212-218.

Fyon, J.A., and Cole, S. 1989. Geology of part of the Temagami greenstone belt, District of Nippissing, including relationships between lithologic, alteration, and structural features and precious-metal occurrences. Ont. Geol. Surv., Misc. Paper 146, pp. 108-115.

Ginsburg, A.I., Timofeyev, I.N., and Feldman, L.G. 1979. Principles of Geology of the Granitic Pegmatites. Nedra, Moscow, in Russian.

Glyuk, D.S., and Anfiligov, V.N. 1974. Phase equillibrium in the system granite - H_2O-HF at a pressure of 1000 Kg/cm^2. Geochemistry Internat. v. 1973, pp. 321-325.

Gorvindaraju, K. 1984. Compilation of working values for 170 international reference samples of mainly silicate rocks and minerals. Geostandards Newsletter, v. 8, Appendix I, pp. 3-16

Gresens, Randall L. 1967. Composition-Volume Relationships of Metasomatism. Chem. Geol., v. 2, pp. 47-65.

Gunow, A.J., Ludington, S., and Munoz, J.L. 1980. Fluorine in micas from the Henderson molybdenite deposit, Colorado. Econ. Geol., v. 75, pp. 1127-1137.

Harker, A. 1909. The Natural History of the Igneous Rocks. New York, 384 p.

Henderson, P. 1986. Inorganic Geochemistry. Pergamon Press, 353 p.

Hildreth, W. 1977. The Bishop Tuff;compositional zonation in a silicic magma chamber without crystal setting (Abstract). Geol. Soc. Amer., Abstr. Programs, 8(6), pp. 918, September 1976. Meeting: The Geol. Soc. Amer., 1976 annual meeting, Nov. 8-11, 1976, Denver, Colo., United States.

Hildreth, Wes. 1981. Gradients in Silicic Magma Chambers: Implications for Lithospheric Magmatism. J. Geophys. Res., v. 86, No. B11, pp. 10153-10192.

Hildreth, Wes. 1979. The Bishop Tuff: Evidence for the origin of compositional zonation in the silicic magma chambers. Geol. Soc. Amer., Special Paper 180, pp. 43-75.

Hutchinson, C.S. 1974. Laboratory Handbook of Petrographic Techniques. John Wiley and Sons, New York, pp. 264-282.

Irvine, T.N, and Barager, W.R.A. 1971. A guide to the chemical classification of the common volcanic rocks. Can. J. Earth Sci., v. 8, pp. 523-549.

Isuk, Edet E. 1976. Solubility of molybdenite in the system Na_2O-K_2O-SiO_2-MoS_2-H_2O-CO_2 with geological application. Unpubl. Ph.D. thesis, Univ. Iowa, 101 p.

Jahns, R.H., and Burnham, C.W. 1969. Experimental studies of pegmatite genesis: I. A model for the derivation and crystallization of granitic pegmatites. Econ. Geol., v. 64, pp. 843-864.

Jensen, L.S. 1976. A new cation plot for classifying subalkalic volcanic rocks. Ont. Div. Mines Misc. Paper 66, 22 p.

Johnston, M. 1987. Stratigraphy and geochemistry of a portion of the Temagami greenstone belt, northeastern Ontario. Unpubl. M.Sc. thesis, Laurentian University, Sudbury, 123 p.

Kamb, W.J. 1959. Ice petrofabric observations from Blue Glacier, Washington, in relation to theory and experiments. J. Geophys. Res., 64, pp. 1891-1919.

Kirkham, R.V., and Sinclair, W.D. 1985. Porphry copper, molybdenum, tungsten: in Canadian mineral deposit types: a geological synopsis (Eckstrand, O.R., editor). Econ. Geol. Report - Geological Survey of Canada, v. 36, pp. 50-52, illus., 1984.

Knutson, J., Ferguson, J., Roberts, W.M.B., Donnelly, T.H., and Lambert, I.B. 1979. Petrogenesis of the Copper-Bearing Breccia Pipes, Redbank, Northern Territory, Australia. Econ. Geol., v. 74, pp. 814-826.

Kovalenko, N.I., Kovalenko, V.I., and Belykh, L.A. 1974. Experimental study of the fusion and crystallization of topaz-bearing quartz keratophyre (ongonite) in the presence of water and hydrofluoric acid. Akad. Nauk. SSSR Doklady, v. 215, pp. 681-684.

Lambeyre, Jean and Bowden, Peter. 1982. Plutonic rocktypes series: Discrimination of various granitoid series and related rocks. J. Volcanology and Geotherm. Res., v. 14, pp. 169-186.

Locke, A. 1926. The formation of certain ore bodies by mineralization stoping. Econ. Geol., v. 21, pp. 431-453.

Lowell, David J., and Guilbert, John M. 1970. Lateral and vertical alteration-mineralization zoning in porphyry ore deposits. Econ. Geol., v. 65, No. 4, pp. 373-408.

Ludington, Steve. 1981. The Redskin Granite: Evidence for Thermogravitational Diffusion in a Precambrian Granite Batholith. J. Geophys. Res., v. 86, No. B11, pp. 10423-10430.

Lynch, G.V., and Pride, C. 1983. Evolution of a high leve, high-silica magma chamber: the Pattison pluton, Nisling Range alaskites, Yukon. Can. J. Earth Sci. v. 21, pp. 407-414.

Manning, D.A.C. 1982. An Experimental Study of the Effects of Fluorine on the Crystallization of Granitic Melts. In Metallization Associated With Acid Magmatism. Edited by A.M. Evans. John Wiley and Sons Ltd., New York. pp. 191-203.

Marchand, M. 1973. Determination of Rb, Sr, and Rb/Sr by XRF. Technical Memo 73-2, Dept. of Geology, McMaster Univ., Hamilton, Ontario.

McCarthy, T.S., and Hasty, R.A. 1976. Trace element distribution patterns and their relationship to the crystallization of granite melts. Geochim. Cosmochim. Acta, v. 40, pp. 1351-1358.

McKinstry, H.E. 1955. Structure of hydrothermal ore deposits. Econ. Geol., 50th Anniv. Vol., Pt. 1, pp. 170-225.

Michael, Peter J. 1983. Chemical differentiation of the Bishop Tuff and other high silica magmas through crystallization processes. Geology, v. 11, pp. 31-34.

Miller, Calvin F., and Mittlefehldt, David W. 1982. Depletion of light rare-earth elements in felsic magmas. Geology (Boulder), v. 10, No. 3, pp. 129-133, illus. (incl. 1 table), 48 ref.

Mills, Joseph W. 1972. Origin of Copper-Bearing Breccia Pipes. Econ. Geol., v. 67, pp. 533-535.

Mittlefehldt, David, and Miller, Calvin F. 1983. Geochemistry of the Sweetwater Wash Pluton, California: Implications for "anomalous" trace element behavior during differentiation of felsic magmas. Geochim. Cosmochim. Acta, v. 47, pp. 109-124.

Moore, James G., and Lockwood, John P. 1973. Origin of Comb Layering and Orbicular Structure, Sierra Nevada Batholith, California. Geol. Soc. Amer. Bulletin, v. 84, pp. 1-20, 22 figs.

Moorehouse, W.M. 1946. The northeastern portion of the Temagami Lake area. Ont. Dept. Mines, v. 51, part 6.

Muecke, G.K., and Clarke, D.B. 1980. Rare earth element geochemistry of the South Mountain batholith, Nova Scotia. Geol. Soc. Can., Abstr. with Progr., v. 5, 72 p.

Mutschler, Felix E., Wright, Ernest G., Ludington, Steve, and Abbott, Jeffrey T. 1981. Granite molybdenite systems. Econ. Geol., v. 76, pp. 874-897.

Noble, Donald C., Rigot, Ward L., Bowman, Harry R. 1979. Rare-earth-element content of some highly differentiated ash-flow tuffs and lavas. Geol. Soc. Amer., Special Paper 180, pp. 77-85.

Norton, Denis L., and Cathles, Lawrence M. 1973. Breccia Pipes - Products of Exsolved Vapor from Magmas. Econ. Geol., v. 68, pp. 540-546.

Ohmoto, H., and Rye, R.O. 1979. Isotopes of sulphur and carbon. In Geochemistry of hydrothermal ore deposits, 2nd ed., pp. 509-567. Edited by H.L. Barnes. John Wiley, New York, 798 p.

Perry, V.D. 1961. The significance of mineralized breccia pipes. Mining Eng., v. 13, pp. 367-376.

Philpotts, J.A., and Schnetzler, C.C. 1970. Phenocrystmatrix partition coefficients for K, Rb, Sr, and Ba, with application to anorthosite and basalt genesis. Geochim. Cosmochim. Acta, v. 34, pp. 307-322.

Ramdohr, P. 1969. The Ore Minerals and Their Intergrowths. Pergamon, New York.

Rice, A. 1981. Convective fractionation: a mechanism to provide cryptic zoning (macrosegregation), layering, in cumulates, banded tuffs and explosive volcanism in igneous processes. J. Geophys. Res. 86, pp. 405-417.

Robin, Pierre-Yves F., and Jowett, Craig E. 1986. Computerized density contouring and statistical evaluation of orientation data using counting circles and continuous weighting functions. Tectonophysics, 121 (2-4), pp. 207-223, illus. incl., 3 tables, 20 ref.

Roedder, Edwin, and Coombs, D.S. 1967. Immiscibility in granitic melts, indicated by fluid inclusions in ejected granitic blocks form Ascension Island. J. Petrol., 8 (3), pp. 417-451.

Shand, S.J. 1943. The Eruptive Rocks, 2nd. ed. New York: Wiley,.

Shannon, J.R., Walker, B.M., Carten, R.B., and Geraghty, E.P. 1982. Unidirectional solidification textures and their significance in determining relative ages of intrusions at the Henderson Mine, Colorado. Geology (Boulder), v. 10, No. 6, pp. 293-297, illus., 20 ref.

Shaw, H.R., Smith, R.L., and Hildreth, W. 1976. Thermogravitational mechanisms for chemical variations in zoned magma chambers. Geol. Soc. Amer., Abstr. Programs, 8, 1102 p.

Shvetsov, M.S. 1955. Summary of Concerning some additional aids in studying sedimentary formations. J. Sed. Petrol., No. 25, pp. 229-234.

Sillitoe, R.H. 1985. Ore-Related Breccias in Volcanoplutonic Arcs. Econ. Geol., v. 80, pp. 1467-1514.

Sillitoe, R.H., and Sawkins, F.J. 1971. Geologic, Mineralogic and Fluid Inclusion Studies Relating to the Origin of Copper-bearing Tourmaline Breccia Pipes, Chile. Econ. Geol., v. 66, pp. 1028-1041.

Soucie, G.E. 1979. A Lithogeochemical Study of Metasomatic Alteration in the Temagami Greenstone Belt, Northeastern Ontario. Unpubl. M.Sc. thesis, Laurentian University, Sudbury.

Spurr, J.E. 1923. The ore magmas. New York, Mcgraw Hill, pp. 431-485.

Stewart, J.P. 1983. Petrology and geochemistry of the intrusives spatially associated with the Logtung W-Mo prospect, south-central Yukon Territory: Unpubl. M.Sc. thesis, Univ. of Toronto, 243 p.

Streckeisen, A.L. 1973. Plutonic rocks: Classification and nomenclature recommended by the IUGS subcommission on the systematics of igneous rocks. Geotimes, v. 18, pp. 26-30.

Strong, David F. 1988. A review and model for granite related mineral deposits. In Recent Advances in the Geology of Granite-Related Mineral Deposits. Edited by R.P. Taylor et al. Special Volume - Canadian Institute of Mining and Metallurgy, 39, pp. 424-445, illus. block diag., geol. sketch maps, 99 ref. Meeting: Sept. 1985, Halifax, NS, Canada.

Taylor, S.R., and Gorton, M.P. 1977. Geochemical application of spark source mass spectrometry-III element sensitivity, precision and accurracy. Geochim. Cosmochim. Acta, v. 41, pp. 1375-1380.

Taylor, S.R. 1965. The application of trace element data to problems in petrology. Phys and Chem of the Earth, v. 6 pp. 133-213.

Tindle, Andrew G., and Pearce, Julian A. 1981. Petrogenetic Modelling of in situ Fractional Crystallization in the Zoned Loch Doon Pluton, Scotland. Contributions to Mineralogy and Petrology, 78, pp. 196-207.

Titley, S.R. 1975. Geological characteristics and environment of some porphyry copper occurrences in the southwestern Pacific. Econ. Geol., v. 70, pp. 499-514.

Walker, Stephen D., and Cregheur, Paul. 1982. The Chadbourne Mine, Noranda, Quebec: A Gold-Bearing Breccia. pp. 58-66. In Geology of Canadian Gold Deposits. Edited by W. Petruk and R.W. Hodder. Canadian Institute of Mining and Metallurgy, Special Vol. 24, 286 p.

Warnaars, F.W. 1983. Copper tourmaline breccias at Los Bronces-Chile. Mining Eng. AIME Trans. v. 272, pp. 1902-1911.

Warnaars, F.W., Holmgren, Carmen D., and Barassi, Sergio F. 1985. Porphyry Copper and Tourmaline Breccias at Los Bronces-Rio Blanco, Chile. Econ. Geol., Spec. Issue, v. 80, pp. 1544-1565.

Whalen, J.B. 1980. Geology and geochemistry of the molybdenite showings of the Ackley City batholith, southeast Newfoundland. Can. J. Earth Sci. v. 17, pp. 1246-1258.

Whalen, J.B. 1983. The Ackley City Batholith, southeastern Newfoundland: evidence for crystal versus liquid-state fractionation. Geochim. Cosmochim. Acta, v. 47, pp. 1443-1457.

White, D.E. 1981. Active geothermal systems and hydrothermal ore deposits, pp. 392-423. In Econ. Geol., 75th Anniv. Vol., Edited by B.J. Skinner. 964 p.

White, Allan J.R., and Chappell, Bruce W. 1977. Ultrametamorphism and Granitoid Genesis. Tectonophysics, 43, pp. 7-22.

White, W.H., Bookstrom, A.A., Kamilli, R.J., Ganster, M.W., Smith, R.P., Ranta, D.E., and Steininger, R.C. 1981. Character and Origin of Climax-Type Molybdenum Deposits, pp. 207-316. In Econ. Geol., 75th Anniv. Vol., Edited by B.J. Skinner. 964 p.

Wilson, J.C. 1978. Ore fluid-magma relationships in a vesicular quartz latite porphyry dike at Bingham, Utah. Econ. Geol., v. 73, pp. 1287-1307.

Wright, A.E., and Bowes, D.R. 1963. Classification of volcanic breccias: a disscussion. Geol. Soc. Amer. Bulletin, v. 74, pp. 79-86.

Wright, Thomas L., and Doherty, Patrick C. 1970. A Linear Programming and Least Squares Computer Method for Solving Petrologic Mixing Problems. Geol. Soc. Amer. Bulletin, v.81, pp. 1995-2008.

APPENDIX A

ANALYTICAL METHODS

A-1 XRF Analysis of Major and Trace Elements

A representative portion of each sample (including quartz samples) was crushed to -200 mesh using a ceramic lined shatterbox.

Fusion pellets, for the determination of major elements, were prepared following the procedure outlined by Hutchinson (1977). A 6:1 ratio of flux (1:1 mixture of lithium metaborate and lithium tetraborate) to rock powder was fused in a metal alloy crucible and poured into a metal alloy pellet mold (97% platinum + 3% gold).

Powder pellets, for the determination of trace elements, were prepared following the procedure outlined by Marchand (1973). Approximately 3 grams of rock powder mixed with 3 drops of MOWIOL (polyvinyl alcohol) were used in an aluminium cup to 15 tons pressure.

A-2 Analysis of Au, As, Sb, Mo and W

Gold, As, Sb, Mo and W were determined by epithermal instrumental neutron activation analysis using the McMaster Nuclear reactor as a neutron source. Samples were packaged in batches of 12 samples and 3 standards for quartz and 13 samples and two standards for granitic samples. Samples were irradiated in the rotated cadmium shielded (transparent only

to epithermal neutrons) RIFLS (Reactor Irradiation Facility--Large samples) position where the approximate total thermal flux was 8 x 10^{12} neutron/cm_2/sec. Samples of 1200 mg were packaged in sealed (aqua regea washed) polyethylene vials. Standards for the quartz samples were prepared by weighing appropriate amounts of acidic aqueous solutions of metals into plastic vials filled with volumes of aqua regea washed silica powder with volumes of powder sufficient to yield nearly equal volumes of standards and samples. For the granitic samples two vials containing the standard G-1 (Govindaraju, 1984) were used.

The schedule of irradiation, cooling, and counting times and the characteristics of analytical γ-rays are tabulated below.

(reactor at 2 megawatt/hr)

Nuclide	Irradiation Time,hrs.	Cooling Time,hrs.	Counting Time,hrs.	Analytical γ-ray,KeV	$T_{1/2}$ hrs.
^{197}Au	1.5	48	1.0	412	64.7
^{76}As	1.5	48	1.0	559	26.3
^{122}Sb	1.5	48	1.0	564	65.3
^{99}Mo	1.5	48	1.0	181,739	66.0
^{187}W	1.5	48	1.0	479,686	23.9

Gamma-ray spectra were taken on a Canberra Series 35 plus multichannel analyzer (MCA) coupled to an intrinsic coaxial germanium detector (Aptec Engineering Ltd., Mississauga, Ontario). The detector characteristics were: active volume, 55 cm^3; resolution 1.8 KeV (FWHM) at 1.33 MeV; relative efficiency 10% and a peak to Compton ratio, 35/1. Spectra were taken in 4096 channels with the MCA calibrated at 0.39 KeV/channel.

The minimum detectable metal concentrations are dependent on sample bulk composition. The detection limits for quartz samples were low since the relatively pure samples had extremely low levels of background radiation. Detection limits were approached when the peak to background rations became low enough to create a large associated error (> 30%) in the peak fitting program, microSAMPO (Copyright 1986 by Logion OY and Canberra industries, Inc.). A summary of approximate detection levels for quartz and granitic samples is listed below. Detection limits for the sulphide separates are approximately an order of magnitude higher than for granitic samples.

Element	Approximate Detection Limit	
(conc.ppm)	Quartz	Granitic
Au	0.3ppb	1ppb

As	0.05	1
Sb	0.005	0.1
W	0.01	0.2
Mo	1	10

A-3 Determination of REE and selected trace elements

The rare earth elements as well as Sc, Ta, Hf and Th were determined by neutron activation analysis under the same conditions used for the Au determinations. The REE were determined from samples also irradiated for Au determination and therefore conditions were not optimal for the REE. Even under the less than optimum conditions the peak to background ratios were large enough to give dependable results. In a few instances the HREE were below detection as was Eu for one sample.

The schedule of irradiation, cooling and counting times are summarized below. Two rock standards G-2 and Scol were used for determination of the REE (Govindaraju, 1984).

Nuclide	Irradiation Time,hrs.	Cooling Time,hrs.	Counting Time,hrs.	Analytical γ-ray,KeV	$T_{1/2}$
^{139}La	1	2 days	1.0	1596	40.23
^{152}Sm	1	2 days	1.0	103.2	46.7h
^{176}Lu	1	8 days	1.0	208.4	6.71d
^{174}Yb	1	8 days	1.0	396.1	4.19d
^{140}Ce	1	40 days	2.0	145.4	32.5d
^{151}Eu	1	40 days	2.0	121.8	13.4y
^{159}Tb	1	40 days	2.0	298.6	72.4d
^{46}Sc	1	40 days	2.0	889,1120	83.9d
^{182}Ta	1	40 days	2.0	1221	115d
$^{233}Pa(Th)$	1	40 days	2.0	311.9	27d
^{181}Hf	1	40 days	2.0	482.2	42d

A-4 Determination of U and Cl

Analysis of Cl and U were done on 0.5 gram and 4 gram samples respectively under the supervision of A. Pidruczny at the Centre for NAA at the McMaster Nuclear reactor. Cl concentrations were determined by neutron activation (detection limit 40ppm). U was determined by delayed neutron activation analysis. The detection limit for U was approximately 0.01ppm for quartz, and 0.5ppm for granitic

Appendix B

Major and trace element data for all samples

Geochemical Analysis of Temagami Samples

INTRUSIVE ROCKS: Major Elements in percent, trace in ppm, Au ppb
(* no analysis; BLD-below detection, analyses normalized to 100%)

rock type—>	grnt	grnt	grnt	grnt	grnt	grnt	grnt	grnt
sample—>	730	750	760	711	780	790	103	131
SiO2	70.1	72.6	72.5	72.5	75.1	75.3	69.1	76.0
Al2O3	15.4	14.5	15.2	14.2	13.0	13.2	16.4	10.9
Fe2O3	3.04	0.95	2.32	2.13	2.00	1.73	3.06	1.27
MgO	0.90	0.94	0.87	0.46	0.42	0.49	1.31	2.91
CaO	3.15	1.37	1.46	1.79	0.99	0.87	2.43	0.27
Na2O	5.15	4.33	4.67	4.33	3.18	4.21	4.29	3.86
K2O	1.44	2.49	2.60	2.85	3.56	3.11	2.34	4.48
TiO2	0.36	0.25	0.23	0.20	0.21	0.13	0.09	BLD(.01)
MnO	0.06	0.06	0.05	0.06	0.05	0.04	0.04	0.02
P2O5	0.10	0.07	0.06	0.04	0.05	0.02	0.10	BLD(.01)
Ba	*	*	*	*	*	*	549.00	47.00
V	38.00	20.00	5.00	13.00	9.00	8.00	*	*
As	*	*	*	*	*	*	0.32	1.80
Co	6.00	4.00	3.00	3.00	2.00	2.00	*	*
Cu	8.00	29.00	18.00	2.00	11.00	5.00	1.00	0.50
Cr	*	*	*	*	*	*	*	*
Ni	5.00	5.00	5.00	5.00	4.00	3.00	*	*
Pb	*	*	*	*	*	*	*	*
Zn	*	*	*	*	*	*	*	*
Rb	37.00	59.00	70.00	82.00	89.00	106.00	84.10	190.00
Sr	214.00	185.00	149.00	116.00	79.00	54.00	142.50	12.90
Y	5.00	5.00	6.30	15.00	20.00	26.00	19.80	41.00
Zr	161.00	127.00	123.00	112.00	164.00	123.00	124.80	70.00
Nb	*	5.00	*	*	6.00	7.00	18.80	27.00
U	*	*	*	*	*	*	1.75	2.76
Th	*	*	12.00	*	12.00	*	6.58	12.55
Sc	5.00	4.00	3.00	3.00	5.00	4.00	3.43	2.25
Cs	*	*	*	*	*	*	2.45	1.69
Au	*	*	*	*	*	*	BLD	BLD
Sb	*	*	*	*	*	*	BLD	BLD
W	*	*	*	*	*	*	BLD	BLD
Mo	*	*	*	*	*	*	BLD	0.33
Sc	5.00	4.00	3.00	3.00	5.00	4.00	3.43	2.25
Cr	BLD	BLD	BLD	BLD	BLD	BLD	BLD	BLD
Co	6.00	4.00	3.00	3.00	2.00	2.00	5.15	BLD
Ba	*	*	*	*	*	*	533.45	36.86
Hf	*	*	*	*	*	*	4.12	4.48
Ta	*	*	*	*	*	*	1.09	2.97
Cl	*	*	*	*	*	*	100.00	180.00
La	17.00	17.00	12.00	14.00	26.00	20.00	17.18	4.81
Ce	34.27	33.27	23.27	29.27	59.27	43.27	31.21	17.08
Sm	2.60	2.50	1.90	2.80	5.10	4.60	2.89	1.86
Eu	0.69	0.70	0.50	0.55	0.92	0.58	0.61	0.07
Tb	0.24	0.25	0.21	0.46	0.67	0.76	0.55	0.58

Y	5.50	5.70	5.65	15.00	21.00	22.50	19.80	41.00
Yb	0.50	0.48	0.48	2.00	2.40	2.80	2.40	2.65
Lu	0.07	0.07	0.08	0.29	0.38	0.46	0.03	BLD

Geochemical Analyses of Temagami Samples

INTRUSIVE ROCKS: Major Elements in percent, trace in ppm, Au ppb

rock type—>	grnt	grnt	grnt	grnt	grnt	quench	quench	aplite
Sample—>	30	308	310	317	323	290	298	712
SiO2	80.8	73.7	75.2	76.1	72.0	72.0	75.7	76.1
Al2O3	9.3	14.5	13.3	13.0	14.7	15.7	13.8	13.5
Fe2O3	0.81	2.20	1.33	1.03	2.91	2.53	0.98	0.29
MgO	0.23	0.47	0.75	0.16	0.73	0.51	0.26	0.32
CaO	0.31	0.79	0.52	0.42	2.59	0.39	0.70	0.32
Na2O	3.68	3.92	3.97	3.83	3.79	4.35	7.52	3.62
K2O	4.41	3.37	4.18	4.78	2.25	2.65	0.20	5.37
TiO2	BLD(.01)	0.14	0.02	0.03	0.25	0.23	0.09	0.06
MnO	0.01	0.04	0.03	0.01	0.03	0.01	0.00	0.03
P2O5	BLD(.01)	0.04	BLD(.01)	BLD(.01)	0.08	0.06	0.03	0.05
Ba	81.00	635.00	522.00	330.00	532.00	418.00	25.00	*
V	*	18.00	7.00	2.00	32.00	34.00	14.00	3.00
As	2.44	0.00	0.46	0.61	2.03	0.84	1.54	*
Co	*	5.30	2.00	2.50	1.55	3.10	4.10	1.00
Cu	114.00	3.10	0.80	2.30	1.60	10.30	7.10	1.00
Cr	*	20.10	14.00	18.40	22.90	19.60	15.60	*
Ni	*	4.00	2.00	1.00	6.50	7.00	3.00	2.00
Pb	*	19.10	7.50	10.40	6.50	4.00	8.80	*
Zn	*	29.00	14.00	12.00	33.50	33.00	7.00	*
Rb	156.00	116.20	125.00	136.80	67.10	125.00	2.30	124.00
Sr	17.80	80.70	28.90	15.50	168.25	68.00	80.20	16.00
Y	51.90	19.70	34.10	30.40	11.90	8.70	16.70	12.00
Zr	56.50	119.20	92.00	67.70	134.95	164.50	181.00	60.00
Nb	22.10	12.20	11.20	11.40	8.35	13.90	17.30	*
U	2.93	1.82	2.56	1.81	1.41	1.15	1.42	*
Th	7.78	5.11	9.77	7.21	5.75	4.06	5.38	*
Sc	1.73	2.88	1.45	1.30	3.62	3.34	1.25	2.00
Cs	1.73	1.42	1.20	1.31	0.90	2.94	0.09	*
Au	BLD	BLD	BLD	BLD	BLD	BLD	BLD	*
Sb	BLD	BLD	BLD	BLD	0.25	0.15	0.22	*
W	0.54	0.34	0.41	BLD	0.45	2.58	0.87	*
Mo	0.39	BLD	0.43	BLD	BLD	BLD	0.53	*
Sc	1.73	2.88	1.45	1.30	3.62	3.34	1.25	2.00
Cr	BLD	6.88	BLD	BLD	15.67	11.25	BLD	BLD
Co	BLD	3.12	1.28	BLD	5.00	5.36	3.42	BLD
Ba	63.23	554.78	472.08	294.60	541.02	395.78	24.57	*
Hf	3.56	3.70	3.34	2.79	4.15	3.77	4.30	*
Ta	2.06	1.08	1.12	1.18	0.84	0.72	0.66	*
Cl	190.00	*	270.00	190.00	370.00	130.00	*	*
La	5.65	9.16	14.07	10.62	18.48	12.36	17.56	7.60
Ce	14.88	28.30	34.47	24.20	47.83	22.73	35.21	19.27

Sm	2.98	1.54	3.59	3.08	2.56	1.99	1.87	1.90
Eu	0.11	0.46	0.34	0.11	0.83	0.54	0.71	0.13
Tb	1.01	0.48	0.87	0.71	0.42	0.28	0.27	0.36
Y	51.90	19.70	34.10	30.40	11.90	8.70	16.70	12.00
Yb	5.20	3.08	3.27	4.11	1.91	0.28	BLD	1.90
Lu	BLD	BLD	0.49	0.45	BLD	0.03	BLD	0.29

Geochemical Analyses of Temagami Samples

INTRUSIVE ROCKS: Major Elements in percent, trace in ppm, Au ppb

rock type—>	peg	peg	peg	dyke	dyke	dyke	dyke	dyke
sample—>	318	319	322	56	307	113	302	320
SiO2	77.2	75.0	75.6	70.5	71.8	69.6	69.9	69.9
Al2O3	12.2	14.2	14.0	14.7	14.2	15.4	15.0	14.9
Fe2O3	1.54	0.78	0.86	4.06	3.05	3.62	3.88	3.39
MgO	0.13	0.06	0.15	0.89	0.87	0.84	0.82	0.94
CaO	0.54	0.11	0.14	2.95	2.30	3.81	2.39	3.04
Na2O	3.74	4.55	3.75	3.92	4.23	4.44	3.99	3.94
K2O	3.85	4.77	4.95	1.33	1.95	0.69	1.65	1.81
TiO2	0.09	0.03	0.03	0.32	0.30	0.37	0.36	0.35
MnO	0.02	0.01	0.01	0.03	0.03	0.04	0.04	0.04
P2O5	0.04	BLD(.01)	0.02	0.13	0.09	0.14	0.11	0.10
Ba	907.00	666.00	1.0E+3	355.00	490.00	179.00	424.00	497.50
V	7.00	4.00	5.00	42.00	37.00	47.00	45.00	41.00
As	0.92	2.75	4.84	1.80	0.61	*	7.44	1.66
Co	0.60	2.23	3.90	2.50	3.00	5.70	4.55	5.30
Cu	29.00	4.23	5.40	84.00	4.90	176.00	6.10	23.00
Cr	13.10	15.87	20.30	24.10	17.20	17.50	21.35	26.20
Ni	2.00	2.00	3.00	7.00	9.00	9.00	6.50	15.00
Pb	11.60	11.00	10.40	9.30	9.60	4.30	8.15	10.90
Zn	21.00	3.33	2.00	54.00	82.00	64.00	40.00	73.00
Rb	103.70	142.50	136.50	58.30	60.60	77.90	80.45	82.35
Sr	52.10	22.83	24.20	183.10	169.20	189.60	173.20	202.50
Y	30.00	34.30	28.80	14.90	13.00	14.80	13.10	9.75
Zr	91.60	74.20	114.60	217.30	168.90	233.00	216.00	204.40
Nb	13.40	11.23	12.00	11.10	12.20	10.20	10.65	10.05
U	3.08	1.38	1.75	0.69	1.04	*	0.65	0.96
Th	8.60	7.10	10.98	2.96	3.62	*	3.95	3.64
Sc	2.12	1.08	1.45	5.61	4.12	*	5.26	4.42
Cs	1.24	1.75	1.95	1.47	0.88	*	1.69	2.11
Au	7.88	1.14	3.39	*	1.73	*	BLD	8.16
Sb	BLD	BLD	BLD	0.39	0.12	*	0.36	0.15
W	0.34	0.66	0.38	0.99	0.34	*	2.57	0.38
Mo	2.81	20.37	12.51	BLD	BLD	*	BLD	0.36
Sc	2.12	1.08	1.45	5.61	4.12	*	5.26	4.42
Cr	5.95	BLD	BLD	20.64	16.01	*	14.71	36.68
Co	1.72	1.16	1.79	7.26	6.06	*	7.34	7.05
Ba	789.02	604.89	874.06	390.77	508.98	*	457.81	490.07
Hf	3.27	2.85	5.12	4.44	3.84	*	4.42	4.47
Ta	1.17	0.96	0.99	0.52	0.61	*	0.59	0.64

Cl	170.00	82.67	250.00	70.00	130.00	*	40.00	40.00
La	25.10	5.08	4.04	13.75	15.51	*	18.41	22.01
Ce	45.67	14.92	19.65	42.40	35.86	*	34.66	42.46
Sm	4.08	1.56	1.21	2.67	1.74	*	2.98	3.00
Eu	0.44	0.16	0.17	1.02	0.71	*	0.88	0.86
Tb	0.61	0.74	0.61	0.37	0.30	*	0.46	0.35
Y	30.00	34.30	28.80	14.90	13.00	*	13.40	9.75
Yb	3.18	4.54	5.02	1.33	2.36	*	0.65	1.49
Lu	0.42	0.50	0.57	0.16	0.14	*	0.04	0.12

Geochemical Analysis of Temagami Samples

VOLCANIC ROCKS: Major elements in percent trace elements in ppm
(* no analysis; results normalized to 100%)

Sample—>	89	152	233	236	238	252	136	138
rock type->	2i	2i	2i	2i	2i	2i	2k	2k
SiO2	50.22	50.29	51.49	52.11	52.38	51.85	51.65	53.51
Al2O3	13.17	13.58	14.19	13.90	13.17	13.62	13.44	13.60
Fe2O3	13.27	14.07	11.99	13.97	17.90	13.40	13.81	15.15
MgO	8.95	7.97	8.95	7.05	4.33	6.89	6.98	4.99
CaO	9.79	10.39	9.43	8.48	8.48	9.07	10.05	7.96
Na2O	2.38	1.72	1.96	1.96	1.35	2.04	2.48	2.54
K2O	1.47	1.09	1.26	1.33	1.08	1.10	0.64	1.14
TiO2	0.51	0.71	0.48	0.91	1.00	0.73	0.70	0.80
MnO	0.15	0.15	0.16	0.19	0.19	0.17	0.18	0.22
P2O5	0.08	0.07	0.08	0.09	0.12	0.08	0.07	0.08
Ba	792	133	173	214	276	153	134	303
V	289	314	283	351	376	319	319	302
As	0.50	2.13	3.50	2.70	0.50	1.00	0.50	1.50
Co	53.5	49.0	33.5	40.1	56.6	52.9	47.1	53.2
Cu	37.0	16.8	35.0	33.0	69.0	8.2	474.0	6.4
Cr	389.9	393.9	468.3	171.3	56.5	248.0	253.9	209.1
Ni	145.0	103.3	119.0	92.0	62.0	108.0	98.0	62.0
Zn	88.0	84.5	94.0	96.0	137.0	214.0	249.0	268.0
Rb	66.5	55.1	48.3	62.1	39.8	59.4	13.8	28.0
Sr	120.2	102.3	158.4	105.7	110.0	168.7	105.3	130.2
Y	22.9	14.7	18.4	15.7	22.7	19.6	17.4	17.4
Zr	33.1	42.2	43.1	55.1	71.5	49.8	42.3	48.7

Sample—>	247	250	133	151	153	228	241	20
rock type->	2k	2k	2j	2j	2j	2j	2j	2o
SiO2	50.24	50.27	52.41	50.13	51.93	50.22	52.26	50.77
Al2O3	12.44	13.42	14.22	15.12	14.97	13.54	13.47	13.93
Fe2O3	18.02	17.70	16.13	15.61	14.31	17.01	17.55	14.62
MgO	7.64	5.13	6.79	5.66	5.82	5.99	3.93	5.70
CaO	7.87	10.32	5.97	9.93	7.28	9.99	9.53	10.68
Na2O	1.60	1.62	2.40	1.67	3.13	1.53	1.23	2.05
K2O	1.26	0.48	0.92	0.83	1.52	0.90	0.83	0.81
TiO2	0.68	0.73	0.89	0.75	0.79	0.55	0.82	1.12
MnO	0.18	0.23	0.19	0.21	0.16	0.20	0.28	0.23
P2O5	0.08	0.09	0.07	0.08	0.10	0.11	0.09	0.08
Ba	267.0	89.0	291.0	156.0	353.0	165.0	163.0	98.0
V	364.0	351.0	360.0	318.0	290.0	334.5	319.0	376.0
As	2.10	1.50	3.40	0.50	0.50	2.25	1.70	0.50
Co	85.6	67.3	54.7	53.9	51.1	64.1	64.3	47.1
Cu	102.0	6.6	6.2	58.0	199.0	69.5	34.0	51.0
Cr	421.1	388.8	207.9	372.2	416.3	403.6	203.5	30.0
Ni	126.0	93.0	64.0	86.0	97.0	128.5	83.0	58.0
Zn	159.0	107.0	130.0	134.0	99.0	129.0	167.0	99.0
Rb	34.8	4.4	38.8	26.1	54.6	21.5	20.2	36.0
Sr	84.2	72.3	84.9	106.8	154.8	145.0	98.2	103.1
Y	23.0	15.1	14.1	14.0	15.6	18.8	20.3	24.0

Zr	48.6	42.5	53.5	46.3	47.4	45.8	51.2	71.8

Geochemical Analysis of Temagami Samples

VOLCANIC ROCKS: Major elements in percent trace elements in ppm
(* no analysis; results normalized to 100%)

Sample—>	265	284	300	174(dup)	306	174(dup)	112	190
rock type->	2o	mts	mts	2p/h	2p/h	2p/h	dyke	dyke
SiO2	53.83	56.75	57.33	47.44	51.81	47.61	54.81	48.20
Al2O3	14.28	14.35	13.45	10.17	12.27	10.07	14.01	15.56
Fe2O3	10.97	9.15	8.91	23.53	14.91	23.69	9.25	15.50
MgO	4.14	5.63	9.00	6.69	6.18	6.57	8.19	6.01
CaO	11.93	8.82	5.60	8.11	10.53	8.19	7.56	6.32
Na2O	1.69	3.51	2.82	0.97	2.30	0.83	4.17	1.32
K2O	1.42	0.80	1.97	1.44	0.41	1.48	0.95	2.95
TiO2	1.35	0.70	0.54	1.32	1.28	1.23	0.67	3.21
MnO	0.21	0.20	0.13	0.28	0.22	0.27	0.14	0.24
P2O5	0.16	0.08	0.25	0.06	0.09	0.06	0.27	0.71
Ba	146.0	271.0	995.0	102.0	136.0	102.0	819.0	512.0
V	335.0	253.0	161.0	578.0	452.0	573.0	154.0	378.5
As	0.50	1.40	3.00	2.30	1.80	1.20	1.00	2.30
Co	38.3	23.7	24.7	86.0	29.7	88.3	30.5	54.2
Cu	10.3	11.1	33.0	598.0	68.0	593.0	87.0	59.5
Cr	70.4	215.8	890.4	242.3	25.3	221.9	719.4	82.7
Ni	65.0	86.0	142.0	272.0	111.0	301.0	234.0	69.0
Zn	78.0	91.0	101.0	119.0	132.0	115.0	142.0	150.0
Rb	64.1	34.7	40.4	127.8	14.8	136.1	30.3	342.6
Sr	179.6	230.2	272.0	58.4	196.3	64.8	425.6	370.1
Y	24.1	23.0	16.4	3.0	20.6	0.9	22.2	21.1
Zr	94.4	60.9	103.8	12.4	64.2	11.1	132.9	203.3

Sample—>	330	52f	56f	61f	63f	67f	71f	114f
Rock type->	dyke	bxx frg	bxx frg	bxx frg	bxx frg	bxx frg	bxx frg	bxx frg
SiO2	47.58	49.75	49.18	49.91	49.68	48.94	49.23	52.41
Al2O3	14.85	13.22	13.97	12.56	12.68	14.28	14.67	14.66
Fe2O3	16.96	14.69	11.72	15.25	15.96	15.83	16.99	13.06
MgO	5.97	7.54	8.97	8.02	7.80	7.71	6.20	6.82
CaO	8.54	9.76	10.47	9.50	9.24	7.85	7.32	8.77
Na2O	1.98	1.41	1.45	1.57	1.13	1.32	1.52	1.81
K2O	0.89	1.00	0.99	1.10	1.07	1.66	1.48	0.91
TiO2	2.51	0.27	0.33	0.26	0.32	0.26	0.34	0.29
MnO	0.18	0.18	0.17	0.20	0.28	0.23	0.21	0.16
P2O5	0.53	0.43	0.12	0.03	0.05	0.03	0.04	0.06
Ba	373.0	285.0	141.0	1.1E+3	138.0	312.0	152.0	139.0
V	296.00	*	*	*	*	*	*	*
As	4.90	*	*	*	*	*	*	*
Co	57.9	*	*	*	*	*	*	*
Cu	56.0	534.0	355.0	152.0	563.0	134.0	251.0	37.0
Cr	91.0	53.1	89.6	56.5	100.4	189.5	169.3	61.1
Ni	109.0	180.6	115.9	107.5	96.7	105.8	123.1	102.2
Zn	116.0	47.6	47.3	48.9	63.3	58.8	61.7	51.1
Rb	19.5	53.1	89.6	56.5	100.4	189.5	169.3	61.1

Sr	423.2	180.6	115.9	107.5	96.7	105.8	123.1	102.2
Y	26.9	31.0	25.6	25.6	30.5	21.1	21.3	20.2
Zr	163.6	47.6	47.3	48.9	63.3	58.8	61.7	51.1

Geochemical Analysis of Temagami Samples

VOLCANIC ROCKS: Major elements in percent trace elements in ppm
(* no analysis; results normalized to 100%)

Sample—>	116f		119f		123f		146f		150f		272f		275f		1344a	
Rock type>	bxx	frg	bxx	frg	bxx	frg	bxx	frg	bxx	frg	bxx	frg	bxx	frg	bxx	frg
SiO2	48.79		48.69		50.16		49.84		49.69		49.56		49.78		50.47	
Al2O3	16.84		14.63		14.71		13.94		13.67		13.76		13.74		13.73	
Fe2O3	13.66		15.80		13.98		14.28		13.10		11.72		15.53		13.01	
MgO	6.00		7.44		7.23		7.52		8.82		10.56		6.65		8.29	
CaO	10.12		7.87		9.41		8.99		10.00		9.52		9.93		9.62	
Na2O	1.90		1.65		1.99		1.91		1.84		1.49		1.15		1.90	
K2O	1.00		1.21		0.93		0.86		0.88		1.24		0.93		1.18	
TiO2	0.36		0.43		0.33		0.29		0.26		0.31		0.29		0.36	
MnO	0.16		0.23		0.13		0.20		0.19		0.17		0.22		0.20	
P2O5	0.11		0.12		0.09		0.21		0.09		0.12		0.26		0.07	
Ba	213.0		447.0		230.0		184.0		147.0		182.0		142.0		153.0	
V	*		*		*		*		*		*		*		*	
As	*		*		*		*		*		*		*		*	
Co	*		*		*		*		*		*		*		*	
Cu	90.0		103.0		11.0		377.0		168.0		200.0		2.2E+3		196.5	
Cr	62.3		79.4		50.2		62.1		70.9		106.7		60.0		93.7	
Ni	105.1		108.4		130.5		130.0		117.6		99.7		113.3		127.3	
Zn	58.3		67.6		47.5		49.9		46.5		45.0		49.3		50.0	
Rb	62.3		79.4		50.2		62.1		70.9		106.7		60.0		93.7	
Sr	105.1		108.4		130.5		130.0		117.6		99.7		113.3		127.3	
Y	24.5		25.0		20.4		28.9		29.7		23.5		24.3		24.2	
Zr	58.3		67.6		47.5		49.9		46.5		45.0		49.3		50.0	

Geochemical Analyses of Temagami Samples

QUARTZ VEINS AND BRECCIA MATRIX: (all cocentrations except for Au(ppb) in ppm; *-no analysis; BLD-below detection)(sample types: 1-unmineralized veins;2-mineralized veins;3-feldspar-bearing veins;4-qtz.breccia unmineralized;5-qtz.breccia mineralized;6-feldspar-bearing breccia unmineralized;7-feldspar-bearing breccia mineralized;8-granite hosted vein)

Type-	1	1	1	1	1	1	2	2	2
Sample-	54	68	69	161	169	263	10	76b	78
Au	0.17	0.44	0.99	0.14	1.22	0.27	BLD	0.41	BLD
As	0.10	0.13	0.31	0.18	0.14	0.22	0.25	0.07	0.16
Sb	0.011	0.019	0.020	0.016	0.010	0.022	0.024	0.014	0.023
W	0.03	0.16	0.03	0.08	0.03	0.03	0.06	0.03	0.03
Mo	0.13	0.51	0.34	5.40	0.90	0.24	20.88	2.51	0.90
Cl	290	120	520	*	*	320	800	*	300
U	0.01	0.02	0.02	0.01	0.01	0.01	0.02	0.01	0.04

Type-	2	2	2	2	2	2	2	2	2
Sample-	147	181	185	187c	189	192	224	225	256
Au	0.49	3.16	BLD	1.04	6.22	13.38	0.39	0.45	0.63
As	0.09	0.04	0.15	0.28	2.16	0.07	0.11	0.07	0.08
Sb	0.019	0.019	0.013	0.025	0.076	0.012	0.022	0.009	0.027
W	0.02	0.02	0.02	0.02	0.07	0.03	BLD	0.01	0.02
Mo	0.80	1.44	0.27	8.50	29.06	1.32	11.83	0.36	5.20
Cl	*	*	230	300	470	380	1,130	*	*
U	0.01	0.02	0.06	0.07	0.04	0.01	0.01	0.01	0.01

Type-	2	2	2	3	3	3	4	4	4
Sample-	257	271	286	75	101	102	61	114	123
Au	9.22	BLD	0.21	0.81	0.27	BLD	0.76	0.28	0.50
As	0.09	0.22	0.24	0.08	0.24	0.23	0.22	0.18	0.20
Sb	0.039	0.028	0.034	0.021	0.008	0.010	0.019	0.008	0.011
W	0.03	0.08	0.01	0.05	0.02	0.03	0.07	0.04	0.47
Mo	5.76	2.16	2.11	2.36	0.20	BLD	2.85	BLD	0.46
Cl	*	*	*	*	*	*	440	*	260
U	*	0.01	0.01	0.04	0.02	0.01	0.04	0.01	0.01

Type-	4	4	5	5	5	5	5	5	5
Sample-	146	150	63	71	144a	144b	272	275	344
Au	0.51	2.27	0.35	0.33	1.12	0.80	0.48	14.93	4.25
As	0.40	0.44	0.83	0.10	0.19	0.22	0.29	0.20	0.19
Sb	0.030	0.032	0.009	0.010	0.010	0.017	0.022	0.019	0.012
W	0.09	0.54	0.01	0.01	0.04	0.06	0.04	0.05	0.05
Mo	0.13	0.80	3.97	0.79	1E+2	68.71	20.45	4.20	66.33
Cl	610	*	170	*	620	620	200	240	*
U	0.02	0.02	0.01	0.01	0.01	*	0.02	0.02	0.01

Type-	6	6	6	6	6	7	8	8	8
Sample-	52	56c	67	116	119	148	29a	48a	130
Au	0.50	BLD	0.13	0.58	0.62	0.37	0.41	1.66	BLD
As	0.21	0.16	0.20	0.19	0.22	0.39	0.11	0.92	0.26
Sb	0.007	0.009	0.009	0.010	0.011	0.037	0.012	0.050	0.008
W	0.02	0.24	0.19	0.07	0.03	0.05	0.08	0.07	0.08
Mo	0.12	BLD	0.65	BLD	BLD	0.50	0.06	0.67	0.24
Cl	130	490	*	410	380	160	730	120	360
U	0.01	0.02	0.02	0.02	0.01	0.02	0.01	0.14	BLD

Appendix C

Precision of XRF Analysis

Relative error for duplicate XRF sanalyses

(Major elements in percent ,trace elements in ppm)

Element	152a	152b	± % Relative error	174a	174b	± % Relative error
SiO2	50.43	50.24	0.38	47.44	47.61	0.36
Al2O3	13.59	13.57	0.15	10.17	10.07	0.99
Fe2O3	13.92	14.11	1.36	23.53	23.69	0.68
MgO	8.04	7.94	1.25	6.69	6.57	1.81
CaO	10.18	10.46	2.71	8.11	8.19	0.98
Na2O	1.74	1.71	1.74	0.97	0.83	15.56
K2O	1.09	1.08	0.92	1.44	1.48	2.74
TiO2	0.79	0.68	14.97	1.32	1.23	7.06
MnO	0.15	0.14	6.90	0.28	0.27	3.64
P2O5	0.07	0.06	15.38	0.06	0.06	0.00
Ba	139.00	*	0.38	102.00	*	0.36
V	309.00	316.00	2.24	578.00	573.00	0.87
As	1.30	2.40	59.46	2.30	1.20	62.86
Cu	7.00	20.00	96.30	598.00	593.00	0.84
Cr	408.00	389.20	4.72	242.30	221.90	8.79
Ni	110.00	101.00	8.53	272.00	301.00	10.12
Pb	12.60	5.40	80.00	16.70	10.80	42.91
Zn	86.00	84.00	2.35	119.00	115.00	3.42
Rb	53.40	55.70	4.22	127.80	136.10	6.29
Sr	99.10	103.40	4.25	58.40	64.80	10.39
Y	15.50	14.40	7.36	3.00	0.90	0.36
Zr	40.80	42.60	4.32	12.40	11.10	11.06

	228a	228b	± % Relative error	302a	302b	± % Relative error
SiO2	50.42	50.02	0.80	71.22	71.28	0.08
Al2O3	13.51	13.56	0.37	15.35	15.22	0.85
Fe2O3	16.96	17.05	0.53	3.94	3.96	0.51
MgO	5.96	6.01	0.84	0.83	0.83	0.00
CaO	9.92	10.05	1.30	2.48	2.39	3.70
Na2O	1.48	1.57	5.90	4.02	4.10	1.97
K2O	0.89	0.90	1.12	1.64	1.71	4.18
TiO2	0.55	0.54	1.83	0.37	0.36	2.74
MnO	0.20	0.20	0.00	0.03	0.05	50.00
P2O5	0.11	0.10	9.52	0.11	0.11	0.00
Ba	165.00	*	0.38	432.00	*	0.36
V	332.00	337.00	1.49	46.00	44.00	4.44
As	2.50	2.00	22.22	2.40	BLD	*
Cu	69.00	70.00	1.44	6.70	5.50	19.67
Cr	408.10	399.00	2.25	24.00	18.70	24.82
Ni	132.00	125.00	5.45	7.00	6.00	15.38
Pb	16.70	20.70	21.39	11.80	4.50	89.57
Zn	137.00	121.00	12.40	41.00	39.00	5.00
Rb	22.90	20.10	13.02	79.50	81.40	2.36
Sr	149.20	140.80	5.79	176.50	169.90	3.81
Y	21.20	16.30	26.13	13.40	12.80	4.58

Zr	50.90	40.60	22.51	214.60	217.40	1.30

Relative error for duplicate XRF sanalyses

(Major elements in percent ,trace elements in ppm)

	323a	323b	± % Relative error	328a	328b	± % Relative error
SiO2	72.57	72.51	0.08	50.91	50.87	0.08
Al2O3	14.75	14.78	0.20	11.91	11.83	0.67
Fe2O3	2.96	2.90	2.05	18.80	18.84	0.21
MgO	0.75	0.71	5.48	4.73	4.75	0.42
CaO	2.59	2.63	1.53	9.68	9.68	0.00
Na2O	3.78	3.85	1.83	1.33	1.43	7.25
K2O	2.25	2.28	1.32	0.61	0.57	6.78
TiO2	0.25	0.24	4.08	1.47	1.46	0.68
MnO	0.03	0.02	40.00	0.31	0.32	3.17
P2O5	0.07	0.08	13.33	0.25	0.26	3.92
Ba	530.00	*	0.38	181.00	*	*
V	30.00	34.00	12.50	293.00	311.00	5.96
As	1.30	6.60	134.18	2.90	BLD	*
Cu	1.10	2.10	62.50	54.00	55.00	1.83
Cr	23.60	22.20	6.11	243.20	239.50	1.53
Ni	4.00	9.00	76.92	124.00	130.00	4.72
Pb	8.50	4.50	61.54	11.30	10.30	9.26
Zn	34.00	33.00	2.99	107.00	105.00	1.89
Rb	64.20	70.00	8.64	23.70	29.60	22.14
Sr	165.90	170.60	2.79	155.40	161.00	3.54
Y	9.70	14.10	36.97	42.90	48.20	11.64
Zr	132.20	137.70	4.08	157.30	166.20	5.50

	190a	190b	± % Relative error	320a	320b	± % Relative error
SiO2	48.21	48.19	0.04	70.98	71.10	0.17
Al2O3	15.66	15.45	1.35	15.10	15.20	0.66
Fe2O3	15.51	15.49	0.13	3.40	3.48	2.33
MgO	5.98	6.04	1.00	1.09	0.81	29.47
CaO	6.29	6.35	0.95	3.07	3.10	0.97
Na2O	1.27	1.37	7.58	4.04	3.97	1.75
K2O	2.98	2.92	2.03	1.84	1.83	0.54
TiO2	3.15	3.26	3.43	0.35	0.36	2.82
MnO	0.24	0.23	4.26	0.04	0.04	0.00
P2O5	0.71	0.70	1.42	0.10	0.10	0.00
Ba	512.00	*	*	497.00	*	*
V	369.00	388.00	5.02	41.00	41.00	0.00
As	1.20	3.40	95.65	6.70	7.20	7.19
Cu	58.00	61.00	5.04	21.00	25.00	17.39
Cr	85.30	80.00	6.41	24.90	27.50	9.92
Ni	67.00	71.00	5.80	14.00	16.00	13.33
Pb	4.50	10.10	76.71	6.70	15.10	77.06
Zn	151.00	149.00	1.33	73.00	*	*
Rb	336.90	348.30	3.33	79.30	85.40	7.41

Sr	373.00	367.10	1.59	199.60	205.40	2.86
Y	22.90	19.30	17.06	9.10	10.40	13.33
Zr	200.50	206.00	2.71	200.20	208.60	4.11

APPENDIX D

CONTOURING METHOD

Contour maps were produced using the program Surfer (Golden Software Inc., Golden Colorado). The first stage of the program algorithm is to divide the area to be contoured into a grid. The spacing or size of grid cells is user specified and depends on the density of data being considered. Where it was possible grid spacing was set so that the number of grid cells was approximately equal to the number of data points. Randomly spaced data points (Z_i), dispersed over the grid, are used to calculate elements or average Z values at the intersection of grid cells, with sides of length d. The calculation of the Z value is determined by the relation:

$$Z = \frac{\sum_{i=1}^{n} Z_i/(d_{i)2}}{\sum_{i=1}^{n} 1/(d_i)^2}$$

For the calculation of Z the program was set to consider the 10 nearest points within a radius of the grid element. Contour lines were drawn at intervals, set by the user, so as to best illustrate the data.

For the data herein the most common limitation of the contouring method is that data is commonly unevenly distributed over the grid area. This results in grid spacings that are not optimal for the data of different areas but are a compromise between the two extremes. Contour maps created for areas of poor data coverage must be interpreted with caution since contours in these areas are based on few and distant data points.

MAP 1

Geology of the Study Area

LEGEND

Volcanics

2 Unsubdivided tholeiitic basalt

2i Salt and pepper textured tholeiitic-basalt (Mg-rich).

2j Very fine-grained tholeiitic basalt (Fe-rich).

2k Very fine-grained amygdaloidal and or pillowed tholeiitic basalt (Fe-rich).

2o Medium-grained quartz and plagioclase altered tholeiitic basalt.

2p Possible mafic intrusive (unit 3); medium to coarse-grained intergrowth of hornblende and plagioclase.

2q Hybridized basalt, adjacent to intrusion breccia: medium grained, local intense feldspar alteration in form of lenses and bands, also local concentrations of aplite dyklets; isolated coarse-grained phases may be unit 3.

Intrusives

3 Mafic intrusive rock, anorthosite/gabbro, unsubdivided.

4a Buff coloured granite-granodiorite.

4b Salmon pink coloured granite.

5 Quartz and quartz-feldspar cemented breccia.

6a Feldspar porphyry.

6b Quartz-feldspar porphyry.

7 Basaltic dykes.

Symbols

- attitude of quartz veins (may be average of several when trends consistent)
- average attitude of prominent joints
- foliation
- trend of dykes
- areas where molybdenite + chalcopyrite mineralization is > 1%
- areas of > 1% Fe + Mo oxide mineralization
- geological contact
- fault
- shaft
- pit or trench
- paved road
- railway
- X (290) sample location

Geology by M. E. Baknes

N

0 100 200 300 m

SCALE 1 : 3500

GAS LINE

NET LAKE

NET LAKE

TEMAGAMI NORTH

4a

4b

3

2q

2p

2i

2j

2j-k

2k

5

6a

6b

7

tr. mo

aplites

pegmatites

bubble structures

tr. cpy

py-cpy

po-cpy

bxx

qtz-plag alteration

x(284)

x(174) po-cpy

x(306)

water tower

mo cpy

(298)

(290)

(300)

Quenched Granite

Qtz-Ksp. alteration

For detail of grid area see map 2

INTRUSION BRECCIA (Matrix 4a Framework 2,3)

py po cpy min.

"069" Shear zone

many small Qtz v.

Vein Stockwork

Intense Silicification

MAP 2

GEOLOGY OF THE BRECCIA AND ADJACENT AREA

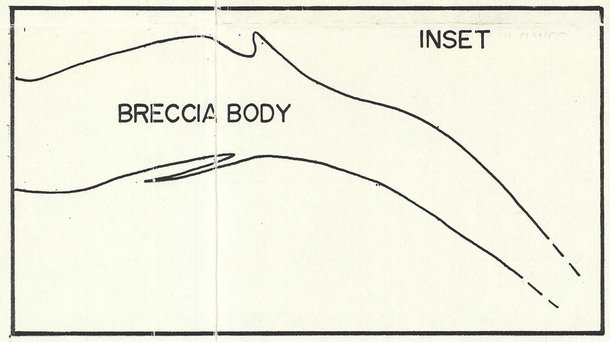

LEGEND

- 2i salt and pepper textured tholeiitic basalt (Mg-rich)
- 2j very fine-grained tholeiitic basalt (Fe-rich)
- 2k very fine-grained amygdaloidal and or pillowed tholeiitic basalt (Fe rich)
- 2o medium-grained silica and plagioclase altered tholeiitic basalt (Mg-rich)
- 4b Salmon pink granite
- 6a feldspar porphyry
- 7 basaltic dyke
- 8 dacite-andesite dyke
- 5a feldspar-bearing veins and breccia
- 5b non feldspar-bearing veins and breccia
- incipient breccia
- pervasive breccia

- average attitude of quartz veins
- average attitude of joint sets
- trend of dykes
- areas where molybdenite + chalcopyrite mineralization is > 1%
- areas of > 1% Fe + Mo oxide mineralization
- abrupt breccia contact
- gradational breccia contact
- geological contact
- fault
- shaft
- pit